

Early to middle Eocene calcareous nannofossils of the SW Pacific:
paleobiogeography and paleoclimate

by

Claire Louise Shepherd

A thesis
submitted to Victoria University of Wellington
in fulfilment of the requirements for the degree of
Doctor of Philosophy
In Geology

Victoria University of Wellington

2017

ABSTRACT

Earth's climate underwent a long-term warming trend from the late Paleocene to early Eocene (~58–51 Ma), with global temperature reaching a sustained maximum during the Early Eocene Climatic Optimum (EECO; 53–50 Ma). Geochemical proxies indicate tropical or warm subtropical sea-surface temperature (SST) conditions in middle and high latitudes in the early Eocene, implying a very low latitudinal temperature gradient. This study investigates whether calcareous nannofossil assemblages in the southwest (SW) Pacific provide evidence of these conditions at middle latitudes in the early to middle Eocene, particularly during the EECO. Specifically, this study documents the biogeographic changes of warm- and cold-water nannofossil species along a paleolatitudinal transect through the EECO to track changes in water masses/ocean circulation at that time.

Early to middle Eocene calcareous nannofossil assemblages were examined from four sites along a latitudinal transect in the SW Pacific, extending from Lord Howe Rise in the north to Campbell Plateau in the south and spanning a paleolatitude of ~46–54°S. All of the sections studied in this project span nannofossil zones NP10–16 (Martini, 1971). The data indicate up to three regional unconformities through the sections: at mid-Waipara, Deep Sea Drilling Project (DSDP) Site 207 and 277, part or all of Zone NP10 (lower Waipawan) is missing; at Sites 207 and 277 a possible hiatus occurs within NP12 (upper Waipawan–lower Mangaorapan); and at all sites part or all of Zone NP15 (lower Bortonian) is missing. Results of this study indicate that nannofossil assemblages in the SW Pacific are more similar to floras at temperate to polar sites rather than those at tropical/subtropical sites. However, variations in the relative abundance of key species in the SW Pacific are broadly consistent with the trends seen in the geochemical proxy records: an increase in warm-water taxa coincided with the EECO, corroborating geochemical evidence for a temperature maximum in the SW Pacific during this interval.

The increase in the abundance and diversity of warm-water taxa and decrease in the abundance of cool-water taxa through the EECO supports previous suggestions that a warm-water mass (northward of the proto-Tasman Front) extended to ~55°S paleolatitude during

this interval in response to enhanced poleward heat transport and intensification of the proto-East Australian Current. At the southernmost site, DSDP Site 277, a relatively short-lived influx of warm-water taxa at ~51 Ma suggests that warm waters expanded south at this time. However, greater diversity and abundance of warm-water taxa throughout the EECO at DSDP Site 207, suggests that the proto-East Australian Current exerted greater influence at this latitude for a longer duration than at Site 277. An increase in the abundance of cool-water taxa and decrease in diversity and abundance of warm-water taxa at all sites is recorded following the termination of the EECO. This corresponds with the contraction of the proto-Tasman Front due to weakened proto-East Australian Current flow and associated amplification of the proto-Ross Gyre.

Previous estimates of SSTs from geochemical proxies in the SW Pacific during the EECO indicate that there was virtually no latitudinal temperature gradient and temperatures were tropical to subtropical ($>20^{\circ}\text{C}$). However, nannofossil data from this study indicate warm temperate conditions ($\sim 15\text{--}20^{\circ}\text{C}$) during the EECO, suggesting that a reduced latitudinal gradient was maintained through this interval, which is in agreement with climate models.

ACKNOWLEDGEMENTS

Firstly, I would like to thank my supervisors: Drs. Chris Hollis, Denise Kulhanek and James Crampton. To Chris, who has been immensely generous with his time and knowledge over the last three years, thank you for your guidance and support. Thanks to Denise who has been an outstanding mentor in all things “nannofossil”. Thank you so much for reviewing anything I sent your way, giving second opinions on the identification of specimens and generally answering my multitude of questions. To James, thank you for reviewing manuscripts, chapters and abstracts, your contribution has been invaluable.

Huge thanks to the people at GNS Science for making me feel like part of the team. Thanks to Erica Crouch and Hugh Morgans for sharing their knowledge on the mid-Waipara and Hampden Beach sections. To Sonja-Bermudez, thanks for being a fantastic office-mate and injecting some humour into my day when I really needed it. Thanks to Kristina Pascher for your friendship over the last three years, it was great to have someone to talk to who was experiencing the same challenges. Marianna Terezow, thanks for the random chats and for giving my microscope a makeover – karaoke board-game night is coming soon. Lastly, thanks to all of those people at GNS that stopped by every now and again, just to see how things were going. Your words of encouragement and support were truly appreciated.

Thanks to overseas colleagues: Leah Schneider at IODP for generously sharing her Eocene nannofossil data; and Jean Self-Trail at USGS for the opportunity to collaborate on the *Tribrachiatulus* study. I would also like to acknowledge the assistance of the New Zealand Government for funding this project through the Marsden Fund and the GNS Science Global Change Through Time Programme.

Last but not least I would like to thank my incredible support team. To my Mum and Dad, who joined me on this crazy ride almost 9 years ago when I decided to “start” Uni. Thank you so much for your love and support, I could not have done this without you. To my dear friend Esther, who provided a weekend escape hatch whenever I needed it. Thank you for your generosity and friendship, I am looking forward to a much needed catch-up with you

and the “kids”. Finally, to Lisa and Jack, thank you for your love, patience and understanding throughout this challenging year. Your combined ability to make me laugh every day kept me from losing my mind.

TABLE OF CONTENTS

ABSTRACT.....	i
ACKNOWLEDGEMENTS.....	iii
TABLE OF CONTENTS.....	v
LIST OF FIGURES.....	ix
LIST OF TABLES.....	xi
CHAPTER 1: INTRODUCTION.....	1
1.1 Overview.....	1
1.2 Eocene climate.....	2
1.3 Eocene proxy reconciliation problem.....	4
1.4 Geochemical temperature proxies.....	5
1.4.1 Oxygen isotopes.....	5
1.4.2 Mg/Ca paleothermometry.....	6
1.4.3 TEX ₈₆	7
1.5 Calcareous nannofossils.....	8
1.5.1 Introduction.....	8
1.5.2 Biostratigraphic utility of calcareous nannofossils.....	9
1.5.3 Paleoenvironmental utility of calcareous nannofossils.....	12
1.6 Aims and structure of this thesis.....	15
CHAPTER 2: METHODOLOGY.....	18
2.1 Slide preparation.....	18
2.2 Assemblage counts.....	18
2.3 Taxonomy.....	18
2.4 Preservation/dissolution indices.....	19
2.4.1 Qualitative evaluation based on visual observation.....	20
2.4.2 Relative abundance of <i>Zygrhablithus bijugatus</i>	20
2.4.3 <i>Chiasmolithus</i> ratio.....	21
2.5 Paleotemperature index.....	21
2.6 Statistical analysis.....	21
2.7 Geochemical proxy data.....	22

2.8 Age models	22
CHAPTER 3: STUDY LOCATIONS	23
3.1 Introduction.....	23
3.2 Site Description	24
3.2.1 Lord Howe Rise: DSDP Leg 21, Site 207	24
3.2.2 Campbell Plateau: DSDP Leg 29, Site 277	25
3.2.3 Canterbury Basin: mid-Waipara River section	26
3.2.4 Canterbury Basin: Hampden Beach section	28
3.3 Previous work.....	30
3.3.1 Lord Howe Rise	30
3.3.2 Campbell Plateau.....	31
3.3.3 Canterbury Basin	31
CHAPTER 4: BIOSTRATIGRAPHY	34
4.1 Introduction.....	34
4.2 Nannofossil zone definitions	34
4.2.1 <i>Tribrachiatus contortus</i> Zone (NP10)	34
4.2.2 <i>Discoaster binodosus</i> Zone (NP11)	35
4.2.3 <i>Tribrachiatus orthostylus</i> Zone (NP12).....	35
4.2.4 <i>Discoaster lodoensis</i> Zone (NP13)	35
4.2.5 <i>Discoaster sublodoensis</i> Zone (NP14).....	35
4.2.6 <i>Nannotetrina fulgens</i> Zone (NP15).....	36
4.2.7 <i>Discoaster tanii nodifer</i> Zone (NP16)	36
4.3 Biostratigraphic results	37
4.3.1 Mid-Waipara River section	38
4.3.2 Hampden Beach section.....	42
4.3.3 DSDP Site 207	45
4.3.4 DSDP Site 277	49
4.4 Age and correlation.....	53
4.5 Summary	57
CHAPTER 5: PALEOENVIRONMENTAL ANALYSIS	59
5.1 Introduction.....	59
5.2 Preservation and diversity	59

5.2.1 Mid-Waipara River section	59
5.2.2 Hampden Beach section	62
5.2.3 DSDP Site 207	64
5.2.4 DSDP Site 277	66
5.2.5 Summary.....	67
5.3 Paleoecological indicators.....	70
5.3.1 <i>Chiasmolithus</i>	70
5.3.2 <i>Coccolithus formosus</i>	70
5.3.3 <i>Coccolithus pelagicus</i>	71
5.3.4 <i>Discoaster</i>	71
5.3.5 <i>Reticulofenestra daviesii</i>	71
5.3.6 <i>Sphenolithus</i>	72
5.3.7 <i>Toweius</i>	72
5.3.8 <i>Zygrhablithus</i>	72
5.4 Paleotemperature	73
5.4.1 Mid-Waipara River section	73
5.4.2 Hampden Beach Section.....	76
5.4.3 DSDP Site 207	79
5.4.4 DSDP Site 277	81
5.5 <i>Toweius-Reticulofenestra</i> Turnover Event	83
CHAPTER 6: DISCUSSION.....	88
6.1 Applicability of established nannofossil zonations to SW Pacific sections	88
6.2 Nannofossil bioevents in the SW Pacific	90
6.2.1 <i>Blackites</i>	90
6.2.2 <i>Ellipsolithus</i>	90
6.2.3 <i>Girgisia gammation</i>	91
6.2.4 <i>Reticulofenestra umbilicus</i>	91
6.3 Utility of preservation indices	92
6.4 Timing of the EECO in the SW Pacific.....	93
6.5 Comparison with low- and high-latitude assemblages.....	96
6.6 Comparison with geochemical temperature proxies	99
6.7 Biogeographic reconstruction of nannofossil assemblages.....	100

CHAPTER 7: CONCLUSIONS.....	106
7.1 Key findings	106
7.2 Future work.....	108
REFERENCES.....	110
APPENDIX A: SYSTEMATIC PALEONTOLOGY	131
APPENDIX B: PLATES	146
APPENDIX C: DISTRIBUTION CHARTS.....	160
APPENDIX D: AGE-DEPTH MODELS.....	171

LIST OF FIGURES

Figure 1.1: Cenozoic deep-sea temperatures derived from oxygen isotopes of benthic foraminifera	2
Figure 1.2: Schematic diagram showing the inferred surface water circulation in the southwest Pacific during the early Eocene (~50 Ma)	5
Figure 1.3: Correlation of the zonations of Martini (1971), Edwards (1971), Okada & Bukry (1980) and Agnini et al. (2014) calibrated to Gradstein et al. (2012).....	11
Figure 3.1: Location of the study sites during the early Eocene	23
Figure 3.2: Map showing the location of DSDP Sites 206–208, Lord Howe Rise.....	24
Figure 3.3: Map showing the location of DSDP Site 277, Campbell Plateau	25
Figure 3.4: Map showing the location of the mid-Waipara River Section, Canterbury Basin, New Zealand (modified from Morgans et al., 2005)	27
Figure 3.5: Map showing the location of the Hampden Beach Section, Canterbury Basin, New Zealand (modified from Morgans, 2009)	29
Figure 4.1: Map of the mid-Waipara River section showing the location of the sections sampled in 2007 (f898-f889) and 2012 (f937–f1047).....	39
Figure 4.2: Range chart of key nannofossil taxa at mid-Waipara River.....	41
Figure 4.3: Map of the Hampden Beach section showing the location of the samples collected in 1998 (f243-f303).....	43
Figure 4.4: Range chart of key nannofossil taxa at Hampden Beach	44
Figure 4.5: Range chart of key nannofossil taxa at Site 207	48
Figure 4.6: Range chart of key nannofossil taxa at Site 277	51
Figure 4.7: Age-depth plot for DSDP Site 207	54
Figure 4.8: Age-depth plot for DSDP Site 277	55
Figure 4.9: Biostratigraphy of all four study sites	58
Figure 5.1: Comparison of calcium carbonate (CaCO ₃) content, preservation/dissolution indices, taxon richness and Shannon diversity for the mid-Waipara River section	61
Figure 5.2: Comparison of preservation, taxon richness and Shannon diversity for the Hampden Beach section	63

Figure 5.3: Comparison of preservation/dissolution indices, taxon richness and Shannon diversity for DSDP Site 207	65
Figure 5.4: Comparison of preservation/dissolution, taxon richness and Shannon diversity for DSDP Site 277	66
Figure 5.5: Cross-plots showing the association between preservation/dissolution indices and diversity measures	69
Figure 5.6: (A) Relative abundance of selected nannofossil species from the mid-Waipara River section.....	75
Figure 5.7: (A) Relative abundance patterns of selected nannofossil species from the Hampden Beach section	78
Figure 5.8: (A) Relative abundance patterns of selected nannofossil species from DSDP Site 207	80
Figure 5.9: (A) Relative abundance patterns of selected nannofossil species from DSDP Site 277	82
Figure 5.10: Abundance patterns of <i>Reticulofenestra</i> , <i>Toweius</i> and <i>Discoaster</i> at all study sites.....	85
Figure 5.11: Relative abundance of <i>Toweius</i> and <i>Reticulofenestra</i> at each study site	86
Figure 6.1: Relative abundance of cool- and warm-water taxa at each study site, compared to TEX ₈₆ ^H SST data from mid-Waipara River	95
Figure 6.2: Relative abundance of key nannofossil genera at each study site.....	98
Figure 6.3: Relative abundance of <i>Toweius</i> , <i>Reticulofenestra</i> , <i>Zygrhablithus</i> and <i>Discoaster</i> at each study site	99
Figure 6.4: Development of the southwest Pacific Subtropical Front in the early to middle Eocene based on nannofossil warm- and cool-water assemblages.....	103
Figure 6.5: Paleogeographic reconstructions for sites in the southern middle to high latitudes in the early to middle Eocene	105

LIST OF TABLES

Table 1: Preservation evaluation scale based on observations by light microscopy	20
Table 4.1: Summary of key bioevents identified at all study sites.	37
Table 5.1: Correlation coefficients for CaCO ₃ content, diversity measures and preservation/dissolution indices	60

CHAPTER 1: INTRODUCTION

1.1 Overview

Earth's climate underwent a distinct warming trend from the late Paleocene to early Eocene (~58–51 Ma), with global temperature reaching its Cenozoic peak (Figure 1.1) during the Early Eocene Climatic Optimum (EECO; 52–50 Ma) (Zachos et al., 2008; Bijl et al., 2009; Huber & Caballero, 2011). A number of short-lived hyperthermal events have been recognised through the interval prior to the EECO, including the Paleocene-Eocene Thermal Maximum (PETM; ~56 Ma), Eocene Thermal Maximum 2 (ETM2; ~53.5 Ma) and Eocene Thermal Maximum 3 (ETM3; ~52 Ma) (Lourens et al., 2005; Röhl et al., 2005; Sluijs et al., 2007). A long period of cooling followed the EECO, culminating in the development of continental ice sheets on Antarctica by late Eocene to early Oligocene (~34 Ma) (Liu et al., 2009; Bijl et al., 2013). This long transition to cooler climates was also punctuated by transient periods of warming, the most pronounced occurring during the middle Eocene, designated the middle Eocene climatic optimum (MECO; ~40 Ma) (Bohaty et al., 2009; Bijl et al., 2010). Improved understanding of the relationship between these intervals of pronounced climate change and ocean systems can provide valuable insights into the potential impacts of future climate change.

Geochemical temperatures proxies (TEX₈₆, Mg/Ca) have estimated that sea-surface temperatures (SSTs) in the high-latitude southwest (SW) Pacific reached 30°C or more during the EECO (Bijl et al., 2009; Hollis et al., 2009; Creech et al., 2010). However, these warm SST estimations are difficult to reconcile with climate models (Huber & Caballero, 2011; Lunt et al., 2012) and proxies for land temperature (Greenwood et al., 2004; Pancost et al., 2013). Furthermore, the high SSTs imply that either the latitudinal temperature gradient between polar and tropical regions was almost non-existent at this time, or they are a reflection of regional climate and ocean circulation anomalies (Hollis et al., 2012).

One of the ways that this apparent mismatch between geochemical proxies and climate models can be addressed is through the study of marine phytoplankton. The biogeography

and diversity of calcareous nannoplankton have been used to identify latitudinal temperature gradients within the ocean (e.g. McIntyre & Bé, 1967; Okada & Honjo, 1973; Haq et al., 1977b), to elucidate changes in sea-surface temperature and productivity (e.g. Aubry, 1992, 1998; Bralower, 2002; Gibbs et al., 2006; Kalb & Bralower, 2012), and as a tool for reconstructing Paleogene Southern Ocean paleoclimatic and paleoceanographic conditions (e.g. Wei & Wise, 1990a; Bralower, 2002; Persico & Villa, 2004; Villa et al., 2008). The present study examines species turnover and changes in geographic distribution of SW Pacific calcareous nannofossils in the early to middle Eocene in order to determine how they responded to periods of pronounced climate change, particularly during the EECO, and to reconcile the apparent inconsistencies between geochemical proxies and climate models.

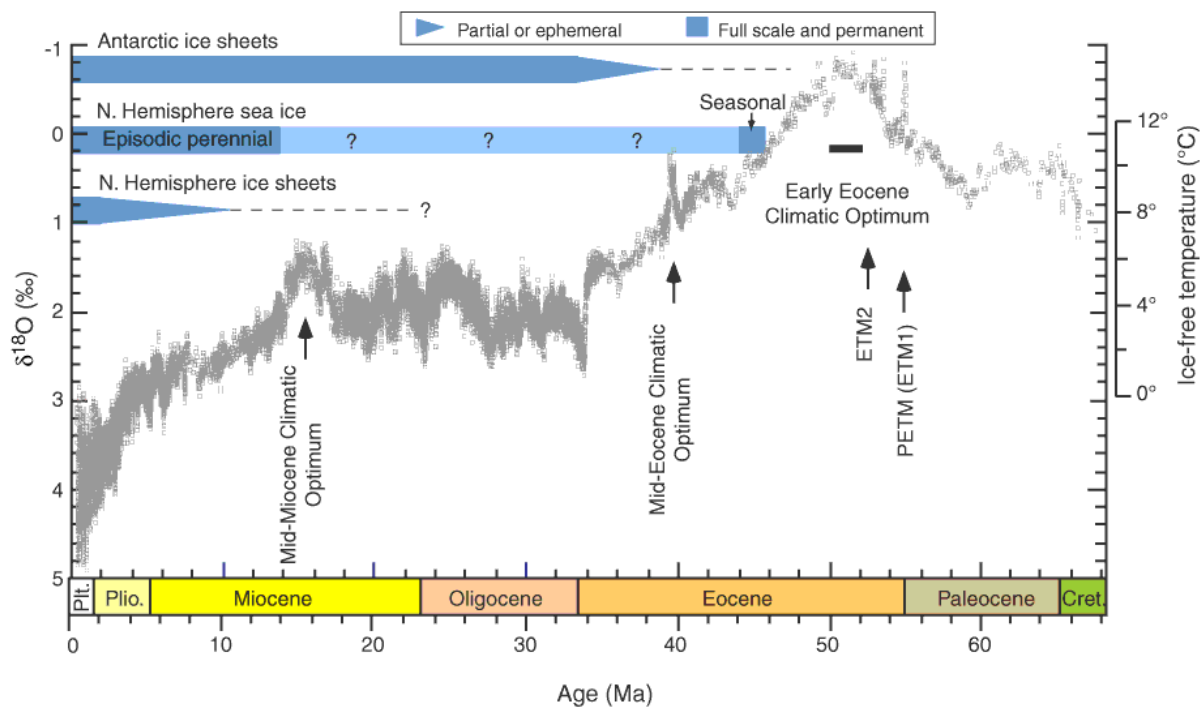


Figure 1.1: Cenozoic deep-sea temperatures derived from oxygen isotopes of benthic foraminifera. Figure modified from Expedition 318 Scientists (2010) (adapted from Zachos et al., 2008) and calibrated to Gradstein et al. (2004). PETM = Paleocene-Eocene Thermal Maximum, ETM1 = Eocene Thermal Maximum 1, ETM2 = Eocene Thermal Maximum 2.

1.2 Eocene climate

A long-term global warming trend initiated in the late Paleocene (~58 Ma), culminated with the EECO (Zachos et al., 2001). A number of transient hyperthermal events were superimposed on this warming trend, the most prominent being the PETM (~56 Ma). This

short-lived event (~220 kyr) is associated with a large negative carbon isotope excursion (CIE) and a global increase in sea-surface temperatures of ~5–8°C (Sluijs et al., 2007, Dunkley-Jones et al., 2013). Temperatures reached a maximum in the Cenozoic with the EECO, a broadly defined event that extends from ~53 to ~50 Ma (Kirtland-Turner et al., 2014), perhaps to ~49 Ma in the SW Pacific (Hollis et al., 2009; Creech et al., 2010; Hollis et al., 2012) and mid-latitude Indian Ocean (Shamrock & Watkins, 2012), and perhaps through the Eocene in the low-latitude Indian Ocean (Pearson et al., 2007).

Following the termination of the EECO, a period of long-term cooling occurred through the middle to late Eocene, culminating in the first major Antarctic glaciation by early Oligocene (Liu et al., 2009; Bijl et al., 2013). The transition to cooler conditions has traditionally been linked to the opening of Southern Ocean gateways (Kennett, 1977; Exon et al., 2004), which led to thermal isolation of Antarctica and subsequent cooling at the Eocene/Oligocene boundary. In contrast, climatic modelling studies suggest that declining atmospheric CO₂ concentrations were the major driving force behind the development of a large ice sheet on Antarctica (DeConto & Pollard, 2003; Huber et al., 2004). This is supported by Inglis et al. (2015) who found that changes in ocean gateways could not explain the majority of high-latitude cooling in the Eocene and instead, these authors suggested that CO₂ drawdown was the primary driver for global surface water cooling during this interval.

Recent studies have focused on understanding the timing of the origin and evolution of the Southern Ocean, particularly regarding the opening of ocean gateways and associated circulation changes. Stickley et al. (2004) indicated that the opening of the Tasmanian Gateway occurred progressively between ~35.2–30.2 Ma, leading to the development of a proto-Leeuwin current that initially delivered warm waters into the SW Pacific Ocean. Furthermore, these authors suggested that deepening of the Tasmanian Gateway occurred at least 1.8 Myr (at ~35.5 Ma) before the Eocene/Oligocene boundary. This is consistent with Lazarus et al. (2008) who concluded that isolation of the Southern Ocean preceded Antarctic glaciation by ~2 Myr. Scher et al. (2015) agreed with the earlier work of Exon et al. (2004), that the Tasmanian Gateway opened at ~33.5 Ma (± 1.5 Ma) with a deep westward flow occurring through the gateway at that time, similar to the present-day Antarctic Slope Current. Additionally, they inferred that the onset of the ACC occurred at ~30 Ma,

coincident with the alignment of the northern margin of the Tasmanian Gateway with the mid-latitude westerly wind belt.

1.3 Eocene proxy reconciliation problem

Several studies have generated SST estimates for the SW Pacific for the Paleogene using geochemical proxies (Burgess et al., 2008; Bijl et al., 2009; Hollis et al., 2009; Creech et al., 2010). However, as mentioned previously, the high SSTs estimated by these studies are difficult to reconcile with climate models and terrestrial temperature estimates (e.g. Greenwood et al., 2004; Huber & Caballero, 2011). Hollis et al. (2012) proposed that geochemical SST proxies for the SW Pacific are affected by a warm bias that may be related to local climate, ocean circulation, or seasonality. One explanation, supported by paleontological evidence from Kennett & Exon (2004), is the southward expansion of a proto-East Australian Current (EAC) during episodes of pronounced warming, concomitant with the contraction of the proto-Ross Gyre (Figure 1.2). Under this scenario, warm subtropical water was brought into the South Tasman Sea and New Zealand region via this current, which combined with the absence of circum-Antarctic circulation, could account for warmer regional SSTs during the early Eocene.

One area of uncertainty in the estimation of SW Pacific SSTs revolves around the use of two calibrations of the TEX_{86} proxy: $\text{TEX}_{86}^{\text{H}}$ and $\text{TEX}_{86}^{\text{L}}$. These calibrations were developed for application across different SST ranges, with $\text{TEX}_{86}^{\text{H}}$ more suitable where SST is $>15^{\circ}\text{C}$, and $\text{TEX}_{86}^{\text{L}}$ where SST is likely to range below 15°C (Kim et al., 2010). Hollis et al. (2012) found that the $\text{TEX}_{86}^{\text{L}}$ calibration was most consistent with other SST proxy results for the southwest Paleogene, providing SSTs that are $5\text{--}9^{\circ}\text{C}$ below previous TEX_{86} estimates. This finding was corroborated by Pancost et al. (2013) who found a good match between mean annual air temperature (MAAT) estimates and $\text{TEX}_{86}^{\text{L}}$ -derived SSTs. However, Bijl et al. (2010) found that $\text{TEX}_{86}^{\text{H}}$ -derived SSTs across the MECO at the same site were consistent with U_{37}^{K} estimates. A recent study by Inglis et al. (2015) suggested that the $\text{TEX}_{86}^{\text{L}}$ calibration should be used with caution because of discrepancies associated with the subsurface export of glycerol dialkyl glycerol tetraethers (GDGTs).

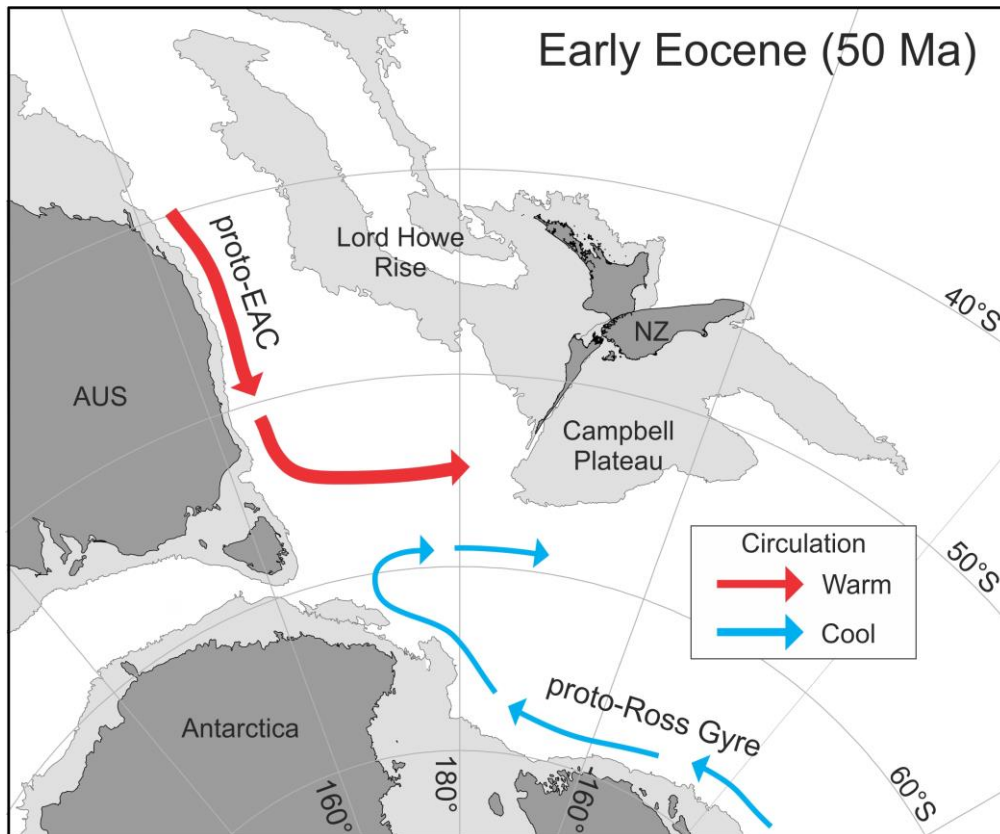


Figure 1.2: Schematic diagram showing the inferred surface water circulation in the southwest Pacific during the early Eocene (~50 Ma). Adapted from Exon et al. (2004) and Nelson & Cooke (2001). Tectonic reconstruction of the southwest Pacific generated in GPlates using the paleomagnetic reference frame of Torsvik et al. (2012). NZ = New Zealand, AUS = Australia, EAC = East Australian Current.

1.4 Geochemical temperature proxies

As discussed in previous sections, a wide range of geochemical proxies are used in paleoclimate studies (e.g. oxygen and carbon isotopes, TEX_{86} , Mg/Ca , $U^{K'}_{37}$, methylation of branched tetraethers/cyclization of branched tetraethers, and leaf-margin analysis). This section provides additional background information for proxies that will form part of the analysis and discussion in subsequent chapters. Additional proxies that involve the use of calcareous nannofossils are discussed in section 1.5.3.

1.4.1 Oxygen isotopes

The early foundations for this proxy were laid by Urey (1947), who investigated the thermodynamic properties and fractionation of isotopes. Subsequent work by Urey and his graduate students (Urey et al., 1951; Epstein et al., 1953) established the use of oxygen isotope composition in calcium carbonate as a thermometer, which is based on the premise

that variation in the abundance of ^{18}O isotope in calcium carbonate is related to changes in the temperature of the water in which the carbonate was deposited (Urey et al., 1951). The first use of oxygen isotope paleothermometry was undertaken by Emiliani (1955), who used the oxygen isotope ratio ($\delta^{18}\text{O}$) of calcite in foraminiferal tests to reconstruct temperature oscillations during the Pleistocene.

Following this early work, deep-sea $\delta^{18}\text{O}$ records derived from benthic foraminifera have been used to develop the general trends in climate change through the Cenozoic (e.g. Zachos et al., 1993, 1994, 2001, 2008). The deep-sea oxygen isotope compilation also provides a record of high-latitude SST, given that deep ocean water formation is a result of the cooling and sinking of water in the polar regions (Zachos et al., 2001).

The reconstruction of temperatures using $\delta^{18}\text{O}$ of foraminifera requires a number of assumptions. Firstly, it assumes knowledge of the $\delta^{18}\text{O}$ of the seawater in which the organism grew. This composition can be affected by changes in global ice volume and the local precipitation/evaporation (P/E) balance (Huber, 2008; Pearson, 2012). A second assumption is the depth habitat of foraminifera. In addition to occupying a range of depths within the water column, planktonic foraminifera also descend to a particular depth when they reach maturity. In order to reconstruct SSTs, it is therefore essential to select a species that remains within the mixed layer for its entire life cycle (Pearson, 2012).

A further complication associated with the $\delta^{18}\text{O}$ proxy is the effect of diagenetic alteration of planktonic foraminiferal calcite, which has been linked to under-estimates of temperature. Sexton et al. (2006) investigated the difference in $\delta^{18}\text{O}$ values for specimens displaying two different states of preservation: frosty (typical pelagic setting) vs glassy (hemipelagic clay-rich settings). Frosty foraminiferal tests were found to have much greater diagenetic alteration and consistently produced higher $\delta^{18}\text{O}$ values than those with a glassy taphonomy.

1.4.2 Mg/Ca paleothermometry

Mg/Ca paleothermometry is based on the ratio of magnesium (Mg) to calcium (Ca) incorporated in planktonic and benthic foraminiferal tests. During the formation of biogenic

calcium carbonate, Mg is one of several divalent cations that can substitute for Ca (Nürnberg et al., 1996). Early studies suggested an association between Mg/Ca ratios and water temperature during calcification (e.g. Chave, 1954; Duckworth, 1977). However, Delaney et al. (1985) found no evidence to support this correlation and instead suggested that differences in Mg/Ca ratios were linked to some other environmental factor. A later study of core-top samples provided evidence of a covariance between magnesium concentration and water temperature (Nürnberg, 1995), and this was further substantiated by culture studies demonstrating that growth temperature was the main control on Mg incorporation in foraminiferal tests (Nürnberg et al., 1996; Lea et al., 1999). Earlier discrepancies were attributed to partial dissolution of foraminiferal calcite following deposition on the seafloor (Rosenthal et al., 2000). Advances in analytical techniques such as laser ablation inductively coupled plasma mass spectrometry (LA-ICP-MS) has helped to reduce the errors associated with the surficial and internal contamination of foraminiferal calcite. This method enables the detection of contaminated zones using a trace element depth profile through the test wall, and these areas can then be excluded from the analysis (Creech et al., 2010).

One of the major advantages of the Mg/Ca paleothermometer is that both Mg/Ca and $\delta^{18}\text{O}$ can be measured from the same medium, thereby reducing the effects of other factors (e.g. seasonality, habitat) that occur when proxy data from different faunal groups are used (Regenberg et al., 2006). Additionally, temperature estimates based on Mg/Ca ratios are species specific, which means that it is possible to determine the temperature in different parts of the water column based on the environmental preferences of the species being used (Barker et al., 2005).

1.4.3 TEX₈₆

TEX₈₆ is a paleothermometer based on GDGTs, a component of the membrane lipids produced by members of the domain Archaea. It was previously believed that Archaea consisted of organisms that only inhabited extreme conditions, generally falling into several major groupings: extreme halophiles, methanogens, (hyper)thermophiles and thermoacidophiles (Woese et al., 1990). However, it was later found that Archaea are also present in a variety of non-extreme environments including soils, ocean and freshwater

sediments (DeLong, 1992; Fuhrman et al., 1992; Jurgens et al., 1997; MacGregor et al., 1997; Schouten et al., 2000).

Different types of GDGTs containing 0–4 cyclopentane moieties are biosynthesized by marine Thaumarchaeota (Sinninghe Damsté et al., 2002) and the relative distribution of the GDGTs has been demonstrated to be strongly dependent upon growth temperatures, i.e. an increase in temperature results in an increase in cyclopentane moieties (De Rosa & Gambacorta, 1988; Uda et al., 2001). Given this relationship between temperature and lipid membrane composition, Schouten et al. (2002) introduced the TEX₈₆ (tetraether index of tetraethers consisting of 86 carbons) temperature proxy based on the relative abundance of isoprenoid GDGTs. This study showed that the TEX₈₆ index had a significant linear correlation with annual mean SST and could be used to estimate past temperatures. As discussed previously, several calibrations of the TEX₈₆ proxy have since been proposed (e.g. Kim et al., 2010). Recent work by Tierney & Tingley (2014, 2015) applied a Bayesian regression approach (BAYSPAR) to the TEX₈₆ SST calibration, which generates absolute temperature values similar to TEX₈₆^H but provides a more robust analysis of uncertainty.

1.5 Calcareous nannofossils

1.5.1 Introduction

Calcareous nannofossil is the collective term used to describe all calcareous fossils that are less than 30 microns (µm) in size. Although this includes a variety of organisms, the dominant group are the calcareous remains of coccolithophores, a type of unicellular marine algae belonging to the division Haptophyta (Bown & Young, 1998a). The test of a coccolithophore, known as the coccosphere, is typically composed of individual calcite plates (coccoliths) that are secreted by the cell. This ability to produce a calcareous exoskeleton differentiates coccolithophores from other phytoplankton and non-calcifying members of Haptophyta (Brand, 1994; Haq, 1998). Following the death of a coccolithophore, the exoskeleton is transported through the water column and often becomes fossilised in sea-floor sediments as disaggregated coccoliths, or less commonly as a complete coccosphere (Bown & Young, 1998a).

Coccoliths are divided into two main groups based on their morphology: heterococcoliths are composed of calcite units that vary in shape and size, and holococcoliths are formed of minute (less than 0.1 μm) crystal elements that are virtually identical (Siesser & Winter, 1994). Nannoliths are a third group of calcareous nannofossil that do not exhibit the typical characteristics of hetero- or holococcoliths but some are known to be produced by haptophytes (e.g. ceratoliths) (Alcober & Jordan, 1997; Sprengel & Young, 2000). Young et al. (1999) proposed four possible modes of origin for nannoliths: modified heterococcoliths, modified holococcoliths, structures formed by haptophytes through different biomineralisation processes, or structures formed by unrelated organisms. Although the biological affinity of some nannoliths remains ambiguous, certain taxa within this group provide important biostratigraphic markers (e.g. Discoasteraceae, Fasciculithaceae, and Sphenolithaceae).

In the past, holo- and heterococcoliths were thought to be so morphologically distinct from each other that they were described and named as separate species. However, Parke & Adams (1960) demonstrated in a culture study that the two different morphologies represent coccolith formation during different phases of the haptophyte life cycle. Additionally, recent studies have shown that holo- and heterococcoliths are formed during alternate phases of a haplo-diploid life cycle (Houdan et al., 2004; Noël et al., 2004), with holococcoliths formed during the haploid phase and heterococcoliths formed during the diploid phase (Young & Henriksen, 2003). Heteromorphic life cycles have also been inferred through the observation of combination coccospheres, which bear both hetero- and holococcoliths (e.g. Cortés & Bollman, 2002; Geisen et al., 2002; Couapel et al., 2009).

1.5.2 Biostratigraphic utility of calcareous nannofossils

The biostratigraphic usefulness of calcareous nannofossils was first recognised by Bramlette & Riedel (1954), who found distinctive forms of microfossils on both sides of the Pacific and Atlantic oceans that were characteristic of particular time horizons within the Cenozoic. From this observation, the authors suggested that these microfossils, particularly discoasters, had the potential to be used in the global correlation of certain horizons. Further studies by Bramlette and his colleagues (Bramlette, 1957; Bramlette & Sullivan,

1961; Bramlette & Martini, 1964) expanded on this concept, promoting the idea that calcareous nannofossils could be used as an effective biostratigraphic tool.

Following the early work of Bramlette and others, biostratigraphic zonation schemes were developed for parts of the Cenozoic (Bramlette & Wilcoxon, 1967; Hay et al., 1967), although these were based either on samples taken from a limited area (i.e. one location) or from correlation between locations that were geographically distant from each other. The initiation of the Deep Sea Drilling Project (DSDP) in 1968 opened the door for nannofossil zonations to become more refined (Siesser, 1994). New zones for the late Miocene to Recent were proposed by Gartner (1969) based on DSDP cores from the Pacific and Atlantic oceans. Martini & Worsley (1970) and Martini (1970) published the first zonations for the Neogene and Paleogene, respectively, using the first or last occurrences of a particular species to define zone boundaries. A total of 46 zones (21 Neogene; 25 Paleogene) were described and each zone was assigned an alpha-numerical code (NN = Neogene nanoplankton zone; NP = Paleogene nanoplankton zone). Around the same time, Bukry & Bramlette (1970) proposed a zonation for the Late Cretaceous to Late Pleistocene based on cores recovered from DSDP sites in the equatorial and south Atlantic Ocean. In addition to using species first or last occurrences, they also utilised characteristics of the assemblage to define their zones.

Martini (1971) published a slightly revised nanoplankton zonation for the Cenozoic, which included range charts of important species and correlations with foraminiferal, radiolarian and dinoflagellate zones. Martini (1971) based his zonation mainly on land sections located in Europe, California and the Caribbean. Bukry (1973c, 1975) published an alternative Cenozoic zonation, which was based primarily on samples collected from low to middle latitude DSDP sites. This was later modified by Okada & Bukry (1980) to refine zones within the Danian and assign alpha-numerical codes (CP = Coccoliths Paleogene zones; CN = Coccoliths Neogene zones) to the scheme.

Although the zonations of Martini (1971) and Bukry (1973c, 1975; Okada & Bukry, 1980) are still used widely, subsequent zonations have been proposed that try to resolve issues arising from these earlier schemes (e.g. unreliable or rare bioevents). Backman et al. (2012) and

Agnini et al. (2014) published new low–middle latitude zonations for the Miocene–Pleistocene and the Paleogene respectively. These new zonations are a combination of reliable bioevents from previous schemes and new datums to replace unreliable to problematic bioevents. The new zonations also include additional bioevents that help to further subdivide some of the zones in the original schemes (Figure 1.3).

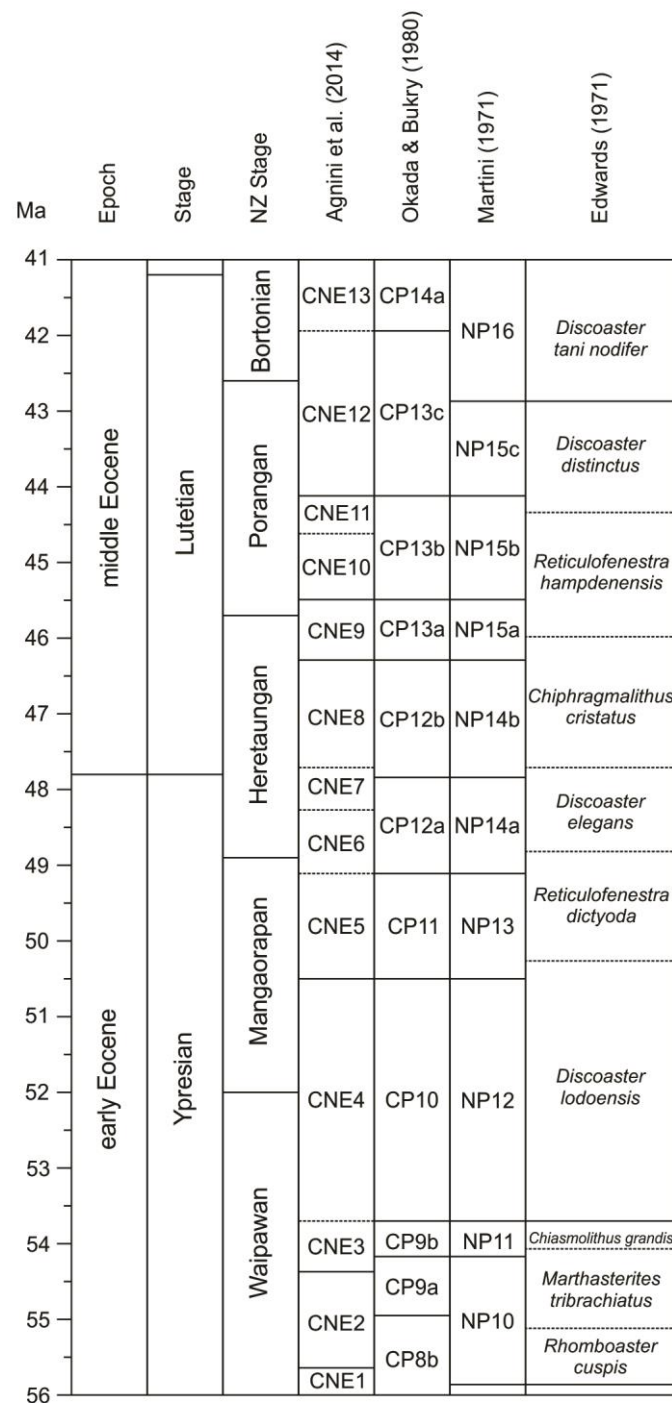


Figure 1.3: Correlation of the zonations of Martini (1971), Edwards (1971), Okada & Bukry (1980) and Agnini et al. (2014) calibrated to Gradstein et al. (2012). New Zealand Stages are based on Raine et al. (2015).

Another problem with the older zonations is their application at high latitudes, particularly in the Southern Ocean, where warm- and temperate-water taxa are often rare or absent (Fiorini et al., 2012). Edwards & Perch-Nielsen (1975) examined sites in the SW Pacific and found that diversity was generally low, especially during the middle Oligocene to early Pliocene, and as a result the biostratigraphic resolution was poorer than low latitude areas. Mid-latitude zonation schemes were first published by Edwards (1971) for the New Zealand Paleogene (Figure 1.3), and Wise (1983) for the Cenozoic of the Falkland Plateau region. Wei and Wise (1990b) established a detailed Eocene–Oligocene zonation scheme for the Southern Ocean and this was later modified by Wei & Thierstein (1991) to include an additional Oligocene zone. Fiorini et al. (2012) published a revised middle Eocene–late Oligocene zonation for the Southern Ocean, which replaces the zones and subzones of Wei & Wise (1990b) and Wei and Thierstein (1991).

1.5.3 Paleoenvironmental utility of calcareous nannofossils

Extant coccolithophores are planktonic, marine organisms that are distributed widely within the oceanic realm. They demonstrate a wide range of ecological tolerances, occurring in the pelagic environment of the open ocean to near-shore and inshore, lagoonal settings (Haq, 1998), and hypersaline environments (Legge et al., 2006, 2008). Coastal or neritic coccolithophores have haploid stages that are often noncalcifying and when they do produce coccoliths they are frequently small or poorly calcified, meaning that they are rarely preserved in the fossil record (de Vargas et al., 2007). As photosynthesising organisms, coccolithophores live within the photic zone (upper 150–200 m) of the ocean, with their highest abundance found at depths of 50 m in the tropics and 10–20 m in temperate regions (Siesser, 1993). Given their presence in the photic zone, and species-dependent requirements for salinity, nutrients and temperature, nannofossil assemblages have the potential to provide a good record of sea-surface conditions that prevailed during the organism's lifespan.

One of the key considerations when using nannofossils in paleoenvironmental reconstructions is the degree to which the fossil assemblages found in seafloor sediments reflect the living assemblages of the overlying surface waters. Honjo (1976) demonstrated that individual coccoliths of *Emiliania huxleyi* settle very slowly through the water column at

rates ranging from less than 1 $\mu\text{m}/\text{second}$ to 1.6 $\mu\text{m}/\text{second}$. This equates to anywhere between 50–150 years for an individual coccolith to reach the seafloor at a depth of 5000 m (Siesser, 1993). Under this scenario, ocean currents could transport coccoliths vast distances from their original water mass, where eventually they would settle on the seafloor and have no relationship to assemblages living in overlying surface waters. However, it has been established that most coccoliths are transported to the seafloor largely via the rapid settling of faecal pellets within marine snow (Roth et al., 1975; Honjo, 1976; Pilska & Honjo, 1987; Alldredge & Silver, 1988). Studies measuring the sinking rates of these larger aggregates show that the rate of descent of faecal pellets is on average around 200 m/day, almost twice as fast as the sinking rate of marine snow (Steinmetz, 1994). Coccoliths transported to the seafloor as components of these larger aggregates are therefore not carried as far laterally by ocean currents and are likely to be displaced by no more than 130–175 km (Honjo, 1976; Steinmetz, 1994).

The biogeographic distribution of modern nanoplankton was first investigated by McIntyre & Bé (1967) using plankton and surface sediment samples from the Atlantic Ocean. They were able to divide coccolithophore assemblages into five major latitudinal zones based on temperature: tropical, subtropical, transitional, subarctic and subantarctic. Additionally, they showed that species diversity was greater in the tropical and subtropical zones than in the subarctic and subantarctic zones. A subsequent study by Okado & Honjo (1973) analysed nanoplankton assemblages along transects in the north and central Pacific Ocean. Similar to the Atlantic study, they were able to identify six latitudinal zones based on the distribution of characteristic species and they also observed a decline in diversity from low to high latitudes. These early studies laid the groundwork for the use of paleobiogeographic data to reconstruct past ocean sea-surface temperatures (e.g. CLIMAP Project Members, 1976; Haq et al., 1977b; Haq, 1980).

The paleoecology and biogeography of calcareous nanofossils have been used as a tool for reconstructing Southern Ocean paleoclimatic and paleoceanographic conditions during the Paleogene. Several studies (Wei & Wise, 1990a; Bralower, 2002; Persico & Villa, 2004; Villa et al., 2008; Schneider et al., 2011) have used statistical analyses of assemblage data (e.g. principal component analysis, cluster analysis, correlation coefficients, non-metric

multidimensional scaling, etc.) to elucidate patterns and relationships among taxa. These observations have then been used to make interpretations about paleoceanographic and paleoclimatic changes. However, it is often difficult with these types of analysis to separate the individual effects of ocean stratification, seasonality, temperature and nutrient availability as commonly these factors are closely intertwined.

In addition to the analysis of assemblage or species-specific data, various geochemical techniques have been applied to nannofossils for the reconstruction of paleotemperature. As previously discussed, the stable isotope analysis of foraminifera has become well established as a paleotemperature and paleoceanographic tool. Application of this technique to calcareous nannofossils was first investigated by Anderson & Cole (1975) and Margolis et al. (1975), who demonstrated that the oxygen isotopic composition of nannofossils could also be used in paleotemperature studies. Later culture studies by Dudley et al. (1980) demonstrated that coccoliths exhibit a vital effect in the fractionation of the oxygen isotope. However, these authors reasoned that this did not exclude the use of calcareous nannofossils in paleotemperature analysis, providing that the degree to which the effect operates over a given temperature range is known. This early work has led to more recent studies that have improved the understanding of these vital effects (Dudley et al., 1986; Ziveri et al., 2003; Bolton et al., 2012; Candelier et al., 2013; Hermoso et al., 2015).

Another geochemical proxy derived from coccolithophores is the alkenone SST proxy (U_{37}^K) that is based on unsaturated, long-chain C_{37} – C_{39} methyl and ethyl ketones produced by certain phytoplankton, including some species of coccolithophores. Volkman et al. (1980) identified these compounds in marine sediments of Recent to Miocene age and also in the coccolithophore *Emiliana huxleyi*. They proposed that this organism and perhaps other coccolithophores could be the major contributor of these compounds to the sedimentary record. Later studies by Brassell et al. (1986a, 1986b), introduced the U_{37}^K index as a measure of the relative degree of unsaturation of alkenones. These workers demonstrated a correlation between the U_{37}^K index and the $\delta^{18}O$ record of planktonic foraminifera, establishing its value as a SST proxy. The U_{37}^K index has subsequently been used widely in sediments dated back to the middle to late Eocene (Bijl et al., 2009, 2010; Liu et al., 2009).

More recently Brassell (2014) proposed an evolutionary adaptation to alkenone biosynthesis that was likely driven by a global cooling following the EECO. The occurrence of alkatrienones, specifically C37:3, has been recognised in sediments of middle Eocene age and younger, but is absent in older alkenone-containing sediments (lower Aptian–lower Eocene). The appearance of alkatrienones directly after the EECO coincides with the expansion of *Reticulofenestra* during the middle Eocene, suggesting that the evolutionary adaptation of alkenones provided a competitive advantage for this group to thrive in conditions that were cooler and nutrient limited.

1.6 Aims and structure of this thesis

Geochemical proxies indicate tropical or warm subtropical conditions in middle and high latitudes in the early Eocene, implying a very low latitudinal temperature gradient. **The aim of this study is to investigate whether calcareous nannofossil assemblages in the SW Pacific provide evidence of these conditions at middle latitudes in the early to middle Eocene, particularly during the EECO.** This will be achieved by examining assemblages from four sites along a latitudinal transect in the SW Pacific spanning paleolatitudes ~46–54°S documenting the biogeographical range of temperature-dependent nannofossil species to determine if their range expanded or contracted in response to the warming and cooling of the Earth's oceans.

One of the main concerns with using nannofossil assemblages in paleoclimatic or paleoenvironmental reconstructions is the degree to which the original assemblage has been influenced/removed by dissolution. Typically, preservation is estimated based on the visual observation of specimens under light microscope, however this method can be rather subjective. This project will explore the use of different preservation indices to determine if there are additional means of quantifying changes in preservation.

Although this thesis constitutes a body of research that can stand alone, it also forms part of a larger Marsden Fund project that aims to interpret SW Pacific paleoclimate and paleoceanography during the Eocene. The early work of Haq et al. (1977b) demonstrated that the combined data from different microfossil groups (nannofossils and foraminifera)

could be used to interpret early Cenozoic biogeographic patterns in the Atlantic Ocean, which in turn could be used to reconstruct the paleoclimatic history of the region. This approach underpins the aims behind the Marsden Fund project, which utilises a multidisciplinary approach incorporating the use of geochemical proxies, climate modelling, and paleontological analysis of microfossil assemblages (calcareous nannofossils, foraminifera and radiolaria). Therefore, another primary aim of this thesis project is to contribute to a synthesis paper that reconciles proxies, models and paleobiogeography for the SW Pacific.

Chapter one provides an introduction to the main components of the thesis: Eocene paleoclimate and calcareous nannofossils. It focuses on the various approaches taken to reconstruct climate through this interval of geological time and serves to highlight areas of conflict arising from current or past methodologies and interpretations. Additionally, it presents an overview of calcareous nannofossils and considers their usefulness as biostratigraphic and paleoclimatic tools. Chapter two outlines the methods used for nannofossil preparation, identification and data collection. It discusses the issue of nannofossil dissolution and outlines the various approaches taken to quantify this factor. Chapter three introduces the study sites, providing information on setting and previous work at each site. Chapters four and five present the biostratigraphic and paleoenvironmental results, respectively. Chapter six provides an integrated discussion of the results to provide a comprehensive review of nannofossil paleobiogeography and paleoclimate in the SW Pacific. Additionally, it compares these results to those from low latitude sites and discusses the paleogeographic distribution of calcareous nannofossils and paleoclimatic implications for the early to middle Eocene. Chapter seven summarises the main conclusions of this study.

Publications resulting from this body of work include a paper describing the biostratigraphy and taxonomy of nannofossils from the mid-Waipara River section (Shepherd & Kulhanek, 2016), and co-authorship on a paper providing a new integrated magneto-biostratigraphic chronology for the mid-Waipara River section (Dallanave et al., 2016). Future publications resulting from this thesis will include a synthesis paper documenting nannofossil assemblages in the SW Pacific and their paleoclimatic and paleoenvironmental significance;

a collaborative paper that integrates microfossil groups (nannofossils, foraminifera and dinocysts) and provides a paleoenvironmental analysis of the mid-Waipara River section for the early Eocene; and contribution towards a synthesis paper that addresses the wider questions of the Marsden Fund project, primarily the reconciliation of proxies, models and paleobiogeography in the SW Pacific. Additional work has involved collaboration with colleagues at the U.S. Geological Survey to describe two new morphotypes of *Tribrachiatus* identified in material from the mid-Waipara River section and two New Jersey cores (Self-Trail et al., in review).

CHAPTER 2: METHODOLOGY

2.1 Slide preparation

A total of 111 samples were analysed from two terrestrial outcrop sites in the Canterbury Basin and two DSDP sites (see details Chapter 4). Calcareous nannofossil smear slides were made directly from unprocessed samples using standard techniques (Bown & Young, 1998b). The outer surface of the sample was cleaned with a razor blade to prevent any outside contamination. A small amount of clean sediment was scraped onto a cover slip and mixed with a drop of distilled water. This was then distributed evenly across the surface of the coverslip with a toothpick and placed on a hot plate to dry. The coverslip was then affixed to a glass microscope slide using Norland Optical Adhesive 61 and placed under ultraviolet light to cure. In some cases, samples contained a large amount of coarse material and strewn slides were prepared. This involved mixing a small amount of sediment with distilled water in a beaker, allowing the coarse particles to settle, and then pipetting the fine-grained suspension onto a cover slip until it was fully covered. Once dry, the coverslip was affixed to a microscope slide using the same method described previously. Slides were analysed using an Olympus BX53 microscope at 1000x magnification in plane-transmitted light (PL), cross-polarised light (XPL) and phase-contrast (PC) light.

2.2 Assemblage counts

A semi-quantitative approach was taken for data collection, counting 450 specimens along random traverses of each slide, followed by a further 30 minutes of scanning to identify rare species not recorded in the initial count. Counts of 456 specimens provide abundance estimates that are within 5% of the actual proportion at the 95% confidence level (Chang, 1967).

2.3 Taxonomy

Specimens were identified to species level following the taxonomic concepts of Perch-Nielsen (1985), Bown (1998, 2005), Dunkley Jones et al. (2009) and Shamrock & Watkins (2012). Results are correlated to the biostratigraphic zonation scheme of Martini (1971),

with subzones as defined by Aubry (1991) and absolute ages for events from Gradstein et al. (2012). Comparison with the biozonation scheme of Agnini et al. (2014) is included where relevant. All taxa discussed in this thesis are listed in the systematic paleontology (Appendix A) and full synonymies are available in the publications mentioned previously in this section.

2.4 Preservation/dissolution indices

Calcareous nannofossils are susceptible to the diagenetic processes of dissolution and overgrowth. Dissolution can affect the composition of an assemblage by preferentially removing some species and leaving the more resistant forms behind. Additionally, calcite that is released through dissolution is reprecipitated onto some taxa, such as discoasters, obscuring ornamentation and causing considerable difficulty with identification (Siesser, 1993).

Although the effect of dissolution can be obvious when observing nannofossils by light microscope, it is often difficult to estimate the degree of overall dissolution. Attempts have been made by some workers to express the degree of overgrowth or etching by categorising the various stages of preservation (e.g. Roth & Thierstein, 1972; Bukry, 1973b; Roth, 1973). However, Gibbs et al. (2004) cautioned against the use of visual observation alone when estimating the overall preservation state of assemblages. These authors demonstrated that assemblages that appear to be well preserved based on visual observation can in fact be significantly affected by dissolution.

Although some workers have used more complex methods to quantify the degree of dissolution (e.g. Gibbs et al, 2004), this study aims to find a relatively simple index that can be calculated based on data collected during the census count and can be used to compliment the visual observation of preservation. Correlation between the different preservation indices and visual observation of preservation are used to determine the degree of covariance.

2.4.1 Qualitative evaluation based on visual observation

The following scale has been developed to assign a qualitative value to the degree of preservation observed in an assemblage using light microscopy. In addition to the three main categories defined below (Table 1), assemblages can be assigned a value that falls somewhere in between i.e. Very Good, Moderate-Good, Poor-Moderate or Very Poor.

Table 1: Preservation evaluation scale based on observations by light microscopy (adapted from Roth, 1973).

Category	Description
Good:	Very little evidence of dissolution or overgrowth; specimens identifiable to the species level.
Moderate:	Some dissolution observed with coccoliths showing irregular outlines. Central crosses and grills are usually preserved, and solution-susceptible species are still present (e.g. <i>Pontosphaera</i>). Overgrowth is noticeable on discoasters as a thickening of the arms. Most specimens identifiable to the species level.
Poor:	Moderate to strong dissolution, central crosses and grills are often destroyed. Some isolated placolith shields are present, and non-resistant genera are less common. Overgrowth on discoasters is strongly noticeable with thickening of the arms and ornamentation becoming obscured. Most specimens cannot be identified at the species and/or generic level.

2.4.2 Relative abundance of *Zygrhablithus bijugatus*

Modern holococcoliths are sensitive to dissolution due to their delicate crystal structure and the lack of imbrication commonly observed in heterococcoliths. Although *Zygrhablithus bijugatus* is not quite as fragile as its modern day counterparts, it has the uniform, minute crystal structure that is typical of all holococcoliths and can therefore be utilised as an indicator of dissolution (Jiang & Wise, 2009). A similar approach to that used by Pea (2011) is adopted in this study, where high relative abundance is interpreted as little dissolution and lower relative abundance is inferred to indicate greater dissolution. It should be noted that in some cases *Z. bijugatus* can become overgrown during early diagenesis, resulting in very dissolution-resistant forms that often persist in samples that have been heavily dissolved (Gibbs et al., 2012). It is also recognised that the relative abundance of *Z. bijugatus* can be affected by paleoenvironmental conditions, such as temperature and nutrient supply. This factor is taken into consideration when comparing results from the different preservation indices.

2.4.3 *Chiasmolithus* ratio

Chiasmoliths are placolith coccoliths that exhibit *Coccolithus*-type shields and tube. The central area is spanned by diagonally crossed bars and it is this feature that enables identification at species level. The central crosses of chiasmoliths are often missing in assemblages that show evidence of dissolution and a rough estimate of the degree of dissolution can be calculated by using a ratio of *Chiasmolithus* that lack a central cross and cannot be differentiated (*Chiasmolithus* spp. indet.) to the total of all *Chiasmolithus* (*Chiasmolithus* spp. including differentiated species), as expressed in Equation 2.1 (Pea, 2011).

$$\text{Equation 2.1: } [\textit{Chiasmolithus} \text{ spp. indet.}/\text{total } \textit{Chiasmolithus}] \times 100$$

2.5 Paleotemperature index

Use of the ratio of *Discoaster* to *Chiasmolithus* (D/C ratio) as a paleotemperature index was based on the observation that *Discoaster* is most abundant at warm-water low latitudes, and *Chiasmolithus* is most abundant at cool-water high latitudes (Bukry, 1973a, 1974). Bukry (1974) hypothesised that an equal proportion of these two genera could therefore be inferred to represent temperate conditions. The use of this ratio has been questioned by some workers (Haq et al., 1977a; Perch-Nielsen, 1977) due to the uncertainty surrounding the exact relationship between water temperature and the D/C ratio.

$$\text{Equation 2.2: } \text{D/C ratio} = \text{total discoasters}/\text{total chiasmoliths}$$

The D/C ratio is calculated for each study site and compared against other proxy data ($\delta^{18}\text{O}$ and $\text{TEX}_{86}^{\text{H}}$) to determine its reliability as a paleotemperature index.

2.6 Statistical analysis

Statistical analysis of census data was performed using the free software package PAST (Paleontological Statistics) (Hammer et al., 2001). Nannofossil diversity at each site was quantified using taxon richness (S) and the Shannon diversity index (H). Taxon richness is a simple measure of diversity, equal to the number of species in a community. In this current

study a counting group approach is used, were named species and undifferentiated genera are given equal weighting. Additionally, a standard count size of 450 specimens was adopted and as such, S does not need to be normalised. The Shannon index accounts for both the evenness and the richness of a community, and is more sensitive to the abundance of rare species than are other indices, e.g. Fisher Alpha, Simpson Index (Krebs, 1999; Colwell, 2012).

2.7 Geochemical proxy data

TEX₈₆ analysis for the mid-Waipara River and Hampden Beach sections was conducted by the University of Bristol (Inglis et al., 2015). Oxygen isotope ($\delta^{18}\text{O}$) measurements for Sites 277 and 207 were conducted in the stable isotope laboratory at the University of California, Santa Cruz following the methodology outlined in Hollis et al. (2015).

2.8 Age models

Age models have been developed for DSDP Sites 207 and 277 using the nannofossil data collected in this project and these are discussed in more detail in Section 4.4. The age model used for the mid-Waipara section is from Dallanave et al. (2016) and is a robust model based on magneto-biostratigraphy. Additionally, nannofossil biostratigraphy from this current study was used in the development of the Dallanave et al. (2016) age model. The Hampden Beach age model is from Inglis et al. (2015) and is based primarily upon foraminifera biostratigraphy. Due to the patchy nature of the nannofossil record at Hampden Beach, no attempt has been made to refine this age model with data collected in this study.

CHAPTER 3: STUDY LOCATIONS

3.1 Introduction

Four key sites in the southwest (SW) Pacific were studied in order to analyse the turnover and geographic distribution of calcareous nannofossils from the early to middle Eocene. These sites span paleolatitudes 46°S to 54°S (Figure 3.1), with Deep Sea Drilling Project (DSDP) Site 277 in the south, DSDP Site 207 in the north, and two sites in between (mid-Waipara River and Hampden Beach sections).

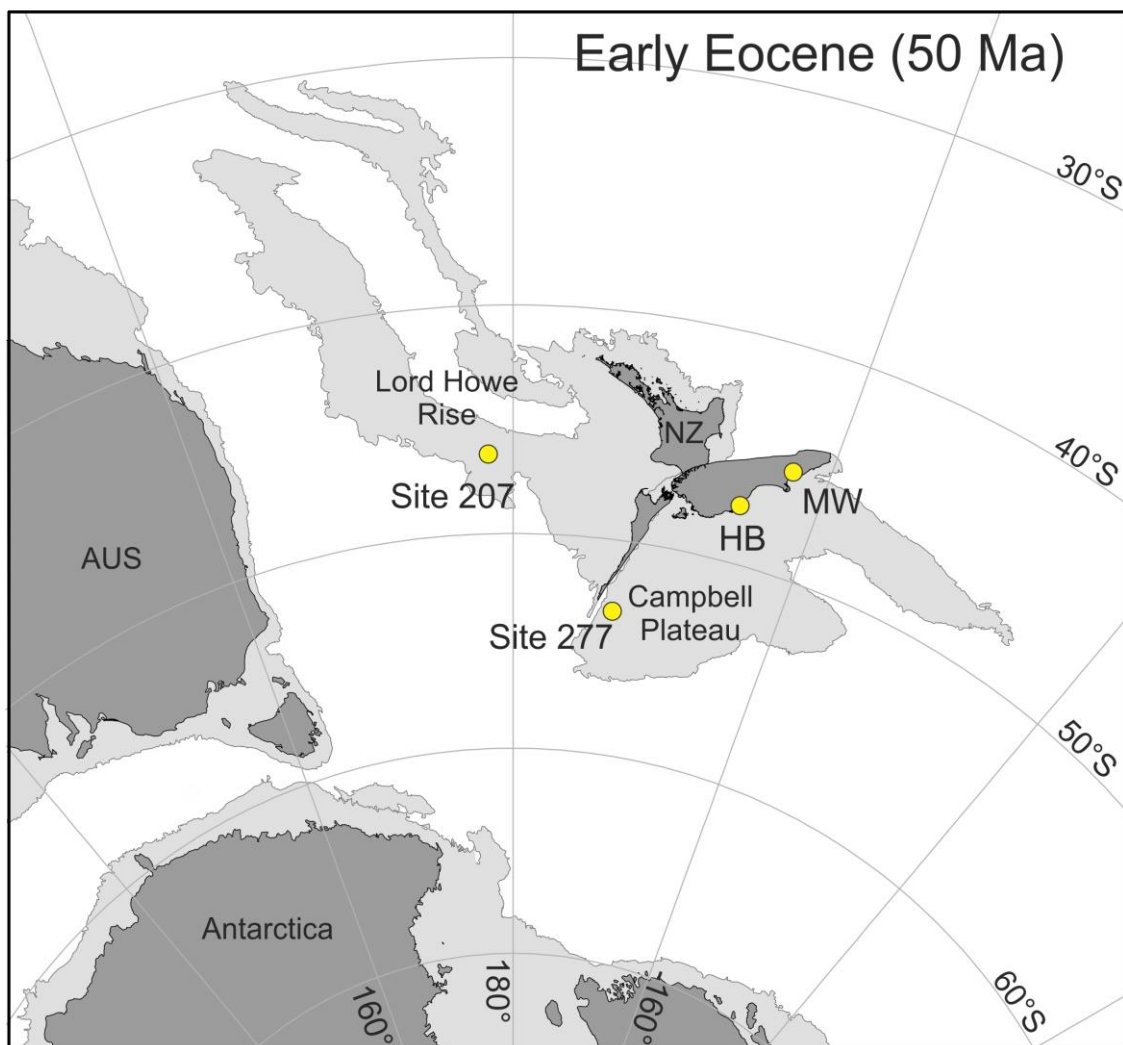


Figure 3.1: Location of the study sites during the early Eocene. Tectonic reconstruction of the southwest Pacific generated in GPlates using the paleomagnetic reference frame of Torsvik et al. (2012). MW = mid-Waipara River, HB = Hampden Beach, NZ = New Zealand, AUS = Australia.

3.2 Site Description

3.2.1 Lord Howe Rise: DSDP Leg 21, Site 207

DSDP Site 207 is located on the southern Lord Howe Rise at a water depth of 1389 m in the northwestern section of the Tasman Sea, northwest of the Bellona Gap and adjacent to the deep-sea Tasman Basin ($36^{\circ} 57.75'S$; $165^{\circ} 26.06'E$) (Figure 3.2). This site was located at a paleolatitude of $\sim 46^{\circ}S$ during the early Eocene (Figure 3.1) Site 207 was drilled in 1973 during DSDP Leg 21 and was cored continuously to a maximum penetration of 513 metres below the seafloor (mbsf). 55 cores were recovered from two holes; 5 cores from Hole 207 and a further 50 cores from Hole 207A. The upper 309 m of the sequence comprises late Pleistocene to Paleocene aged sediments, primarily foraminiferal-nannofossil ooze and chalk, with some siliceous microfossil bearing foraminiferal-nannofossil ooze. Sediments from 309–513 mbsf are Late Cretaceous age and are comprised mainly of rhyolitic tuffs and vitrophyric rhyolite flows, with ~ 50 m of glauconitic silty claystone at 309–357 mbsf (Burns et al., 1973). This current study focuses on lower to middle Eocene sediments taken from cores 14–26.

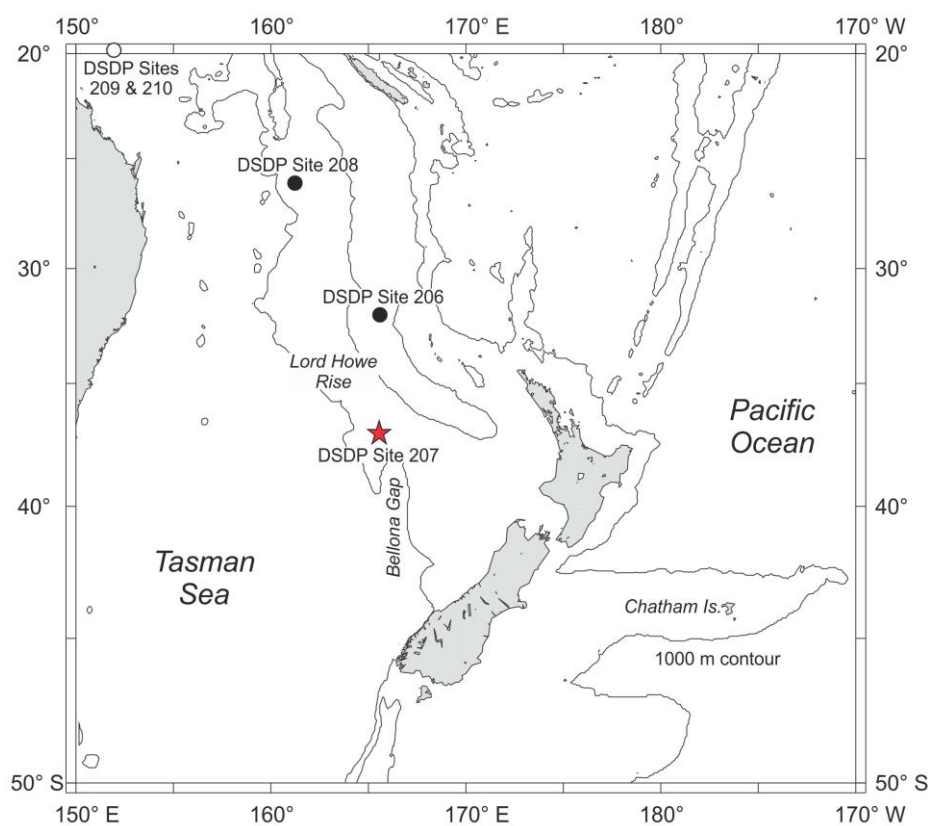


Figure 3.2: Map showing the location of DSDP Sites 206–208, Lord Howe Rise. Sites 209 and 210 are located to the northwest of Site 208, as indicated by the open circle. The 1000 m contour line represents the regional bathymetry.

3.2.2 Campbell Plateau: DSDP Leg 29, Site 277

DSDP Site 277 is located on the southern Campbell Plateau between Auckland and Campbell Islands ($52^{\circ} 13.43'S$; $166^{\circ} 11.48'E$) at a water depth of 1214 m (Figure 3.3). During the early Eocene Site 277 was located at a paleolatitude of $\sim 54^{\circ}S$ (Figure 3.1). Drilled in 1973 during DSDP Leg 29, the primary objectives were to obtain a Cenozoic biostratigraphic sequence from subantarctic latitudes and identify any disconformities that might be present. Forty-six cores were recovered with a maximum penetration of 472.5 m. Sediments comprise 462 m of upper Oligocene to middle Paleocene nannofossil ooze and chalk, overlain disconformably by 10 m of Plio-Pleistocene foraminifera and nannofossil ooze (Kennett et al., 1975). This current study analyses sediments from cores 36–41, spanning the lower to lower middle Eocene.

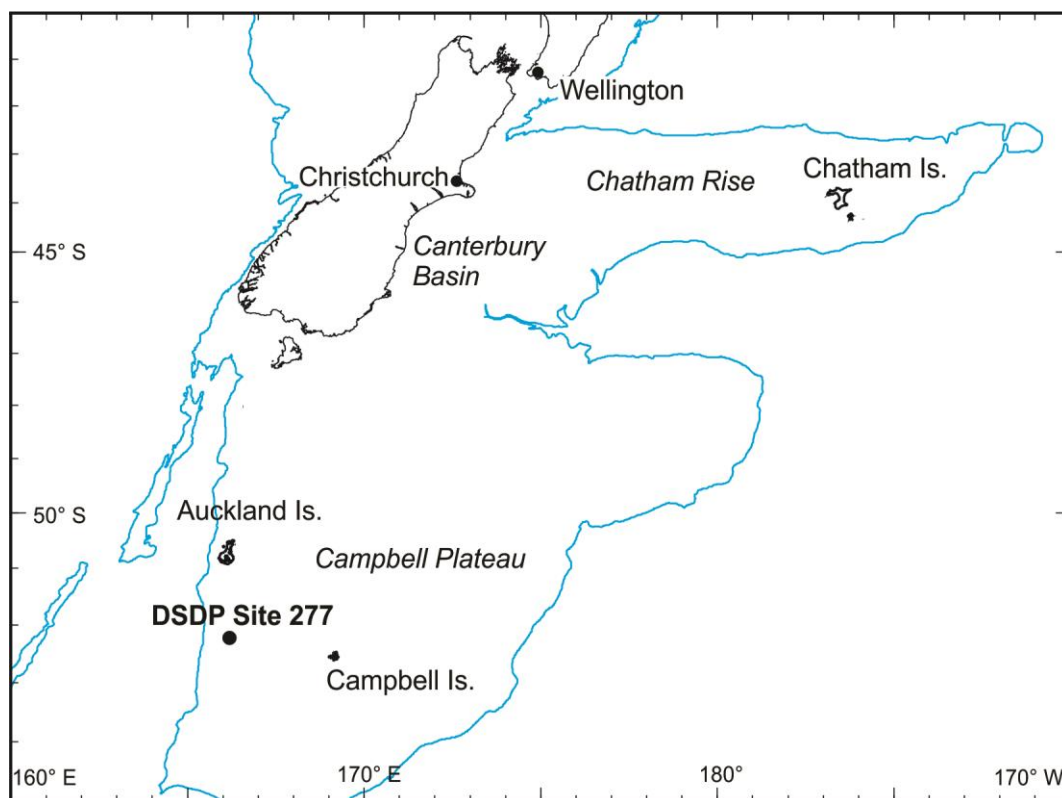


Figure 3.3: Map showing the location of DSDP Site 277, Campbell Plateau. Black lines indicate the modern coastline and blue lines show the regional bathymetry (1000 m contour).

3.2.3 Canterbury Basin: mid-Waipara River section

The mid-Waipara River section is located along the middle part of the Waipara River, northern Canterbury Basin (Figure 3.4). During the early Eocene the New Zealand landmass was positioned $\sim 3\text{--}4^\circ$ further south than its current location, with the mid-Waipara River section located at a paleolatitude of $\sim 47^\circ\text{S}$ (Figure 3.1). At that time there was widespread deposition of transgressive sediment along the passive margin of New Zealand (Ballance, 1993; King et al., 1999). Previous work by Morgans et al. (2005) integrated samples from six stratigraphic sections (Columns 1 to 6) in mid-Waipara River into a single composite section, spanning the Upper Cretaceous to middle Eocene. This study focuses on sediments of the Ashley Mudstone in Column 6 (grid reference NZTM BV24/156831 523323 to BV24/156849 523306; New Zealand topomap 50 BV24, 1:50,000, Edition 1, 2009)¹. The unit is a calcareous mudstone that was deposited at upper bathyal depths in the early to middle Eocene (Morgans et al., 2005; Hollis et al., 2012).

The Ashley Mudstone was first described by Mason (1941) and the formation definition was later revised by Browne & Field (1985). At mid-Waipara, basal Ashley Mudstone is separated from the underlying Paleocene strata (Waipara Greensand) by a sharp and unconformable contact. Hollis et al. (2012) identified the Paleocene-Eocene Thermal Maximum (PETM) in the basal Ashley Mudstone by a negative $\delta^{13}\text{C}$ excursion (measured from bulk organic carbon) and dinoflagellate assemblages. The PETM interval is overlain by a 50–75 m thick section of Ashley Mudstone that extends from lower to middle Eocene (New Zealand Waipawan to Bortonian Stages) (Hollis et al., 2012). This encompasses a time interval of 16 million years (56–40 Ma) based on the recently recalibrated New Zealand Geological Time Scale (Raine et al., 2015). The Amuri Limestone of late Eocene–Oligocene age conformably overlies the Ashley Mudstone (Morgans et al., 2005).

¹ Original grid reference: NZMS260 M34/7831 9486 to M34/7848 9469; New Zealand Map Series 260 topomap M34, 1:50,000, Edition 1, 1991

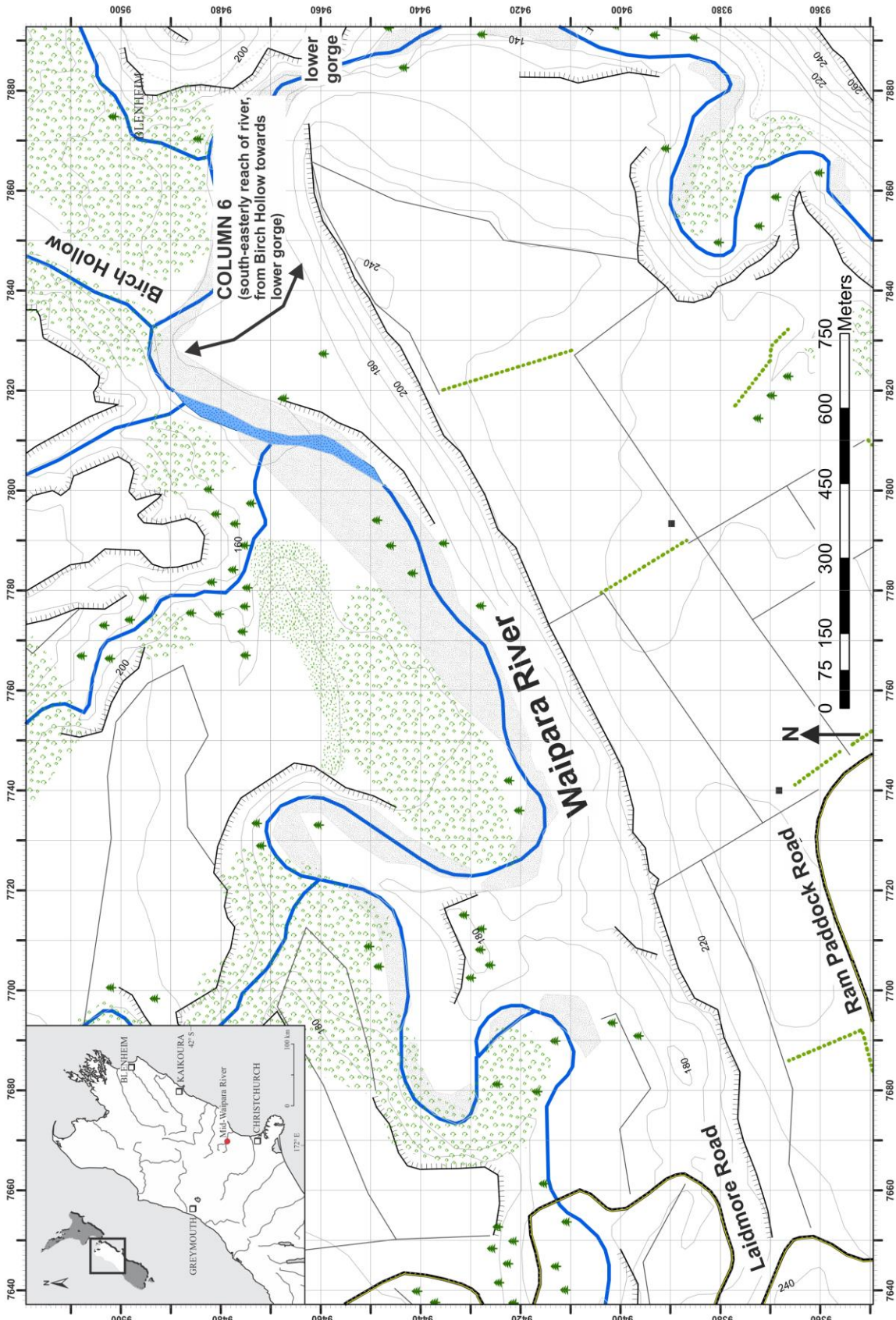


Figure 3.4: Map showing the location of the mid-Waipara River Section, Canterbury Basin, New Zealand (modified from Morgans et al., 2005). Map grid from New Zealand Map Series 260 topomap M34, 1:50,000, Edition 1, 1991. Inset shows the location of the section on the South Island.

3.2.4 Canterbury Basin: Hampden Beach section

The Hampden Beach section represents a near-complete onshore Paleogene succession spanning the Paleocene to upper Eocene. It is the designated boundary stratotype section and point (SSP) for the Bortonian Stage (Morgans, 2009 and references therein). The section represents a 256.5 m thick sequence that extends along Hampden Beach, and spans the Moeraki, Kurinui and Hampden Formations.

The section is located on the North Otago coastline in the southern Canterbury Basin, extending from just below Lookout Bluff to Moeraki (Figure 3.5). As with the mid-Waipara River section, during the Paleogene the Hampden Beach section was located ~3–4° further south from its current position, at a paleolatitude of ~49°S (Figure 3.1). This current study focuses mainly on the lower to middle Eocene sediments of the Kurinui Formation, with some analysis of the underlying Moeraki and overlying Hampden formations (grid reference NZTM CC18/142948 497806 to CC18/143144 498333; New Zealand topomap 50 CC18, 1:50,000, Edition 2, 2010)². Sediments were deposited in shelf to upper bathyal depths in a neritic environment that became progressively more calcareous over time (Morgans, 2009).

The Moeraki Formation was first defined as the Moeraki Series by Hochstetter (as cited in Morgans, 2009) and later as the Moeraki Formation (Brown, 1959). At Hampden Beach the upper Moeraki Formation consists of 30 m of medium grey-green, micaceous, non-calcareous mudstone of Paleocene age (New Zealand Teurian stage) (Morgans, 2009).

The overlying Kurinui Formation was described as the Kurinui Series by Benson (1943) and later as the Kurinui Formation by Brown (1959). The Kurinui Formation spans the lower to middle Eocene (New Zealand Waipawan-Heretaungan Stages) and consists of non-calcareous basal greensand overlain by slightly calcareous siltstone and claystone that display a fining upwards sequence (Morgans, 2009). The maximum thickness of the formation at Hampden Beach is 104.7 m and contact with the underlying Moeraki Formation is considered to be unconformable (Crouch & Brinkhuis, 2005).

² Original grid reference: grid reference NZMS260 J42/3935 3969 to J42/4101 4496; New Zealand Map Series 260 topomap J42, 1:50,000, Edition 1, 1984

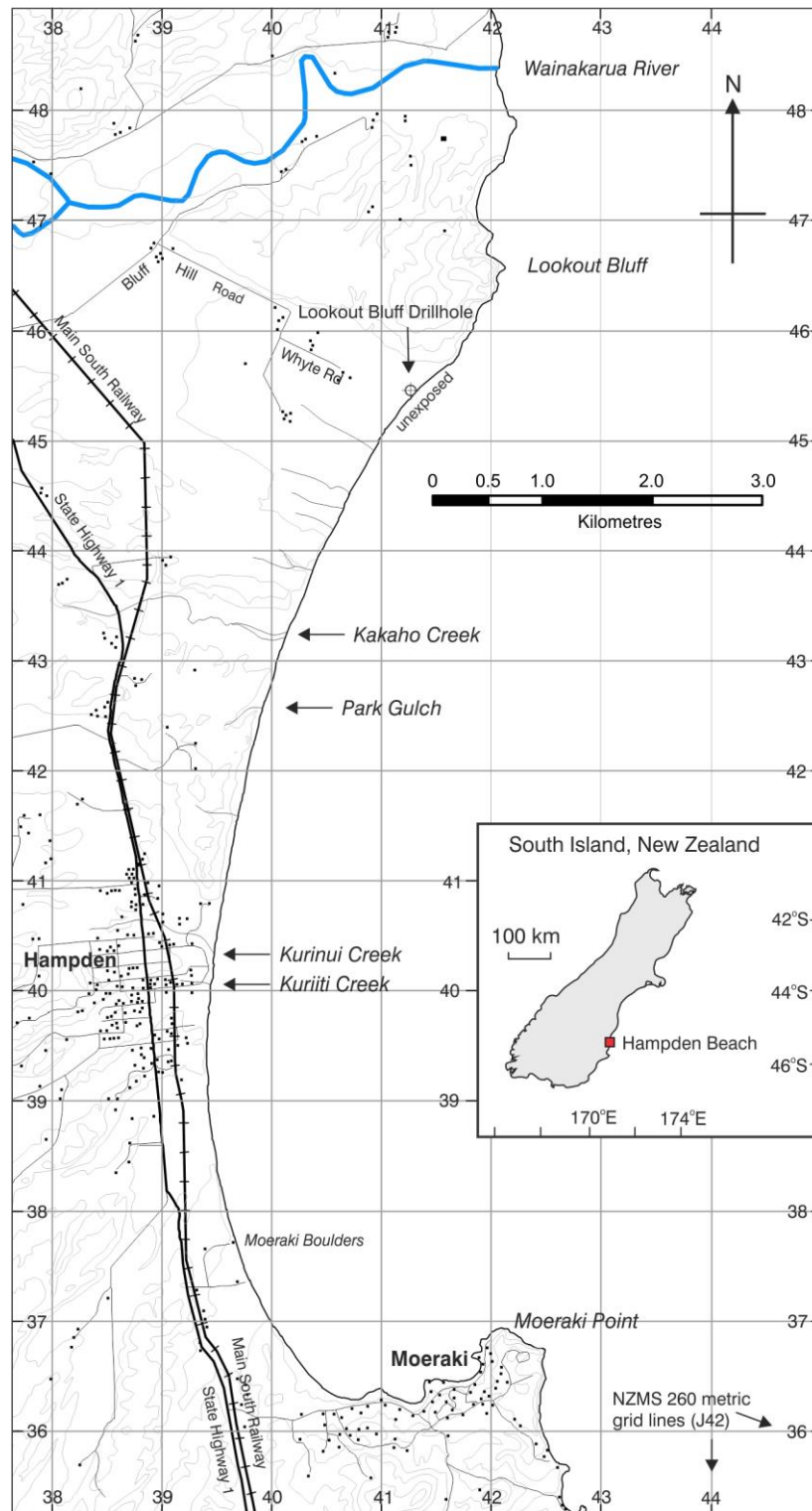


Figure 3.5: Map showing the location of the Hampden Beach Section, Canterbury Basin, New Zealand (modified from Morgans, 2009). Map grid from New Zealand Map Series 260 topomap J42, 1:50,000, Edition 1, 1984. Inset shows the location of the section within the South Island.

McMillan (1999) published the first detailed geological map of the Hampden Beach region and considered the Moeraki and Kurinui formations of earlier workers to be members of the Abbotsford Formation. However, for the purpose of consistency with previous studies (e.g. Morgans, 2009), here the Moeraki and Kurinui members are retained as formations.

Marshall (1916) erected the Hampden Formation informally and Brown (1959) raised it to formation status. At Hampden Beach the Hampden Formation is comprised of basal glauconitic silty sandstone (~5–6 m) overlain by slightly glauconitic, micaceous, calcareous sandy siltstone (~116 m). The transition from the underlying Kurinui Formation is represented by a rapidly coarsening upwards sequence from dark grey, calcareous claystone to extremely glauconitic sandstone. The Hampden Formation is dated as middle Eocene with a very condensed basal section (30–50 cm) spanning the New Zealand Heretaungan and Porangan stages and the remainder of the formation of Bortonian age, with the exception of the uppermost 5.5 m which is Kaiatan (Morgans, 2009).

3.3 Previous work

3.3.1 Lord Howe Rise

A summary of nannofossil biostratigraphy at Site 207 was presented by Burns et al. (1973) following the DSDP Leg 21 expedition. The lithology and paleontology of the sequence at Site 207, particularly in the lower part, were found to have close similarities with sequences of equivalent age in eastern New Zealand. Bukry (1973a) provided a summary of nannofossil assemblages for all sites drilled during Leg 21 (Sites 203–210), and discussed changes in preservation and the use of the *Discoaster/Chiasmolithus* ratio to estimate paleotemperature at different latitudes. The most comprehensive account of calcareous nannofossils from Leg 21 was given by Edwards (1973a), although detailed reports were only provided for Sites 203–205. Much of the nannofossil material from Leg 21 was only subjected to cursory inspection, resulting in identification of only the more conspicuous taxa. Edwards (1973a) found that nannofossil assemblages from Sites 207–208 provided a better correlation to their equivalent New Zealand assemblages than assemblages from DSDP Leg 21 sites to the northwest of Site 208, i.e. Sites 209 and 210 that have closer

affinities with low-latitude assemblages. There have been no significant paleoclimate studies at this site.

3.3.2 Campbell Plateau

Kennett et al. (1975) provided a summary of nannofossil biostratigraphy at Site 277 following the DSDP Leg 29 expedition. Edwards & Perch-Nielsen (1975) also documented nannofossils from Leg 29, discussing biostratigraphy, paleoecology and correlations between northern and southern high-latitude nannofossils in the Cenozoic. In addition, they provided a distribution chart for taxa found at Site 277 from Upper Pleistocene to mid-Paleocene. Later work by Waghorn (1981) examined core material from Site 277 and provided a detailed biostratigraphy for the middle Oligocene to upper Eocene interval. Hollis et al. (1997) provided a review of these earlier studies and included new nannofossil data from three samples collected from cores 45 and 44. These data were integrated with data from other fossil groups to provide a detailed biostratigraphic scheme for Site 277. Recent work reporting on the discovery of the PETM at Site 277 (Hollis et al., 2015) included an examination of calcareous nannofossils across this interval, which extends and refines the existing data set.

Shackleton & Kennett (1975) provided an early record of paleoclimate at Site 277 using oxygen and carbon isotopes. They found that SST decreased from $\sim 19^{\circ}\text{C}$ in the early Eocene to $\sim 7^{\circ}\text{C}$ by the Oligocene. Hollis et al. (2015) showed an increase in seafloor temperatures of $\sim 5\text{--}6^{\circ}\text{C}$ across the PETM interval at Site 277, reaching $\sim 19^{\circ}\text{C}$ in the basal PETM. A recent study by Pascher et al. (2015) presented a detailed record of climate change through the middle to late Eocene at Site 277. These authors identify the Middle Eocene Climatic Optimum (MECO; ~ 40 Ma), Priabonian Oxygen Isotope Maximum (PrOM; ~ 37 Ma) and late Eocene warming event (~ 36.4 Ma) based on radiolarian assemblages and $\delta^{18}\text{O}$ values.

3.3.3 Canterbury Basin

The Canterbury Basin has been the focus of a number of previous studies investigating biostratigraphy, paleoclimate, magnetostratigraphy and paleoenvironment. Calcareous nannoplankton from the mid-Waipara River section were first examined by Edwards (1966).

Analysis of assemblages in Haumurian- to Waipawan-aged sediments revealed three distinctive biostratigraphic zones that correlated with those found across the Cretaceous/Paleogene boundary in Europe and North America.

Early work at Hampden Beach was carried out by Cameron & Waghorn (1985), who presented a summary of the key foraminiferal and nannofossil events across the Bortonian/Kaiatan boundary at this locality. These authors correlated the section with the standard zonation scheme of Martini (1971) but conceded that exact correlation of zone boundaries was problematic. Based on the *Discoaster/Chiasmolithus* ratio, Cameron & Waghorn (1985) inferred that paleotemperatures increased from cooler conditions in the early Bortonian to warmer conditions in the late Bortonian.

The Paleocene-Eocene transition at Hampden Beach was studied from a marine palynological perspective (Crouch & Brinkhuis, 2005) in an attempt to better understand environmental change during this period at southern high latitudes. The authors found that fluctuations in the dinocyst assemblages coincided with increases in temperature and excess carbon related to the PETM. They suggested that the dominant factor affecting dinoflagellate assemblage composition was changes in SST. They also identified short-lived episodes of raised SST during the PETM and early Eocene, as evidenced by high relative abundance of the *Apectodinium* complex.

Morgans (2009) conducted a study of upper Paleocene to middle Eocene foraminifera from the Hampden Beach section. New data were combined with existing biostratigraphic records to refine the resolution of New Zealand stage boundaries and improve correlation with offshore basins. In addition to refining the biostratigraphy of the Hampden section, Morgans (2009) discussed aspects of paleoclimate, paleogeography and paleoenvironment based on the integrated data.

Paleoclimate of the middle Eocene at Hampden Beach has been well documented by Burgess and colleagues (Burgess, 2008; Burgess et al., 2008, 2009). These workers used geochemical, sedimentary and fossil assemblage records to generate a multi-proxy paleoclimate record. They showed that middle Eocene SSTs at Hampden Beach were ~23–

25°C, which is warmer than previous estimates for Southern Ocean sites on Maud Rise and Kerguelen Plateau (10–12°C; Zachos et al., 1994), and Campbell Plateau (13°C; Shackleton & Kennett, 1975). They also identified a transient warm interval (~2.5°C) between 40 and 39.6 Ma, which they interpreted as MECO.

Hollis et al. (2009) used a geochemical multiproxy approach to estimate SSTs at mid-Waipara and found that paleotemperature estimates from TEX_{86} , Mg/Ca and $\delta^{18}\text{O}$ were indicative of tropical conditions (~30°C) from the late–early to early-middle Eocene (50.7–46.5 Ma). Creech et al. (2010) also estimated SSTs for the Eocene at mid-Waipara and found close agreement between Mg/Ca temperature estimates (24–30°C) and the previously published data of Hollis et al. (2009).

Later work by Hollis et al. (2012) developed a paleo-calibration for TEX_{86} based on an Eocene data set and found that it coincided most closely with the $\text{TEX}_{86}^{\text{L}}$ proxy. SSTs using the $\text{TEX}_{86}^{\text{L}}$ proxy were at ~25–26°C during the PETM and EECO in the Canterbury Basin, suggesting that previous SST estimates may have been overestimated by 5–9°C. Using the MBT'/CBT proxy, Pancost et al. (2013) presented a record of terrestrial Paleocene–Eocene climate for the SW Pacific, showing that mean annual air temperature (MAAT) estimates matched more closely to $\text{TEX}_{86}^{\text{L}}$ -derived SSTs than to other calibrations of the TEX_{86} proxy (Hollis et al., 2009, 2012). Mg/Ca ratios indicate that the Hampden section may have been slightly warmer during the Mangaorapan than mid-Waipara, with average SSTs of 28°C. This is likely a reflection of the shallower depositional setting at Hampden Beach (Morgans, 2009).

Recent studies by Dallanave et al. (2014, 2016) provide a new integrated magneto-biostratigraphic chronology for the Eocene interval (~51–47 Ma) of the mid-Waipara section. The biostratigraphy was based on foraminiferal, calcareous nannofossil and dinoflagellate cyst analyses of new samples collected at the same levels as mini-cores used for paleomagnetic analysis, and spans the Waipawan to lowermost Bortonian Stages.

CHAPTER 4: BIOSTRATIGRAPHY

4.1 Introduction

This chapter presents the biostratigraphic results of all study sites. Section 4.2 outlines the zonations used in this study (Martini, 1971; Aubry, 1991), including remarks on changes/updates to zone markers and correlation to the zonation of Agnini et al. (2014). Section 4.3 provides detailed biostratigraphic results for each site. Age-depth models for DSDP Sites 277 and 207 are presented in Section 4.4, and these are used to compare sedimentation rates and hiatuses between the two locations. The final section provides a summary of the chapter, including a correlation of all study sites based on biostratigraphy.

4.2 Nannofossil zone definitions

The zonation (=NP zones) of Martini (1971) has been shown to provide good biostratigraphic resolution in the SW Pacific (e.g. Kulhanek et al., 2015, Dallanave et al., 2016, Shepherd & Kulhanek, 2016). As such, this is the main zonation used for this study, with subzones defined by Aubry (1991). The zonation (=CNE zones) of Agnini et al. (2014) was developed for use at low to middle latitudes; however, it has recently been applied to a high-latitude section in the SW Pacific (Dallanave et al., 2015). It is used here to supplement the zonation of Martini (1971) and provide additional age control. Zone boundaries are calibrated to Gradstein et al. (2012). It should be noted that the zonation of Okada & Bukry (1980) is not used in this study, as it does not offer any additional improvement to age control across the interval studied. The relevant Martini (1971) zones are outlined below and correlations to other zones illustrated in Figure 1.3.

4.2.1 *Tribrachiatus contortus* Zone (NP10)

Definition: Interval from the first occurrence (FO) of *Rhomboaster bramlettei* to the last occurrence (LO) of *Tribrachiatus contortus* (Martini, 1971).

Remarks: The last occurrence of *Fasciculithus* has been reported as late NP9–early NP10 (Raffi et al., 2005), hence the co-occurrence of this taxon with *R. bramlettei* can be used to constrain samples to NP10.

Correlation: The base of Zone CNE1 is marked by the LO of the *Fasciculithus richardii* group, with the FO of *Rhomboaster* spp. following just a short time later (Agnini et al., 2014), making the base of CNE1 nearly equivalent to the base of NP10. The base of Zone CNE2 is defined by the LO of *Fasciculithus tympaniformis*, which Agnini et al. (2014) indicate is the last member of *Fasciculithus* to go extinct. This event correlates to lower Zone NP10. The FO of *T. orthostylus* marks the base of Zone CNE3 and this correlates to upper Zone NP10 (Agnini, et al., 2014).

4.2.2 *Discoaster binodosus* Zone (NP11)

Definition: Interval from the LO of *T. contortus* to the FO of *Discoaster lodoensis* (Martini, 1971).

Remarks: *T. contortus* is absent from all of the studied sections. This species is part of the *Rhomboaster* lineage, which is documented as being incomplete or absent in the New Zealand region (Edwards, 1971; Hollis et al., 2015). Instead, we use the FO of *Sphenolithus radians*, which can be used as a secondary marker to define the base of Zone NP11 (Backman, 1986).

Correlation: Zone NP11 is included within Zone CNE3 (Agnini et al., 2014).

4.2.3 *Tribrachiatulus orthostylus* Zone (NP12)

Definition: Interval from the FO of *D. lodoensis* to the LO of *Tribrachiatulus orthostylus* (Martini, 1971).

Correlation: The first common occurrence (FCO) of *D. lodoensis* defines the base of Zone CNE4 and this event correlates to the base of Zone NP12 (Agnini et al., 2014).

4.2.4 *Discoaster lodoensis* Zone (NP13)

Definition: Interval from the LO of *T. orthostylus* to the FO of *Discoaster sublodoensis* (Martini, 1971).

Correlation: The base of Zone CNE5 is defined by the LO of *T. orthostylus* and this is equivalent to the base of Zone NP13 (Agnini et al., 2014).

4.2.5 *Discoaster sublodoensis* Zone (NP14)

Definition: Interval from the FO of *D. sublodoensis* to the FO of *Nannotetrina fulgens* (Martini, 1971).

Remarks: *D. sublodoensis* is rare in the New Zealand region (especially in the higher latitude sections), making it difficult to distinguish the base of Zone NP14.

Correlation: The FO of common 5-rayed *D. sublodoensis* marks the base of Zone CNE6 and this is equivalent to the base of Zone NP14. The base of CNE7 is defined by the LO of *D. lodoensis* and is correlated to lower Zone NP14. The FO of *N. cristata* marks the base of Zone CNE8 and this event is correlated with middle Zone NP14 (Agnini et al., 2014).

4.2.6 *Nannotetrina fulgens* Zone (NP15)

Definition: Interval from the FO of *N. fulgens* to the LO of *Blackites gladius* (Martini, 1971).

Remarks: The total range of *Chiasmolithus gigas* is used to define Subzone NP15b (Aubry, 1991).

Correlation: The base of Zone CNE9 is defined by the FO of *Nannotetrina alata* group and this is equivalent to the base of Zone NP15. The FO of *C. gigas* marks the base of CNE10 and this correlates to the base of Subzone NP15b. The base of CNE11 is marked by the FO of common *Sphenolithus cuniculus* and this event is within subzone NP15b. The LO of *C. gigas* defines the base of Zone CNE12 and this event is correlated to the base of Subzone NP15c (Agnini et al., 2014).

4.2.7 *Discoaster tanii nodifer* Zone (NP16)

Definition: Interval from the LO of *B. gladius* to the LO of *Chiasmolithus solitus* (Martini, 1971);

Remarks: *B. gladius* is often missing in assemblages (Gradstein et al., 2012; Shamrock & Watkins, 2012; Dallanave et al., 2015), therefore, the LO of *Nannotetrina alata/fulgens* is used as a secondary marker to define the base of NP16 (Backman, 1986; Expedition 320/321 Scientists, 2010).

Correlation: The FCO of *R. umbilicus* defines the base of CNE13 and this event correlates to lower Zone NP16. The definition of *R. umbilicus* follows that of Backman & Hermelin (1986), which includes all specimens $\geq 14 \mu\text{m}$. The base of CNE14 is marked by the FCO of *R. reticulata* and this event is correlated to middle Zone NP16 (Agnini et al., 2014).

4.3 Biostratigraphic results

The key biostratigraphic results for each site are outlined below and summarised in Table 4.1. Zone boundaries are positioned at the midpoint between consecutive samples in which the FO or LO of key taxa are observed. Individual tables showing the distribution of taxa at each site are presented in Appendix C. Due to the poor biostratigraphic resolution of the Hampden Beach section, no attempt has been made to correlate it with the zonation of Agnini et al. (2014).

Table 4.1: Summary of key bioevents identified at all study sites.

Bioevent	NP Zone (base)	CNE Zone (base)	Lower limit	Upper limit	Zonal Boundary Placement (midpoint)
Mid-Waipara River section					
FO <i>Reticulofenestra umbilicus</i>		CNE13	62.26	58.55	60.41
LO <i>Discoaster lodoensis</i>		CNE7	40.76	43.00	41.88
LO <i>Tribrachiatulus orthostylus</i>	NP13	CNE5	11.13	12.55	11.84
FO <i>Discoaster lodoensis</i>	NP12	CNE4	-2.87	-3.99	-3.43
FO <i>Sphenolithus radians</i> ¹	NP11		-6.61	-13.20	-9.91
FO <i>Tribrachiatulus orthostylus</i>		CNE3	-6.61	-13.20	-9.91
FO <i>Rhomboaster bramlettei</i> ²	(in) NP10		-15.25		
Hampden Beach section					
FO <i>Discoaster lodoensis</i>	(in) NP13–14		46.70	49.70	48.20
DSDP Site 207					
FO <i>Reticulofenestra umbilicus</i>		CNE13	170.19	171.51	170.85
FO <i>Nannotetrina cristata</i>		CNE8	219.47	230.01	224.74
LO <i>Discoaster lodoensis</i>		CNE7	230.01	219.47	224.74
LO <i>Tribrachiatulus orthostylus</i>	NP13	CNE5	273.00	269.60	271.30
FO <i>Discoaster lodoensis</i>	NP12	CNE4	276.51	282.00	279.26
FO <i>Sphenolithus radians</i> ¹	NP11		284.20	286.00	285.10
FO <i>Tribrachiatulus orthostylus</i>		CNE3	284.20	286.00	285.10
DSDP Site 277					
FO <i>Reticulofenestra umbilicus</i>		CNE13	369.00	370.58	369.79
FO <i>Nannotetrina cristata</i>		CNE8	370.58	372.08	371.33
LO <i>Discoaster lodoensis</i>		CNE7	387.59	381.50	384.73
FO <i>Discoaster sublodoensis</i>	NP14	CNE6	389.50	391.00	390.25
LO <i>Tribrachiatulus orthostylus</i>	NP13	CNE5	426.53	419.60	423.07
FO <i>Discoaster lodoensis</i>	NP12	CNE4	429.40	434.57	431.99
FO <i>Sphenolithus radians</i> ¹	NP11		446.50	446.92	446.71
FO <i>Tribrachiatulus orthostylus</i>		CNE3	446.50	446.92	446.71

¹Secondary marker for base of Zone NP11

²Base of studied section

4.3.1 Mid-Waipara River section

This study utilises 27 samples collected in 2012 from a ~66 m succession of Ashley Mudstone and 7 samples collected in 2007 from above the Paleocene-Eocene Thermal Maximum (PETM) interval in the basal Ashley Mudstone (Figure 4.1). The two sample sets were correlated using foraminifera, dinocyst and nannofossil bioevents to produce a composite section (Figure 4.2; refer to Dallanave et al., 2016).

The FO of *R. bramlettei* is observed at mid-Waipara in sample M34/f0898 (-15.25 m), which indicates that the base of the studied section is within Zone NP10. The presence of *Rhomboaster* and *Fasciculithus* in samples M34/f0898 (-15.25 m) to M34/f0896 (-13.2 m) confines this interval to Zone NP10. The base of CNE2 is marked by the LO of *F. tympaniformis* at -13.2 m, suggesting that the entire Zone NP10 interval correlates with Zone CNE1 (Figure 4.2). The assemblage of Zone NP10 contains abundant *Toweius callosus* and common *Coccolithus pelagicus*. Other taxa include few to rare *Discoaster lenticularis*, *Toweius eminens*, *Toweius pertusus*, *Toweius serotinus* and *Toweius tovae*. *Discoaster multiradiatus* and *Discoaster salisburgensis* are common in the lowermost sample examined but are rarer towards the top of this interval.

At mid-Waipara, the FO of *S. radians* is found in sample M34/f0894 (-6.61 m) and consequently the base of Zone NP11 is placed at -9.91 m, the midpoint between this sample and the next underlying sample (-13.2 m). Samples M34/f0894 (-6.61 m) to M34/f0892 (-3.99 m) are assigned to Zone NP11. The FO of *T. orthostylus* is used to mark the base of Zone CNE3 and this event is correlated to the upper part of Zone NP10. At mid-Waipara this event is in the same sample as the FO of *S. radians*, suggesting that all of Zone CNE2 and part of CNE3 is missing. For this reason, an unconformity is placed at the base of NP11 (-9.91 m). However, it should also be noted that a large sampling gap of ~6.6 m occurs between the sample at -6.61 m and the underlying one (Figure 4.2). Samples in Zone NP11 contain abundant *C. pelagicus* and *T. callosus*, with few *Chiasmolithus bidens*, *Discoaster barbadiensis*, *Discoaster kuepperi*, *Sphenolithus anarrhopus*, *Sphenolithus editus*, *Sphenolithus moriformis* and *T. orthostylus*. Rare taxa include *Calcidiscus pacificanus*, *Cyclicargolithus parvus*, *Discoaster binodosus*, *Girgisia gammation*, *Lophodolithus nascens*, *Neochiastozygus imbrii* and *Reticulofenestra* spp.

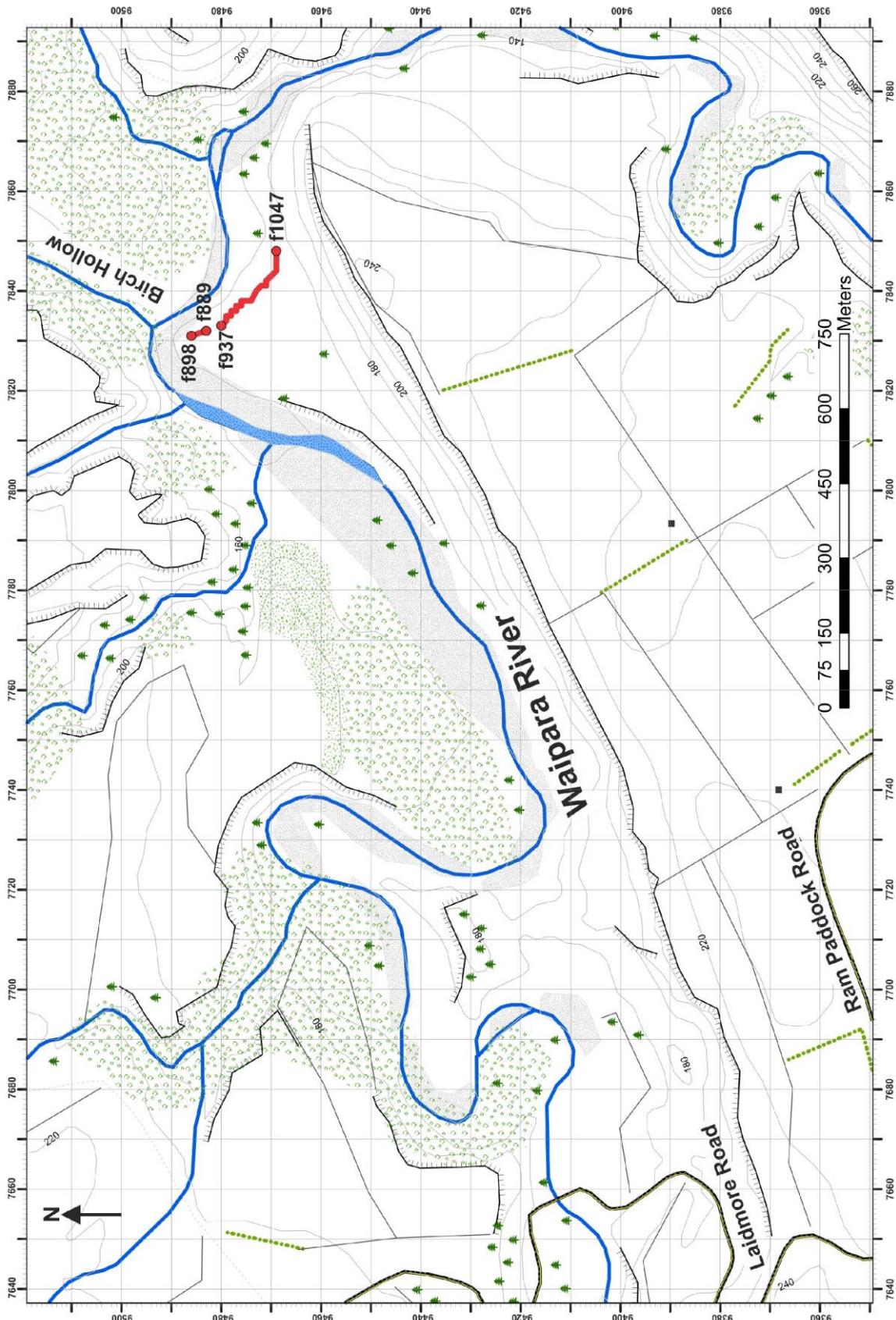


Figure 4.1: Map of the mid-Waipara River section showing the location of the sections sampled in 2007 (f898–f889) and 2012 (f937–f1047). Modified from Morgans et al. (2005).

The FO of *D. lodoensis* is in sample M34/f0891 (-2.87 m) in the mid-Waipara section, which places the base of Zone NP12 at the midpoint between -3.99 and -2.87 m (-3.43 m), with samples from M34/f0891 (-2.87 m) to M34/f0959 (11.13 m) assigned to this zone. The base of Zone CNE4 is defined by the FCO of *D. lodoensis* and this is placed at the same position as the base of Zone NP12. The assemblage of Zone NP12 is characterised by abundant *C. pelagicus* and *Toweius occultatus*, with common *D. kuepperi* and *Reticulofenestra samodurovii*. *Toweius callosus* is abundant in the lower part of Zone NP12 but becomes less so towards the top of the zone. Less common taxa include *Blackites* spp., *Chiasmolithus grandis*, *C. solitus*, *Coccolithus formosus*, *G. gammation*, *Helicosphaera seminulum*, *Markalius inversus*, *Neococcolithes dubius*, *Neococcolithes minutus*, *Orthozygus occultus*, *Pontosphaera exilis*, *Pontosphaera pulchra*, *Reticulofenestra daviesii*, *Reticulofenestra dictyoda*, *Reticulofenestra minuta*, *Reticulofenestra producta*, *S. moriformis*, *S. radians*, *T. orthostylus* and *Zygrhablithus bijugatus bijugatus*.

The LO of *T. orthostylus* is observed in sample M34/f0959 (11.13 m), placing the base of Zones NP13 and CNE5 at the midpoint between 11.13 and 12.55 m. *Discoaster sublodoensis* is not observed at mid-Waipara making it impossible to define the base of Zones NP14 and CNE6. The LO of *D. lodoensis* defines the base of Zone CNE7 and is found in the sample at 40.76 m, with the zone boundary placed at the midpoint between 40.76 m and 43.00 m. Samples M34/f0963 (12.55 m) to M34/f1039 (58.55 m) are placed in a combined NP13–NP14 zone and contain abundant *C. pelagicus*, with common *R. dictyoda* and *R. samodurovii*. The FO of *Reticulofenestra wadeae* is near the base of this combined zone and the species is relatively common throughout the rest of the samples assigned to this zone. *Discoaster kuepperi*, *T. callosus* and *T. occultatus* are generally more common in the lower part of the zone, with decreased abundance in the upper part. *Discoaster elegans* first occurs in low numbers towards the top of this combined zone.

The absence of *N. fulgens* and *C. gigas*, suggests that all or part of Zone NP15 is missing at the mid-Waipara section. The absence of markers for the bases of Zones CNE8 (FO of *N. cristata*), CNE9 (FO of *Nannotetrina alata* group), CNE10 (FO of *C. gigas*), CNE11 (FO of common *S. cuniculus*) and CNE12 (LO of *C. gigas*) means that these zones cannot be recognised at mid-Waipara. These taxa occur in the New Zealand region but are generally

rare (e.g. *Nannotetrina*, (Edwards & Perch-Nielson, 1975; Hines et al., 2013); *C. gigas*, (Martini, 1986)). The Porangan Stage is inferred to be missing from this section due to the absence of foraminiferal datums (Dallanave et al., 2016). Based on this finding and the absence of nannofossil datums for this interval, an unconformity is placed between the combined NP13–14 zone and Zone NP16.

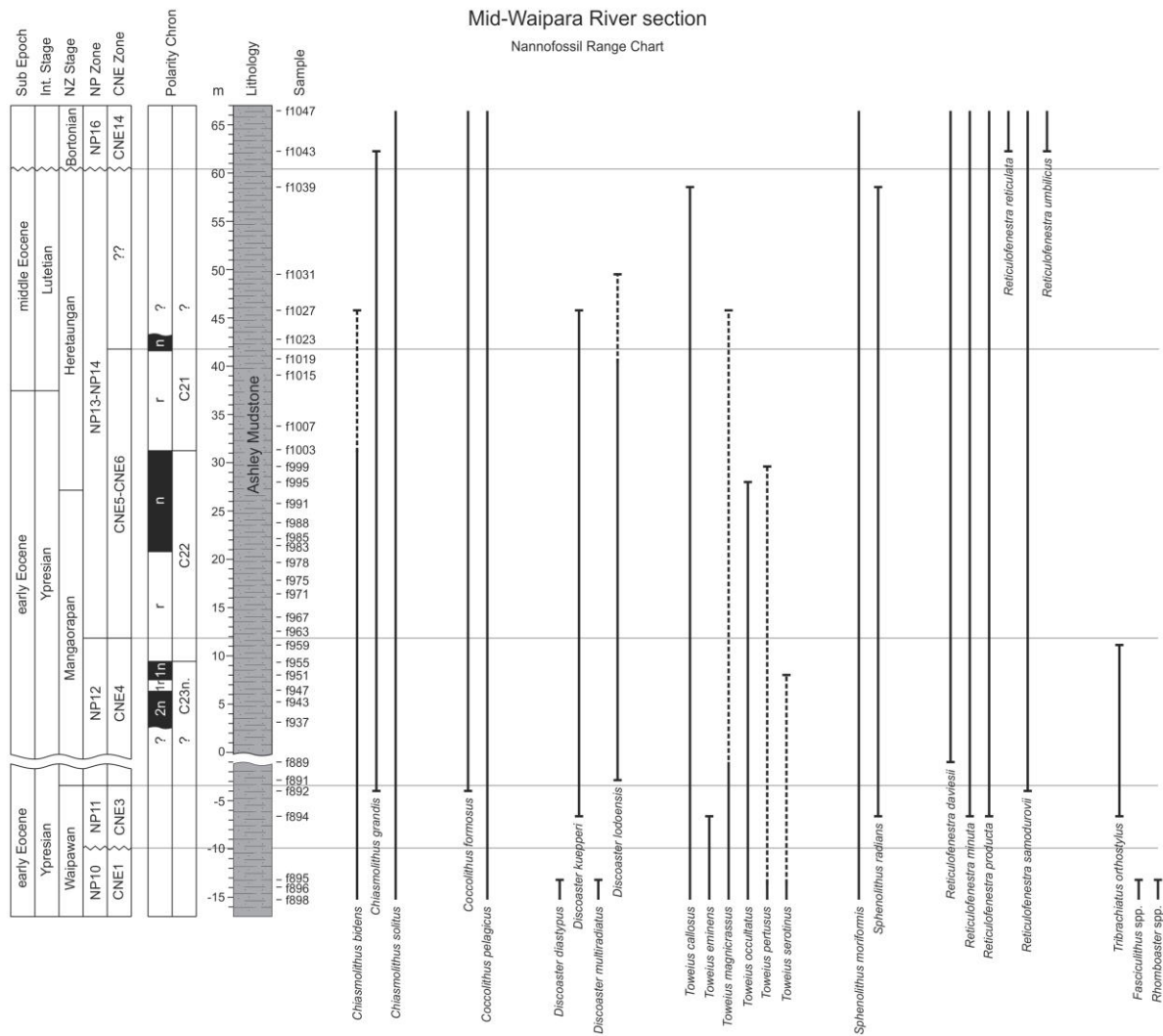


Figure 4.2: Range chart of key nannofossil taxa at mid-Waipara River. Magnetostratigraphy and correlation to international and local stages is based on Dallanave et al. (2016). Solid vertical lines indicate consistent occurrence, dashed vertical lines indicate intermittent occurrence, and short horizontal lines indicate limits of stratigraphic range. Nannofossil zone boundaries are placed at the midpoints between samples and are denoted by grey horizontal lines across the figure. The break in the column at 0 m represents the separation between the two sample sets.

The marker for the base of NP16 (*N. alata/fulgens*) is absent from mid-Waipara. Instead, the presence of *R. umbilicus* (>14 μm) and *R. reticulata* in samples M34/f1043 (62.26 m) to

M34/f1047 (66.45 m) places them within Zone NP16. *Reticulofenestra umbilicus* marks the base of Zone CNE13 and *R. reticulata* the base of CNE14, indicating that CNE13 (lower Zone NP16) is missing or occurs within the 3.71 m sampling gap. Zone NP16 contains common to abundant *C. pelagicus* and common *Reticulofenestra* taxa. Other taxa include *Chiasmolithus expansus* and *Discoaster saipanensis*.

4.3.2 Hampden Beach section

This study is based on 36 samples collected from the Hampden Beach section in 1998 in conjunction with the earlier study of Morgans (2009), spanning the upper Paleocene to middle Eocene (Figure 4.3). Six samples were taken from the Moeraki Formation, 29 samples were collected from the Kurinui Formation, and one sample was collected from the Hampden Formation. This section includes intervals where nannofossils are completely absent or preservation and abundance are extremely poor, making it difficult to identify nannofossil zone boundaries (Figure 4.4). Results are therefore presented in the context of each formation, from oldest to youngest, and are related to New Zealand Stages using the foraminiferal biostratigraphy of Morgans (2009).

The basal part of the Hampden Beach section (Teurian Moeraki Formation), from samples J42/f243 (1.6 m) to J42/f249 (25.4 m), is completely barren of calcareous nannofossils and it is not possible to correlate this interval with a particular nannofossil zone (Figure 4.4). Samples J42/f250 (30 m) to J42/f258 (46.7), lowermost Kurinui Formation, are also devoid of nannofossils and cannot be correlated with a nannofossil zone. The FO of *D. lodoensis* is observed in sample J42/f261 (49.7 m) and the absence of *Tribrachiatulus orthostylus* together with the presence of *D. lodoensis* from samples J42/f0261 (49.7 m) to J42/f0273 (79.2 m) indicates correlation with Zone NP13 or NP14. *Discoaster sublodoensis* is also absent at Hampden Beach making it difficult to identify the base of NP14 and sediments of this interval are therefore assigned to a combined NP13–14 zone (Figure 4.4). The assemblages contain abundant to common *C. pelagicus*, *R. minuta* and *R. samodurovii*, with common to few *D. kuepperi*, *R. daviesii* and *R. dictyoda*. Less common taxa include *C. bidens*, *C. solitus*, *Coccolithus foraminis*, *D. elegans*, *D. lodoensis*, *Discoaster wemmelensis*, *N. dubius*, *Reticulofenestra circus*, *R. producta*, *R. wadeae*, *S. moriformis*, *S. radians* and *T. callosus*.

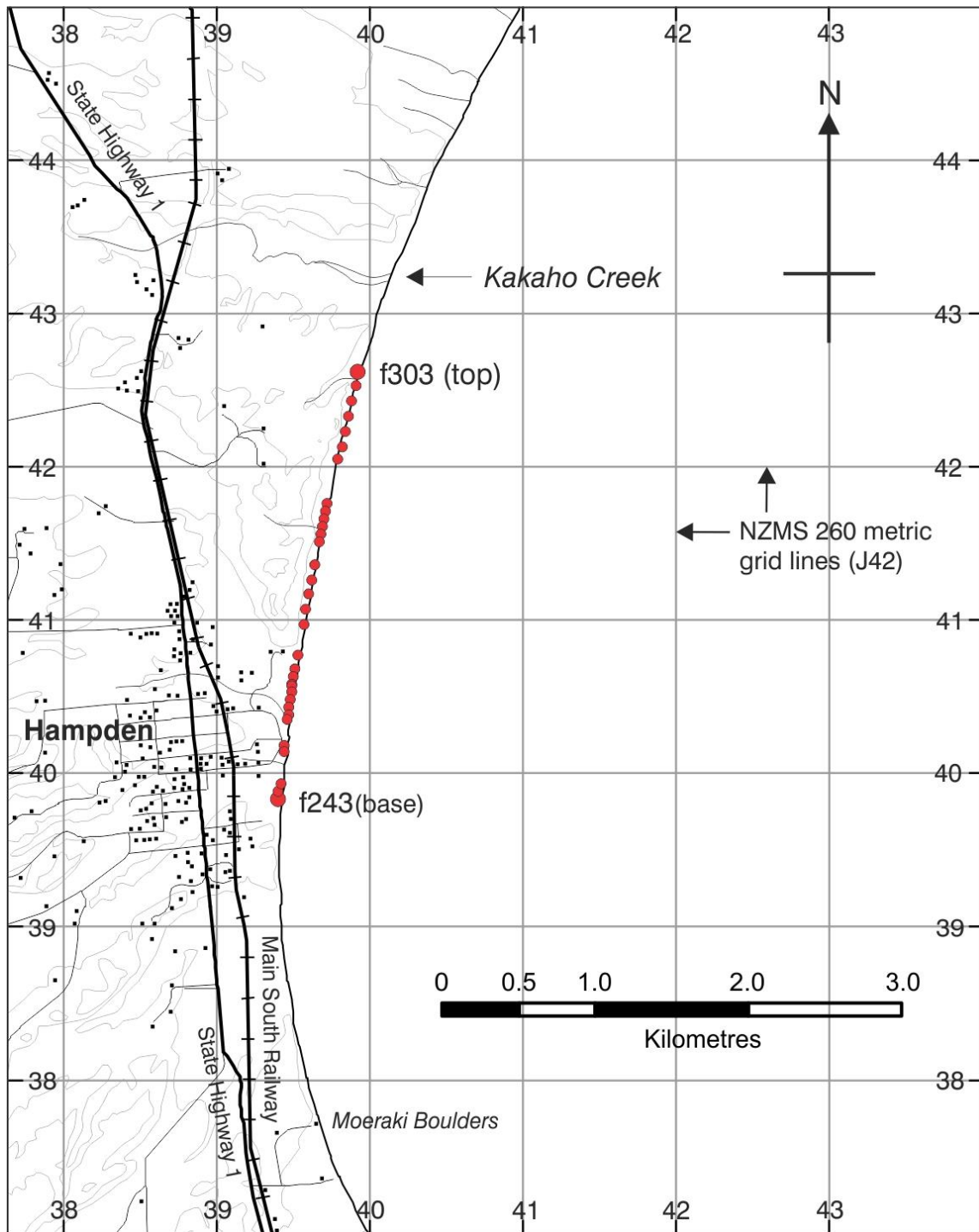


Figure 4.3: Map of the Hampden Beach section showing the location of the samples collected in 1998 (f243-f303). Modified from Morgans (2009).

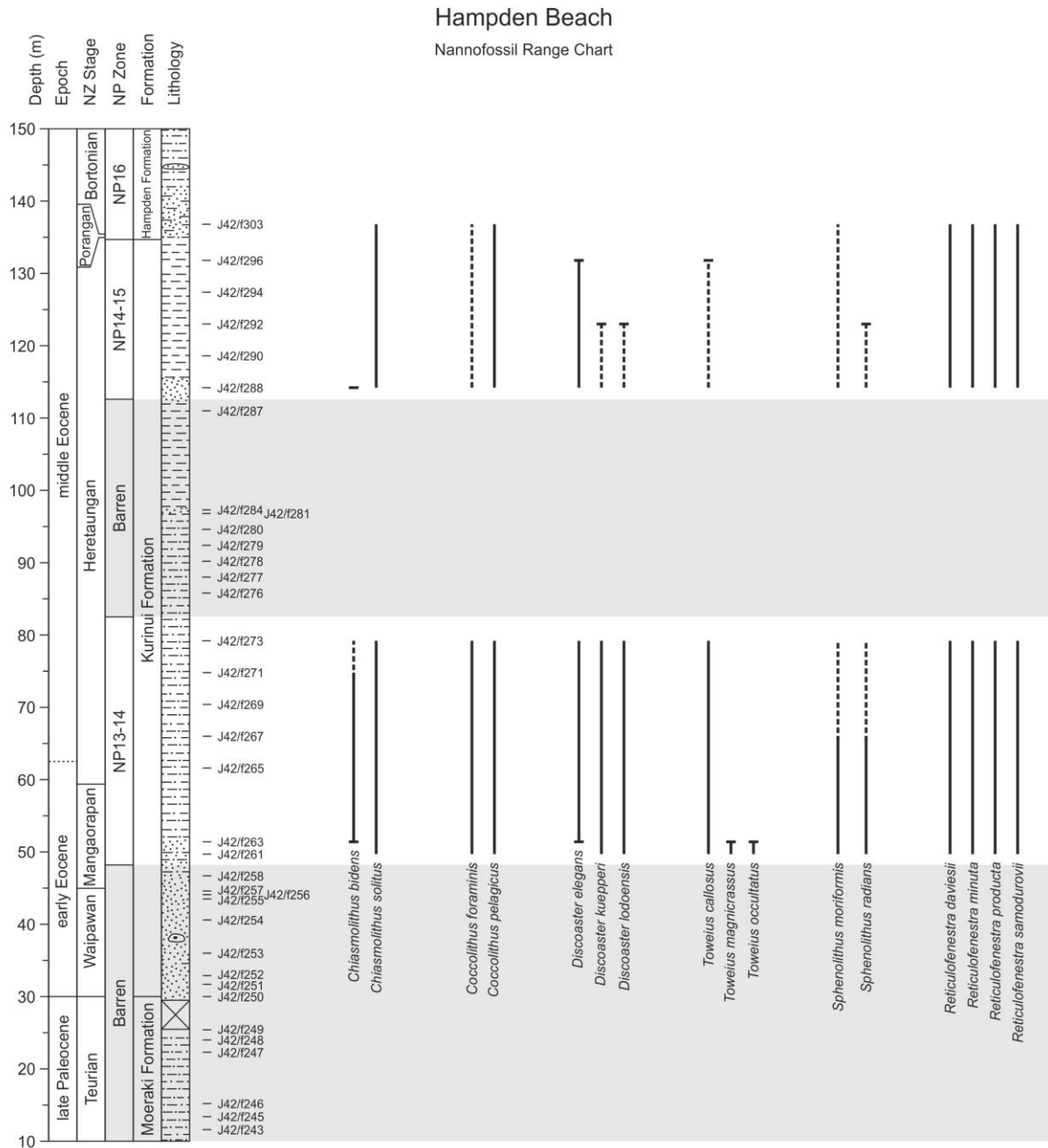


Figure 4.4: Range chart of key nannofossil taxa at Hampden Beach. Epochs and New Zealand Stages are from Morgans (2009). Solid vertical lines indicate consistent occurrence, dashed vertical lines indicate intermittent occurrence, and short horizontal lines indicate limits of stratigraphic range. Nannofossil zone boundaries are placed at the midpoints between samples. Grey shading represents barren intervals.

The middle section of the Kurinui Formation from J42/f276 (85.8 m) to J42/f287 (111 m) contains no nannofossils; however, samples J42/f0288 (114.2 m) to J42/f0296 (131.8 m) taken from the uppermost interval contain rare to abundant nannofossil assemblages. The absence of *R. umbilicus* and *R. reticulata* suggests that these sediments are lower NP16 or

older but the absence of *C. gigas* and *N. alata/fulgens* makes it impossible to differentiate zones NP14–NP16 (Figure 4.4). Morgans (2009) assigned a Heretaungan age to the interval from 114.2 to 131.8 m and this age control is used to constrain samples J42/f0288 to J42/f0296 to a combined NP14–NP15 zone. Assemblages in the upper Kurinui Formation contain abundant *R. samodurovii* with common to few *C. pelagicus*, *R. daviesii*, *R. dictyoda*, *R. minuta* and *R. wadeae*.

Only one sample, J42/f303 (136.8 m), was analysed from the Hampden Formation and it contains a more diverse assemblage than the underlying Kurinui Formation, likely due to better preservation, at least in part. As with the previous samples the absence of key marker taxa makes it difficult to assign it to an NP zone but the absence of *R. reticulata* and *R. umbilicus* suggests that it is lower NP16 or older (Figure 4.4). The assemblage contains abundant *R. minuta* and *R. samodurovii*, with common *R. dictyoda*. Less common taxa include *Blackites* spp., *C. expansus*, *C. pelagicus*, *Discoaster bifax* *P. pulchra*, *R. producta* and *R. wadeae*.

4.3.3 DSDP Site 207

This study analyses 22 samples (cores 14–26) obtained from the Kochi Core Center, Kochi University, Japan. These samples span the lower to middle Eocene (Figure 4.5).

Rhomboaster bramlettei is not observed at DSDP Site 207, but the genus *Fasciculithus* is present in sample 21-207A-26R-3, 100-104 cm (286 m below sea floor [mbsf]). Given the absence of *R. bramlettei* and presence of *Fasciculithus*, it is possible that this lowermost sample correlates with upper NP9. However, there is a sampling gap of ~1.8 m between this sample and the overlying one, which is correlated with NP11, and as such, this interval is assigned to a combined NP9–10 zone. Because the LO of *F. tympaniformis* is in the sample at 286 mbsf, the top of CNE1 is placed at the midpoint between 286 and 284.2 mbsf (Figure 4.5). The assemblage of this combined NP9–10 zone contains abundant *C. pelagicus* with common *T. callosus*, *T. occultatus* and *T. pertusus*. Other taxa include *C. bidens*, *Chiasmolithus californicus*, *C. parvus*, *D. multiradiatus*, *D. salisburgensis*, *Ellipsolithus bollii*, *Ellipsolithus macellus*, *Fasciculithus involutus*, *F. tympaniformis*, *Hornibrookina australis*,

Jakubowskia leoniae, *Neochiastozygus distentus*, *Neochiastozygus junctus*, *S. moriformis*, *T. eminens*, *T. tovae* and *Z. bijugatus bijugatus*.

The FO of *S. radians* is in sample 21-207A-26R-2, 70-74 cm (284.2 mbsf) and therefore the base of Zone NP11 is placed at 285.1 mbsf, the midpoint between this sample (284.2 mbsf) and the underlying sample (286 mbsf). Samples 21-207A-26R-2, 70-74 cm (284.2 mbsf) to 21-207A-25R-CC (279 mbsf) are assigned to Zone NP11. The FO of *T. orthostylus* is in the same sample as the FO of *S. radians* indicating that the base of Zone CNE3 occurs in the same position as the base of Zone NP11. As at mid-Waipara, this provides evidence for an unconformity between Zones NP9–10 and NP11, with possibly all of Zone CNE2 and part of CNE3 missing (Figure 4.5). It should be noted, however, that there is only a 200 kyr difference in age between these two events (Gradstein et al., 2012) and it is possible that there is some separation between these events in the 1.8 m of section between the bounding samples. Assemblages of Zone NP11 contain abundant *C. pelagicus* and common *D. kuepperi*, *T. callosus* and *Z. bijugatus bijugatus*. Less common taxa include *Braarudosphaera bigelowii*, *C. bidens*, *C. californicus*, *C. grandis*, *Chiasmolithus nitidus*, *C. parvus*, *Clausicoccus fenestratus*, *Clausicoccus subdistichus*, *J. leoniae*, *Lophodolithus* spp., *Micrantholithus* spp., *P. exilis*, *P. pulchra*, *S. moriformis*, *Sphenolithus spiniger*, *T. eminens*, *T. occultatus*, *T. pertusus* and *T. tovae*. The FOs of *Reticulofenestra minuta*, *R. producta* and *R. samodurovii* are within this zone.

The FO and FCO of *D. lodoensis* are in sample 21-207A-25R-3, 51-55 cm (276.51 mbsf); therefore, the base of Zones NP12 and CNE4 is placed at the midpoint between 276.51 and 279 mbsf (Figure 4.5). Samples from 21-207A-25R-3, 51-55 cm (276.5 mbsf) to 21-207A-24R-CC (271.5 mbsf) are assigned to Zone NP12. The assemblages are characterised by abundant *C. pelagicus* and *Z. bijugatus bijugatus* and common *D. kuepperi*. Less common taxa include *B. bigelowii*, *C. californicus*, *C. grandis*, *C. nitidus*, *C. solitus*, *C. subdistichus*, *C. foraminis*, *C. formosus*, *Cyclicargolithus luminis*, *D. wemmelensis*, *G. gammation*, *H. seminulum*, *M. inversus*, *Neococcolithes protenus*, *O. occultus*, *R. daviesii*, *R. dictyoda*, *R. minuta*, *R. producta*, *R. samodurovii*, *S. moriformis*, *S. spiniger*, *S. radians*, and *T. orthostylus*. Identification of discoasters to species level in this interval is difficult due to overgrowth.

The base of Zones NP13 and CNE5 is placed at the midpoint between 269.9 and 271.5 mbsf because the LO of *T. orthostylus* is observed in sample 21-207A-24R-CC (271.5 mbsf). Samples 21-207A-24R-4, 110-114 cm (269.9 mbsf) to 21-207A-22R-1, 126-130 cm (247.26 mbsf) are assigned to Zone NP13 (Figure 4.5). Assemblages contain abundant *C. pelagicus* and *Z. bijugatus bijugatus*, with the latter becoming less abundant towards the top of the zone. *Reticulofenestra daviesii*, *R. dictyoda*, *R. minuta*, *R. producta* and *R. samodurovii* are rare to few in the lower part of this zone but become more common towards the top, where *R. circus* makes its first appearance. Other taxa characteristic of Zone NP13 at this site include *C. solitus*, *C. subdistichus*, *C. foraminis*, *C. formosus*, *Coronocyclus bramlettei*, *C. luminis*, *D. barbadiensis*, *D. lodoensis*, *N. protenus*, *R. wadeae*, *S. moriformis*, *S. spiniger* and *S. radians*. *Discoaster kuepperi* is common in the lower part of this zone but decreases in abundance in the upper part.

The FOs of *D. sublodoensis* and common 5-rayed *D. sublodoensis* are found together in sample 21-207A-21R-4, 96-100 cm (242.46 mbsf), which places the base of Zones NP14 and CNE6 at the midpoint between 242.46 and 247.26 mbsf. The base of CNE7 is identified by the LO of *D. lodoensis* at 230.01 mbsf. However, the primary marker for the base of Zone CNE8 (FO of *N. cristata*) is in the succeeding sample at 219.47 mbsf. Because it is possible that an interval corresponding to CNE7 occurs within the ~10.5 m sampling gap, this interval is assigned to combined zone CNE7–CNE8 (Figure 4.5). Samples from 21-207A-21R-4, 96-100 cm (242.46 mbsf) to 21-207A-18R-2, 102-106 cm (207.52 mbsf) are assigned to Zone NP14. The assemblages have common to abundant *C. pelagicus* and *R. samodurovii* and common *R. daviesii*, *R. dictyoda* and *Z. bijugatus bijugatus*. Less common taxa include *C. grandis*, *C. solitus*, *C. subdistichus*, *C. foraminis*, *C. bramlettei*, *D. barbadiensis*, *D. lenticularis*, *D. wemmelensis*, *N. protenus*, *O. occultus*, *R. circus*, *R. minuta*, *R. producta*, *R. wadeae* and *S. moriformis*. *Chiasmolithus expansus* and *N. cristata* first occur in low numbers towards the middle of this zone. *Toweius callosus* is present in low numbers throughout most of the interval and *Toweius magnicrassus* occurs sporadically.

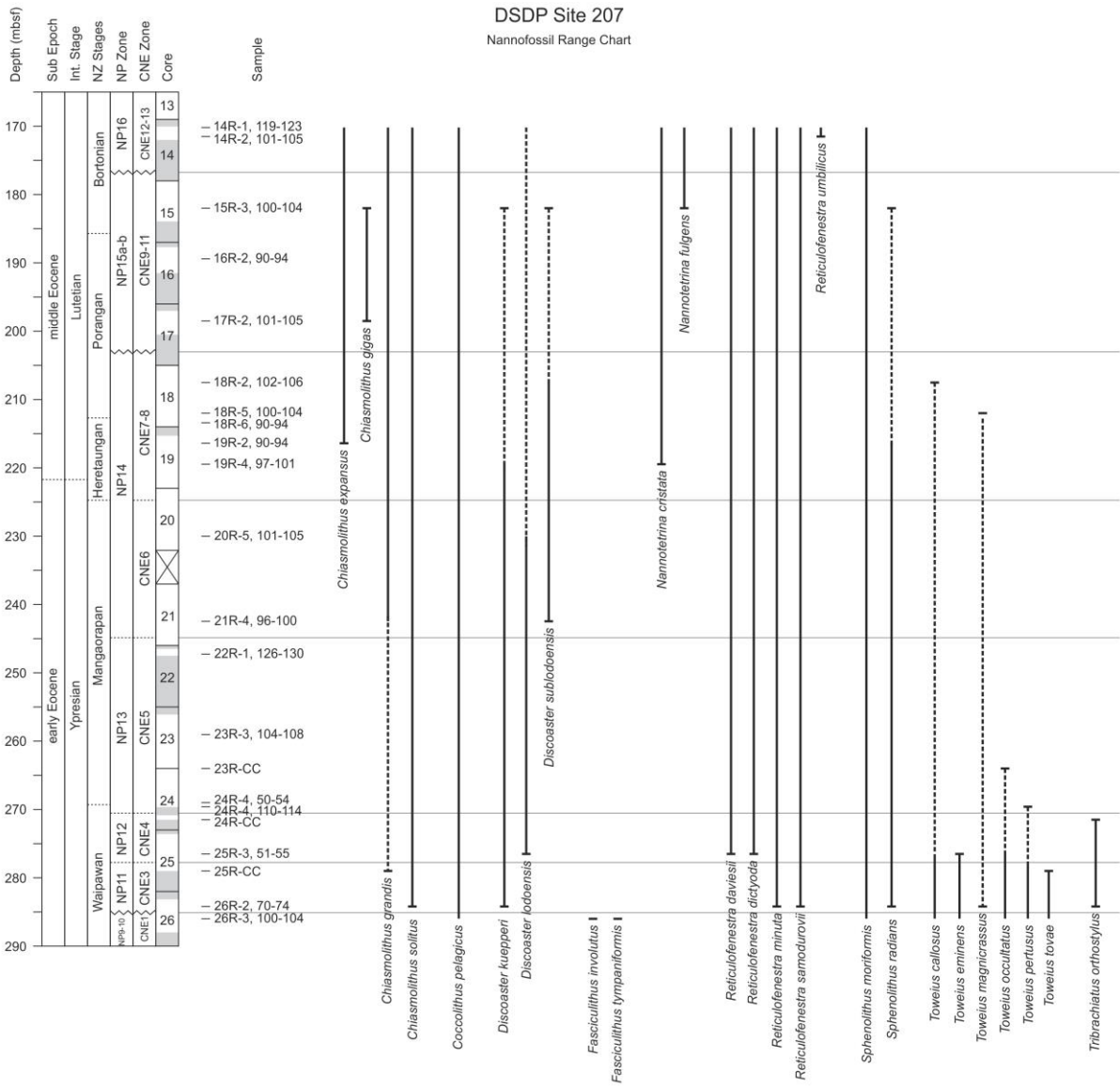


Figure 4.5: Range chart of key nannofossil taxa at Site 207. Solid vertical lines indicate consistent occurrence, dashed vertical lines indicate intermittent occurrence, and short horizontal lines indicate limits of stratigraphic range. Nannofossil zone boundaries are placed at the midpoints between samples and are denoted by grey horizontal lines across the figure. Grey shading represents no core recovery and crosses represent core gaps.

The FO of *C. gigas* is in sample 21-207A-17R-2, 101-105 cm (198.51 mbsf), placing the base of Subzone NP15b and Zone CNE10 at the midpoint between 198.51 and 207.52 mbsf. The base of CNE11 is defined by FO of common *S. cuniculus*. Because this species is absent at Site 207, this interval is assigned to combined CNE10–11. The absence of *N. fulgens* in samples below the FO of *C. gigas* suggests that Subzone NP15a (=Zone CNE9) is missing at Site 207. However, this species is rare at Site 207 and does not occur until the upper part of Subzone NP15b. Therefore, this interval is assigned to combined Subzones NP15a–b (=Zones

CNE9–11) (Figure 4.5). This interval encompasses samples 21-207A-17R-2, 101-105 cm (198.51 mbsf) to 21-207A-15R-3, 100-104 cm (182 mbsf). The assemblages contain abundant *R. samodurovii* and common *C. pelagicus*, *R. dictyoda* and *Z. bijugatus bijugatus*. *Reticulofenestra circus* is common in the lower part of this combined subzone but becomes less abundant towards the top. Conversely *R. daviesii* becomes more abundant towards the top of the combined subzone. Other taxa present include *Blackites* spp., *C. expansus*, *Chiasmolithus modestus*, *C. solitus*, *C. fenestratus*, *C. subdistichus*, *C. formosus*, *D. barbadiensis*, *D. wemmelensis*, *M. inversus*, *N. cristata*, *N. dubius*, *N. minutus*, *R. minuta*, *R. producta*, *R. wadeae* and *S. moriformis*. *Discoaster lodoensis* also occurs within this interval in extremely low numbers.

At DSDP Site 207 the LO of *N. fulgens* is in sample 21-207A-14R-1, 119-123 cm (170.19 mbsf), above the FO of *R. umbilicus* in sample 21-207A-14R-2, 101-105 cm (171.51 mbsf). It is likely that this record of *N. fulgens* is due to reworking. However, it is also possible that *R. umbilicus* occurred earlier in the SW Pacific, given that the genus is thought to have arisen in high southern latitudes (Schneider et al., 2011). Nevertheless, until this can be substantiated by further studies, the presence of *R. umbilicus* is used to assign these samples to Zone NP16 (Figure 4.5). The zone boundary is therefore placed at the midpoint between sample 21-207A-14R-2, 101-105 cm (171.51 mbsf) and 21-207A-15R-3, 100-104 cm (182 mbsf). The base of CNE12 is defined by the LO of *C. gigas*, which is found at 182 mbsf, the same level as the base of Zone NP16. The FCO of *R. umbilicus* marks the base of Zone CNE13; however, this event cannot be identified at Site 207 because the species is rare throughout the interval. Zone NP16 assemblages contain abundant *R. samodurovii* and common *C. pelagicus*, *R. daviesii*, *R. dictyoda*, *R. minuta* and *Z. bijugatus bijugatus*. Less common taxa include *C. solitus*, *C. subdistichus*, *C. bramlettei*, *D. barbadiensis*, *D. wemmelensis*, *G. gammation*, *H. seminulum*, *N. cristata*, *R. circus*, *Reticulofenestra hillae*, *R. producta*, *R. wadeae* and *S. moriformis*.

4.3.4 DSDP Site 277

Smear slides for nineteen samples (cores 36–41) were made from sediment samples held at the Micropaleontology Reference Centre, GNS Science. These samples continue up core from the sequence analysed in a recent PETM study (Hollis et al., 2015) and span the lower

to lower middle Eocene (Figure 4.6). The following results include data collected from the current study as well as raw count data from Hollis et al. (2015) for the lower interval of this section (samples 29-277-44R-3, 145-148 cm to 29-277-42R-2, 3-5 cm [448.45–426.53 mbsf]).

The marker for the base of Zone NP10, *R. bramlettei*, is not observed at DSDP Site 277. *Fasciculithus* is present in samples 29-277-44R-3, 145-148 cm (448.45 mbsf) to 29-277-44R-2, 142-145 cm (446.92 mbsf), indicating that this interval corresponds with NP9–10. As with Site 207, the absence of *R. bramlettei* and presence of *Fasciculithus* may be an indication that part or all of NP10 is missing. However, it is difficult to ascertain the reason for the absence of *R. bramlettei* and these samples are assigned to a combined NP9–10 zone (Figure 4.6). The LO of *F. tympaniformis* is in the sample at 446.92 mbsf and the base of CNE2 is placed at the midpoint between 446.92 and 446.5 mbsf (Figure 4.6). The assemblages in the combined NP9–10 zone contain abundant *C. pelagicus*, *T. callosus* and *T. pertusus*, with few to rare *C. bidens*, *C. luminis*, *D. multiradiatus*, *D. salisburgensis*, *Fasciculithus* spp., *Hornibrookina australis*, *M. inversus*, *N. distentus*, *N. protenus*, and *S. moriformis*.

The base of Zone NP11 is placed at 446.71 mbsf, the midpoint between this sample (446.5 mbsf) and the underlying sample (446.92 mbsf) because the FO of *S. radians* is in sample 29-277-44R-2, 100-103 cm (446.5 mbsf). Samples 29-277-44R-2, 100-103 cm (446.5 mbsf) to 29-277-43R-1, 7-10 cm (434.57 mbsf) are assigned to Zone NP11. The FO of *T. orthostylus* is in the same sample as the FO of *S. radians*, indicating that the base of Zone CNE3 coincides with the base of Zone NP11. As at the previous two sites, this indicates that there is an unconformity between Zones NP9–10 and NP11, with possibly all of Zone CNE2 and part of CNE3 missing (Figure 4.6). However, given the consistency of the co-occurrence of these species across all three study sites, there is also the possibility that these two events occurred at approximately the same time in the SW Pacific. Assemblages in Zone NP11 contain abundant *C. pelagicus* and *T. callosus*, with common to abundant *Z. bijugatus*. Other taxa include *C. bidens*, *Chiasmolithus consuetus*, *C. subdistichus*, *D. kuepperi*, *N. protenus*, *S. moriformis*, *S. radians*, *T. pertusus* and *T. orthostylus*. *Reticulofenestra* spp. first occurs in low numbers towards the middle of this zone.

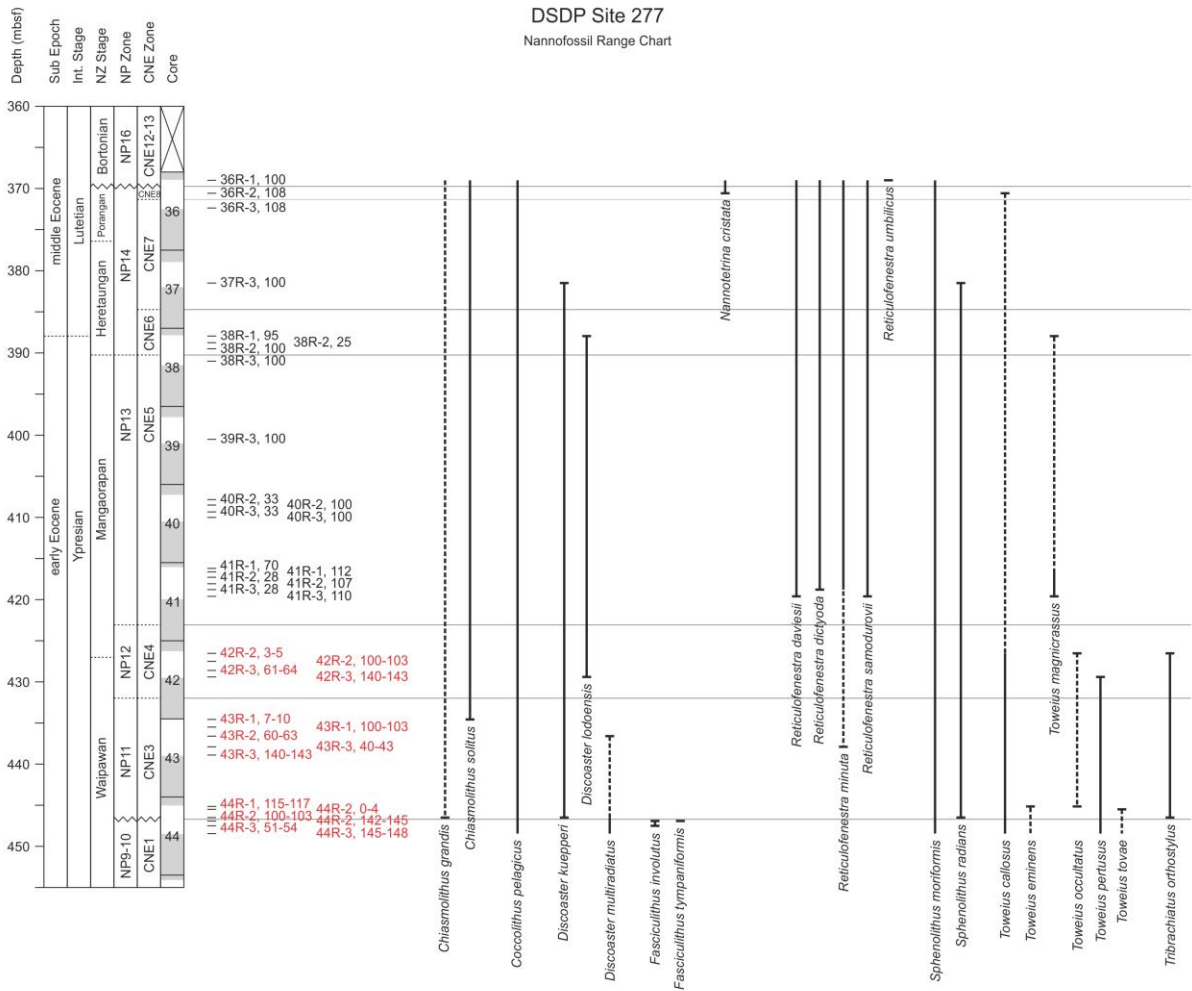


Figure 4.6: Range chart of key nannofossil taxa at Site 277. Solid vertical lines indicate consistent occurrence, dashed vertical lines indicate intermittent occurrence, and short horizontal lines indicate limits of stratigraphic range. Nannofossil zone boundaries are placed at the midpoints between samples and are denoted by grey horizontal lines across the figure. Grey shading represents no core recovery and crosses represent core gaps. Samples shown in red are from Hollis et al. (2015).

The FO and FCO of *D. lodoensis* are defined together in sample 29-277-42R-3, 140-143 cm (429.4 mbsf). The base of Zones NP12 and CNE4 is placed at the midpoint between 434.57 and 429.4 mbsf (431.99 mbsf). Samples from 29-277-42R-3, 140-143 cm (429.4 mbsf) to 29-277-42R-2, 3-5 cm (426.53 mbsf) are assigned to Zone NP12 (Figure 4.6) and the assemblages contain abundant *C. pelagicus* and *Z. bijugatus bijugatus*, and common to abundant *T. callosus*. Less common taxa include *C. bidens*, *C. consuetus*, *C. solitus*, *C. fenestratus*, *C. subdistichus*, *C. luminis*, *Lophodolichus* spp., *M. inversus*, *N. protenus*, *Reticulofenestra* spp., *S. anarrhopus*, *S. moriformis*, *S. radians* and *T. orthostylus*. *Discoaster kuepperi* is rare at the base of this zone but becomes common towards the top.

The base of Zones NP13 and CNE5 is placed at the midpoint between 419.6 and 426.53 mbsf because the LO of *T. orthostylus* is in sample 29-277-42R-2, 3-5 cm (426.53 mbsf). Samples from 29-277-41R-3, 110 cm (419.6 mbsf) to 29-277-38R-3, 100 cm (391 mbsf) are assigned to Zone NP13 (Figure 4.6). Assemblages contain abundant *C. pelagicus* and *Z. bijugatus*, and common *D. kuepperi*, which becomes rare towards the top of the zone. As at Site 207, *R. daviesii*, *R. dictyoda*, *R. minuta*, and *R. samodurovii* are rare in the lower part of this zone but become more abundant towards the top. The FOs of *R. circus*, *R. producta* and *Reticulofenestra scrippsae* are in the middle to upper part of Zone NP13. Other taxa characteristic of this zone include *Calcidiscus bicircus*, *C. solitus*, *C. fenestratus*, *C. subdistichus*, *C. formosus*, *Coccolithus latus*, *C. bramlettei*, *D. barbadiensis*, *D. lodoensis*, *M. inversus*, *N. protenus*, *R. wadeae*, *S. moriformis* and *S. radians*.

The FO of *D. sublodoensis* and the FO of 5-rayed *D. sublodoensis* are found together in sample 29-277-38R-2, 100 cm (389.5 mbsf), which places the base of Zones NP14 and CNE6 at the midpoint between 389.5 and 391 mbsf. The LO of *D. lodoensis* is in the sample at 387.95 mbsf and this marks the base of CNE7, with the boundary placed at the midpoint between 387.95 and 381.5 mbsf. Samples from 389.5 to 387.5 mbsf are therefore assigned to Zone CNE6, which corresponds to lower NP14 (Figure 4.6). The FO of *N. cristata* defines the base of CNE8 and at Site 277 this is in the sample at 370.58 mbsf. Samples 29-277-38R-2, 100 cm (389.5 mbsf) to 29-277-36R-2, 108 cm (370.58 mbsf) are assigned to Zone NP14. Assemblages contain common to abundant *C. pelagicus*, *R. dictyoda* and *R. samodurovii*, with common *R. daviesii*. *Zygrhablithus bijugatus* is common in the lower to middle part of this zone but becomes less abundant towards the top. Less common taxa include *C. modestus*, *C. solitus*, *C. formosus*, *M. inversus*, *R. circus*, *R. minuta*, *R. producta*, *R. wadeae* and *S. moriformis*. *Discoaster barbadiensis*, *D. kuepperi* and *S. radians* are rare in the lower part of this interval and absent towards the top.

As in the mid-Waipara River section, the absence of *N. fulgens* and *C. gigas* suggests that some, if not all, of Zone NP15 is missing at Site 277. Additionally, the markers for the bases of Zones CNE9 (FO of *N. alata* group), CNE10 (FO of *C. gigas*), CNE11 (FO of common *S. cuniculus*) and CNE12 (LO of *C. gigas*) are absent at Site 277 and therefore these zones cannot be defined (Figure 4.6).

The marker for the base of Zone NP16 (*N. alata/fulgens*) is absent at Site 277. Instead, the presence of *R. umbilicus* (>14 µm) in sample 29-277-36R-1, 100cm (369 mbsf) is used to place it within Zone NP16, with the zone boundary placed at the midpoint between 369 and 370.58 mbsf (Figure 4.6). As at Site 207, the abundance of *R. umbilicus* is rare at Site 277, making it difficult to identify the base of Zone CNE13. Assemblages in Zone NP16 contain abundant *R. samodurovii* and common *C. pelagicus*, *R. daviesii*, *R. dictyoda*, *R. minuta*, *R. producta* and *R. wadaeae*. Less common taxa include *C. expansus*, *C. modestus*, *C. solitus*, *M. inversus*, *N. cristata*, *N. dubius*, *R. circus*, *S. moriformis* and *Z. bijugatus bijugatus*.

4.4 Age and correlation

Biostratigraphic datums for DSDP Sites 277 and 207 have been used to construct age-depth plots (Figures 4.7–4.8) using the following conditions: i) compacted sediment accumulation rate (SAR) is assumed to be relatively constant where lithology is uniform; ii) the correlation line should lie above the LO and below the FO of biomarkers; and iii) hiatuses are inferred based on the biostratigraphic evidence outlined in the preceding section and where applicable, the clustering of bioevents. The second condition is based on the assumption that events are isochronous, therefore, this condition would fail if the events prove to be diachronous. In addition to the nannofossil events outlined in the preceding section, foraminiferal (H. Morgans, P. Strong pers. comm. 2016) and radiolarian (K. Pascher pers. comm. 2016) datums have also been included in order to improve the robustness of the age models (Appendix D).

Correlation lines represent the line of best fit and are placed to accommodate as many of the biostratigraphic datums as possible, with primary importance given to nannofossil and foraminiferal events. Intervals of very low sedimentation rate, which are indicated on the plots as alternative lines of fit (Figures 4.7–4.8), are interpreted as hiatuses. Vertical lines on the age depth plots indicate the distance between bounding samples and the arrow indicates the direction in which an event could move. A FO can move downwards, as the biomarker may be present in the interval between the sample it was found in and the underlying one. Likewise, a LO can move upwards, as the biomarker may be present in the interval between the sample it was found in and the overlying one.

DSDP Site 207

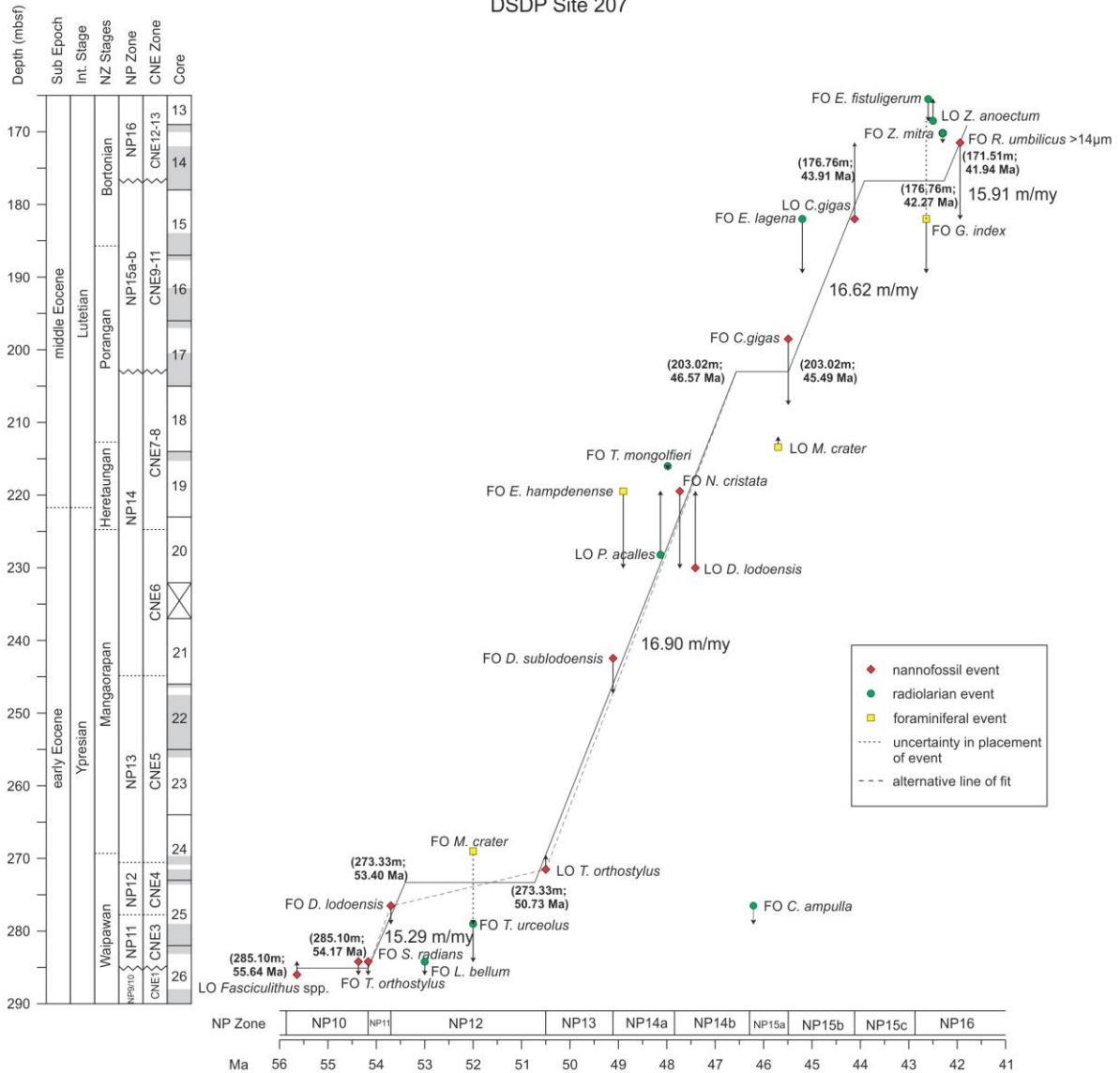


Figure 4.7: Age-depth plot for DSDP Site 207. Vertical lines represent the uncertainty between bounding samples and arrows indicate the direction in which the event could move (see text for explanation). The line of correlation represents intervals of constant sediment accumulation rate (SAR) and hiatuses. Bold labels (depth; age) represent points on the line where there is a change in SAR. New Zealand (NZ) Stages are based on bioevents in Raine et al. (2015). FO = first occurrence, LO = last occurrence. Grey shading represents no core recovery and crosses represent core gaps.

DSDP Site 207 has a relatively constant SAR (~15–16 m/Myr) interrupted by four hiatuses (Figure 4.7). A similar pattern is observed at Site 277 (Figure 4.8), although the SAR is higher (~16–25 m/Myr). This higher SAR is consistent with previous estimates of 19–22 m/Myr within the Paleogene at Site 277 (Kennett et al., 1975). Hollis et al. (1997) found a much lower rate of sedimentation of 5.6 m/Myr across a similar interval. However, their rate is calculated from the line of best fit in their age-depth plot, which excludes three potential

hiatuses through the interval. The dotted line shown in figure 5 of their publication is a closer fit with the age-depth plot shown in this study.

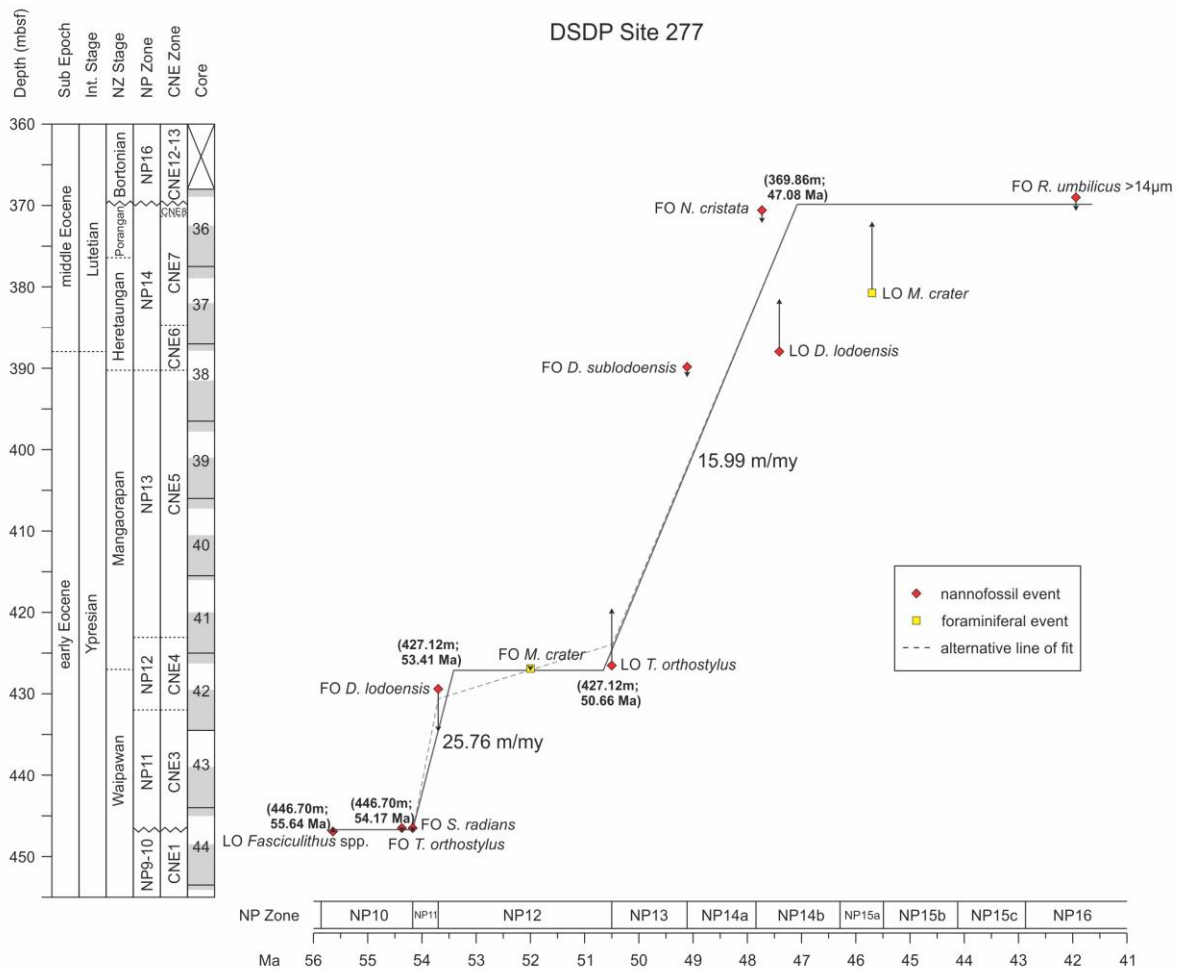


Figure 4.8: Age-depth plot for DSDP Site 277. Vertical lines represent the uncertainty between bounding samples and arrows indicate the direction in which the event could move (see text for explanation). The line of correlation represents intervals of constant sediment accumulation rate (SAR) and hiatuses. Bold labels (depth; age) represent points on the line where there is a change in SAR. New Zealand (NZ) Stages are based on bioevents in Raine et al. (2015). FO = first occurrence, LO = last occurrence. Grey shading represents no core recovery and crosses represent core gaps.

A hiatus spanning parts of Zones NP9–10 and NP11 is identified at both sites, based on the LO of *Fasciculithus* spp., FO of *T. orthostylus* and FO of *S. radians*, as previously discussed. Identification of this hiatus at Site 207 is in agreement with Edwards (1973b) who noted an unconformity at ~285 mbsf. Furthermore, he suggested that this is a regional unconformity also identified at Sites 206 and 208 and is associated with the Paleocene/Eocene boundary. Colour changes in the core are observed in the core logs at Site 207 at ~284.92 and 285.71

mbsf and either of these changes may be associated with this unconformity. Kennett et al. (1975) suggested that this regional unconformity may also be present at Site 277 and a disrupted interval is observed in core logs between 446.5–446.92 mbsf, with a colour change at ~446.83 mbsf.

A second hiatus is placed at ~427.12 mbsf at Site 277 and ~273.33 mbsf at Site 207. The FO of *D. lodoensis*, LO of *T. orthostylus* and FO of the foraminifera *Morozovella crater* are in close proximity to each other at both sites and this clustering of events suggests very low SARs or a hiatus spanning part of Zone NP12 (Figures 4.7–4.8). At Site 277 the colour of the core changes at ~426.66 mbsf, which may represent a change in lithology associated with this unconformity. At Site 207 there is no distinct change in colour from 271.5–276.51 mbsf; however, there was less than 100% recovery in core 24 and the unconformity may actually occur within this non-recovered interval.

At Site 207 a third hiatus is tentatively placed at ~203.02 mbsf, between Zone NP14 and Subzone NP15a–b. This is based on the FO of *C. gigas*, which marks the base of NP15b, and the absence of *N. fulgens* in underlying samples, suggesting that Subzone NP15a is missing. However, as noted in the preceding section, a sampling gap of ~9 m occurs at this part of the section, which may contain the boundary between Zone NP14 and Subzone NP15a. This hiatus is placed between the base of core 17 and top of core 18; however, poor recovery in core 17 makes it impossible to identify this unconformity in core logs.

At Site 277 the uppermost hiatus is placed at ~369.86 mbsf and represents time missing between Zones NP14 and NP16. This is based on the absence of *N. fulgens* and *C. gigas*, which mark the base of Subzones NP15a and NP15b, respectively. A similar hiatus is observed at Site 207 at ~176.76 mbsf, between Subzone NP15b and Zone NP16, based on the LO of *C. gigas* and FO of the foraminifera *Globigerinatheka index*. At both sites it is difficult to accurately identify the base of NP16 due to the absence of *B. gladius* and sporadic occurrence of *N. fulgens*. *Reticulofenestra umbilicus* >14 µm is used to approximate the base of NP16; however, at Site 207 this taxon first occurs in low numbers at the same depth as the LO of *C. gigas*. This suggests that *R. umbilicus* >14 µm may evolve earlier at this particular latitude. This hiatus is unable to be recognised in core logs at Site 207 because of

the incomplete recovery of core 14. At Site 277 the core is fragmented between 369 and 370.58 mbsf and the unconformity could occur between any of the breaks in core through this interval.

4.5 Summary

All four study sites span the interval from lower Eocene to uppermost middle Eocene (nannofossil Zones NP10 to NP16; Waipawan to Bortonian NZ stages) (Figure 4.9). Due to poor preservation and barren intervals in the Hampden Beach section, identification of nannofossil zones is difficult. Consequently, NZ Stages determined by foraminiferal biostratigraphy for Hampden Beach (Morgans, 2009) are used to improve correlation with the other sections.

SARs at Sites 207 and 277 are relatively constant at ca. 15–17 m/Myr but are interrupted by three unconformities that can generally be correlated across sites. The first of these is recognised in the mid-Waipara River section and DSDP Sites 207 and 277 (Figure 4.9). It occurs at the base of the interval, in the lower Eocene (lower Waipawan), where part or all of Zone NP10 is missing. The second hiatus is identified at Sites 207 and 277, where the clustering of events (*T. orthostylus*, *D. lodoensis* and *M. crater*) indicates a very low sedimentation rate or hiatus during NP12 (upper Waipawan–lower Mangaorapan). Significantly, this interval is relatively expanded at mid-Waipara. The next unconformity that is observed at mid-Waipara and DSDP Site 277 and is also evident in the Hampden section, lies at or near the base of the Bortonian stage. At Hampden a very thin Porangan interval lies above the unconformity. At mid-Waipara the entire Porangan is missing, which includes all of Zone NP15. At Site 277, foraminiferal biostratigraphy indicates a Porangan interval underlies the unconformity even though Zone NP15 is missing. At Site 207, the overall succession is more complete over this stratigraphic interval but two unconformities are inferred. The first occurs within the middle Eocene (Porangan), where a potential hiatus is implied between Zones NP14 and NP15a–b. The uppermost unconformity at Site 207 lies at the base of the Bortonian stage with the upper part of Zone NP15 is missing.

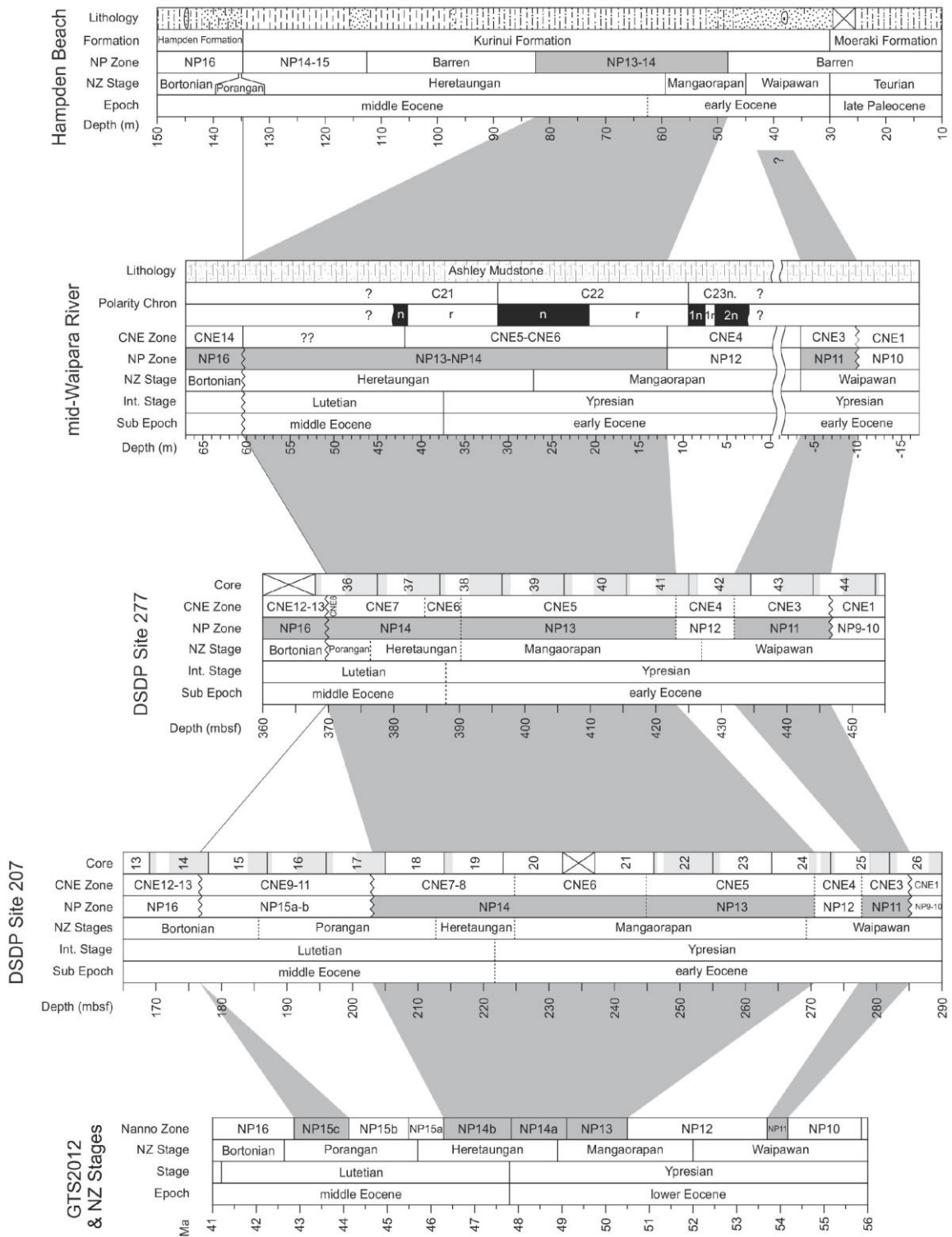


Figure 4.9: Biostratigraphy of all four study sites compared with the geologic time scale of Gradstein et al. (2012; GTS2012) integrated with the New Zealand (NZ) Stages calibrated by Raine et al. (2015). Calcareous nannofossil zonation is from Martini (1971; NP zones) and Agnini et al. (2014; CNE zones).

CHAPTER 5: PALEOENVIRONMENTAL ANALYSIS

5.1 Introduction

This chapter presents the paleoenvironmental results for all study sites. In Section 5.2, preservation and diversity are analysed for each site. Pearson's Correlation coefficient (r) is used to determine the degree of covariance between preservation indices, as well as between diversity measures and carbonate content, where available (Table 5.1). In Section 5.3, the paleoecological affinities of key taxa/species are discussed with reference to past studies and this information is used in Section 5.4 to compare assemblage data with other paleotemperature data (e.g. TEX_{86} and $\delta^{18}O$). In Section 5.5, the early Eocene *Toweius–Reticulofenestra* turnover event is discussed and the timing of the event is compared between SW Pacific sites and to other areas beyond this study.

5.2 Preservation and diversity

In this section the following conventions are adopted regarding the discussion of correlation coefficients: >0.8 is described as a strong correlation, >0.5 to ≤ 0.8 is described as a moderate correlation, and ≤ 0.5 is described as a weak correlation. P-values are also calculated to determine the significance of the correlation.

5.2.1 Mid-Waipara River section

Three indices have been used to analyse preservation/dissolution at this site (see Chapter 2): visual observation of preservation (VOP), relative abundance of *Zygrhablithus bijugatus* and the *Chiasmolithus* ratio. All indices are significantly correlated with each other and with $CaCO_3$ content ($p < 0.02$; Table 5.1). These correlations indicate that in this section, all indices can be used as guides to preservation and that preservation is linked to carbonate content.

Table 5.1: Correlation coefficients for CaCO₃ content, diversity measures and preservation/dissolution indices. P-values only included where p<0.1. VOP = visual observation of preservation.

	Preservation/dissolution indices				Diversity measures	
	<i>Z. bijugatus</i> %	VOP	<i>Chiasmolithus</i> ratio	Unidentified rims %	Taxon richness (S)	Shannon diversity (H)
mid-Waipara River						
CaCO ₃ content	0.6379 n=29 p<0.001	0.5866 n=29 p<0.002	-0.4598 n=29 p<0.02		0.3906 n=29 p<0.05	0.2961 n=29
<i>Z. bijugatus</i> %		0.7019 n=34 p<0.001	-0.4080 n=34 p<0.02		0.3517 n=34 p<0.05	0.3466 n=34 p<0.05
VOP			-0.5309 n=34 p<0.002		0.3521 n=34 p<0.05	0.2308 n=34
<i>Chiasmolithus</i> ratio					-0.4812 n=34 p<0.005	-0.3833 n=34 p<0.05
Taxon richness (S)						0.7878 n=34 p<0.001
Hampden Beach						
VOP					0.6373 n=13 p<0.02	-0.2939 n=13
Taxon richness (S)						0.5080 n=13 p<0.1
DSDP Site 207						
<i>Z. bijugatus</i> %		-0.2999 n=22	0.2802 n=22	-0.1061 n=22	0.0502 n=22	-0.1996 n=22
VOP			-0.4203 n=22 p<0.1	-0.5785 n=22 p<0.005	0.2039 n=22	0.3004 n=22
<i>Chiasmolithus</i> ratio				0.0286 n=22	-0.0822 n=22	0.1841 n=22
Unidentified rims %					-0.1234 n=22	-0.5771 n=22 p<0.005
Taxon richness (S)						0.3307 n=22
DSDP Site 277						
<i>Z. bijugatus</i> %		0.1785 n=34	0.3436 n=19	-0.2032 n=19	-0.0883 n=34	-0.4141 n=34 p<0.02
VOP			-0.0258 n=19	-0.1612 n=19	-0.4751 n=34 p<0.005	-0.6310 n=34 p<0.001
<i>Chiasmolithus</i> ratio				-0.1462 n=19	0.1897 n=19	-0.0346 n=19
Unidentified rims %					-0.1132 n=19	-0.3202 n=19
Taxon richness (S)						0.8160 n=34 p<0.001

Preservation is poor in Zones NP10—NP11 where CaCO₃ is <15% (Figure 5.1). Preservation is moderate to good from the base of Zone NP12 to lower NP13–14 (with CaCO₃ content fluctuating through this interval but overall higher than elsewhere in the section (max. 26.3%). Preservation declines from moderate to very poor in upper NP13–14 where CaCO₃ content decreases to a minimum of 8.5%. An improvement in preservation is observed in Zone NP16, although CaCO₃ content remains low, which may be due to a lithological change across the unconformity at the base of this zone from mudstone to glauconite dominated mudstone. It is possible that a change in clay content may account for improved preservation even though CaCO₃ content declines, as has been suggested by previous workers (Pearson & Burgess, 2008; Firth et al., 2013).

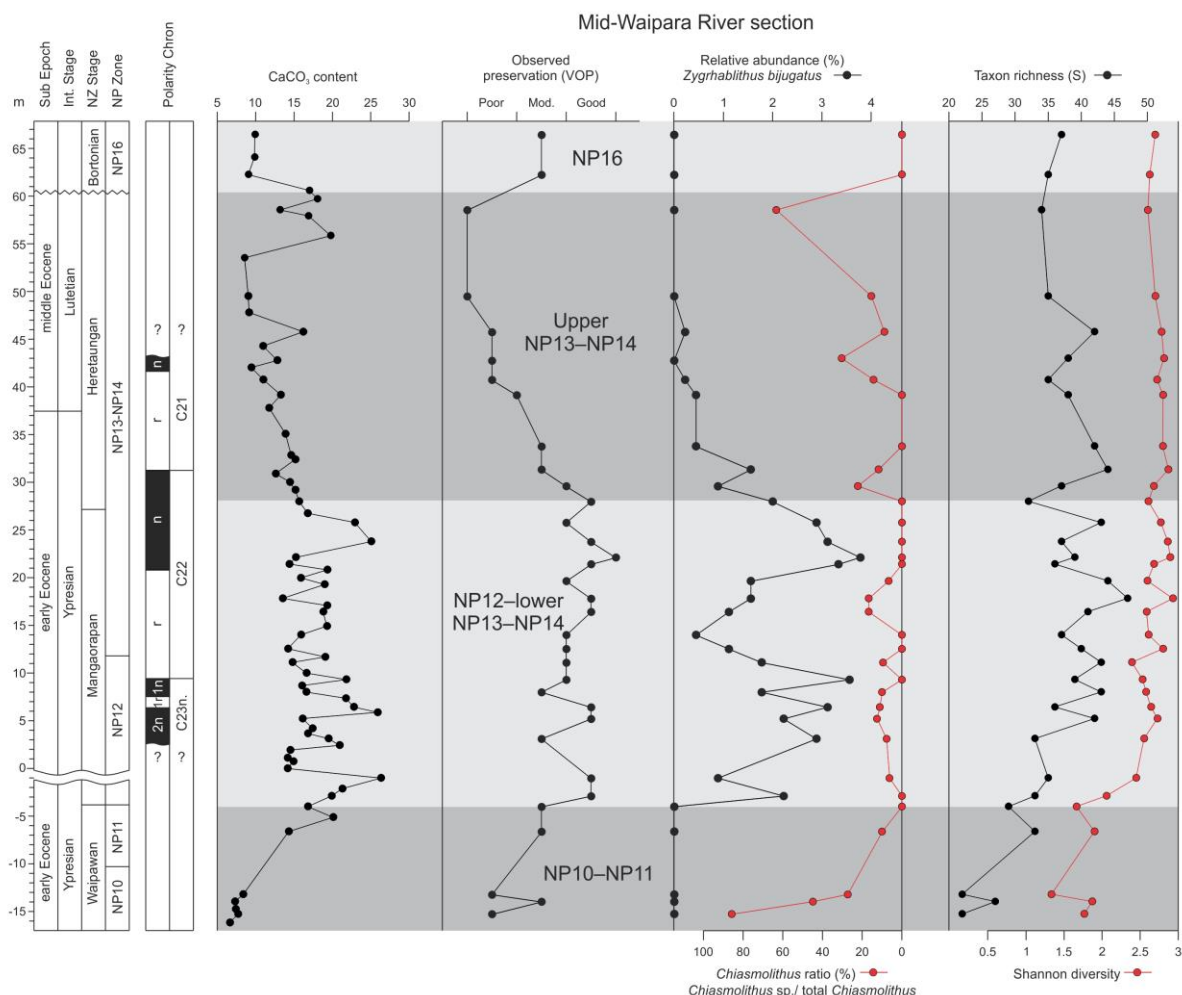


Figure 5.1: Comparison of calcium carbonate (CaCO₃) content, preservation/dissolution indices, taxon richness and Shannon diversity for the mid-Waipara River section. Grey shading represents intervals discussed in the text.

Diversity has previously been correlated with paleotemperature, where high diversity is generally associated with warmer climates and vice versa (Shamrock & Watkins, 2012). However, diversity is also affected by preservation. Differential dissolution may remove some taxa from the assemblage, thereby skewing the actual representative number of species present and biasing community composition towards more resistant taxa (Roth & Thierstein, 1972; Jiang & Wise, 2009). For instance, *Discoaster* is one of the most resistant genera of nannofossils and an increase in dissolution can result in an artificial increase in abundance of this group (Roth & Thierstein, 1972). Census data based on standard counts of 450 specimens were used to calculate Taxon Richness (S) and Shannon Diversity (H), which were both compared with the preservation indices to determine if a correlation exists between the two factors.

Taxon richness, Shannon diversity and preservation indices are weakly correlated (Table 5.1). Diversity and richness are lowest in NP10–11, corresponding to poor preservation through this interval. An increase in diversity and richness is seen from the base of NP12, reaching maximum values in lower Zone NP13–14 and this is consistent with the increase in preservation. In the upper part of the combined NP13–14 zone, diversity remains stable. Richness decreases slightly across this upper interval and is consistent with the decrease in preservation but still remains higher than values in the lower interval. Overall, the covariance between preservation and diversity indices suggests that preservation is the primary factor influencing diversity in this section. This observation needs to be borne in mind when analysing changes in assemblage composition (Section 5.3).

5.2.2 Hampden Beach section

The lack of nannofossils in some intervals at Hampden Beach precludes use of some of the preservation/dissolution indices and, therefore, only the VOP index is analysed for this section (Figure 5.2). Additionally, CaCO₃ measurements are not available for this section, but based on lithology, it is generally less calcareous than the mid-Waipara River section, with two intervals that are non-calcareous (Figure 5.2). The lower portion of the section, spanning the Teurian to lower Mangaorapan, is completely barren of calcareous nannofossils. Assemblages in the combined NP13–14 zone (Mangaorapan–lower Heretaungan) have moderate to good preservation and this is comparable to the record at

mid-Waipara River. Preservation begins to deteriorate in the lower Heretaungan and nannofossils are absent in the mid-Heretaungan. Improved preservation is observed at the base of the combined Zone NP14–15 (upper Heretaungan) and this is likely associated with a change in lithology at this level from silty mudstone to glauconitic sandy siltstone. Preservation is poor to moderate through the remainder of this combined zone and this parallels the record seen at mid-Waipara, where preservation is poor in the upper Heretaungan. The topmost sample in Zone NP16 (Bortonian) contains well-preserved nannofossils, which is similar to mid-Waipara River.

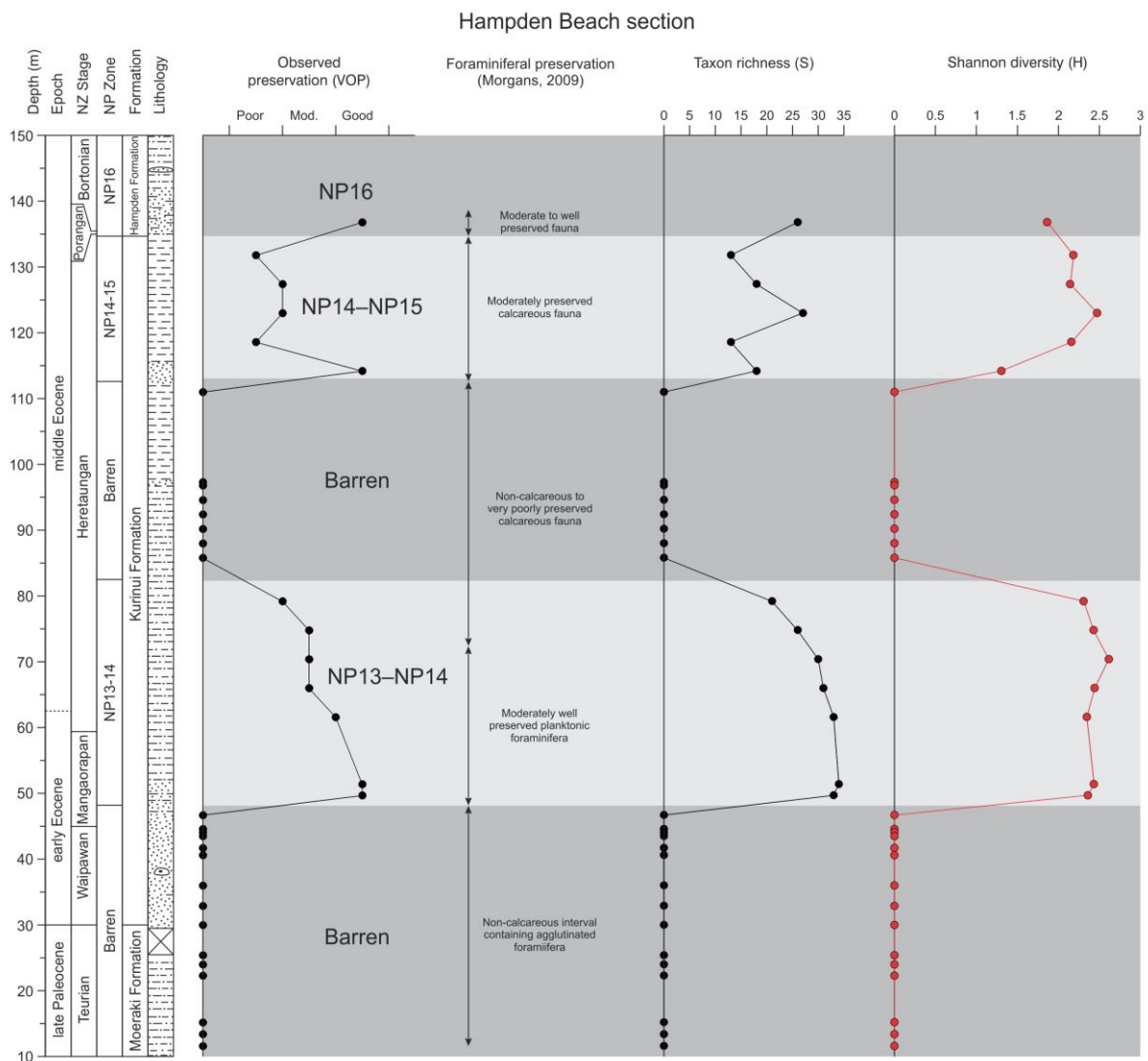


Figure 5.2: Comparison of preservation, taxon richness and Shannon diversity for the Hampden Beach section. Estimates of foraminiferal preservation are from Morgans (2009). Grey shading represents the intervals discussed in the text.

Taxon richness and the VOP preservation index are moderately correlated (Table 5.1). Shannon diversity and taxon richness at Hampden Beach have similar patterns to mid-Waipara River. Both diversity measures are at their highest within the combined Zone NP13–14 at Hampden Beach and this corresponds with moderate to good preservation through this interval. Taxon richness is lower in the combined Zone NP14–15, which coincides with a decrease in preservation. Shannon diversity, however, remains high through this combined zone at Hampden Beach.

5.2.3 DSDP Site 207

As at mid-Waipara River, three indices have been used to analyse preservation/dissolution: VOP, relative abundance of *Z. bijugatus* and the *Chiasmolithus* ratio. Additionally, there are a large number of unidentified nannofossil rims throughout the section, which are likely a result of dissolution. The relative abundance of these rims is therefore used as a fourth preservation index at this site and at DSDP Site 277. A moderate correlation is observed between this proxy and VOP (Table 5.1). However, the relative abundance of *Z. bijugatus* is not correlated with these other indices, indicating that this index is not a robust guide to preservation at this site. It is likely that *Z. bijugatus* has become overgrown during early diagenesis at Site 207, making it resistant to dissolution. Also, there is only a weak correlation between the *Chiasmolithus* ratio and other indices. This might be explained by the low abundance of this genus in parts of the section, particularly in Zones NP9–10 to NP13, where relative abundance averaged <1% of the total assemblage. Such low values make it difficult to calculate an accurate ratio between complete versus incomplete *Chiasmolithus* in the assemblage.

Based on the VOP and rim indices, preservation is poor to moderate and dissolution levels are moderately high at the base of the section in Zones NP10–12. A slight improvement in preservation is observed through Zones NP13 and NP14 and dissolution levels are low through this interval. Preservation is good in upper NP14 and dissolution levels are at a minimum, but preservation worsens and dissolution increases through NP15a–b. The indices indicate good preservation and low dissolution at the very top of the section in NP16 (Bortonian), similar to the pattern seen in the mid-Waipara and Hampden sections.

Shannon diversity and the percentage of unidentified rims are negatively correlated (Table 5.1), suggesting that diversity is strongly influenced by dissolution. The diversity and richness trends are consistent with this correlation for much of the record, with low values at the base of the section, and then increasing through the lower part and decreasing in the upper part. There is also a small increase in richness in the Bortonian. However, the maximum values for diversity and richness occur within the NP13–lower NP14 interval (Mangaorapan Stage) rather than the interval where preservation is best (upper NP14). This suggests that this diversity peak is not an artefact of preservation.

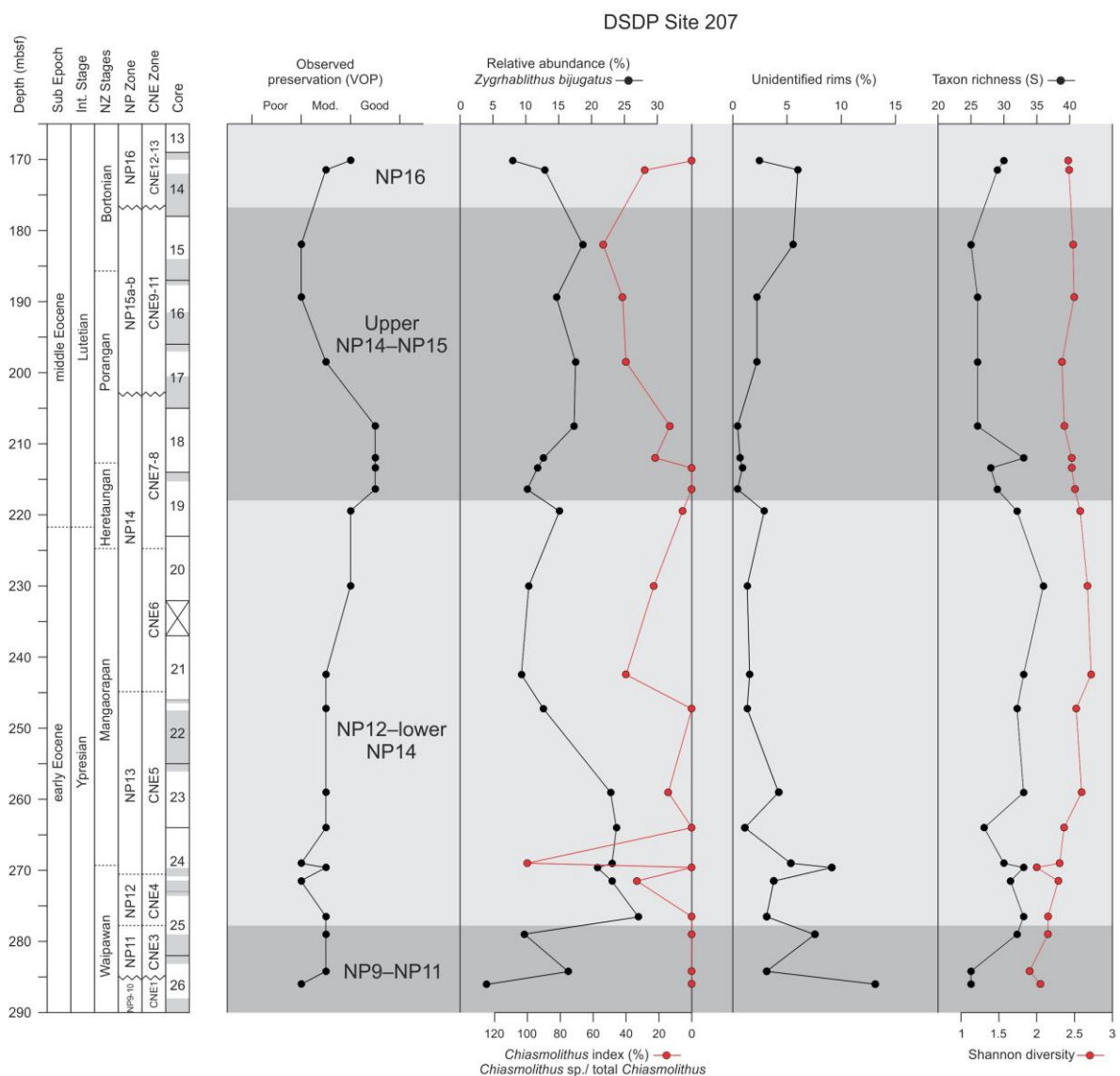


Figure 5.3: Comparison of preservation/dissolution indices, taxon richness and Shannon diversity for DSDP Site 207. Grey shading represents intervals discussed in the text.

5.2.4 DSDP Site 277

As at DSDP Site 207, four indices are used to analyse preservation/dissolution: VOP, relative abundance of *Z. bijugatus*, the *Chiasmolithus* ratio and percentage of unidentified rims (Figure 5.4). Because the results for DSDP Site 277 are a combination of data from this study and that from Hollis et al. (2015), some of the indices do not extend to the base of the studied interval. At Site 277, none of the other preservation indices exhibit a significant correlation with VOP (Table 5.1). This is probably due to relatively little variation in preservation as indicated by VOP ranging from poor to moderate through the section. Despite the lack of covariance between indices, a parallel trend is noted in the upper part of the section, where preservation worsens (VOP) and dissolution increases (*Z. bijugatus*, unidentified rims) within Zones NP13–14. As with the previous sites, preservation improves (VOP) and dissolution decreases (unidentified rims) in NP16 (Bortonian).

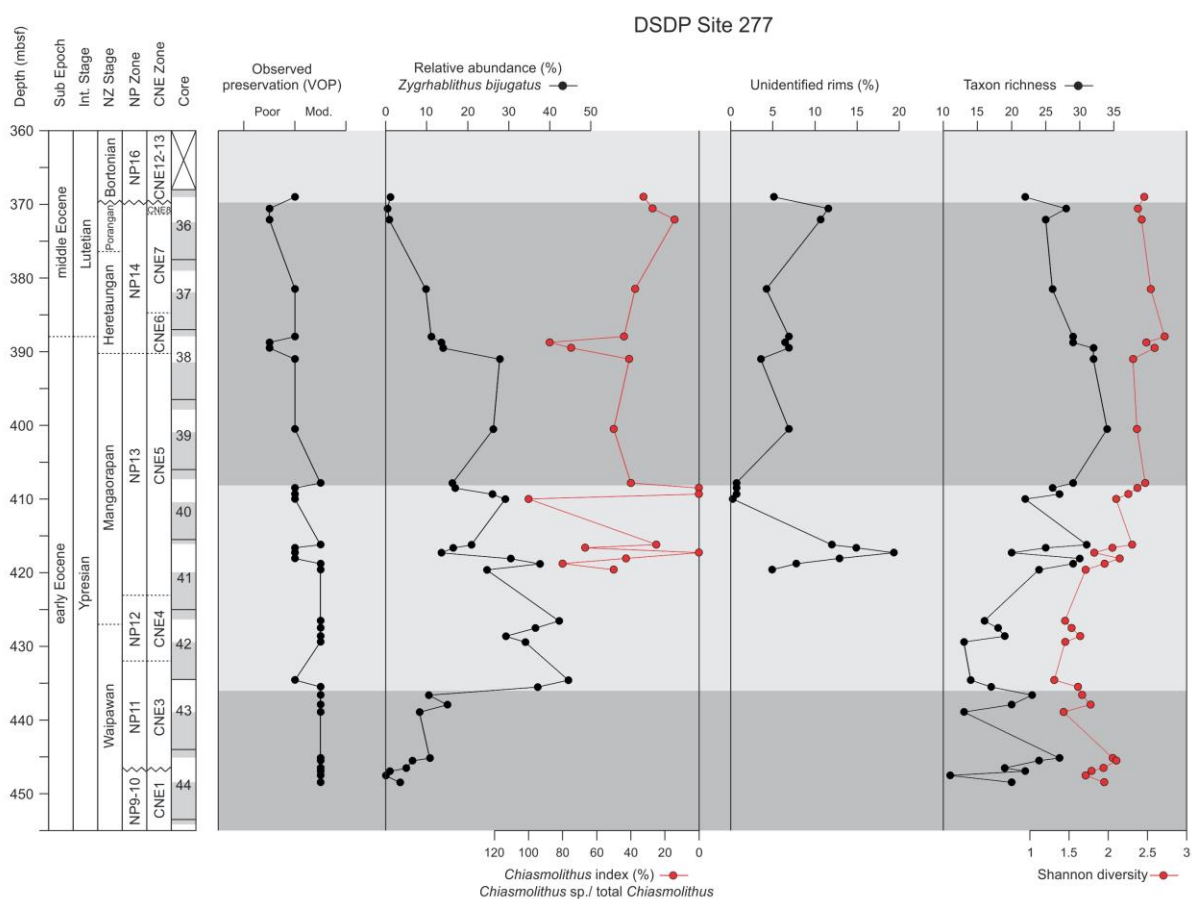


Figure 5.4: Comparison of preservation/dissolution, taxon richness and Shannon diversity for DSDP Site 277. Grey shading represents intervals discussed in the text.

In the lower part of the section the relative abundance of *Z. bijugatus* increases sharply in upper Zone NP11 (Waipawan) and this is also observed at Site 207 and mid-Waipara. Abundance of this species decreases in Zones NP13–14 at mid-Waipara and Site 277, eventually becoming absent towards the top of Zone NP14. This parallels the general trend of moderate–good preservation across Zones NP12 to lower NP13 and decreasing preservation through Zones NP13–14.

At Site 277, Shannon diversity is negatively correlated with VOP and *Z. bijugatus* abundance (Table 5.1). Additionally, taxon richness has a moderate negative correlation with VOP. In both these cases, the correlation is difficult to reconcile with the observed trends and is not thought to relate to a causal relationship. Diversity and richness tend to increase through the section over the same interval that preservation deteriorates, which suggests that in this section preservation has little influence on diversity.

5.2.5 Summary

Application of the preservation/dissolution indices provides variable results across the four study sites (Figure 5.5A–C). VOP is considered to be the most consistent index because it exhibits the strongest correlations with other indices at mid-Waipara and Site 207, and also exhibits a clear relationship to CaCO₃ content at mid-Waipara. The relative abundance of *Z. bijugatus* is moderately correlated with VOP at mid-Waipara and proves to be an effective guide to preservation at that site (Figure 5.5A). Correlation of *Z. bijugatus* with other indices at DSDP Sites 207 and 277 is not as strong. However, at Site 277 this index parallels general preservation trends. Interpretation of this index at Site 207 is more difficult, but an increase in abundance through Zone NP11–lower NP13 and decrease through upper NP13–NP14 is consistent with mid-Waipara and Site 277.

The *Chiasmolithus* ratio proves useful at mid-Waipara River, where it is moderately correlated with VOP (Figure 5.5B). Although correlation coefficients are not as high between these indices at Site 207, there is still a moderate association between the two. The difference in the degree of correlation of these indices across these two sites is probably due to the difference in relative abundance of *Chiasmolithus*, with lower values at Site 207 making it difficult to capture an accurate representation of the ratio between incomplete

and complete specimens. The *Chiasmolithus* ratio does not appear to perform well as an index at Site 277, as it fails to record the deterioration in preservation in the upper part of the section that is evident in all other indices.

The percentage of unidentified rims is used as an additional index at DSDP Sites 207 and 277 and is moderately correlated with VOP at Site 207 (Figure 5.5C). Although the association between these two indices is not as strong at Site 277, a parallel trend is observed in the upper part of the section, with decreases in VOP and *Z. bijugatus*, and concomitant increase in unidentified rims.

Similar trends in preservation are evident in the mid-Waipara River and Hampden Beach sections. Intervals of poor preservation at mid-Waipara River correspond to barren intervals at Hampden Beach and the primary interval of good to moderate preservation corresponds with the NP12–14 interval in both sections. The barren intervals at Hampden Beach probably represent the extreme end of high dissolution or no original carbonate.

As mentioned previously, the level of preservation at Site 277 is difficult to ascertain for the base of the section due to the lack of indices through this interval. Preservation through NP12 to lower NP13 is moderate to good but then declines across NP12–14. At Site 207 preservation is similar to mid-Waipara River and Hampden Beach, where preservation in the lower part of the section is poor to moderate. Preservation improves in upper Zone NP14 at Site 207, which differs from the poor to moderate preservation at the onshore sections. Preservation deteriorates across the combined NP15a–b zone but, as at mid-Waipara River and Hampden Beach, it improves at the top of the section in the Bortonian.

As expected, Shannon diversity and taxon richness are positively correlated for all four sites (Figure 5.5D). Diversity and richness are at their lowest through Zones NP9–11 at all sites. There is more variability at Site 277 through this interval with slightly higher diversity and richness in lower Zone NP11 and lower diversity and richness in upper Zone NP11–12. At mid-Waipara River and Site 207, diversity increases in Zone NP12 and becomes stable across Zones NP13–NP16. At Site 277, diversity increases across Zones NP13–14 but there is more variability than at the other sites. Diversity at Hampden Beach is highest during the

combined Zones NP13–14 and remains at similar levels in the combined Zones NP14–15. Taxon richness increases in Zone NP12 at mid-Waipara and Sites 207 and 277, reaching a maximum in NP13–14. A slight decrease in richness occurs in Zone NP14 at mid-Waipara and Site 277, and in late NP14–NP15 at Site 207. At Hampden Beach richness is highest in the combined Zones NP13–14 but begins to decrease towards the upper part of this zone and is variable through the combined Zones NP14–15. Both onshore sites and DSDP Site 207 increase in richness in NP16; however, this is probably exaggerated due to the unconformity between Zones NP14–15 and NP16.

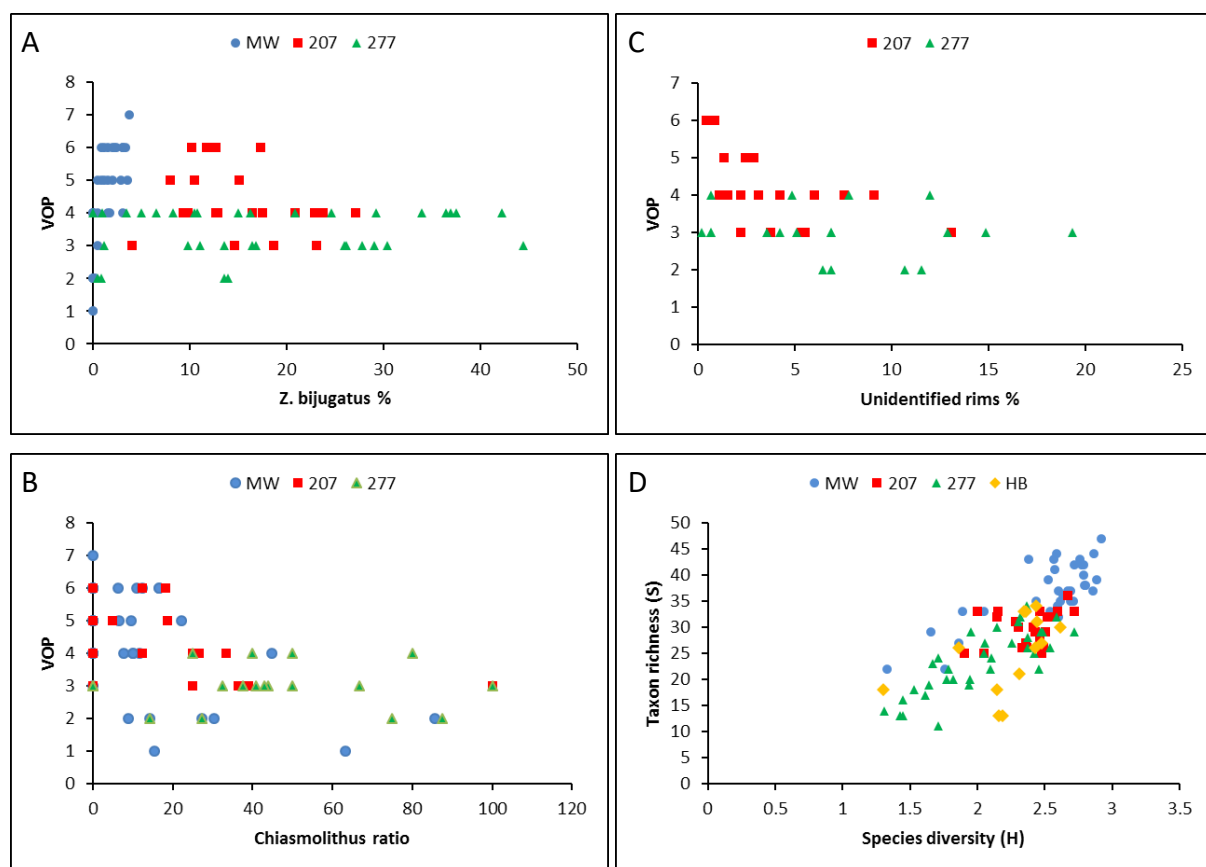


Figure 5.5: Cross-plots showing the association between preservation/dissolution indices and diversity measures. MW = mid-Waipara River, HB = Hampden Beach, 207 = DSDP Site 207 and 277= DSDP Site 277.

A global compilation of nannofossil data indicates that nannofossil diversity was extremely high in the early Eocene with 120 recorded species (Bown et al., 2004). Diversity remained high into the middle Eocene (~85–100 species) but was followed by a rapid decrease into the Oligocene (~39 species) (Bown et al., 2004; Aubry, 1998). Taxon richness data from this

current study supports this general trend, with an increase through the early to early middle Eocene, followed by the onset of a gradual decrease. Shannon diversity also follows this overall pattern with an increase through the early Eocene at all sites, followed by relatively stable diversity into the middle Eocene.

5.3 Paleoecological indicators

Determining the ecological preferences of extinct nannofossils can be problematic due to the interconnectivity of environmental factors such as temperature and nutrient supply (Agnini et al., 2007b). In addition, some fossil species are inferred to have undergone an evolutionary shift in their ecological preference over time (Haq & Lohmann, 1976). Despite these problems, there is general agreement that certain species reflect specific environmental conditions (e.g. Wei & Wise, 1990a; Wei et al., 1992; Bralower, 2002; Gibbs et al., 2006; Villa et al., 2008). This section outlines the ecological preferences of key taxa/species used in this study.

5.3.1 *Chiasmolithus*

Chiasmolithus spp. is largely regarded as having a preference for cool-water environments (Bralower, 2002; Persico & Villa, 2004; Villa, et al., 2008). Bukry (1973a) suggested that during the Eocene this genus was most abundant at cool-water, high-latitude sites. However, Wei & Wise (1990a) suggested that an increase in chiasmoliths towards higher latitudes during the middle Eocene–Oligocene only applies to the group as a whole and some of the larger species, such as *Chiasmolithus gigas* and *Chiasmolithus grandis*, are rare to absent at higher latitudes. Aubry (1998) proposed that this group was adapted to mesotrophic or eutrophic environments.

5.3.2 *Coccolithus formosus*

Coccolithus formosus (also known as *Ericsonia formosa* by some workers) is thought to prefer warm-water environments (Wei et al., 1992; Villa et al., 2008). A latitudinal transect of the South Atlantic Ocean demonstrated that this species was virtually absent at high latitudes in the middle Eocene–Oligocene but abundant at low to middle latitudes (Wei &

Wise, 1990a). Furthermore, a decrease in the abundance of *C. formosus* from ~44 Ma was associated with cooling at that time (Wei & Wise, 1990a).

5.3.3 *Coccolithus pelagicus*

The ecological preference of *C. pelagicus* appears to have undergone a shift in temperature preference through time (Haq & Lohman, 1976). The modern species has a preference for cool-water (McIntyre & Bé, 1967) but the fossil species is inferred to have had a temperate-water preference in the Paleogene (Wei & Wise, 1990a; Persico & Villa, 2004; Villa et al., 2008).

5.3.4 *Discoaster*

Discoasters are considered to have a preference for warm-water environments, and their abundance generally decreases towards higher latitudes (Bukry, 1973a; Wei & Wise, 1990a). On the other hand, some studies indicate that discoaster abundance at some equatorial sites is lower than that at mid-latitudes (Haq & Lohmann, 1976; Wei & Wise, 1990a), suggesting that abundance of this genus is likely affected by factors other than just temperature. Aubry (1992) suggested that discoasters were adapted to oligotrophic conditions and the abundance of this group at high latitudes during the early Eocene can be attributed to this factor as much as it can to temperature. Likewise, their decrease in abundance through the late Eocene could be due to the contraction of oligotrophic environments and not solely a response to cooling conditions. Villa et al. (2008) argued that although there was evidence to suggest that discoaster abundance was affected by nutrient supply during the middle Eocene, the reason for their eventual disappearance at Southern Ocean sites in the late middle Eocene was most likely due to a decrease in sea-surface temperature (SST).

5.3.5 *Reticulofenestra daviesii*

Reticulofenestra daviesii was abundant at high latitude sites but virtually absent or very rare at equatorial sites (Wei & Wise, 1990a; Wei, et al., 1992). The abundance of *R. daviesii* generally parallels that of the *Chiasmolithus* group and it is therefore regarded as a cool-water indicator (Wei & Wise, 1990a; Persico & Villa, 2004; Villa & Persico, 2006). The

absence of *R. daviesii* from the base of the sections in this study should not be interpreted as an indication of warmer temperatures, as *Reticulofenestra* did not evolve until Zone NP11–NP12 in the SW Pacific (Schneider et al., 2011).

5.3.6 *Sphenolithus*

Sphenolithus spp. is a dominant component of assemblages at equatorial sites but its abundance declines in mid- to high latitudes. Diversity follows a similar pattern, with high diversity at low latitudes and decreasing at mid- to high latitudes. These factors, combined with its close association with *Discoaster*, are interpreted as a preference for oligotrophic, warm-water conditions (Wei & Wise, 1990a; Bralower, 2002). At some localities, *Sphenolithus* decreased in abundance across the PETM, which is contrary to what is expected, given their preference for warm conditions. Instead, it appears that their low abundance through this interval was driven by high nutrient supply and increased eutrophic conditions at the sites where this decrease is observed (Gibbs et al., 2006; Agnini et al., 2007b).

5.3.7 *Toweius*

This genus was interpreted by Bralower (2002) to be mesotrophic because of its ability to endure a wide variation in temperature and nutrient availability. Other authors have interpreted it to have a preference for cooler, meso-eutrophic waters (Bown et al., 2004). Self-Trail et al. (2012) proposed that species-level abundance of this genus could be used to interpret paleoceanographic changes during the Paleocene and Eocene. These authors suggested that *T. eminens* and *T. tovae* were dominant in the cool, mesotrophic conditions of the late Paleocene; *T. serotinus* was adapted to warm, eutrophic conditions during the PETM; and *T. occultatus* and *T. callosus* were adapted to warm, mesotrophic conditions following the PETM.

5.3.8 *Zygrhablithus*

Wei & Wise (1990a) considered the distribution of *Z. bijugatus* to be controlled by productivity and water depth; however, it has been found at both shallow- and deep-water sites. Edwards (1973b; Edwards & Perch-Neilsen, 1975) proposed that the presence of this

species was an indication of deposition in water depths above the lysocline, due to its tendency to dissolve below this depth. However, it has since been recognised that in some cases *Z. bijugatus* can become overgrown during early diagenesis, resulting in very dissolution-resistant forms that often persist in sediments (Gibbs et al., 2012). Other workers have proposed that *Z. bijugatus* has an affinity for deep-water, oligotrophic environments (Aubry, 1998), yet this species is common in the South Dover Bridge core, Maryland, which is located in a middle to outer neritic setting (Self-Trail, 2011).

5.4 Paleotemperature

In addition to using trends in the abundance of individual taxa, various proxies for temperature have been developed that use the combined abundance of certain taxa or species with known biogeographic affinities i.e. warm-water (>15°C) or cool-water (<15°C) species; or ratios of warm-water to cool-water species (e.g. Bukry, 1973a, 1974; Wei & Wise, 1990a; Villa & Persico, 2006; Shamrock & Watkins, 2012).

In this section the individual and grouped abundance of temperature indicator species are described for each site and are compared with the *Discoaster/Chiasmolithus* paleotemperature index and geochemical proxies where available. TEX_{86}^L has been shown to be influenced by factors other than temperature (Taylor et al., 2013). TEX_{86}^H yields SSTs that are very similar to BAYSPAR (Tierney & Tingley, 2014) and although both appear to yield SSTs that are too warm when compared to other proxies (Hollis et al., 2012), they are the best available. For this reason, TEX_{86}^H is used here but primarily as a guide to relative temperature change.

5.4.1 Mid-Waipara River section

At mid-Waipara the temperate species *C. pelagicus* forms a significant part of the assemblage, varying in abundance from ~8% to 38% throughout the section (Figure 5.6A). Warm-water taxa are most abundant in Zone NP10 to lower combined Zone NP13–14, with values ranging between ~9–19% (Figure 5.6B). This is reflected in a high percentage of *Discoaster* spp. through this interval, fluctuating in abundance from 2–18%. *Sphenolithus* spp. are most abundant in Zone NP11 and interestingly, this peak in abundance correlates

with a decrease in the abundance of *Discoaster* spp. (Figure 5.6A). Cool-water taxa are less abundant through this interval, only reaching a maximum of 7% (Figure 5.6B).

The abundance of warm-water taxa begins to decrease in lower Zone NP13–14 and this is reflected mainly in the decrease in *Discoaster* spp. Through this part of the section cool-water taxa begin to increase in abundance, reaching a peak of 16.67% midway through the combined Zone NP13–14. The lower part of this increase is related to *R. daviesii*, which begins to increase in abundance in the lower part of this combined zone, steadily rising to a peak abundance of 10.9%. *Chiasmolithus* spp. start to increase in abundance at around the same interval that *R. daviesii* reaches its maximum abundance.

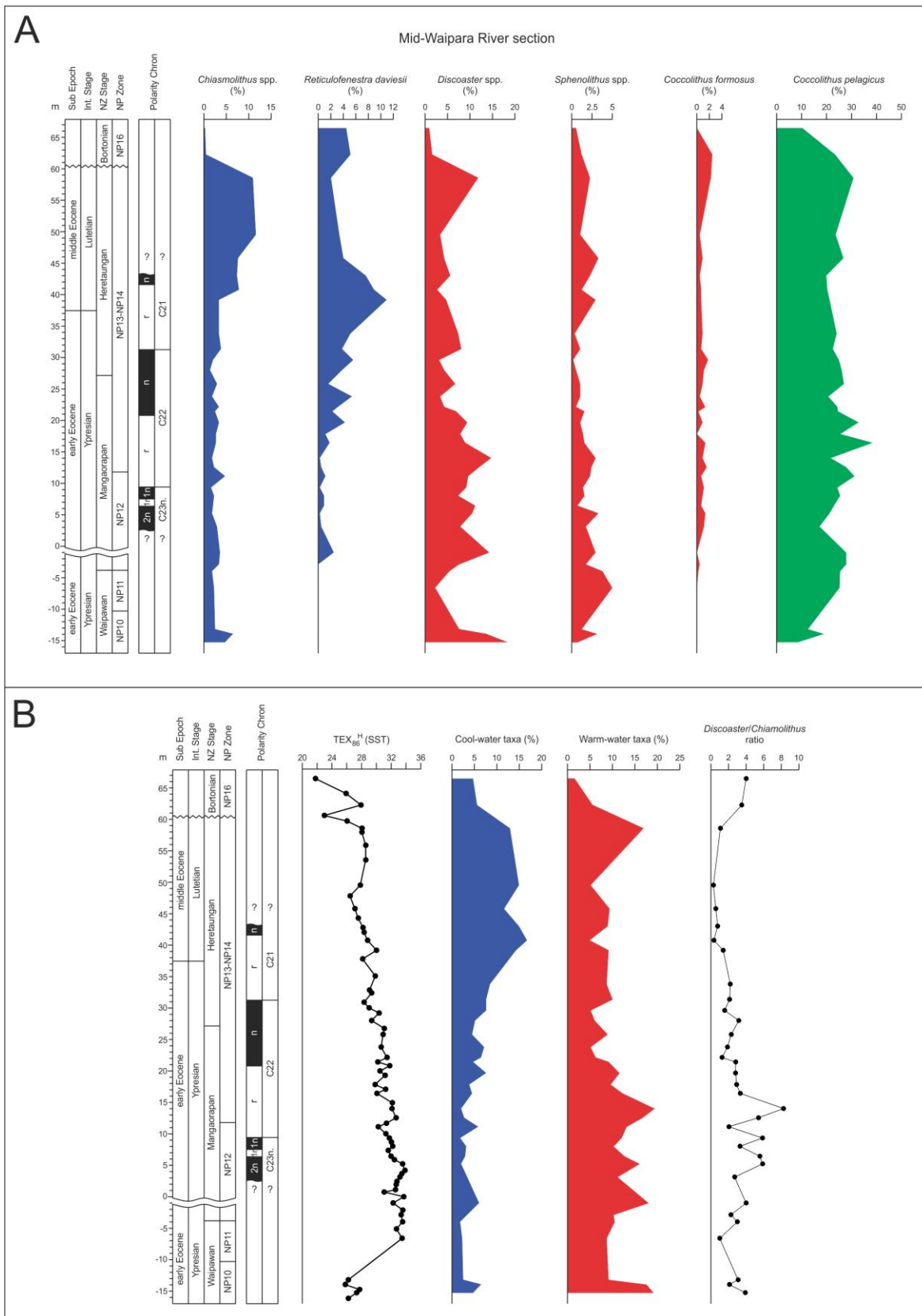


Figure 5.6: (A) Relative abundance of selected nannofossil species from the mid-Waipara River section plotted against depth, nannofossil zones, NZ Stages and magnetostratigraphy. (B) Combined relative abundance of cool- and warm-taxa from panel A, compared to TEX_{86}^H SST data and the D/C paleotemperature index. Blue = cool-water taxa, red = warm-water taxa, and green = temperate-water taxa. TEX_{86}^H analysis conducted at the University of Bristol.

The abundance of warm-water taxa increases in abundance in upper Zone NP13–14 and this is signified by an increase in abundance of all three warm-water indicators. A concomitant decrease in cool-water taxa is also observed at this level and although the group abundance only records a slight drop in abundance, *R. daviesii* decreases considerably at this point, whereas *Chiasmolithus* spp. remains constant. A drop in both cool- and warm-water taxa is observed in NP16; however, *R. daviesii* increases in abundance through this interval. It should be noted that an unconformity is observed between Zone NP16 and the underlying combined NP13–14 Zone, resulting in large variations in assemblage composition across this boundary.

The general patterns in the nannofossil assemblages correlate well with the TEX₈₆ record ($r=0.53$, $p<0.005$), which indicates that SST peaks in NP11, followed by a gradual decrease towards the top of the section (Figure 5.6B). A drop in SST in NP16 correlates with the increased abundance of *R. daviesii* and drop in warm-water taxa. TEX₈₆^H values at the base of the section are low relative to the high percentage of warm-water taxa and this is probably a reflection of the preferential preservation of *Discoaster*. Lack of exposure precludes further sampling to fill the sampling gap above this interval, which is needed to clarify the onset of warmer temperatures.

The D/C ratio is in good agreement with the group abundance patterns and the relative temperature trend in the TEX₈₆ record, with higher values across Zone NP12 to lower Zone NP13–14 (Figure 5.6B). An increase in the D/C ratio occurs in NP16, which appears to be inconsistent with the decrease in SST and warm-water taxa, but does coincide with the large drop in *Chiasmolithus* spp. As previously mentioned, variations at the top of the section are likely a result of the unconformity, with the constituent species in the two genera changing dramatically.

5.4.2 Hampden Beach Section

At Hampden Beach, warm-water taxa are more abundant than cool-water taxa through the combined Zone NP13–14, reaching a maximum abundance of 18.8% (Figure 5.7B). *Discoaster* spp. accounts for the majority of the warm-water taxa through this interval (Figure 5.7A). *Reticulofenestra daviesii* is the main constituent of the cool-water assemblage

within this combined zone, reaching a maximum abundance of 10.15%. As at mid-Waipara River, *C. pelagicus* is a major component, accounting for 34.7% of the assemblage.

Proportions of cool- and warm-water taxa in the combined Zone NP14–15 remain similar to the lower interval, but abundance of the two groups is slightly lower. *Reticulofenestra daviesii* remains at higher abundance than *Chiasmolithus* spp., which accounts for less than 3% of the total assemblage. A spike in warm-water taxa in this upper interval is attributed mainly to an increase in *Discoaster* spp. abundance, with a small increase in *Sphenolithus moriformis*. This peak in discoaster abundance is probably exaggerated due to poor preservation at this level. Nannofossils are very rare in this part of the section and the assemblage is comprised of two main genera, suggesting that much of the original assemblage has been removed by diagenesis. *Coccolithus pelagicus* is less abundant in this upper Zone NP14–15 than the lower Zone NP13–14.

As at mid-Waipara, the nannofossil temperature indicators can be compared with SST inferred from the TEX₈₆ proxy. For all data shown, the Index of Branched and Isoprenoid Tetrathers (BIT) index is <0.3, which indicates that terrestrial GDGTs have had minimal impact on the SST estimates (Weijers et al., 2006). Because of the patchy recovery of nannofossils and a significant gap in the TEX₈₆ record, only a general comparison is possible with the TEX₈₆ record. In the lower interval where warm-water taxa comprise ~5–18% of the assemblage and the D/C ratio ranges from ~2–17.3, high SSTs of 29–33°C are inferred from the TEX₈₆^H index. A weak cooling trend in the SST record is paralleled by a small increase in cool-water taxa. However, a spike in the D/C ratio is not matched by a peak in SST. There are too few TEX₈₆ samples in the upper interval to draw any conclusions, except that there appears to be an overall cooling trend from lower to middle Eocene at Hampden Beach.

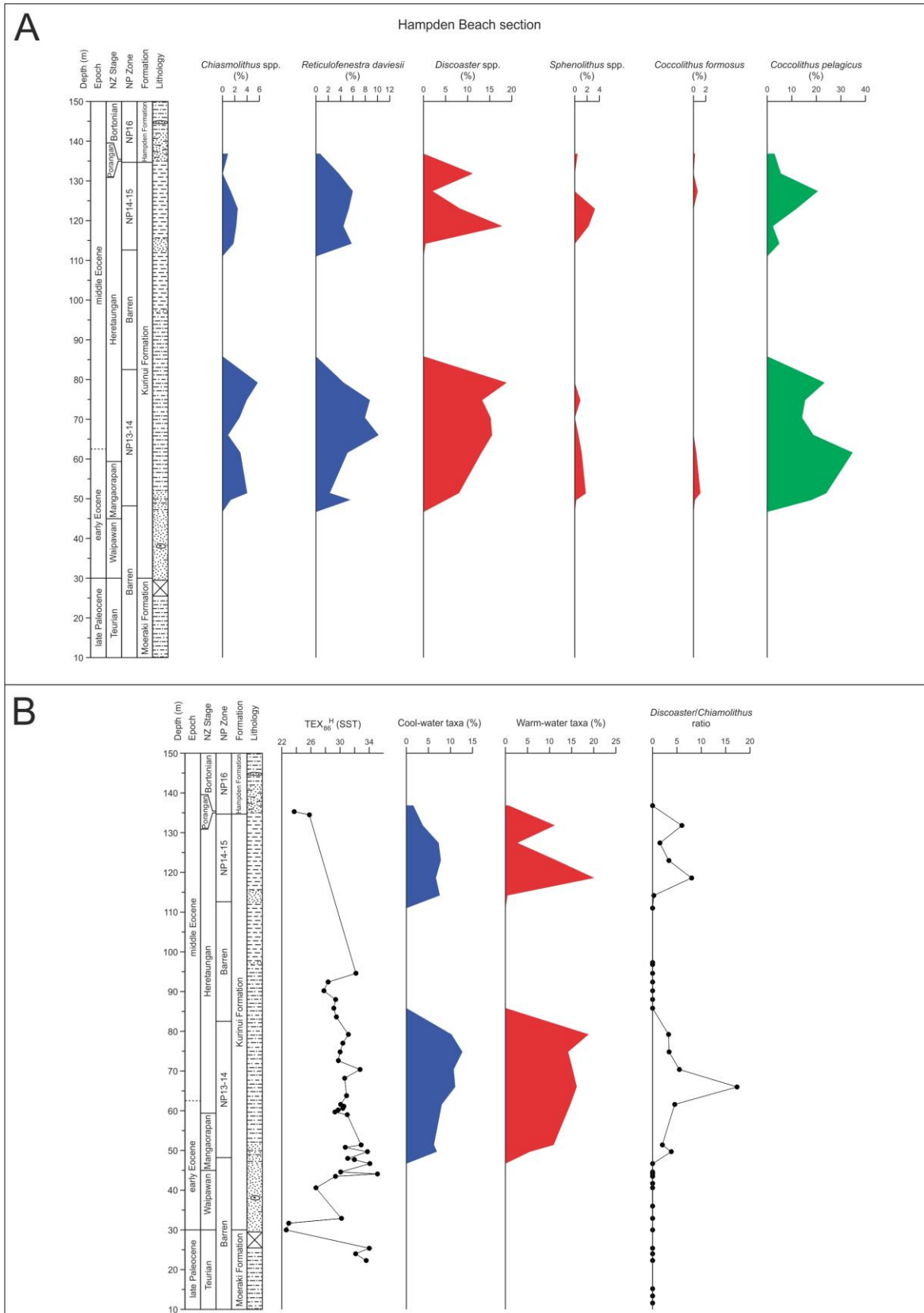


Figure 5.7: (A) Relative abundance patterns of selected nanofossil species from the Hampden Beach section plotted against depth, nanofossil zones and NZ Stages. (B) Combined relative abundance of cool- and warm-taxa from panel A, compared to TEX_{86}^H SST data and the D/C paleotemperature index. Blue = cool-water taxa, red = warm-water taxa, and green = temperate-water taxa. TEX_{86} analysis conducted at the University of Bristol.

5.4.3 DSDP Site 207

Coccolithus pelagicus is a significant constituent of assemblages from the combined Zone NP9–10 to lower Zone NP13, comprising 32–44.4% of the assemblage (Figure 5.8A). Warm-water taxa increase in abundance through this interval, reaching a maximum of 26.67% in NP12. This increase in warm-water taxa corresponds with peak abundance of all three warm-water indicators (Figure 5.8). Cool-water taxa are least abundant through this basal part of the section, reaching no more than 3.3% of the assemblage.

The abundance of *C. pelagicus* remains fairly constant through the remainder of Zone NP13 to upper Zone NP14, ranging between ~16–22%. In this interval, the abundance of cool-water taxa increases steadily, reaching a maximum of 14.2%. As seen at mid-Waipara, *R. daviesii* increases in abundance before *Chiasmolithus*, reaching a peak of 9.6% in upper Zone NP14. *Chiasmolithus* begins to increase in abundance in lower Zone NP14, attaining a maximum of 7.1% but then begins to decrease to lower values by upper Zone NP14. Warm-water taxa decrease in abundance through this interval, dropping to a low of 1.33% in upper Zone NP14. This is reflected across all three warm-water indicators, with *Sphenolithus* spp. and *C. formosus* dropping to an abundance of less than 1%.

From upper Zone NP14 to Zone NP16 the abundance of warm-water taxa remains low, not reaching more than 5.5% of the assemblage. *Coccolithus pelagicus* abundance remains constant through this interval but is less abundant than in the lower part of the section (~10–15%). Cool-water taxa decrease slightly in abundance in lower NP15a–b, but increase again towards the top of the section where they make up 8.7–11.3% of the assemblage. Similar to mid-Waipara, the increase in cool-water taxa is mainly due to an increase in the abundance of *R. daviesii*.

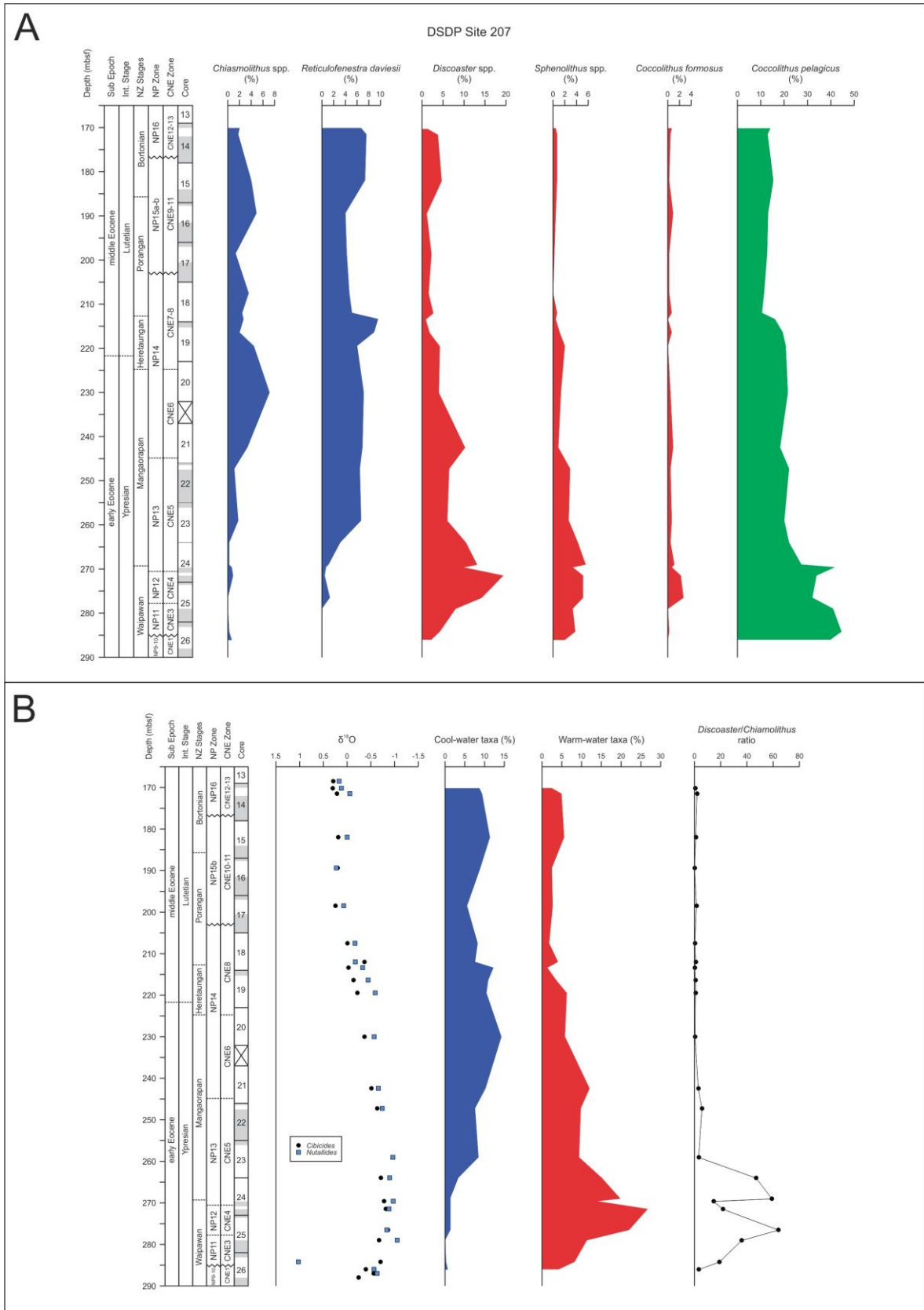


Figure 5.8: (A) Relative abundance patterns of selected nannofossil species from DSDP Site 207 plotted against depth, nannofossil zones and NZ Stages. (B) Combined relative abundance of cool- and warm-taxa from panel A, compared to the D/C paleotemperature index and the oxygen isotope record ($\delta^{18}\text{O}$) derived from benthic foraminifera. Blue = cool-water taxa, red = warm-water taxa, and green = temperate-water taxa. $\delta^{18}\text{O}$ analysis conducted at the University of California, Santa Cruz.

The cooling trend evident from the nannofossil assemblages is paralleled by the oxygen isotope ($\delta^{18}\text{O}$) record from benthic foraminifera (Figure 5.8B). A positive shift in $\delta^{18}\text{O}$ values is observed from the base of Zone NP14 up into Zone NP16, and this is consistent with the decrease in warm-water taxa and increase in cool-water taxa across this interval. The D/C ratio agrees broadly with the patterns seen in the assemblage data (Figure 5.8B). The ratio is high at the base of the section where warm-water taxa are a dominant component of the assemblage. The ratio drops dramatically in the middle of Zone NP13 and remains close to zero throughout the rest of the section, corresponding with an increase in cool-water taxa over this interval. The lack of variation in the D/C ratio throughout most of the record may be an indication that this site is too far north for it to be effective, as *Chiasmolithus* are generally less abundant at lower latitudes (Bukry, 1973a).

5.4.4 DSDP Site 277

At Site 277 the abundance of both warm- and cool-water taxa is low in Zones NP10 to upper NP12 (Figure 5.9B). The only exception to this is a spike in the abundance of warm-water taxa near the boundary between combined Zone NP9–10 and NP11. This peak in abundance is mainly due to an increase *Discoaster* spp. (Figure 5.9A) and is mostly likely exaggerated because of the unconformity located at this level. *Coccolithus pelagicus* is a major component through this lower part of the section, accounting on average for ~33% of the assemblage.

Warm-water taxa become much more abundant in lower Zone NP13 and, although there are small increases in *Sphenolithus* spp. and *C. formosus*, the bulk of this increase is due to *Discoaster* spp. (30.9%). The abundance of warm-water taxa drops above this large peak, but remains at fairly constant values through to the middle of Zone NP13. The abundance of cool-water taxa continues to be low through this interval, at less than 5% of the total assemblage. *Coccolithus pelagicus* remains a significant component of the assemblage but starts to gradually decrease, dropping to 25% by the middle of Zone NP13.

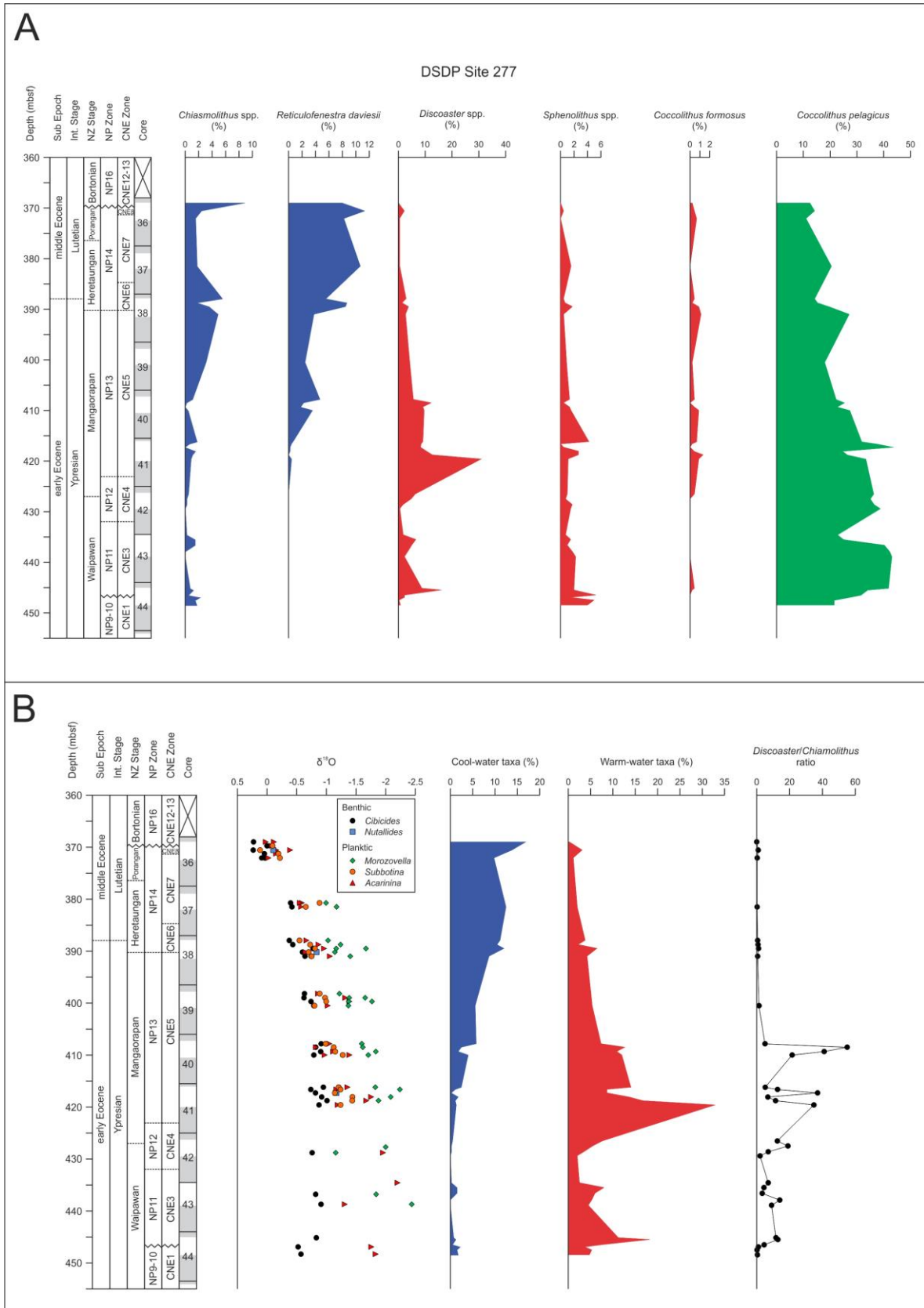


Figure 5.9: (A) Relative abundance patterns of selected nannofossil species from DSDP Site 277 plotted against depth, nannofossil zones and NZ Stages. (B) Combined relative abundance of cool- and warm-taxa from panel A, compared to the D/C paleotemperature index and the oxygen isotope record ($\delta^{18}\text{O}$) derived from benthic and planktic foraminifera. Blue = cool-water taxa, red = warm-water taxa, and green = temperate-water taxa. $\delta^{18}\text{O}$ analysis conducted at the University of California, Santa Cruz.

Cool-water taxa begin to increase in abundance in the middle of Zone NP13, peaking in Zone NP16 (16.9%). This peak in abundance coincides with an unconformity at the boundary between Zones NP14 and NP16. As at Hampden Beach and Site 207, *Chiasmolithus* spp. decrease in the upper portion of the section but *R. daviesii* increases. Warm-water taxa continue to decrease in abundance from the middle of Zone NP13, reaching less than 1% in Zone NP16. This is reflected in the low abundance of all three warm-water indicators. *Coccolithus pelagicus* continues to decrease in abundance towards the top of the section but still accounts for ~12.4% of the assemblage.

The $\delta^{18}\text{O}$ records from benthic and planktic foraminifera parallel the cooling trend evident from the nannofossil assemblages (Figure 5.9B). A gradual positive shift in $\delta^{18}\text{O}$ values is observed from lower Zone NP13 up into Zone NP16, and this is consistent with the decrease in warm-water taxa and increase in cool-water taxa across this interval. The gradient between benthic and planktic foraminifera decreases towards the top of the section and this may reflect greater diagenesis as waters become cooler or greater vertical mixing.

The D/C ratio is low in the basal part of the section but is consistent with a slightly higher abundance of warm-water taxa compared to cool-water taxa (Figure 5.9B). The ratio increases from upper NP12 to lower NP13, coinciding with the increase in warm-water taxa across this interval and the low abundance of cool-water taxa. The ratio drops sharply in the middle of Zone NP13 and stays close to zero through to the top of the section. This agrees with the decrease in warm-water taxa and increase in cool-water taxa over this interval.

5.5 *Toweius-Reticulofenestra* Turnover Event

The abundance turnover between *Toweius* and *Reticulofenestra* in the early Eocene has been well documented in the Mediterranean (Agnini et al., 2006) and the eastern Indian Ocean (Shamrock & Watkins, 2012). This event occurred within the EECO and is described by Agnini et al. (2014) as occurring in three phases: 1) high abundance of *Toweius* in upper Zone CNE4 (NP12); 2) a significant decrease in the abundance of *Toweius* and the concomitant sporadic FO of *Reticulofenestra* in uppermost Zone CNE4 (NP12); and 3) the LO of *Toweius* in Zone CNE5 (NP13). Another key feature within this event is an acme of

Discoaster within the dominance shift from *Toweius* to *Reticulofenestra* (Agnini et al., 2006; Shamrock & Watkins, 2012). Agnini et al. (2006) suggested two explanations for this turnover event: 1) the *Discoaster* acme was driven by changes in SST during the EECO; or 2) the peak in *Discoaster* abundance and subsequent origination and increase in *Reticulofenestra* was controlled by changes in nutrient availability and ocean conditions.

At all sites in this study, the timing of the turnover event is comparable to the studies of Agnini et al. (2006) and Shamrock & Watkins (2012), although there are differences in the FO of *Reticulofenestra* and LO of *Toweius* (Figure 5.10). Agnini et al. (2014) indicated that the FO of *Reticulofenestra* occurs within Zone CNE4 (NP12) in low and middle latitudes. However, *Reticulofenestra* is known to have evolved earlier in the high southern latitudes (Schneider et al., 2011) and data from the New Zealand region support this observation. Data from this current study indicate that at least three species of *Reticulofenestra* first occur within Zone NP11 (Zone CNE3) at DSDP Site 207 and the mid-Waipara River section. This older FO of the *Reticulofenestra* group is also documented at DSDP Site 277, Campbell Plateau (Hollis et al., 2015).

The extinction of *Toweius* is reported to occur in Zone NP13 (Zone CNE5) (Agnini et al., 2006; Agnini et al., 2014). However, at mid-Waipara River and Hampden Beach, *Toweius* ranges well up into the combined Zone NP13–14 (CNE5–6) and into Zone NP14 at Sites 207 and 277. This extended range of *Toweius* is also observed in the Tora section, Southwest Wairarapa, New Zealand (Hines et al., 2013).

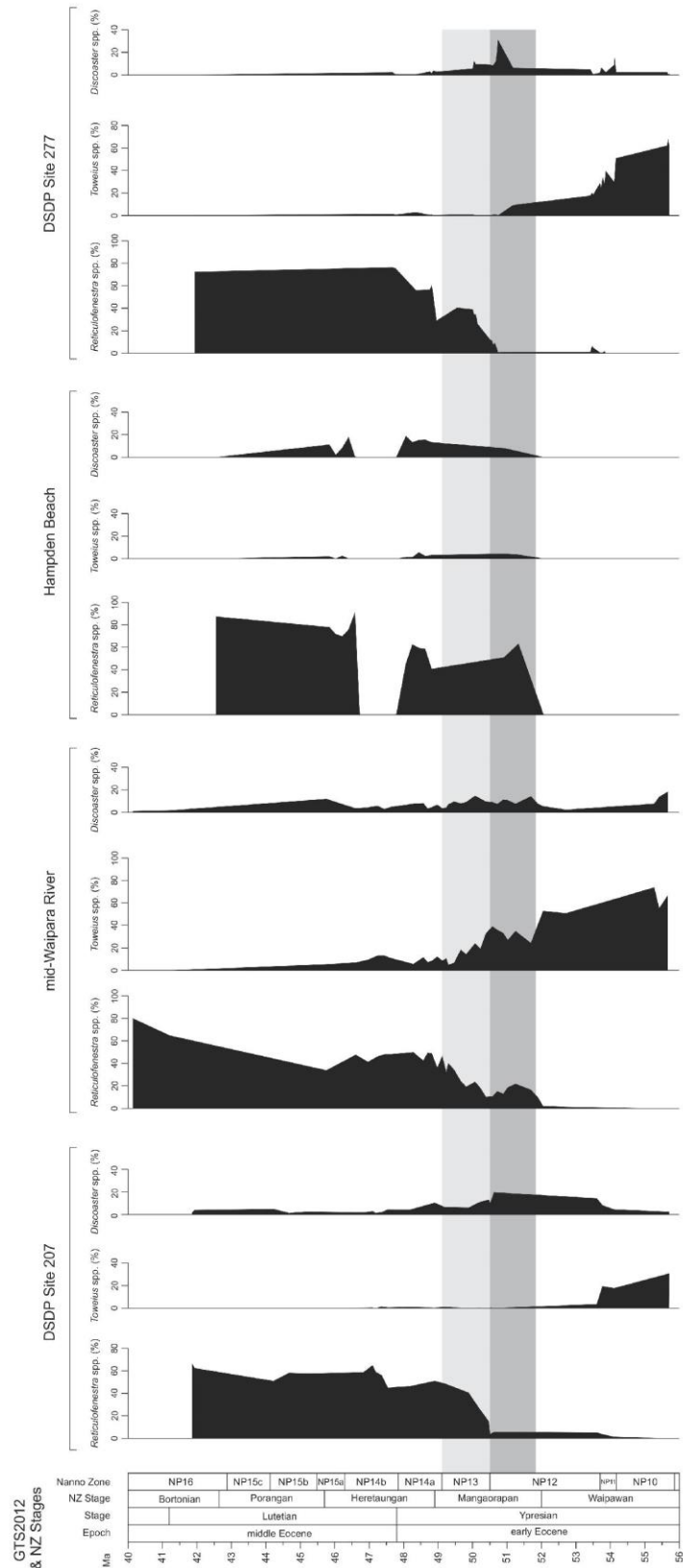


Figure 5.10: Abundance patterns of *Reticulofenestra*, *Toweius* and *Discoaster* at all study sites. Sample depths for DSDP Sites 207 & 277 are converted to ages using the age-depth models presented in Section 4.4. Ages for mid-Waipara River are from Dallanave et al. (2016) and for Hampden Beach from Inglis et al. (2015). NZ Local stages are based on the bioevents in Raine et al. (2015). Grey shading represents the timing of the *Discoaster* acme from previous studies; light grey from Shamrock & Watkins (2012), dark grey from Agnini et al. (2006).

In the current study, the turnover between *Toweius* and *Reticulofenestra* varies between sites (Figure 5.11). At DSDP Site 207, this event occurs earlier than at other sites and there is a gradual shift in dominance between the two groups. The abundance of *Toweius* decreases considerably by the end of NP11 and remains low up into NP14. There is a slight increase in *Reticulofenestra* through NP12, followed by a large increase in abundance at the base of NP13. An increase in *Discoaster* abundance (maximum ~19.3%) is observed within the turnover interval. At mid-Waipara there is considerably more crossover between the two groups, with *Toweius* gradually decreasing in abundance in NP12 as *Reticulofenestra* abundance increases. *Discoaster* abundance increases across this interval, ranging between ~7.3–14.6% of the total assemblage. At Site 277 the shift in dominance occurs abruptly at the base of NP13, with a clear change in the abundance of both groups. This is accompanied by a noticeable peak in *Discoaster* abundance, which reaches ~30% of the total assemblage. The onset and termination of the turnover event is difficult to identify at Hampden Beach, but the high abundance of *Reticulofenestra* and low abundance of *Toweius* across the turnover interval are consistent with other sites (Figure 5.10).

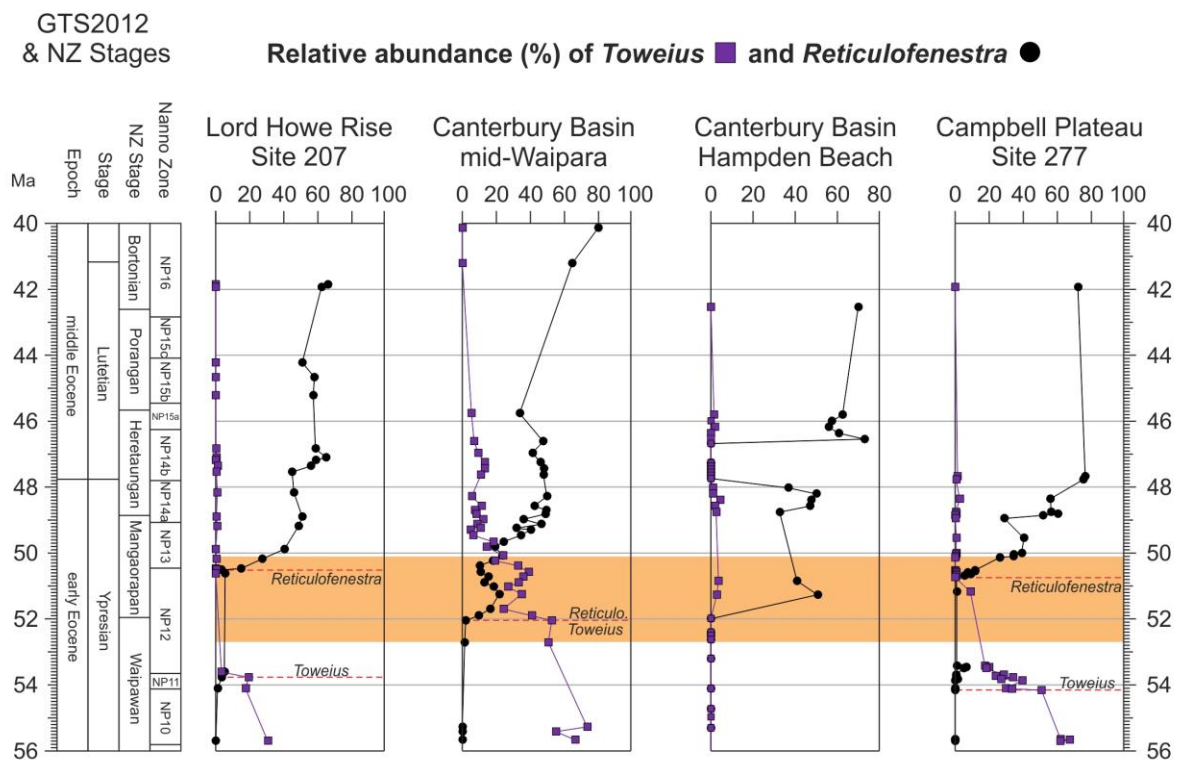


Figure 5.11: Relative abundance of *Toweius* and *Reticulofenestra* at each study site. Red dashed lines mark key abundance shifts within each genus.

In summary, the *Toweius–Discoaster* turnover event described by previous workers (Agnini et al., 2006; Shamrock & Watkins, 2012) is also evident in the SW Pacific. Despite the general agreement of the timing of this event, there are differences in the origination of *Reticulofenestra*, which evolved earlier at high southern latitudes than at low to middle latitudes. Additionally, the extinction of *Toweius* occurred later in the SW Pacific, in Zone NP14. Differences in the duration of the crossover between *Toweius* and *Reticulofenestra* are likely a reflection of different oceanographic settings (i.e. open ocean versus coastal).

CHAPTER 6: DISCUSSION

6.1 Applicability of established nannofossil zonations to SW Pacific sections

The zonations of Martini (1971) and Agnini et al. (2014) provide good stratigraphic resolution through most of the examined sections, although some of the zone markers appear to be absent or extremely rare in the SW Pacific. The absence of *Rhomboaster bramlettei* at DSDP Sites 207 and 277 makes it difficult to identify the base of Zone NP10. However, it is not clear whether the absence of *R. bramlettei* at these sites is due to a hiatus between NP9 and NP10, a sampling gap, or the sporadic presence of this species in the SW Pacific. *Rhomboaster bramlettei* is rare in the mid-Waipara River section and is absent from the Mead Stream section (Hollis et al., 2005; Dallanave et al., 2015) and Toi Flat-1 core (Kulhanek et al., 2015).

The last occurrence (LO) of *Tribrachiatus contortus* marks the base of NP11 but this species is absent from all of the studied sections and at Mead Stream (Dallanave et al., 2015). Previous workers have suggested that the first occurrence (FO) of *Sphenolithus radians* (54.17 Ma) can be used to approximate the base of NP11 (Backman, 1986) and this event has been used at mid-Waipara River and DSDP Sites 207 and 277. As such, it appears to be a reliable marker in the SW Pacific region.

The base of Zone NP14 is marked by the FO of *Discoaster subloensis* and identification of this species in both onshore sections was problematic, due to overgrowth and rarity of specimens, making it impossible to confidently define the boundary between Zones NP13 and NP14. *Discoaster subloensis* is also absent from the Tora and Mead Stream sections (Hines et al., 2013; Dallanave et al., 2015), but is present in other open-ocean settings at lower latitudes in the SW Pacific (e.g. Site 287 and Site 210, Coral Sea Basin; Shafik, 1973; Villa & Wise, 1993). The absence of *D. subloensis* in coastal settings may be an indication that this species has a preference for more distal settings. The LO of *Discoaster lodoensis* is used to define the base of Zone CNE7 and is correlated to lower Zone NP14. This event provides additional age control at mid-Waipara and DSDP Sites 207 and 277 within Zone

NP14. The base of CNE8 is defined by the FO of *Nannotetrina cristata* and this event helps to refine the correlation at DSDP Sites 207 and 277 in upper Zone NP14. As with *D. subladoensis*, occurrences of *Nannotetrina* spp. at mid-Waipara River and Hampden Beach are rare and questionable, and this genus is completely absent at Mead Stream (Dallanave et al., 2015).

The FO of *Nannotetrina fulgens* is used to mark the base of Zone NP15; however, it is difficult to determine the reliability of this marker, given that Zone NP15 is missing or incomplete in the studied sections. Of the four sites examined in this study, *N. fulgens* is only present at Site 207 but its delayed appearance in this section makes it an unreliable marker. The first common occurrence (FCO) of *Sphenolithus cuniculus* defines the base of CNE11 and is correlated to subzone NP15b; however, this species is also absent at all sites.

The base of Zone NP16 is defined by the LO of *Blackites gladius* but this species is absent at all four sites. This is consistent with the global unreliability of this marker, as previously mentioned. The LO of *Nannotetrina alata/fulgens* is used as a secondary marker to define the base of this zone (Backman, 1986; Expedition 320/321 Scientists, 2010). However, as mentioned above, this genus is absent from three of the four study sites and *N. fulgens* is not a reliable marker at Site 207. The FCO of *Reticulofenestra umbilicus* $\geq 14 \mu\text{m}$ is used to mark the base of Zone CNE13, which correlates to lower Zone NP16. At Sites 207 and 277, this species is rare throughout the interval and does not provide any additional age control within Zone NP16 for these two sections.

Despite the absence of several zone markers, the zonations of Martini (1971) and Agnini et al. (2014) allow reasonable correlation between all of the studied sections. Application of the Agnini et al. (2014) zonation provides additional age control at some of the sites within NP14 and, as such, provides a useful supplementary zonation in the SW Pacific. However, further work is needed in the SW Pacific to identify events that can help to refine the stratigraphic resolution through Zones NP14–16, as several of the markers used by Martini (1971) and Agnini et al. (2014) are rare or absent in this region.

6.2 Nannofossil bioevents in the SW Pacific

There are several nannofossil bioevents that have utility in global studies but have mixed utility in the SW Pacific.

6.2.1 *Blackites*

Blackites consists of a base comprised of various cycles of calcite elements and a process or stem. The different species of *Blackites* are distinguished by the shape of the process, but often the process and the base are separated in the fossil record and it is difficult to identify bases to species level. At mid-Waipara, specimens of *Blackites* are difficult to identify to species level and many of the counts of this genus are based on the observation of undifferentiated bases. At Site 207, *Blackites* spp. occur in low numbers through upper NP14 to lower NP16 and are only identifiable to genus level. This genus is observed to occur very sporadically at DSDP Site 277 in mid- to upper NP11 (Hollis et al., 2015) and upper NP14–NP15. This is consistent with previous studies in the New Zealand region where *Blackites* is found to occur sporadically or in low numbers. It is absent from NP10 at Toi Flat, East Coast Basin (Kulhanek et al., 2015) and is present in low numbers at Tora, southeast Wairarapa (Hines et al., 2013). In addition, Edwards & Perch-Nielsen (1975) reported the continuous observation of rare to few *Blackites* (as *Rhabdolithus* sp.) through middle to upper Eocene at DSDP Site 277. This is in contrast to sites located in coastal Tanzania and southeastern Maryland, USA, where abundant and diverse assemblages of rhabdoliths are observed (Bown, 2005; Self-Trail, 2011). Bown (2005) suggested that the absence of this group in many fossil assemblages may be due to dissolution effects.

6.2.2 *Ellipsolithus*

At mid-Waipara and DSDP Sites 207 and 277, *Ellipsolithus* is rare and sporadic, and this is consistent with other New Zealand sections. *Ellipsolithus* is very sporadic and rare at Tora (Hines et al., 2013), and present in low numbers through Zones NP9–10 at Toi Flat (Kulhanek et al., 2015). *Ellipsolithus bolli* is present in low numbers at mid-Waipara River and Sites 207 and 277 in Zones NP9–NP10 and also in NP13 at Site 277. *Ellipsolithus macellus* is observed in Zones NP9–NP10 at all three sites and also ranges into NP11 at Site 277. *Ellipsolithus distichus* has a greater range in the SW Pacific than the other two species. Its oldest

occurrence is in NP10 at mid-Waipara River and its youngest occurrence is in the combined NP14–15 zone at Hampden Beach. It occurs sporadically through zones NP13–14 at all sites.

The rare and sporadic occurrence of *Ellipsolithus* in the SW Pacific is contrary to low latitude sites. At Site 1262, southeastern Atlantic, this group is rare and sporadic at the base of the section immediately following the evolution of the genus (Zones NP4–NP6) but becomes more abundant and continuous through Zones NP7–NP12 (Agnini et al., 2007a). At South Dover Bridge, Maryland, USA, *Ellipsolithus* occurs fairly consistently through Zones NP9–NP12, with *E. distichus* the most abundant species in Zones NP9–10 and *E. macellus* more abundant in Zone NP11 (Self-Trail, 2011). This indicates that this genus is more restricted in the SW Pacific than in the Atlantic and it is known to have migrated into the region significantly later than in other areas (late Paleocene to early Eocene; Edwards, 1971; Kulhanek et al., 2015).

6.2.3 *Girgisia gammation*

Agnini et al., (2014) placed the FO of *Girgisia gammation* within Zone CNE3, slightly older than the base of common *D. lodoensis* (CNE3/CNE4 boundary). At mid-Waipara, the FO of *G. gammation* occurs at the CNE2/CNE3 (NP10/NP11) boundary and, given the sampling gap discussed previously, it is possible that it extends even lower in the section. This is supported by other observations from the SW Pacific where it is found to occur sporadically in Zone NP9 (Hollis et al., 2015; Kulhanek et al., 2015). Conversely, the FO of *G. gammation* is within Zone NP12 (CNE4) at DSDP Site 207. The FO is also found within NP12 in Exmouth Plateau, ODP Site 762 (Schneider et al., 2011). It is possible that this species evolved earlier in the high-latitude Southern Hemisphere and migrated northwards, similar to *Reticulofenestra* (Schneider et al., 2011).

6.2.4 *Reticulofenestra umbilicus*

This species is used in the zonation of Agnini et al. (2014) and Okada & Bukry (1980) to define zone boundaries that are correlated to lower Zone NP16. The FO of larger *R. umbilicus* (>14 µm) is dated at 41.94 Ma within Chron C19r (Gradstein et al., 2012) and the event is used to approximate lower NP16 when *B. gladius* or *N. alata/fulgens* are absent.

There is some ambiguity around the age of this event, however, as it has been placed in basal Chron C20r in the Contessa section, Italy (Lowrie et al., 1982), and Chron C19r in the South Atlantic (Backman, 1987), suggesting that its FO is diachronous.

At Site 207, rare *R. umbilicus* (>14 µm) occurs in one sample that also contains *Chiasmolithus gigas*, which is the marker for Subzone NP15b. The co-occurrence of these two species has been documented in previous studies from offshore New Jersey and Kerguelen Plateau, ODP Site 1138 (e.g. Applegate & Wise, 1987; Arney & Wise, 2003). The latter authors suggested that the FO of *R. umbilicus* may be older in high latitude sections or alternatively, the LO of *C. gigas* is later in low latitude sections. Given that *Reticulofenestra* is known to have originated in the high latitudes (Schneider et al., 2011), it is reasonable to speculate that *R. umbilicus* also evolved earlier in the SW Pacific.

6.3 Utility of preservation indices

The relative abundance of *Z. bijugatus* proves to be an effective guide to preservation at mid-Waipara and to a lesser degree at Sites 277 and 207. However, there is some doubt that variation in the abundance of this species is controlled primarily by dissolution. Dunkley Jones et al. (2008) found that this species declined in abundance across the Eocene-Oligocene transition in well preserved material from Tanzania and suggests that this was in response to a change in nutrient availability. Further work is needed to understand the primary controls on this species.

The *Chiasmolithus* ratio also appears to be useful at mid-Waipara but less so at the other sites. At Site 277 this index produces mixed results and this may be related to poor core recovery at this site. The lower abundance of *Chiasmolithus* at Site 207 makes it difficult to accurately capture the ratio between incomplete to complete specimens and given the preference of *Chiasmolithus* for cool conditions, use of this proxy may only prove to be effective at cooler, high-latitude sites.

At sites 207 and 277 the unidentified rim index parallels preservation trends in certain intervals, despite a weak–moderate covariance with the visual estimation of preservation.

One of the problems with this index is that fluctuations may be recording abundance changes in particular taxa. For example, at Site 207, the large number of unidentified rims at the base of the section corresponds with a high relative abundance of *Toweius*, which is likely the main constituent of the unidentified rims. The subsequent decline in the number of unidentified rims may therefore be an artefact of the decline in *Toweius* over time and not a real signal of preservation change.

Although some inferences can be made based on the correlations between indices, it is clear that these interpretations can be somewhat spurious depending on other factors influencing the abundance of the taxa used (e.g. nutrient availability, SST, biogeographical range). Furthermore, the results of this study do not suggest that visual observation is the best method of measuring preservation and in some cases, one of the other indices may provide a more accurate reflection of preservation changes. It would be useful to compare the preservation indices from this study with results generated using a more complex measure of preservation to determine the usefulness of each individual index.

6.4 Timing of the EECO in the SW Pacific

Maximum values in the TEX_{86} record for mid-Waipara River indicate that the Early Eocene climatic Optimum (EECO) spanned an interval from ~53–50 Ma (Figure 6.1). The onset of the EECO at mid-Waipara is not well constrained due to the sampling gap between upper (~52.7 Ma) and lower (~55.2 Ma) Waipawan samples. However, the age is consistent with Mead Stream, where the onset of the EECO is defined by a negative carbon isotope excursion (~53 Ma; J event) that occurred within a transition interval between limestone-rich and marl-rich facies (Slotnick et al., 2012).

The EECO coincides with the increase in abundance of warm-water taxa at all study sites (Figure 6.1). At Sites 207 and 277, warm-water taxa increase in abundance at ~54 Ma, which is prior to the onset of the EECO. However, the data are poorly constrained through this interval and it is possible that the abundance peaks relate to hyperthermal events, such as the Eocene Thermal Maximum 2 (ETM2), I event or Eocene Thermal Maximum 3 (ETM3) (Cramer et al., 2003; Lourens et al., 2005; Galeotti et al., 2010) prior to the onset of the

EECO. The abundance of cool-water taxa began to increase noticeably at all three sites around 49 Ma, which is slightly later than the termination of the EECO. The placement of the termination of the EECO is somewhat arbitrary, however, based on a small decrease in the TEX_{86} record at ~50 Ma. The TEX_{86} record indicates that sea-surface temperature (SST) began to decline from ~51 Ma to a minimum at ~47 Ma, and this interval of cooling matches with the maxima in cool-water taxa at all sites.

During this cooling interval, a concomitant decrease in warm-water taxa occurred at mid-Waipara River and Sites 207 and 277. At Hampden Beach the abundance of warm-water taxa continued to increase up to 48 Ma, although the *Discoaster/Chiasmolithus* (D/C) ratio decreased across this interval as did the abundance of temperate-water taxa (Figure 5.7). It is possible that the increase in warm-water taxa is partly a result of decreasing preservation through this interval, with more robust warm-water taxa (e.g. *Discoaster*) being preferentially preserved. This same explanation most likely accounts for the brief increase in warm-water taxa at mid-Waipara River at ~45 Ma, as preservation was also extremely poor during this interval.

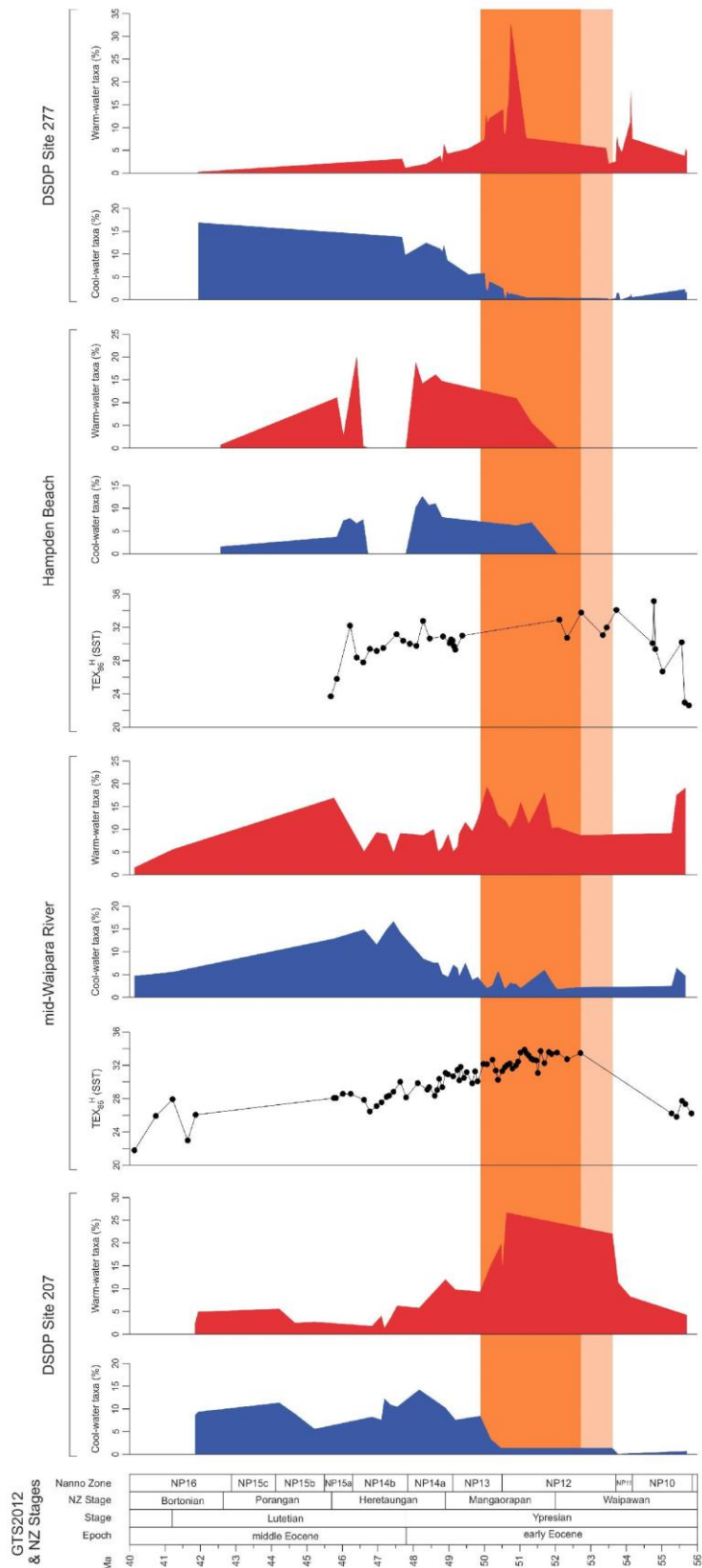


Figure 6.1: Relative abundance of cool- and warm-water taxa at each study site, compared to TEX_{86}^H SST data from mid-Waipara River. Dark orange shading represents the duration of the EECO at mid-Waipara, determined from the TEX_{86} record. Light orange shading indicates uncertainty in the onset of the EECO due to the sampling gap at the base of the mid-Waipara section.

6.5 Comparison with low- and high-latitude assemblages

Schneider et al. (2011) considered how the abundance of key nannofossil genera varied through the early to middle Eocene in a series of DSDP and Ocean Drilling Program (ODP) sites from tropical/subtropical (>20°C), temperate (15–20°C) and polar (<15°C) provinces. Comparison with data from the current study indicates that nannofossil assemblages in the SW Pacific were more similar to assemblages at temperate sites than to assemblages at tropical/subtropical sites in the early to middle Eocene (Figure 6.2). Warm-water taxa constituted a major part of the nannofossil assemblage at tropical/subtropical sites, but were less abundant in temperate regions and formed a very minor part of assemblages in polar regions. Conversely, cool-water taxa were much more abundant at polar sites than at temperate or tropical sites.

A significant decrease in *Toweius* occurred in the early Eocene at all latitudes (~54 Ma) with abundance becoming less than 5% by the end of the EECO (Figure 6.3A). Mid-Waipara River and Kerguelen Plateau are exceptions, where the decline in *Toweius* occurred later, at ~52 and 53 Ma respectively. The global decrease in *Toweius* abundance coincided with an increase in global temperature in the late Paleocene and reflects the preference of *Toweius* for cooler, mesotrophic or eutrophic waters (Bown et al., 2004). A concomitant increase in *Reticulofenestra* occurred in the EECO at middle to high latitudes but not until ~48 Ma at low latitudes (Figure 6.3A). At mid-Waipara River, the gradual decline of *Toweius* could be a reflection of the neritic coastal setting of this site, where higher nutrient supply and less oceanic influence may have resulted in favourable conditions that allowed this genus to endure for longer. Schneider et al. (2011) linked the eventual demise of *Toweius* and expansion of *Reticulofenestra* to environmental changes associated with thermal destratification at the termination of the EECO.

Discoaster and *Zygrhablithus* also increased in abundance across the EECO (Figure 6.3B) and the patterns are generally in agreement with Schneider et al. (2011) who reported a shift between *Toweius* to *Discoaster/Zygrhablithus* to *Reticulofenestra* at temperate to subtropical latitudes. At mid-Waipara River, the relatively small change in *Discoaster* and *Zygrhablithus* abundance provides further evidence that conditions at this site were more

eutrophic, given that both of these genera have been reported to prefer oligotrophic environments. At Site 277 there was an increase in the abundance of *Zygrhablithus* prior to the EECO at ~54 Ma and this parallels a similar increase in this genus at Site 207. The reasons for the increase of *Zygrhablithus* are not clear, however, and have been linked to temperature or changes in nutrient supply (Schneider et al., 2011). At Sites 207 and 277, the increase in *Zygrhablithus* coincided with the initial decline of *Toweius*, suggesting that changes in the oceanic environment detrimental to *Toweius* were more favourable for *Zygrhablithus*. As mentioned previously, the data through the base of the EECO at Sites 207 and 277 is poorly constrained due to large sampling gaps and further analysis is needed to determine whether the increase in *Zygrhablithus* was sustained or whether it was a short-lived event. A similar increase in warm-water taxa occurred at ~54 Ma at these two sites, and it is possible that these assemblage shifts were related to an earlier hyperthermal event.

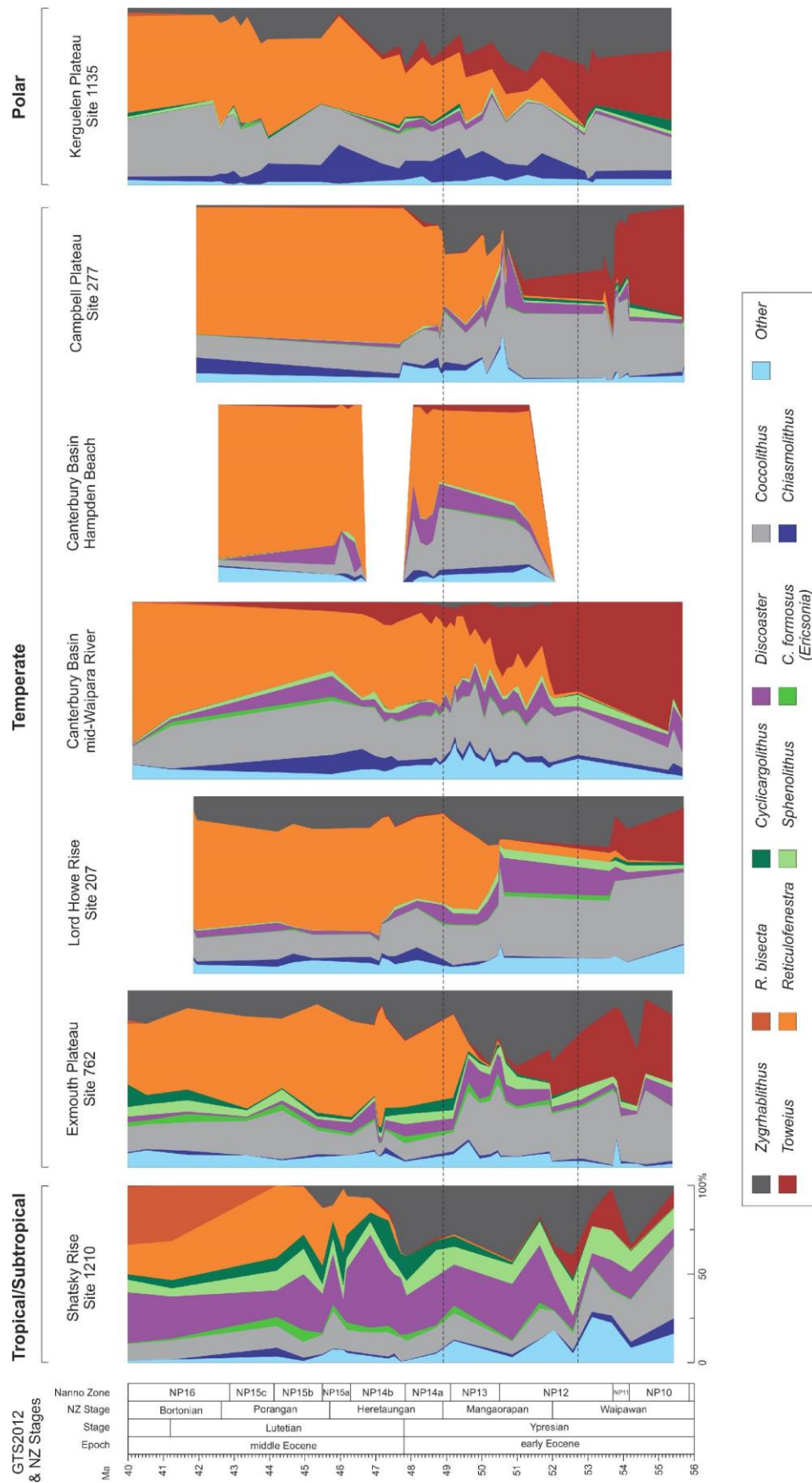


Figure 6.2: Relative abundance of key nannofossil genera at each study site. Data for Shatsky Rise, Exmouth Plateau and Kerguelen Plateau are taken from Schneider et al. (2011) and converted to the timescale of Gradstein et al. (2012). Horizontal dotted lines represent the EECO interval defined at mid-Waipara River.

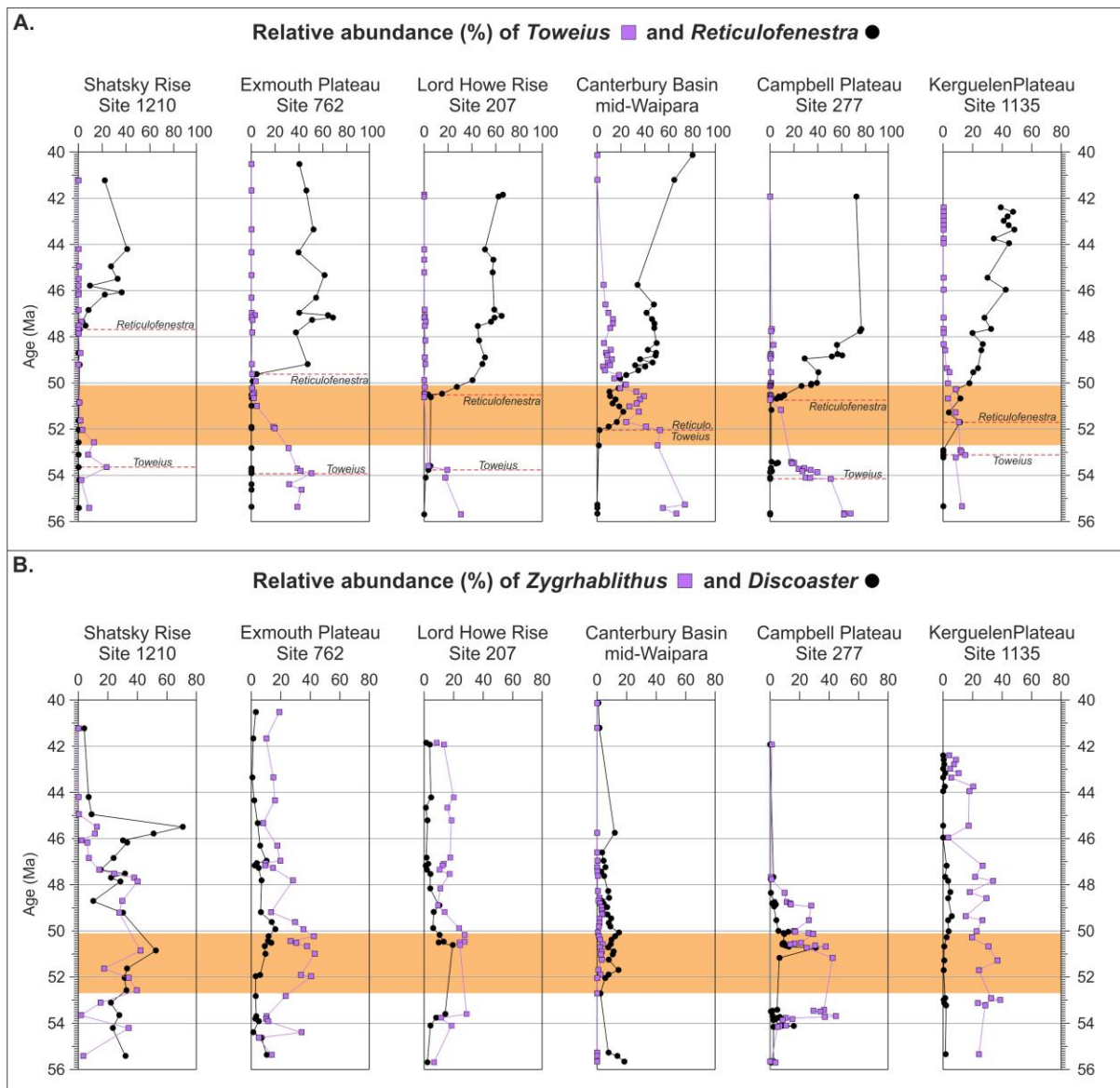


Figure 6.3: Relative abundance of *Toweius*, *Reticulofenestra*, *Zygrabliithus* and *Discoaster* at each study site. Data for Shatsky Rise, Exmouth Plateau and Kerguelen Plateau are taken from Schneider et al. (2011) and converted to the timescale of Gradstein et al. (2012). Red dashed lines mark key abundance shifts within genera. Orange shading represents the Early Eocene Climatic Optimum (EECO).

6.6 Comparison with geochemical temperature proxies

As discussed in the previous section, early Eocene nannofossil assemblages in the SW Pacific are indicative of warm temperate conditions (~15–20°C), rather than tropical conditions estimated by geochemical proxies (~26–30°C; Bijl et al., 2009; Hollis et al., 2009; Creech et al., 2010; Hollis et al., 2012, 2015). This is in agreement with radiolarian assemblages in the SW Pacific, which were dominated by cosmopolitan taxa and only low numbers of low-latitude, tropical-subtropical taxa during the early Eocene (Hollis et al., 2014).

Although all four sites in the SW Pacific show an increase in warm-water assemblages through the EECO, abundance is not as high as that recorded at low latitudes (Schneider et al., 2011). Site 277 shows the highest peak in warm-water taxa during the EECO, accounting for 32% of the total assemblage (Figure 6.1). However, this increase represents a short-lived incursion of warm-water taxa rather than a sustained increase throughout the duration of the EECO. The generally low abundance of warm-water taxa at SW Pacific sites and relatively short episodes of warm-water incursions are difficult to reconcile with the geochemical temperature estimates, which indicate tropical temperatures throughout the entire EECO.

This study appears to confirm suspicions that geochemical proxies are overestimating SSTs in the SW Pacific (Hollis et al., 2012; Pancost et al., 2013). The warm bias in the TEX_{86} proxy may be explained by the effects of seasonality in high latitudes and/or the shallow location of the local sites (Taylor et al., 2013; Inglis et al., 2015; Ho & Laepple, 2016). There may also be problems associated with application of the Mg/Ca proxy in SW Pacific records (Creech et al., 2010; Hollis et al., 2005). Diagenesis causes Mg to substitute for Ca when diagenesis increases, resulting in temperatures that are too hot (Kozdon et al., 2013). In general, the problem is reversed for oxygen isotopes with diagenesis resulting in anomalously low SSTs (Sexton et al. 2006). However, in onshore sections such as Mid-Waipara, meteoric water interactions can cause a significant negative shift in $\delta^{18}O$ values, resulting in anomalously warm SSTs. Preservation of a significant offset between benthic and planktic $\delta^{18}O$ values in this section indicates that diagenesis has not had a major impact on the temperature reconstructions previously reported (Hollis et al., 2009, 2012).

6.7 Biogeographic reconstruction of nannofossil assemblages

Studies of modern and Quaternary oceanography document changes in the SW Pacific Ocean during intervals of warm climate. Hill et al. (2008) found that temperature and salinity has increased off the east coast of Tasmania since 1944. They related these changes to the poleward expansion of the East Australian Current (EAC), linked to changes in the regional mean wind stress curl. Cai (2006) demonstrated that changes to surface winds

caused a spin-up and southward shift of the Southern Ocean super gyre, thus leading to a strengthening of the EAC and the southward migration of marine species in the SW Pacific.

Similar mechanisms can be proposed for changes in ocean circulation during the Cenozoic. Nelson & Cooke (2001) proposed that during the Paleocene, the Southern Ocean around New Zealand was largely influenced by subtropical surface waters fed by the western limb of a South Pacific gyre. This is in agreement with later studies which suggested that the southward expansion of a proto- EAC, prior to the opening of the Tasman gateway, resulted in tropical to warm subtropical water in the south Tasman Sea and New Zealand region (Kennet & Exon, 2004; Sijp et al., 2011). Although Nelson & Cooke (2001) found no evidence of oceanic frontal systems in the Paleocene, they noted that Jenkins (1973) recognised a transition zone between warm subtropical and temperate (cool subtropical) waters at $\sim 55^{\circ}\text{S}$ paleolatitude. Nelson & Cooke (2001) inferred that this transition zone was located $\sim 5^{\circ}\text{S}$ further south during the early-middle Eocene, based on the presence of warm subtropical to marginally tropical marine biota and relatively high SSTs estimated from oxygen isotopes during this interval.

Nannofossil data from this study are broadly in agreement with the inferences drawn in these previous studies. Calculation of the ratio between warm- and cool-water taxa at each site identifies a clear pattern of warm and cool assemblages through the early to middle Eocene (Figure 6.4). During the early Eocene ($\sim 50\text{--}56$ Ma) assemblages from the SW Pacific sites were comprised predominantly of warm-water taxa, suggesting that a warm-water mass extended to $\sim 55^{\circ}\text{S}$ paleolatitude at this time. Although SW Pacific nannofossil assemblages appear to have been influenced by warmer surface waters, it is unlikely that temperatures reached tropical levels, as the ratio of warm- to cool-water taxa is still well below that of low-latitude sites (e.g. Shatsky Rise; Figure 6.5C), even though diversity of warm-water taxa is comparable at both latitudes (Figure 6.5E). Instead, it appears that the boundary between warm subtropical and temperate waters, here referred to as the proto-Tasman Front (proto-TF), migrated southward in response to enhanced poleward heat transport (Figure 6.4).

During the middle Eocene (47–40 Ma), cool-water taxa became more abundant in SW Pacific nanofossil assemblages and diversity also decreased, indicating a shift towards cooler conditions (Figures 6.5B & D). It is likely that the proto-TF shifted north of ~45°S paleolatitude and this was accompanied by an intensification of the proto-Ross Gyre (proto-RG; Figure 6.5B & D). This is in agreement with Nelson & Cooke (2001), who suggested that cooling in the middle Eocene was likely accompanied by a return of the transition zone between warm subtropical and temperate waters to ~50°S paleolatitude. This pattern of frontal movement during cooler intervals is also consistent with Quaternary studies, which indicate northerly migration of the Subtropical Front to around 45–46°S during cool phases such as the last marine isotope stages 3 and 4 (Sikes, et al., 2009).

The abundance of warm-water taxa was lower in the Canterbury Basin than at Sites 207 and 277 during the EECO, suggesting that the warming of surface waters associated with the expansion of the proto-EAC was not as influential in the eastern region of New Zealand as in the west. The relatively short-lived influx of warm-water taxa at Site 277 during the EECO suggests that warm waters expanded south during this interval. However, diversity and abundance of warm-water taxa was greatest at Site 207, implying that the proto-EAC exerted greater influence at this site throughout the EECO. As mentioned previously, data are not well constrained through the lower part of the EECO at Site 207 due to large sampling gaps and as such it is not possible to determine whether the increase in warm-water taxa was sustained throughout the entire interval.

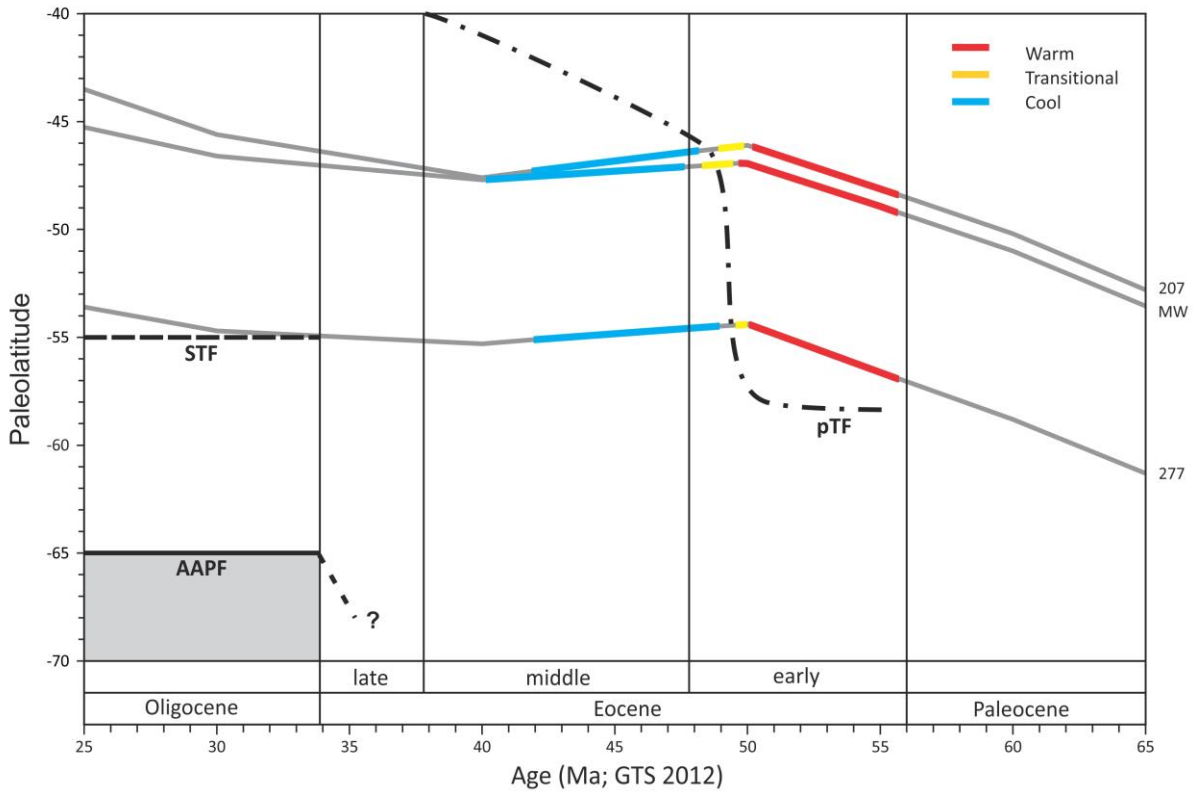
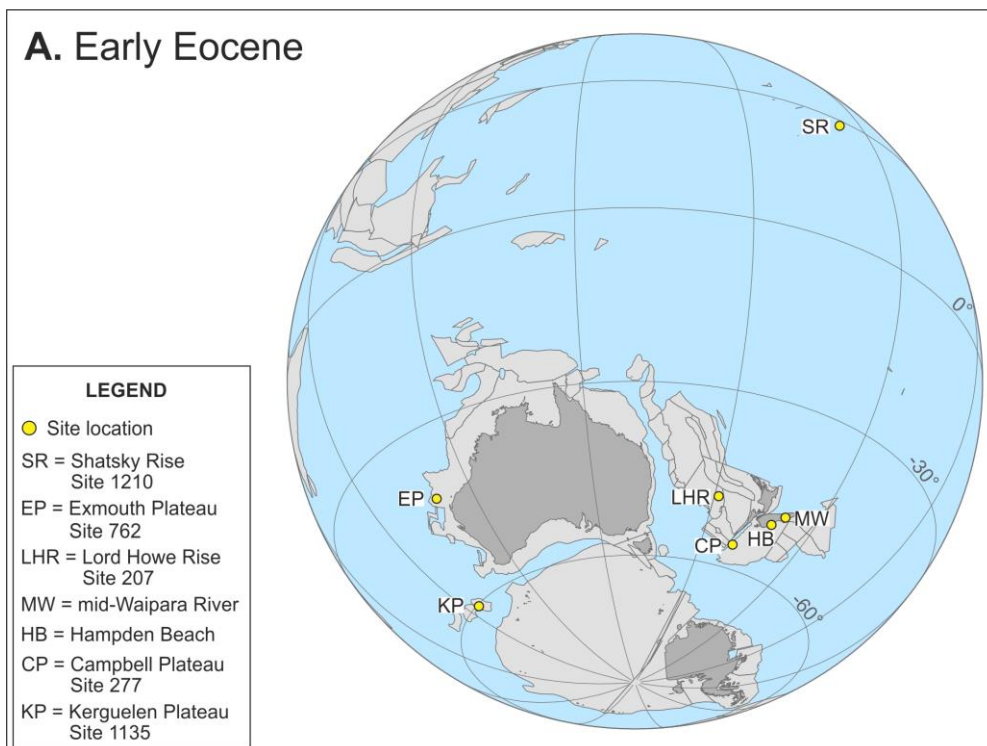
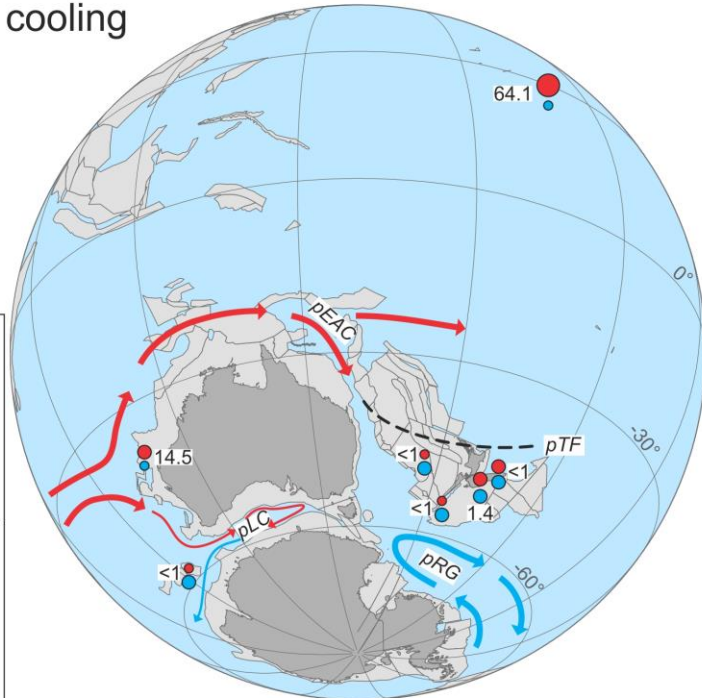
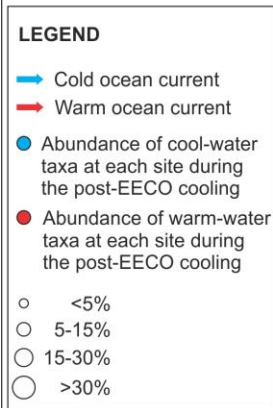


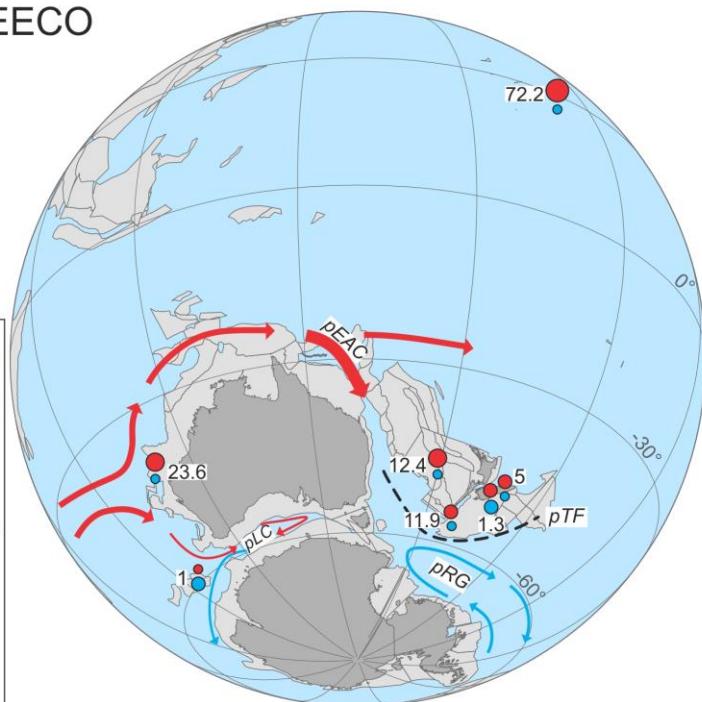
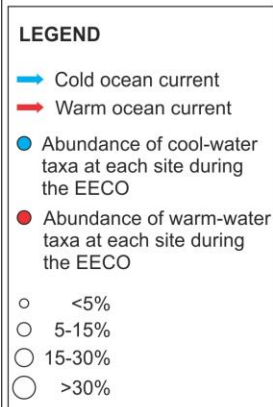
Figure 6.4: Development of the southwest Pacific Subtropical Front in the early to middle Eocene based on nannofossil warm- and cool-water assemblages. Red lines indicate intervals where the ratio of warm- to cool-water taxa > 2 ; blue lines indicate intervals where the ratio is less than 1; and yellow lines represent a transitional interval in between. The grey lines represent the paleolatitude of each site at 5 Ma time intervals. Paleolatitudes were calculated at www.paleolatitude.org and are based on the reference frame of Torsvik et al. (2012). AAPF = Antarctic Polar Front; pTF = proto-Tasman Front; STF = Subtropical Front; GTS = Geological Time Scale.



B. Post-EECO cooling ~47–40 Ma



C. During the EECO ~52–50 Ma



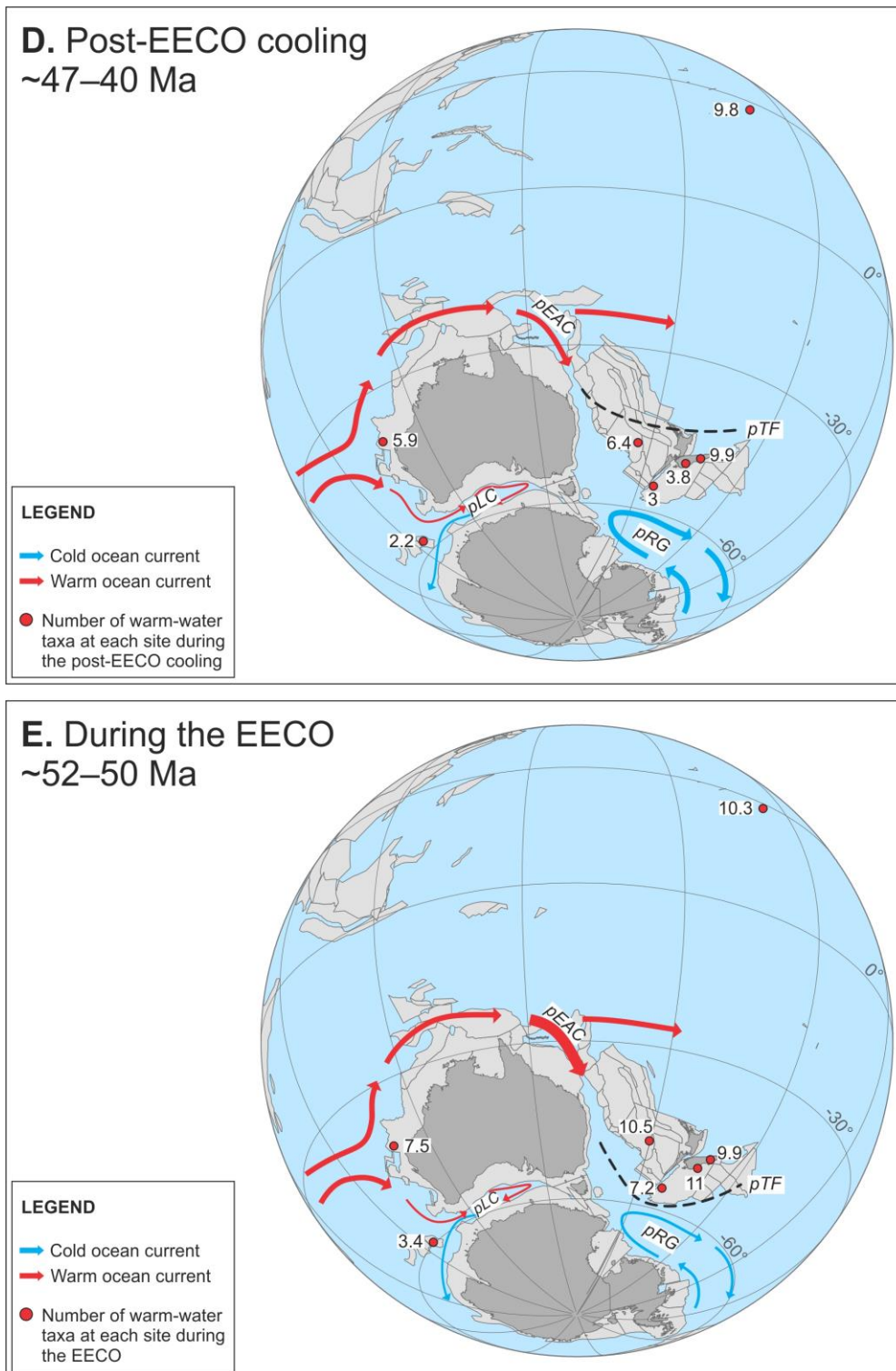


Figure 6.5: Paleogeographic reconstructions for sites in the southern middle to high latitudes in the early to middle Eocene (A) Location of each site in the early Eocene. (B) and (C) Ratio of warm- to cool-water taxa at each site. (D) and (E) Number of warm-water taxa at each site. Data for Shatsky Rise (SR), Exmouth Plateau (EP) and Kerguelen Plateau (KP) are from Schneider et al. (2011). Values are taken as the average over each time interval. Paleogeographic reconstructions are based on the absolute reference frame of Torsvik et al. (2012). pEAC = proto-East Australian Current; pTF = proto-Tasman Front; pRG = proto-Ross Gyre; pLC = proto-Leeuwin Current.

CHAPTER 7: CONCLUSIONS

7.1 Key findings

The objective of this study was to examine species turnover and changes in biogeographic distribution of southwest (SW) Pacific calcareous nannofossils in the early to middle Eocene, in order to determine how they responded to an increase in global temperatures during the Early Eocene Climatic Optimum (EECO). In particular, this study investigates whether calcareous nannofossil assemblages provide evidence of subtropical to tropical conditions at middle latitudes during the early to middle Eocene and evidence of a negligible equator to pole gradient in sea-surface temperature (SST).

The key findings of this study are summarised below:

- 1) All of the sections studied in this project span nannofossil zones NP10–16 (Waipawan to Bortonian NZ Stages). The data indicate up to three regional unconformities through the sections: at mid-Waipara and DSDP Sites 207 and 277, part or all of Zone NP10 (lower Waipawan) is missing; at Sites 207 and 277 a possible hiatus occurs within NP12 (upper Waipawan–lower Mangaorapan); and at all sites, part or all of Zone NP15 (lower Bortonian) is missing.
- 2) All preservation indices are in good agreement at the siliciclastic mid-Waipara section and are significantly correlated with CaCO₃ content, i.e. preservation decreases as carbonate content decreases up-section. Greater variability is observed in indices at the pelagic DSDP Sites, although there is a general consistency between visual observation and unidentified rims at both sites. The results of this study demonstrate that the preservation indices have varying utility at each of the sites and further work is needed to determine their individual reliability.
- 3) Early to middle Eocene nannofossil assemblages in the SW Pacific are more similar to floras at temperate sites rather than those at tropical/subtropical sites.

- 4) Variations in the relative abundance of key species in the SW Pacific are consistent with the trends seen in the geochemical proxy records. A peak in the abundance and diversity of warm-water taxa coincided with the EECO, which is in agreement with global evidence for this interval being a sustained period of prolonged global warmth in the Cenozoic.
- 5) Nannofossil data have been used to refine an existing oceanographic model (Nelson & Cook, 2001). A boundary between warm subtropical water and cooler temperate water, here referred to as the proto-Tasman Front, is identified based on changes in temperature-dependent species. High abundance of warm-water taxa in the early Eocene indicate that a warm-water mass (northward of the proto-Tasman Front) migrated southward to $\sim 55^{\circ}\text{S}$ paleolatitude, in response to enhanced poleward heat transport and intensification of the proto-East Australian Current. At Site 277, on the Campbell Plateau (paleolatitude $\sim 54^{\circ}\text{S}$), a relatively short-lived influx of warm-water taxa at ~ 51 Ma indicates that this southernmost site was influenced by warmer waters at that time. However, greater diversity and abundance of warm-water taxa at Site 207, Lord Howe Rise (paleolatitude $\sim 46^{\circ}\text{S}$), throughout the EECO implies that the proto-East Australian Current exerted greater influence in this northwestern region.
- 6) Following the termination of the EECO, changes in nannofossil assemblages are consistent with the northwards contraction of the proto-Tasman Front and associated amplification of the proto-Ross Gyre. Cool-water taxa became more abundant during this interval and the diversity and abundance of warm-water taxa decreased.
- 7) Previous estimates of high SSTs in the SW Pacific during the EECO suggest that there was virtually no latitudinal SST gradient, whereas nannofossil data from this study indicate that a reduced SST gradient was maintained through the EECO.
- 8) This study offers insights into the potential impacts of future climate change, providing a better understanding of the tolerance of marine plankton to global warming and ocean acidification. Results indicate that nannofossil assemblages thrive during prolonged warm periods such as the EECO, with an increase in the abundance of warm-

water taxa and overall diversity. Additionally, the preservation of assemblages is not adversely affected by warmer SSTs. This study also helps to improve estimates from polar amplification of temperature due to global warming. Geochemical proxies are inferred to have overestimated the degree of polar amplification during the Eocene. This is an area that requires further study in order to determine the true degree of amplification.

7.2 Future work

This study opens up several avenues of research that would help to refine or expand on the results presented thus far.

- 1) Biostratigraphic resolution was hampered at some sites by large sampling gaps or incomplete sections. Further sampling/analysis at these sites is needed to better constrain zone boundaries and improve correlation between sites.
- 2) The zonations of Martini (1971) and Agnini et al. (2014) provided reasonable biostratigraphic resolution and enabled correlation between sites, but further work is needed to improve the zonation for the SW Pacific.
- 3) The age models presented in this study for Sites 207 and 277 are fairly rudimentary, with large error bars. Further integration with other microfossil groups and magnetostratigraphy would help to refine these age models and allow a more accurate interpretation of the timing of events in the SW Pacific.
- 4) The study of other sections/cores within the SW Pacific region is required in order to determine whether the key findings of this study are consistent across the region. Upcoming International Ocean Discovery Program (IODP) expeditions in the SW Pacific provide an ideal opportunity to extend this research. In particular, Expedition 378 (South Pacific Paleogene Climate) offers the potential to recover Eocene nannofossil assemblages in the southern Pacific Ocean from sites situated at ~59°S paleolatitude.

- 5) The data collected in this study could be used to explore in more detail the dominance of particular genera across different intervals and latitudes. In particular, the effects of *Reticulofenestra* evolution on the structuring of coccolith communities through the Eocene would provide a better understanding of the evolutionary impact of this genera during the Cenozoic.

REFERENCES

- Agnini, C., Fornaciari, E., Raffi, I., Catanzariti, R., Pälike, H., Backman, J., et al. (2014). Biozonation and biochronology of Paleogene calcareous nannofossils from low and middle latitudes. *Newsletters on Stratigraphy*, 47(2), 131–181.
- Agnini, C., Fornaciari, E., Raffi, I., Rio, D., Röhl, U., & Westerhold, T. (2007a). High-resolution nannofossil biochronology of middle Paleocene to early Eocene at ODP Site 1262: Implications for calcareous nannoplankton evolution. *Marine Micropaleontology*, 64(3–4), 215–248, doi: 10.1016/j.marmicro.2007.05.003.
- Agnini, C., Fornaciari, E., Rio, D., Tateo, F., Backman, J., & Giusberti, L. (2007b). Responses of calcareous nannofossil assemblages, mineralogy and geochemistry to the environmental perturbations across the Paleocene/Eocene boundary in the Venetian Pre-Alps. *Marine Micropaleontology*, 63(1–2), 19–38, doi: 10.1016/j.marmicro.2006.10.002.
- Agnini, C., Muttoni, G., Kent, D. V., & Rio, D. (2006). Eocene biostratigraphy and magnetic stratigraphy from Possagno, Italy: The calcareous nannofossil response to climate variability. *Earth and Planetary Science Letters*, 241, 815–830.
- Alcober, J., & Jordan, R. W. (1997). An interesting association between *Neosphaera coccolithomorpha* and *Ceratolithus cristatus* (Haptophyta). *Eur. J. Phycol.*, 32, 91–93.
- Allredge, A. L., & Silver, M. W. (1988). Characteristics, dynamics and significance of marine snow. *Progress in Oceanography*, 20(1), 41–82.
- Anderson, T. F., & Cole, S. A. (1975). The stable isotope geochemistry of marine coccoliths: a preliminary comparison with planktonic foraminifera. *Journal of Foraminiferal Research*, 5(3), 188–192.
- Applegate, J. L., & Wise, S. W. (1987). Eocene calcareous nannofossils, Deep Sea Drilling Project Site 205, upper continental rise off New Jersey, U.S.A. In van Hinte, J. E., Wise, S. W., et al., *Initial Reports of the Deep Sea Drilling Project* (Vol. 93, pp. 685–698). Washington, DC: US Government Printing Office.
- Arney, J. E., & Wise, S. W. (2003). Paleocene–Eocene nannofossil biostratigraphy of ODP Leg 183, Kerguelen Plateau. In Frey, F. A., Coffin, M. F., et al., *Proceedings of the Ocean Drilling Program, Scientific Results, 183* (pp. 1–59). College Station, TX.
- Aubry, M.-P. (1991). Sequence stratigraphy: Eustasy or tectonic imprint? *Journal of Geophysical Research*, 96(B4), 6641–6679, doi: 10.1029/90JB01204.

- Aubry, M. P. (1992). Late Paleogene calcareous nannoplankton evolution: a tale of climatic deterioration. In Prothero, D. R., & Berggren, W. A. (Eds.), *Eocene–Oligocene Climate and Biotic Evolution* (pp. 272–309). Princeton, NJ: Princeton University Press.
- Aubry, M. P. (1998). Early Paleogene calcareous nannoplankton evolution: a tale of climatic amelioration. In Aubry, M. P., Lucas, S., et al. (Eds.), *Late Paleocene–Early Eocene Climatic and Biotic Events in the Marine and Terrestrial Records* (pp. 158–203). New York: Columbia University Press.
- Backman, J. (1986). Late Paleocene to middle Eocene calcareous nannofossil biochronology from the Shatsky Rise, Walvis Ridge and Italy. *Palaeogeography, Palaeoclimatology, Palaeoecology*, *57*, 43–59.
- Backman, J. (1987). Quantitative calcareous nannofossil biochronology of middle Eocene through early Oligocene sediment from DSDP Sites 522 and 523. *Abhandlungen der Geologische Bundesanstalt*, *39*, 21–31.
- Backman, J., & Hermelin, J. O. R. (1986). Morphometry of the Eocene nannofossil *Reticulofenestra umbilicus* lineage and its biochronological consequences. *Palaeogeography, Palaeoclimatology, Palaeoecology*, *57*, 103–116.
- Backman, J., Raffi, I., Rio, D., Fornaciari, E., & Pälike, H. (2012). Biozonation and biochronology of Miocene through Pleistocene calcareous nannofossils from low and middle latitudes. *Newsletters on Stratigraphy*, *45*(3), 221–244.
- Ballance, P. F. (1993). The paleo-Pacific, post-subduction, passive margin thermal relaxation sequence (Late Cretaceous–Paleogene) of the drifting New Zealand continent. In Ballance, P. F. (Ed.), *South Pacific Sedimentary Basins of the World 2* (pp. 93–110): Elsevier Science Publishers.
- Barker, S., Cacho, I., Benway, H., & Tachidawa, K. (2005). Planktonic foraminiferal Mg/Ca as a proxy for past oceanic temperatures: a methodical overview and data compilation for the Last Glacial Maximum. *Quaternary Science Reviews*, *24*, 821–834.
- Benson, W. N. (1943). The basic igneous rocks of eastern Otago and their tectonic environment. Part IV – The mid-Tertiary basalts, tholeiites, and dolerites of north-eastern Otago. Section A: distribution and geological occurrence. *Transactions of the Royal Society of New Zealand*, *73*, 116–138.
- Bijl, P. K., Bendle, J. A., Bohaty, S. M., Pross, J., Schouten, S., Tauxe, L., et al. (2013). Eocene cooling linked to early flow across the Tasmanian Gateway. *PNAS*, *110*(24), 9645–9650, doi: 10.1073/pnas.1220872110.

- Bijl, P. K., Houben, A. J. P., Schouten, S., Bohaty, S. M., Sluijs, A., Reichart, G.-J., et al. (2010). Transient middle Eocene atmospheric CO₂ and temperature variations. *Science*, *330*, 819–821.
- Bijl, P. K., Schouten, S., Sluijs, A., Reichart, G.-J., Zachos, J. C., & Brinkhuis, H. (2009). Early Palaeogene temperature evolution of the southwest Pacific Ocean. *Nature*, *461*(7265), 776–779, doi: 10.1038/nature08399.
- Billard, C., & Inouye, I. (2004). What is new in coccolithophore biology? In Thierstein, H. R., & Young, J. R. (Eds.), *Coccolithophores: From Molecular Processes to Global Impact* (pp. 1–29). Berlin: Springer-Verlag.
- Bohaty, S. M., Zachos, J. C., Florindo, F., & Delaney, M. L. (2009). Coupled greenhouse warming and deep-sea acidification in the middle Eocene. *Paleoceanography*, *24*(2), PA2207, doi: 10.1029/2008pa001676.
- Bolton, C. T., Stoll, H., & Mendez-Vicente, A. (2012). Vital effects in coccolith calcite: Cenozoic climate-pCO₂ drove the diversity of carbon acquisition strategies in coccolithophores? *Paleoceanography*, *27*(4), 16 p.
- Bown, P. R. (1998). *Calcareous Nannofossil Biostratigraphy*. Cambridge: Cambridge University, 315 p.
- Bown, P. R. (2005). Paleogene calcareous nannofossils from the Kilwa and Lind areas of coastal Tanzania (Tanzania Drilling Project 2003–4). *Journal of Nannoplankton Research*, *27*(1), 21–95.
- Bown, P. R., Lees, J. A., & Young, J. R. (2004). Calcareous nannoplankton evolution and diversity through time. In Thierstein, H. R., & Young, J. R. (Eds.), *Coccolithophores: From Molecular Processes to Global Impact* (pp. 481–508). Berlin: Springer-Verlag.
- Bown, P. R., & Young, J. R. (1998a). Introduction. In Bown, P. R. (Ed.), *Calcareous Nannofossil Biostratigraphy* (pp. 1–15). London: Kluwer Academic Publishers.
- Bown, P. R., & Young, J. R. (1998b). Techniques. In Bown, P. R. (Ed.), *Calcareous Nannofossil Biostratigraphy* (pp. 16–28). London: Kluwer Academic Publishers.
- Bralower, T. J. (2002). Evidence of surface water oligotrophy during the Paleocene-Eocene thermal maximum: Nannofossil assemblage data from Ocean Drilling Program Site 690, Maud Rise, Weddell Sea. *Paleoceanography*, *17*(2), 13-1–13-12, doi: 10.1029/2001pa000662.
- Bramlette, M. N. (1957). Geology of Saipan, Mariana Islands: Discoasters and some related microfossils. *U.S. Geological Survey Professional Paper*, *280*, 247–255.

- Bramlette, M. N., & Martini, E. (1964). The great change in calcareous nannoplankton fossils between the Maestrichtian and Danian. *Micropaleontology*, 10(3), 291–322.
- Bramlette, M. N., & Riedel, W. R. (1954). Stratigraphic value of discoasters and some other microfossils related to recent coccolithophores. *Journal of Paleontology*, 28(4), 385–403.
- Bramlette, M. N., & Sullivan, F. R. (1961). Coccolithophorids and related nannoplankton of the Early Tertiary in California. *Micropaleontology*, 7(2), 129–188.
- Bramlette, M. N., & Wilcoxon, J. A. (1967). Middle Tertiary calcareous nannoplankton of the Cipero Section, Trinidad, W.I. *Tulane Studies in Geology*, 5, 93–132.
- Brand, L. E. (1994). Physiological ecology of marine coccoliths. In Winter, A., & Siesser, W. G. (Eds.), *Coccolithophores* (pp. 39–49). Cambridge: Cambridge University Press.
- Brassell, S. C. (2014). Climatic influences on the Paleogene evolution of alkenones. *Paleoceanography*, 29, 255–272, doi: 10.1002/2013PA002576.
- Brassell, S. C., Brereton, R. G., Eglinton, G., Grimalt, J., Liebezeit, G., Marlowe, I. T., et al. (1986a). Palaeoclimatic signals recognized by the chemometric treatment of molecular stratigraphic data. *Organic Geochemistry*, 10, 649–660.
- Brassell, S. C., Eglinton, G., Marlowe, I. T., Pflaumann, U., & Sarnthein, M. (1986b). Molecular stratigraphy: a new tool for climatic assessment. *Nature*, 320, 129–133.
- Brown, D. A. (1959). Hampden Formation, Kurinui Formation, Moeraki Formation. In Fleming, C. A. (Ed.), *Lexique stratigraphic international 6, Oceania 4, New Zealand* (pp. 118–119, 184, 237).
- Browne, G. H., & Field, B. D. (1985). The lithostratigraphy of Late Cretaceous to early Pleistocene rocks of northern Canterbury, New Zealand. *New Zealand Geological Survey record 6* (pp. 63).
- Bukry, D. (1973a). Coccolith and silicoflagellate biostratigraphy, Tasman Sea and southwest Pacific Ocean, Deep Sea Drilling Project Leg 21. In Burns, R. E., Andrews, J. E., et al., *Initial Reports of the Deep Sea Drilling Project* (Vol. 21, pp. 885–893). Washington, DC: US Government Printing Office.
- Bukry, D. (1973b). Coccolith stratigraphy, eastern equatorial Pacific, Leg 16 Deep Sea Drilling Project. In van Andel, T. H., Heath, G. R., et al., *Initial Reports of the Deep Sea Drilling Project* (Vol. 16, pp. 653–711). Washington DC: US Government Printing Office.

- Bukry, D. (1973c). Low-latitude coccolith biostratigraphic zonation. In Edgar, N. T., Saunders, J. B., et al., *Initial Reports of the Deep Sea Drilling Project* (Vol. 15, pp. 685–703). Washington, DC: U.S. Government Printing Office.
- Bukry, D. (1974). Phytoplankton stratigraphy, offshore East Africa, Deep Sea Drilling Project Leg 25. In Simpson, E. S. W., Schlich, R., et al., *Initial Reports of the Deep Sea Drilling Project* (Vol. 25, pp. 635–646). Washington DC: US Government Printing Office.
- Bukry, D. (1975). Coccolith and silicoflagellate stratigraphy, Northwestern Pacific Ocean, Deep Sea Drilling Project Leg 32. In Larson, R. L., Moberly, R., et al., *Initial Reports of the Deep Sea Drilling Project* (Vol. 32, pp. 677–701). Washington D.C.: U.S. Government Printing Office.
- Bukry, D., & Bramlette, M. N. (1970). Coccolith age determinations, Leg 3, Deep Sea Drilling Project. In Maxwell, A. E., von Herzon, R. P., et al., *Initial Reports of the Deep Sea Drilling Project* (Vol. 3, pp. 589–611). Washington, DC: US Government Printing Office.
- Burgess, C. E. (2008). *Palaeoclimate and palaeoenvironment of the middle Eocene southern Pacific; insights from New Zealand*. Unpublished PhD Thesis, Cardiff University, Wales. 219 pp.
- Burgess, C. E., Pearson, P. N., Lear, C. H., & Morgans, H. E. G. (2009). A Middle Eocene Southern Pacific climate record from Hampden Beach: the MECO in New Zealand. In Strong, C. P., Crouch, E. M., et al., *Climatic and biotic events of the Paleogene, 12–15 January 2009, Te Papa, Wellington, New Zealand: GNS Science Miscellaneous Series 16: 47*.
- Burgess, C. E., Pearson, P. N., Lear, C. H., Morgans, H. E. G., Handley, L., Pancost, R. D., et al. (2008). Middle Eocene climate cyclicity in the southern Pacific: implications for global ice volume. *Geology*, 36, 651–654, doi: 10.1130/G24762A.1.
- Burns, R. E., Andrews, J. E., Van der Lingen, G. J., Churkin, M., Galehouse, J. S., Packham, G. H., et al. (1973). Initial Reports of the Deep Sea Drilling Project. (Vol. 21, pp. 197–212). Washington DC: US Government Printing Office.
- Cai, W. (2006). Antarctic ozone depletion causes an intensification of the Southern Ocean super-gyre circulation. *Geophysical Research Letters*, 33, 4 p.
- Cameron, A. A., & Waghorn, D. B. (1985). Bortonian/Kaiatan foraminifera and calcareous nanofossils from Hampden Beach and McCulloch's Bridge. In Cooper, R. A., *Hornibrook Symposium, 1985, extended abstracts: New Zealand Geological Survey Record 9: 18–20*.

- Candelier, Y., Minoletti, F., Probert, I., & Hermoso, M. (2013). Temperature dependence of oxygen isotope fractionation in coccolith calcite: a culture and core top calibration of the genus *Calcidiscus*. *Geochimica et Cosmochimica Acta*, *100*, 264–281.
- Chang, Y. (1967). Accuracy of fossil percentage estimation. *Journal of Paleontology*, *41*(2), 500–502.
- Chave, K. E. (1954). Aspects of the biochemistry of magnesium: 1. calcareous marine organisms. *The Journal of Geology*, *62*(3), 266–283.
- CLIMAP Project Members. (1976). The surface of the ice-age earth. *Science*, *191*(4232), 1131–1137.
- Colwell, R. K. (2012). Biodiversity: concepts, patterns, and measurement. In Levin, S. A. (Ed.), *The Princeton Guide to Ecology* (pp. 257–263). Princeton, NJ: Princeton University Press.
- Cortés, M. Y., & Bollman, J. (2002). A new combination coccosphere of the heterococcolith species *Coronosphaera mediterranea* and the holococcolith species *Calyptrolithophora hasleana*. *European Journal of Phycology*, *37*, 145–146, doi: 10.1017/S0967026201003523.
- Couapel, M. J. J., Beaufort, L., & Young, J. R. (2009). A new *Helicosphaera*-*Syracolithus* combination coccosphere (Haptophyta) from the western Mediterranean Sea. *Journal of Phycology*, *45*, 914–916, doi: 10.1111/j.1529-8817.2009.00703.x.
- Cramer, B. S., Wright, J. D., Kent, D. V., & Aubry, M. P. (2003). Orbital climate forcing of $\delta^{13}\text{C}$ excursions in the late Paleocene–early Eocene (chrons C24n–C25n). *Paleoceanography*, *18*(4), 1097.
- Creech, J. B., Baker, J. A., Hollis, C. J., Morgans, H. E. G., & Smith, E. G. C. (2010). Eocene sea temperatures for the mid-latitude southwest Pacific from Mg/Ca ratios in planktonic and benthic foraminifera. *Earth and Planetary Science Letters*, *299*(3–4), 483–495, doi: 10.1016/j.epsl.2010.09.039.
- Crouch, E. M., & Brinkhuis, H. (2005). Environmental change across the Paleocene-Eocene transition from eastern New Zealand: A marine palynological approach. *Marine Micropaleontology*, *56*, 138–160.
- Dallanave, E., Agnini, C., Bachtadse, V., Muttoni, G., Crampton, J. S., Strong, C. P., et al. (2015). Early to middle Eocene magneto-biochronology of the southwest Pacific Ocean and climate influence on sedimentation: Insights from the Mead Stream section, New Zealand. *GSA Bulletin*, *127*, 643–660, doi: 10.1130/B31147.1.

- Dallanave, E., Bachtadse, V., Agnini, C., Muttoni, G., Hollis, C., Hines, B. R., et al. (2014). Early–middle Eocene magneto-biochronology of the Southern Pacific Ocean: new data from the South Island of New Zealand. *Rendiconti Online Societa Geologica Italiana*, *31*, 50–51.
- Dallanave, E., Bachtadse, V., Crouch, E. M., Tauxe, L., Shepherd, C. L., Morgans, H. E. G., et al. (2016). Constraining early to middle Eocene climate evolution of the southwest Pacific and Southern Ocean. *Earth and Planetary Science Letters*, *433*, 380–392, doi: 10.1016/j.epsl.2015.11.010.
- De Rosa, M., & Gambacorta, A. (1988). The lipids of archaebacteria. *Progress in Lipid Research*, *27*, 153–175.
- de Vargas, C., Aubry, M. P., Probert, I., & Young, J. (2007). Origin and evolution of coccolithophores: from coastal hunters to oceanic farmers. In Falkowski, P. G., & Knoll, A. H. (Eds.), *Evolution of Primary Producers in the Sea* (pp. 251–285). Burlington: Academic Press.
- DeConto, R., & Pollard, D. (2003). Rapid Cenozoic glaciation of Antarctica induced by declining atmospheric CO₂. *Nature*, *421*, 245–249, doi: 10.1038/nature01290.
- Delaney, M. L., Bé, A. W. H., & Boyle, E. A. (1985). Li, Sr, Mg, and Na in foraminiferal calcite shells in laboratory culture, sediments traps, and sediment cores. *Geochimica et Cosmochimica Acta*, *49*, 1327–1341.
- DeLong, E. F. (1992). Archaea in coastal marine environments. *PNAS*, *89*, 5685–5689.
- Duckworth, D. L. (1977). Magnesium concentration in the tests of the planktonic foraminifer *Globorotalia truncatulinoides*. *Journal of Foraminiferal Research*, *7*(4), 304–312.
- Dudley, W. C., Blackwelder, P. L., Brand, L., & Duplessy, J. C. (1986). Stable isotopic composition of coccoliths. *Marine Micropaleontology*, *10*, 1–8.
- Dudley, W. C., Duplessy, J. C., Blackwelder, P. L., Brand, L. E., & Guillard, R. R. L. (1980). Coccoliths in Pleistocene–Holocene nannofossil assemblages. *Nature*, *285*, 222–223.
- Dunkley Jones, T., Bown, P. R., & Pearson, P. N. (2009). Exceptionally well preserved upper Eocene to lower Oligocene calcareous nannofossils (Prymnesiophyceae) from the Oande Formation (Kilwa Group), Tanzania. *Journal of Systematic Paleontology*, *7*(4), 359–411.
- Dunkley Jones, T., Lunt, D. J., Schmidt, D. N., Ridgwell, A., Sluijs, A., Valdes, P. J., et al. (2013). Climate model and proxy data constraints on ocean warming across the Paleocene–Eocene Thermal Maximum. *Earth-Science Reviews*, *125*, 123–145.

- Edwards, A. R. (1966). Calcareous nannoplankton from the uppermost Cretaceous and lowermost Tertiary of the mid-Waipara section, South Island, New Zealand. *New Zealand Journal of Geology & Geophysics*, 9(4), 481–490, doi: 10.1080/00288306.1966.10422492.
- Edwards, A. R. (1971). *A calcareous nannoplankton zonation of the New Zealand Paleogene*. Paper presented at the Proceedings of the Second Planktonic Conference, Roma.
- Edwards, A. R. (1973a). Calcareous nanofossils from the southwest Pacific, Deep Sea Drilling Project, Leg 21. In Burns, R. E., Andrews, J. E., et al., *Initial Reports of the Deep Sea Drilling Project* (Vol. 21, pp. 641–691). Washington, DC: US Government Printing Office.
- Edwards, A. R. (1973b). Southwest Pacific regional unconformities encountered during Leg 21. In Burns, R. E., Andrews, J. E., et al., *Initial Reports of the Deep Sea Drilling Project* (Vol. 21, pp. 701–720). Washington, DC: US Government Printing Office.
- Edwards, A. R., & Perch-Nielson, K. (1975). Calcareous nanofossils from the southern southwest Pacific, Deep Sea Drilling Project, Leg 29. In Kennett, J. P., Houtz, R. E., et al., *Initial Reports of the Deep Sea Drilling Project* (Vol. 29, pp. 469–539). Washington, DC: US Government Printing Office.
- Emiliani, C. (1955). Pleistocene temperatures. *The Journal of Geology*, 63(6), 538–578.
- Epstein, S., Buchsbaum, R., Lowenstam, H. A., & Urey, H. C. (1953). Revised carbonate-water isotopic temperature scale. *Bulletin of the Geological Society of America*, 64, 1315–1325.
- Exon, N. F., Kennett, J. P., & Malone, M. J. (2004). Leg 189 synthesis: Cretaceous - Holocene history of the Tasmanian Gateway. In Exon, N. F., Kennett, J. P., et al., *Proceedings of the Ocean Drilling Program, Scientific Results, 189* (pp. 1–38). College Station, Texas.
- Expedition 318 Scientists. (2010). Wilkes Land Glacial History: Cenozoic East Antarctic Ice Sheet evolution from Wilkes Land margin sediments. *IODP Preliminary Report, 318*.
- Expedition 320/321 Scientists. (2010). Methods. In Pälike, H., Lyle, M., et al., *Proceedings of the Integrated Ocean Drilling Program, 320/321*. Tokyo: Integrated Ocean Drilling Program Management International.
- Fioroni, C., Villa, G., Persico, D., Wise, S. W., & Pea, L. (2012). Revised middle Eocene-upper Oligocene calcareous nanofossil biozonation for the Southern Ocean. *Revue de Micropaléontologie*, 55(2), 53–70, doi: 10.1016/j.revmic.2012.03.001.
- Firth, J. V., Eldrett, J. S., Harding, I. C., Coxall, H. K., & Wade, B. S. (2013). Integrated biomagnetostratigraphy for the Palaeogene of ODP Hole 647A: implications for

correlating palaeoceanographic events from high to low latitudes. In Jovane, L., Herrero-Bervera, E., et al. (Eds.), *Magnetic Methods and the Timing of Geological Processes* (pp. 29–78). London: Geological Society, Special Publications, 373.

Fuhrman, J. A., McCallum, K., & Davis, A. A. (1992). Novel major archaeobacterial group from marine plankton. *Nature*, *356*, 148–149.

Galeotti, S., Krishnan, S., Pagani, M., Lanci, L., Gaudio, A., Zachos, J. C., et al. (2010). Orbital chronology of early Eocene hyperthermals from the Contessa Road section, central Italy. *Earth and Planetary Science Letters*, *290*, 192–200.

Gartner, S. (1969). Correlation of Neogene planktonic foraminifera and calcareous nannofossil zones. *Transactions of the Gulf Coast Association of Geological Societies*, *19*, 585–599.

Geisen, M., Billard, C., Broerse, A., Cros, L., Probert, I., & Young, J. (2002). Life-cycle associations involving pairs of holococcolithophorid species: intraspecific variation or cryptic speciation? *European Journal of Phycology*, *37*(4), 531–550, doi: 10.1017/S0967026202003852.

Gibbs, S., Bown, P. R., Murphy, B. H., Sluijs, A., Edgar, K. M., Palike, H., et al. (2012). *Interactive comment on Scaled biotic disruption during early Eocene global warming events. Biogeosciences Discussions*, *9*, C618–C620.

Gibbs, S. J., Bralower, T. J., Bown, P. R., Zachos, J. C., & Bybell, L. M. (2006). Shelf and open-ocean calcareous phytoplankton assemblages across the Paleocene–Eocene Thermal Maximum. *Earth and Planetary Science Letters*, *295*, 583–592.

Gibbs, S. J., Shackleton, N. J., & Young, J. R. (2004). Identification of dissolution patterns in nannofossil assemblages: a high-resolution comparison of synchronous records from Ceara Rise, ODP Leg 154. *Palaeoceanography*, *19*, 12 p, doi: 10.1029/2003PA000958.

Gradstein, F. M., Ogg, J. G., Schmitz, M., & Ogg, G. (2012). *The Geologic Time Scale 2012*: Elsevier, 1176 p.

Greenwood, D. R., Wilf, P., Wing, S. L., & Christophel, D. C. (2004). Paleotemperature estimation using leaf-margin analysis: Is Australia different? *PALAIOS*, *19*, 129–142, doi: 10.1669/0883-1351(2004)019<0129:PEULAI>2.0.CO;2.

Hammer, Ø., Harper, D. A. T., & Ryan, P. D. (2001). PAST: paleontological statistics software package for education and data analysis. *Palaeontologia Electronica*, *4*(1), 9 p.

Haq, B. U. (1980). Biogeographic history of Miocene calcareous nannoplankton and paleoceanography of the Atlantic Ocean. *Micropaleontology*, *26*(4), 414–443.

- Haq, B. U. (1998). Calcareous nannoplankton. In Haq, B. U., & Boersma, A. (Eds.), *Introduction to marine micropaleontology* (pp. 79–108). Singapore: Elsevier Science.
- Haq, B. U., & Lohmann, G. P. (1976). Early Cenozoic calcareous nannoplankton biogeography of the Atlantic Ocean. *Marine Micropaleontology*, *1*, 119–194, doi: 10.1016/0377-8398(76)90008-6.
- Haq, B. U., Lohmann, G. P., & Wise, S. W. (1977a). Calcareous nannoplankton biogeography and its paleoclimatic implications: Cenozoic of the Falkland Plateau (DSDP Leg 36) and Miocene of the Atlantic Ocean. In Barker, P. F., Dalziel, L. W. D., et al., *Initial Reports of the Deep Sea Drilling Project* (Vol. 36, pp. 745–760). Washington D.C.: U.S. Government Printing Office.
- Haq, B. U., Premoli-Silva, I., & Lohmann, G. P. (1977b). Calcareous plankton paleobiogeographic evidence for major climatic fluctuations in the early Cenozoic Atlantic Ocean. *Journal of Geophysical Research*, *82*(27), 3861–3876.
- Hay, W. W., Mohler, H. P., Roth, P. H., Schmidt, R. R., & Boudreaux, J. E. (1967). Calcareous nannoplankton zonation of the Cenozoic of the Gulf Coast and Caribbean-Antillean area, the transoceanic correlation. *Transactions of the Gulf Coast Association of Geological Societies*, *17*, 428–480.
- Hermoso, M., Candelier, Y., Browning, T. J., & Minoletti, F. (2015). Environmental control of the isotopic composition of subfossil coccolith calcite: Are laboratory culture data transferable to the natural environment? *GeoResJ*, *7*, 35–42.
- Hill, K. L., Rintoul, S. R., Coleman, R., & Ridgway, K. R. (2008). Wind forced low frequency variability of the East Australia Current. *Geophysical Research Letters*, *35*, 5 p.
- Hines, B. R., Kulhanek, D. K., Hollis, C. J., Atkins, C. B., & Morgans, H. E. G. (2013). Paleocene–Eocene stratigraphy and paleoenvironment at Tora, Southeast Wairarapa, New Zealand. *New Zealand Journal of Geology and Geophysics*, *56*(4), 243–262, doi: 10.1080/00288306.2013.836112.
- Ho, S. L., & Laepple, T. (2016). Flat meridional temperature gradients in the early Eocene in the subsurface rather than surface ocean. *Nature Geoscience*, *9*, 606–610, doi: 10.1038/ngeo2763.
- Hollis, C. J., Dickens, G. R., Field, B. D., Jones, C. M., & Strong, C. P. (2005). The Paleocene–Eocene transition at Mead Stream, New Zealand: a southern Pacific record of early Cenozoic global change. *Palaeogeography, Palaeoclimatology, Palaeoecology*, *215*, 313–343.

- Hollis, C. J., Handley, L., Crouch, E. M., Morgans, H. E. G., Baker, J. A., Creech, J., et al. (2009). Tropical sea temperatures in the high-latitude South Pacific during the Eocene. *Geology*, *37*(2), 99–102, doi: 10.1130/G25200A.
- Hollis, C. J., Hines, B. R., Littler, K., Villasante-Marcos, V., Kulhanek, D. K., Strong, C. P., et al. (2015). The Paleocene-Eocene Thermal Maximum at DSDP Site 277, Campbell Plateau, southern Pacific Ocean. *Climates of the Past*, *11*, 1009–1025, doi: 10.5194/cp-11-1009-2015.
- Hollis, C. J., Pascher, K. M., Hines, B. R., Littler, K., Kulhanek, D. K., Strong, C. P., et al. (2014). Was the early Eocene ocean unbearably warm or are the proxies unbelievably wrong? *Rendiconti Online Societa Geologica Italiana*, *31*, 109–110.
- Hollis, C. J., Taylor, K. W. R., Handley, L., Pancost, R. D., Huber, M., Creech, J. B., et al. (2012). Early Paleogene temperature history of the Southwest Pacific Ocean: Reconciling proxies and models. *Earth and Planetary Science Letters*, *349–350*, 53–66, doi: 10.1016/j.epsl.2012.06.024.
- Hollis, C. J., Waghorn, D. B., Strong, C. P., & Crouch, E. M. (1997) Integrated Paleogene biostratigraphy of DSDP site 277 (Leg 29): foraminifera, calcareous nannofossils, Radiolaria, and palynomorphs. *Institute of Geological & Nuclear Sciences science report 97/07* (pp. 87).
- Honjo, S. (1976). Coccoliths: Production, transportation and sedimentation. *Marine Micropaleontology*, *1*, 65–79.
- Houdan, A., Billard, C., Marie, D., Not, F., Sáez, A. G., Young, J. R., et al. (2004). Hollococcolithophore-heterococcolithophore (Haptopyhta) life cycles: Flow cytometric analysis of relative ploidy levels. *Systematics and Biodiversity*, *1*(4), 453–465, doi: 10.1017/S1477200003001270.
- Huber, M., Brinkhuis, H., Stickley, C. E., Döös, K., Sluijs, A., Warnaar, J., et al. (2004). Eocene circulation of the Southern Ocean: Was Antarctica kept warm by subtropical waters? *Paleoceanography*, *19*(4), PA4026, doi: 10.1029/2004pa001014.
- Huber, M., & Caballero, R. (2011). The early Eocene equable climate problem revisited. *Climate of the Past*, *7*, 603–633, doi: 10.5194/cp-7-603-2011.
- Inglis, G. N., Farnsworth, A., Lunt, D., Foster, G. L., Hollis, C. J., Pagani, M., et al. (2015). Descent towards the Icehouse: Eocene sea surface cooling inferred from GDGT distributions. *Paleoceanography*, *30*, 1000–1020.
- Jenkins, D. G. (1993). The evolution of the Cenozoic southern high- and mid-latitude planktonic foraminiferal faunas. In Kennett, J. P., & Warnke, D. A., *The Antarctic*

Paleoenvironment: a Perspective on Global Change, Part 2 (Vol. 60, pp. 175–194): American Geophysical Union, Antarctic Research Series.

- Jiang, S., & Wise, S. W. (2009). Distinguishing the influence of diagenesis on the paleoecological reconstruction of nannoplankton across the Paleocene/ Eocene Thermal Maximum: an example from the Kerguelen Plateau, southern Indian Ocean. *Marine Micropaleontology*, *72*, 49–59.
- Jurgens, G., Lindström, K., & Saano, A. (1997). Novel group within the Kingdom Crenarchaeota from Boreal Forest Soil. *Applied and Environmental Microbiology*, *63*(2), 803–805.
- Kalb, A. L., & Bralower, T. J. (2012). Nannoplankton origination events and environmental changes in the late Paleocene and early Eocene. *Marine Micropaleontology*, *92–93*, 1–15.
- Kennett, J. P. (1977). Cenozoic evolution of Antarctic glaciation, the circum-Antarctic Ocean and their impact on global paleoceanography. *Journal of Geophysical Research*, *82*(27), 3843–3860.
- Kennett, J. P., & Exon, N. F. (2004). Paleooceanographic evolution of the Tasmanian Seaway and its climatic implications. In Exon, N. F., Kennett, J. P., et al. (Eds.), *The Cenozoic Southern Ocean: Tectonics, Sedimentation, and Climate Change between Australia and Antarctica* (pp. 345–367). Washington, DC: AGU.
- Kennett, J. P., Houtz, R. E., Andrews, P. B., Edwards, A. R., Gostin, V. A., Hajos, M., et al. (1975). Initial Reports of the Deep Sea Drilling Project. (Vol. 29, pp. 45–120). Washington DC: US Government Printing Office.
- Kim, J.-H., van der Meer, J., Schouten, S., Helmke, P., Willmott, V., Sangiorgi, F., et al. (2010). New indices and calibrations derived from the distribution of crenarchaeal isoprenoid tetraether lipids: Implications for past sea surface temperature reconstructions. *Geochimica et Cosmochimica Acta*, *74*, 4639–4654.
- King, P. R., Naish, T. R., Browne, G. H., Field, B. D., & Edbrooke, S. W. (1999). Cretaceous to Recent Sedimentary Patterns in New Zealand, 1. *Institute of Geological and Nuclear Sciences Folio Series* (pp. 35).
- Kirtland Turner, S., Sexton, P. F., Charles, C. D., & Norris, R. D. (2014). Persistence of carbon release events through the peak of early Eocene global warmth. *Nature Geoscience*, *7*, 748–751.
- Kozdon, R., Kelly, D. C., Kitajima, K., Strickland, A., Fournelle, J. H., & Valley, J. W. (2013). In situ $\delta^{18}\text{O}$ and Mg/Ca analyses of diagenetic and planktic foraminiferal calcite

preserved in a deep-sea record of the Paleocene-Eocene thermal maximum. *Paleoceanography*, 28, 517–528, doi: 10.1002/palo.20048.

Krebs, C. J. (1999). *Ecological Methodology* (2nd ed.). Menlo Park, CA: Benjamin Cummings.

Kulhanek, D. K., Crouch, E. M., Tayler, M. J. S., & Hollis, C. (2015). Paleocene calcareous nanofossils from East Coast, New Zealand: Biostratigraphy and paleoecology. *Journal of Nannoplankton Research*, 35(2), 155–176.

Lazarus, D. B., Hollis, C. J., & Apel, M. (2008). Patterns of opal and radiolarian change in the Antarctic mid-Paleogene: clues to the origin of the Southern Ocean. *Micropaleontology*, 54(1), 41–48.

Lea, D. W., Mashiotta, T. A., & Spero, H. J. (1999). Controls on magnesium and strontium uptake in planktonic foraminifera determined by live culturing. *Geochimica et Cosmochimica Acta*, 63(16), 2369–2379.

Legge, H. L., Mutterlose, J., & Arz, H. W. (2006). Climatic changes in the northern Red Sea during the last 22,000 years as recorded by calcareous nanofossils. *Paleoceanography*, 21, 16 p, doi: 10.1029/2005PA001142.

Legge, H.-L., Mutterlose, J., Arz, H. W., & Pätzold, J. (2008). Nannoplankton successions in the northern Red Sea during the last glaciation (60 to 14.5 ka BP): Reactions to climate change. *Earth and Planetary Science Letters*, 270(3–4), 271–279.

Liu, Z., Pagani, M., Zinniker, D., DeConto, R., Huber, M., Brinkhuis, H., et al. (2009). Global Cooling During the Eocene-Oligocene Climate Transition. *Science*, 323(5918), 1187–1190, doi: 10.1126/science.1166368.

Lourens, L. J., Sluijs, A., Kroon, D., Zachos, J. C., Thomas, E., Röhl, U., et al. (2005). Astronomical pacing of late Paleocene to early Eocene global warming events. *Nature*, 435, 1083–1087.

Lowrie, W., Alvarez, W., Napoleone, G., Perch-Nielsen, K., Silva, I. P., & Toumarkine, M. (1982). Paleogene magnetic stratigraphy in Umbrian pelagic carbonate rocks: the Contessa sections, Gubbio. *Geological Society of America Bulletin*, 93, 414–432.

Lunt, D. J., Dunkley Jones, T., Heinemann, M., Huber, M., LeGrande, A., Winguth, A., et al. (2012). A model-data comparison for a multi-model ensemble of early Eocene atmosphere-ocean simulations: EoMIP. *Climate of the Past*, 8, 1717–1736.

MacGregor, B. J., Moser, D. P., Alm, E. W., Nealson, K. H., & Stahl, D. A. (1997). Crenarchaeota in Lake Michigan sediment. *Applied and Environmental Microbiology*, 63(3), 1178–1181.

- Margolis, S. V., Kroopnick, P. M., Goodney, D. E., Dudley, W. C., & Mahoney, M. E. (1975). Oxygen and carbon isotopes from calcareous nannofossils as paleoceanographic indicators. *Science*, 189(4202), 555–557.
- Marshall, P. (1916). Relations between Cretaceous and Tertiary rocks. *Transactions of the New Zealand Institute*, 48, 100–119.
- Martini, E. (1970). Standard Palaeogene calcareous nannoplankton zonation. *Nature*, 226, 560–561.
- Martini, E. (1971). *Standard Tertiary and Quaternary calcareous nannoplankton zonation*. Paper presented at the Proceedings of the Second Planktonic Conference, Roma.
- Martini, E. (1986). Paleogene calcareous nanoplankton from the Southwest Pacific Ocean, Deep Sea Drilling Project, Leg 60 *Initial Reports of the Deep Sea Drilling Project* (pp. 747–761): US Government Printing Office.
- Martini, E., & Worsley, T. (1970). Standard Neogene calcareous nannoplankton zonation. *Nature*, 225, 289–290.
- Mason, B. H. (1941). The Geology of Mount Grey District, North Canterbury. *Transactions of the Royal Society of New Zealand*, 71, 103–127.
- McIntyre, A., & Bé, A. W. H. (1967). Modern Coccolithophoridae of the Atlantic Ocean - I. Placoliths and cyrtoliths. *Deep-Sea Research*, 14, 561–597.
- McMillan, S. G. (1999). Geology of Northeast Otago: Hampden (J42) and Palmerston (J43). *Institute of Geological & Nuclear Sciences Science Report 98/25*.
- Morgans, H. E. G. (2009). Late Paleocene to middle Eocene foraminiferal biostratigraphy of the Hampden Beach Section, eastern South Island, New Zealand. *New Zealand Journal of Geology & Geophysics*, 52(4), 273–320, doi: 10.1080/00288306.2009.9518460.
- Morgans, H. E. G., Jones, C. M., Crouch, E. M., Field, B. D., Raine, J. I., Strong, C. P., et al. (2005). Upper Cretaceous to Eocene stratigraphy and sample collections, mid-Waipara River section, North Canterbury. *Institute of Geological & Nuclear Sciences report 2003/08*.
- Nelson, C. S., & Cooke, P. J. (2001). History of oceanic front development in the New Zealand sector of the Southern Ocean during the Cenozoic—a synthesis. *New Zealand Journal of Geology and Geophysics*, 44(4), 535–553, doi: 10.1080/00288306.2001.9514954.

- Noël, M.-H., Kawachi, M., & Inouye, I. (2004). Induced dimorphic life cycle of a coccolithophorid, *Calyptosphaera sphaeroidea* (Prymnesiophyceae, Haptophyta). *Journal of Phycology*, *40*, 112–129, doi: 10.1046/j.1529-8817.2004.03053.x.
- Norris, R. D., Wilson, P. A., Blum, P., Fehr, A., Agnini, C., Bornemann, A., et al. (2014). Methods. In Norris, R. D., Wilson, P. A., et al., *Proceedings of the Integrated Ocean Drilling Program*, 342. College Station, TX: Integrated Ocean Drilling Program.
- Nürnberg, D. (1995). Magnesium in tests of *Neogloboquadrina pachyderma* sinistral from high northern and southern latitudes. *Journal of Foraminiferal Research*, *25*(4), 350–368.
- Nürnberg, D., Buma, J., & Hemleben, C. (1996). Assessing the reliability of magnesium in foraminiferal calcite as a proxy for water mass temperatures. *Geochimica et Cosmochimica Acta*, *60*(5), 803–814.
- Okada, H., & Bukry, D. (1980). Supplementary modification and introduction of code numbers to the low-latitude coccolith biostratigraphic zonation (Bukry, 1973; 1975). *Marine Micropaleontology*, *5*, 321–325.
- Okada, H., & Honjo, S. (1973). The distribution of oceanic coccolithophorids in the Pacific. *Deep-Sea Research*, *20*, 355–374.
- Pancost, R. D., Taylor, K. W. R., Inglis, G. N., Kennedy, E. M., Handley, L., Hollis, C. J., et al. (2013). Early Paleogene evolution of terrestrial climate in the SW Pacific, Southern New Zealand. *Geochemistry Geophysics Geosystems*, *14*(12), 5413–5429, doi: 10.1002/2013GC004935.
- Parke, M., & Adams, I. (1960). The motile (*Crystallolithus hyalinus* Gaarder & Markali) and non-motile phases in the life history of *Coccolithus pelagicus* (Wallich) Schiller. *Journal of the Marine Biological Association of the UK*, *39*(2), 263–274, doi: 10.1017/S002531540001331X.
- Pascher, K. M., Hollis, C. J., Bohaty, S. M., Cortese, G., McKay, R. M., Seebeck, H., et al. (2015). Expansion and diversification of high-latitude radiolarian assemblages in the late Eocene linked to a cooling event in the southwest Pacific. *Climate of the Past*, *11*, 1599–1620.
- Pea, L. (2011). *Eocene-Oligocene paleoceanography of the subantarctic South Atlantic: calcareous nannofossil reconstructions of temperature, nutrient, and dissolution history*. Unpublished PhD Thesis, University of Parma, Italy. 205 pp.
- Pearson, P. N. (2012). Oxygen isotopes in foraminifera: overview and historical review. *The Paleontological Society Papers*, *18*, 38 p.

- Pearson, P. N., & Burgess, C. E. (2008). Foraminifer test preservation and diagenesis: comparison of high latitude Eocene sites. In Austin, W. E. N., & James, R. H. (Eds.), *Biogeochemical Controls on Paleoceanographic Environmental Proxies* (pp. 59–72). London: Geological Society, Special Publications 303.
- Pearson, P. N., van Dongen, B. E., Nicholas, C. J., Pancost, R. D., Schouten, S., Singano, J. M., et al. (2007). Stable warm tropical climate through the Eocene Epoch. *Geology*, *35*, 211–214, doi: 10.1130/G23175A.1.
- Perch-Nielsen, K. (1977). Albanian to Pleistocene calcareous nannofossils from the western South Atlantic. In Perch-Nielsen, K., Supko, P. R., et al., *Initial Reports of the Deep Sea Drilling Project* (Vol. 39, pp. 699–823). Washington D.C.: U.S. Government Printing Office.
- Perch-Nielsen, K. (1985). Cenozoic calcareous nannofossils. In Bolli, H., Perch-Nielsen, K., et al. (Eds.), *Plankton Stratigraphy* (pp. 427–554). New York: Cambridge University Press.
- Persico, D., & Villa, G. (2004). Eocene–Oligocene calcareous nannofossils from Maud Rise and Kerguelen Plateau (Antarctica): paleoecological and paleoceanographic implications. *Marine Micropaleontology*, *52*(1–4), 153–179, doi: 10.1016/j.marmicro.2004.05.002.
- Pilskaln, C. H., & Honjo, S. (1987). The fecal pellet fraction of biogeochemical particle fluxes to the deep sea. *Global Biogeochemical Cycles*, *1*(1), 31–48.
- Raffi, I., Backman, J., & Palike, H. (2005). Changes in calcareous nannofossil assemblages across the Paleocene/Eocene transition from the paleo-equatorial Pacific Ocean. *Palaeoceanography, Palaeoclimatology, Palaeoecology*, *266*, 93–126.
- Raine, J. I., Beu, A. G., Boyes, A. F., Campbell, H. J., Cooper, R. A., Crampton, J. S., et al. (2015). Revised calibration of the New Zealand Geological Timescale: NZGT2015/1 *GNS Science Report 2012/39* (pp. 53).
- Regenberg, M., Nürnberg, D., Steph, S., Groeneveld, J., Garbe-Schönberg, D., Tiedemann, R., et al. (2006). Assessing the effect of dissolution on planktonic foraminiferal Mg/Ca ratios: evidence from Caribbean core tops. *Geochemistry Geophysics Geosystems*, *7*(7), 1–23, doi: 10.1029/2005GC001019.
- Röhl, U., Westerhold, T., Monechi, S., Thomas, E., Zachos, J. C., & Donner, B. (2005). *The third and final early Eocene Thermal Maximum: characteristics, timing and mechanisms of the "X" event*. Paper presented at the GSA Annual Meeting 37, Salt Lake City, USA.

- Rosenthal, Y., Lohmann, G. P., Lohmann, K. C., & Sherrell, R. M. (2000). Incorporation and preservation of Mg in Globigerinoides sacculifer: implications for reconstructing the temperature and $^{18}\text{O}/^{16}\text{O}$ of seawater. *Paleoceanography*, 15(1), 135–145.
- Roth, P. H. (1973). Calcareous nannofossils - Leg 17, Deep Sea Drilling Project. In Winterer, E. L., Ewing, J. I., et al., *Initial Reports of the Deep Sea Drilling Project* (Vol. 17, pp. 695–795). Washington, DC: US Government Printing Office.
- Roth, P. H., Mullin, M. M., & Berger, W. H. (1975). Coccolith sedimentation by fecal pellets: Laboratory experiments and field observations. *Geological Society of America Bulletin*, 86, 1079–1084.
- Roth, P. H., & Thierstein, H. R. (1972). Calcareous nannoplankton: Leg 14 of the Deep Sea Drilling Project. In Hayes, D. E., Pimm, A. C., et al., *Initial Reports of the Deep Sea Drilling Project* (pp. 421–485). Washington DC: US Government Printing Office.
- Scher, H. D., Whittaker, J. M., Williams, S. E., Latimer, J. C., Kordesch, W. E., & Delaney, M. L. (2015). Onset of Antarctic Circumpolar Current 30 million years ago as Tasmanian Gateway aligned with westerlies. *Nature*, 523, 580–583.
- Schneider, L. J., Bralower, T. J., & Kump, L. R. (2011). Response of nannoplankton to early Eocene ocean de-stratification. *Palaeoceanography, Palaeoclimatology, Palaeoecology*, 310, 152–162.
- Schouten, S., Hopmans, E. C., Pancost, R. D., & Sinninghe Damsté, J. S. (2000). Widespread occurrence of structurally diverse tetraether membrane lipids: evidence for the ubiquitous presence of low-temperature relatives of hyperthermophiles. *PNAS*, 97(26), 14421–14426.
- Schouten, S., Hopmans, E. C., Schefuß, E., & Sinninghe Damsté, J. S. (2002). Distributional variations in marine crenarchaeotal membrane lipids: a new tool for reconstructing ancient sea water temperatures? *Earth and Planetary Science Letters*, 204, 265–274.
- Self-Trail, J. M. (2011). Paleogene Calcareous Nannofossils of the South Dover Bridge core, Southern Maryland (USA). *Journal of Nannoplankton Research*, 32(1), 1–28.
- Self-Trail, J. M., Powars, D. S., Watkins, D. K., & Wandless, G. A. (2012). Calcareous nannofossil assemblage changes across the Paleocene-Eocene Thermal Maximum: evidence from a shelf setting. *Marine Micropaleontology*, 92–93, 61–80.
- Self-Trail, J. M., Seefelt, E. L., Shepherd, C. L., & Martin, V. A. (in review). Biostratigraphic and morphometric analysis of specimens from the calcareous nannofossil genus *Tribrachiatus*.

- Sexton, P. F., Wilson, P. A., & Pearson, P. N. (2006). Microstructural and geochemical perspectives on planktic foraminiferal preservation: "Glassy" versus "Frosty". *Geochemistry Geophysics Geosystems*, 7(12), 29 p, doi: 10.1029/2006GC001291.
- Shackleton, N. J., & Kennett, J. P. (1975). Paleotemperature history of the Cenozoic and the initiation of Antarctic glaciation: oxygen and carbon isotope analyses in DSDP Sites 277, 279, and 281. In Kennett, J. P., Houtz, R. E., et al., *Initial Reports of the Deep Sea Drilling Project* (Vol. 29, pp. 743–755). Washington, DC: US Government Printing Office.
- Shafik, S. (1973). Nannofossil biostratigraphy of the southwest Pacific Deep Sea Drilling Project, Leg 30. In Andrews, J. E., Packham, G., et al., *Initial Reports of the Deep Sea Drilling Project* (Vol. 30, pp. 549–598). Washington DC: US Government Printing Office.
- Shamrock, J. L., & Watkins, D. K. (2012). Eocene calcareous nannofossil biostratigraphy and community structure from Exmouth Plateau, Eastern Indian Ocean (ODP Site 762). *Stratigraphy*, 9(1), 54 pp.
- Shepherd, C. L., & Kulhanek, D. K. (2016). Eocene nannofossil biostratigraphy of the mid-Waipara River section, Canterbury Basin, New Zealand. *Journal of Nannoplankton Research*, 36(1), 33–59.
- Siesser, W. G. (1993). Calcareous nannoplankton. In Lipps, J. H. (Ed.), *Fossil Prokaryotes and Protists* (pp. 169–201). Oxford: Blackwell Scientific Publications, Inc.
- Siesser, W. G. (1994). Historical background of coccolithophore studies. In Winter, A., & Siesser, W. G. (Eds.), *Coccolithophores* (pp. 1–11). Cambridge: Cambridge University Press.
- Siesser, W. G., & Winter, A. (1994). Composition and morphology of coccolithophore skeletons. In Winter, A., & Siesser, W. G. (Eds.), *Coccolithophores* (pp. 51–62). Cambridge: Cambridge University Press.
- Sijp, W., England, M. H., & Huber, M. (2011). Effect of the deepening of the Tasman Gateway on the global ocean. *Paleoceanography*, 26, 1–18, doi: 10.1029/2011PA002143, 2011.
- Sinninghe Damsté, J. S., Schouten, S., Hopmans, E. C., van Duin, A. C. T., & Geenevasen, J. A. J. (2002). Crenarchaeol: the characteristic core glycerol dibiphytanyl glycerol tatrether membrane lipid of cosmopolitan pelagic crenarchaeota. *Journal of Lipid Research*, 43, 1641–1651.
- Slotnick, B. S., Dickens, G. R., Nicolo, M. J., Hollis, C. J., Crampton, J. S., Zachos, J. C., et al. (2012). Large-amplitude variations in carbon cycling and terrestrial weathering

- during the latest Paleocene and earliest Eocene: the record at Mead Stream, New Zealand. *The Journal of Geology*, 120(5), 487–505.
- Sluijs, A., Bowen, G. J., Brinkhuis, H., Lourens, L. J., & Thomas, E. (2007). The Paleocene-Eocene Thermal Maximum super greenhouse: biotic and geochemical signatures, age models and mechanisms of global change. In Williams, M., Haywood, A. M., et al. (Eds.), *Deep time perspectives on climate change: marrying the signal from computer models and biological proxies* (pp. 323–349): The Geological Society of London.
- Sprengel, S., & Young, J. R. (2000). First direct associations of *Ceratolithus cristatus* ceratoliths, hoop-coccoliths and *Neosphaera coccolithomorpha* planoliths. *Marine Micropaleontology*, 39, 39–41.
- Steinmetz, J. C. (1994). Sedimentation of coccolithophores. In Winter, A., & Siesser, W. G. (Eds.), *Coccolithophores* (pp. 179–197). Cambridge: Cambridge University Press.
- Stickley, C. E., Brinkhuis, H., Schellenberg, S. A., Sluijs, A., Röhl, U., Fuller, M., et al. (2004). Timing and nature of the deepening of the Tasmanian Gateway. *Paleoceanography*, 19, 1–18.
- Taylor, K. W. R., Huber, M., Hollis, C. J., Hernandez-Sanchez, M. T., & Pancost, R. D. (2013). Re-evaluating modern and Palaeogene GDGT distributions: Implications for SST reconstructions. *Global and Planetary Change*, 108, 158–174.
- Tierney, J. E., & Tingley, M. P. (2014). A Bayesian, spatially-varying calibration model for the TEX₈₆ proxy. *Geochimica et Cosmochimica Acta*, 127, 83–106, doi: 10.1016/j.gca.2013.11.026.
- Tierney, J. E., & Tingley, M. P. (2015). A TEX₈₆ surface sediment database and extended Bayesian calibration. *Scientific Data*, 1–10, doi: 10.1038/sdata.2015.29.
- Torsvik, T. H., Van der Voo, R., Preeden, U., Mac Niocaill, C., Steinberger, B., Doubrovine, P. V., et al. (2012). Phanerozoic polar wander, palaeogeography and dynamics. *Earth Science Review*, 114, 325–368.
- Uda, I., Sugai, A., Itoh, Y. H., & Itoh, T. (2001). Variation in molecular species of polar lipids from *Thermoplasma acidophilum* depends on growth temperature. *Lipids*, 36(1), 103–105.
- Urey, H. C. (1947). The thermodynamic properties of isotopic substances. *Journal of the Chemical Society of London*, 562–581.
- Urey, H. C., Lowenstam, H. A., Epstein, S., & McKinney, C. R. (1951). Measurement of paleotemperatures and temperatures of the Upper Cretaceous of England, Denmark

and the southeastern United States. *Bulletin of the Geological Society of America*, 62, 399–416.

- Villa, G., Fioroni, C., Pea, L., Bohaty, S., & Persico, D. (2008). Middle Eocene–late Oligocene climate variability: Calcareous nannofossil response at Kerguelen Plateau, Site 748. *Marine Micropaleontology*, 69(2), 173–192, doi: 10.1016/j.marmicro.2008.07.006.
- Villa, G., & Persico, D. (2006). Late Oligocene climatic changes: Evidence from calcareous nannofossils at Kerguelen Plateau Site 748 (Southern Ocean). *Palaeogeography, Palaeoclimatology, Palaeoecology*, 231(1–2), 110–119, doi: 10.1016/j.palaeo.2005.07.028.
- Villa, G., & Wei, W. (1993). Data report: Paleogene calcareous nannofossil biostratigraphy of DSDP Site 210 offshore northeastern Australia. In Davies, P. J., McKenzie, J. A., et al., *Proceedings of the Ocean Drilling Program, Scientific Results*, 133. College Station, Texas.
- Volkman, J. K., Eglinton, G., Corner, E. D. S., & Sargent, J. R. (1980). Novel unsaturated straight-chain C₃₇–C₃₉ methyl and ethyl ketones in marine sediments and a coccolithophore *Emiliania huxleyi*. *Physics and Chemistry of the Earth*, 12, 219–227, doi: 10.1016/0079-1946(79)90106-X.
- Waghorn, D. B. (1981). *New Zealand and Southwest Pacific Late Eocene and Oligocene calcareous nannofossils*. Unpublished PhD Thesis, Victoria University of Wellington, New Zealand. 562 pp.
- Wei, W., & Thierstein, H. R. (1991). Upper Cretaceous and Cenozoic calcareous nannofossils of the Kerguelen Plateau (southern Indian Ocean) and Prydz Bay (east Antarctica). In Barron, J., Larsen, B., et al., *Proceedings of the Ocean Drilling Program, Scientific Results*, 119 (pp. 467–493). College Station, TX.
- Wei, W., Villa, G., & Wise, S. W. (1992). Paleoceanographic implications of Eocene–Oligocene calcareous nannofossils from Sites 711 and 748 in the Indian Ocean. In Wise Jr, S. W., Schlich, R., et al., *Proceedings of the Ocean Drilling Program, Scientific Results*, 120 (pp. 979–999). College Station, TX.
- Wei, W., & Wise, S. W. (1990a). Biogeographic gradients of middle Eocene–Oligocene calcareous nanoplankton in the South Atlantic Ocean. *Palaeogeography, Palaeoclimatology, Palaeoecology*, 79(1–2), 29–61, doi: 10.1016/0031-0182(90)90104-F.
- Wei, W., & Wise, S. W. (1990b). Middle Eocene to Pleistocene calcareous nannofossils recovered by Ocean Drilling Program Leg 113 in the Weddell Sea. In Barker, P. F., Kennett, J. P., et al., *Proceedings of the Ocean Drilling Program, Scientific Results*, 113 (pp. 639–666). College Station, TX.

- Weijers, J. W. H., Schouten, S., Spaargaren, O. C., & Sinninghe Damsté, J. S. (2006). Occurrence and distribution of tetraether membrane lipids in soils: Implications for the use of the TEX₈₆ proxy and BIT index. *Organic Geochemistry*, *37*, 1680–1693.
- Wise, S. W. (1983). Mesozoic and Cenozoic calcareous nannofossils recovered by Deep Sea Drilling Project, Leg 71 in the Falkland Plateau region, southwest Atlantic Ocean. In Ludwig, W. J., Krasheninnikov, V. A., et al., *Initial Reports of the Deep Sea Drilling Project* (Vol. 71, pp. 481–550). Washington, DC: U.S. Government Printing Office.
- Woese, C. R., Kandler, O., & Wheelis, M. L. (1990). Towards a natural system of organisms: proposal for the domains Archaea, Bacteria, and Eucarya. *PNAS*, *87*, 4576–4579, doi:10.1073/pnas.87.12.4576.
- Young, J. R., & Bown, P. R. (2014). Some emendments to calcareous nannoplankton taxonomy. *Journal of Nannoplankton Research*, *33*(1), 39–46.
- Young, J. R., Davis, S. A., Bown, P. R., & Mann, S. (1999). Coccolith ultrastructure and biomineralisation. *Journal of Structural Biology*, *126*, 195–215.
- Young, J. R., & Henriksen, K. (2003). Biomineralization within vesicles: the calcite of coccoliths. *Reviews in Mineralogy and Geochemistry*, *54*, 189–215.
- Zachos, J. C., Dickens, G. R., & Zeebe, R. E. (2008). An early Cenozoic perspective on greenhouse warming and carbon-cycle dynamics. *Nature*, *451*, 279–283, doi:10.1038/nature06588.
- Zachos, J. C., Lohmann, K. C., Walker, J. C. G., & Wise, S. W. (1993). Abrupt climate change and transient climates during the Paleogene: a marine perspective. *The Journal of Geology*, *101*(2), 191–213.
- Zachos, J., Pagani, M., Sloan, L., Thomas, E., & Billups, K. (2001). Trends, Rhythms, and Aberrations in Global Climate 65 Ma to Present. *Science*, *292*(5517), 686–693, doi:10.1126/science.1059412.
- Zachos, J. C., Stott, L. D., & Lohmann, K. C. (1994). Evolution of Early Cenozoic marine temperatures. *Paleoceanography*, *9*(2), 353–387, doi:10.1029/93pa03266.
- Ziveri, P., Stoll, H., Probert, I., Klaas, C., Geisen, M., Ganssen, G., et al. (2003). Stable isotope 'vital effects' in coccolith calcite. *Earth and Planetary Science Letters*, *210*, 137–149.

APPENDIX A: SYSTEMATIC PALEONTOLOGY

The following provides a list of all calcareous nannofossils considered in this thesis. Full references for taxa can be found in Perch-Nielsen (1985), Bown (1998, 2005) and Shamrock & Watkins (2012). Plate and figure references refer to images shown in Appendix B.

Placolith coccoliths

Order **ISOCHRYSIDALES** Pascher, 1910

Family **PRINSIACEAE** Hay & Mohler, 1967 emend. Young & Bown, 1997

Girgisia gammation (Bramlette & Sullivan, 1961) Varol, 1989

Pl.1, figs 28–30

Hornibrookina australis Edwards & Perch-Nielsen, 1975

Pl.12, figs 24–27

Toweius callosus Perch-Nielsen, 1971

Pl.1, figs 1–4

Remarks: In the lower part of the mid-Waipara River section, outer shields appear to have been lost and only the bright central tube remains.

Toweius eminens (Bramlette & Sullivan, 1961) Gartner, 1971

Pl.1, figs 5–7

Toweius? magnicrassus (Bukry, 1971) Romein, 1979

Pl.1, figs 8–11

Remarks: This species is fairly consistently present in low numbers through NP10 to NP12 at mid-Waipara, a range that is similar to that seen at South Dover Bridge, Maryland, USA (Self-Trail, 2011). However, it is not present through this range at Site 277 and is only present in low numbers at Site 207.

Toweius occultatus (Locker, 1967) Perch-Nielsen, 1971

Pl.1, figs 12–14

Toweius pertusus (Sullivan, 1965) Romein, 1979

Pl.1, figs 15–16

Toweius rotundus Perch-Nielsen in Perch-Nielsen *et al.*, 1978

Pl.1, figs 17–18

Toweius serotinus Bybell & Self-Trail, 1995

Pl.1, figs 19–20

Toweius tovae Perch-Nielsen, 1971

Pl.1, figs 21–23

Toweius sp. 1

Pl.1, fig. 24

Remarks: Medium, subcircular placolith with a bright central area spanned by a visible net. Possible variation of *Toweius* sp. 1 of Bown (2005).

Toweius sp. 2

Pl.1, figs 25–27

Remarks: Small to medium, elliptical to subcircular placoliths with a wide central area spanned by a visible plate. Similar to *Toweius* sp. 2 of Bown (2005).

Family **NOELAEHRHABDACEAE** Jerkovic, 1970 emend. Young and Bown, 1997

Cyclicargolithus floridanus (Roth & Hay in Hay *et al.*, 1967) Bukry, 1971

Pl.3, figs 1–2

Cyclicargolithus luminis (Sullivan, 1965) Bukry, 1971

Pl.3, fig. 3

Cyclicargolithus parvus Shamrock & Watkins, 2012

Pl.3, figs 4–5

Reticulofenestra bisecta (Hay *et al.*, 1966) Roth, 1970

Pl.2, figs 5–7

Reticulofenestra circus de Kaenel & Villa, 1996

Pl.2, figs 17–18

Remarks: Medium to large, subcircular reticulofenestrids with narrow central area.

Differentiation: Similar to *Reticulofenestra wadeae* (Bown 2005) but the central area is narrower.

Reticulofenestra clatrata Müller, 1970

Pl.2, figs 21–22

Reticulofenestra daviesii (Haq, 1968) Haq, 1971

Pl.2, figs 23–24

Reticulofenestra dictyoda (Deflandre *in* Deflandre & Fert, 1954) Stradner *in* Stradner & Edwards, 1968

Pl.2, fig. 14

Remarks: Described by some workers as elliptical with an open central area. Name used here for small to very large (3–14 µm) elliptical reticulofenestrids with a narrow central region.

Reticulofenestra filewiczii (Wise & Wiegand *in* Wise, 1983) Dunkley Jones *et al.*, 2009

Pl.2, figs 25–26

Reticulofenestra hampdenensis Edwards, 1973

Pl.2, figs 19–20

Reticulofenestra hillae Bukry & Percival, 1971

Pl.12, figs 1–4

Reticulofenestra lockeri Müller, 1970

Pl.2, figs 27–28

Reticulofenestra minuta Roth, 1970

Pl.2, figs 8–9

Reticulofenestra producta (Kamptner, 1963) Backman, 1980

Pl.2, figs 1–2

Reticulofenestra reticulata (Gartner & Smith, 1967) Roth & Thierstein, 1972

Pl.2, figs 29–30

Reticulofenestra samodurovii (Hay *et al.* 1966) Roth, 1970

Pl.2, figs 10–11

Reticulofenestra scrippsae Bukry & Percival, 1971

Pl.2, figs 3–4

Reticulofenestra umbilicus (Levin, 1965) Martini & Ritkowski, 1968

Pl.2, figs 12–13

Reticulofenestra wadeae Bown, 2005

Pl.2, figs 15–16

Order **COCCOSPHAERALES** Haeckel, 1894 emend. Young & Bown, 1997

Family **COCCOLITHACEAE** Poche, 1913 emend. Young & Bown, 1997

Campylosphaera dela (Bramlette & Sullivan, 1961) Hay & Mohler, 1967

Pl.3, fig. 6

Chiasmolithus bidens (Bramlette & Sullivan, 1961) Hay & Mohler, 1967

Pl.3, figs 7–8

Chiasmolithus californicus (Bramlette & Sullivan, 1961) Hay & Mohler, 1967

Pl.3, figs 9–10

Chiasmolithus consuetus (Bramlette & Sullivan, 1961) Hay & Mohler, 1967

Pl.12, figs 5–6

Chiasmolithus expansus (Bramlette & Sullivan, 1961) Gartner, 1970

Pl.3, fig. 11

Chiasmolithus gigas (Bramlette & Sullivan, 1961) Radomski, 1968

Pl.12, figs 7–8

Chiasmolithus grandis Bramlette & Riedel, 1954

Pl.3, figs 12–14

Chiasmolithus medius Perch-Nielsen, 1971

Pl.3, figs 15–16

Chiasmolithus modestus Perch-Nielsen, 1971

Pl.3, figs 17–18

Chiasmolithus nitidus Perch-Nielsen, 1971

Pl.3, figs 19–21

Chiasmolithus solitus (Bramlette & Sullivan, 1961) Locker, 1968

Pl.3, figs 22–23

Clausicoccus fenestratus (Deflandre & Fert, 1954) Prins, 1979

Pl.3, figs 24–25

Clausicoccus subdistichus (Roth & Hay in Hay *et al.*, 1967) Prins, 1979

Pl.3, figs 26–27

Clausicoccus vanheckiae (Perch-Nielsen, 1986) de Kaenel & Villa, 1996

Pl.3, figs 28–29

Coccolithus cachaoi (Bown, 2005)

Pl.12, figs 9–13

Coccolithus eopelagicus (Bramlette & Riedel, 1954) Bramlette & Sullivan, 1961

Pl.12, figs 14–15

Coccolithus foraminis Bown, 2005

Pl.4, figs 1–2

Remarks: Bown (2005) reported *C. foraminis* from Zone NP10 in Tanzania. Here we document an expanded stratigraphic range, with the taxon present in low numbers in NP12 at mid-Waipara River and DSDP Site 207. It is more consistently present in low numbers in Zones NP13–14 and NP16 at all four sites.

Coccolithus formosus (Kamptner, 1963) Wise, 1973

Pl.4, figs 3–4

Coccolithus latus Bown, 2005

Pl.4, figs 5–6

Coccolithus pelagicus (Wallich, 1977) Schiller, 1930

Pl.4, figs 7–8

Cruciplacolithus primus Perch-Nielsen, 1977

Family **CALCIDISCACEAE** Young & Bown, 1997

Calcidiscus bicircus Bown, 2005

Pl.4, figs 9–13

Remarks: Medium to large (6–9 μm) subcircular placolith with a non-birefringent distal shield and a narrow to closed central region. There is a great deal of variation seen in the central region across specimens, but generally they show a narrow, bright tube cycle.

Calcidiscus pacificanus (Bukry, 1971) Varol, 1989

Pl.4, figs 14–16

Remarks: Medium to large (6–9 μm) subcircular placolith with a closed centre.

Calcidiscus protoannulus (Gartner, 1971) Loeblich & Tappan, 1978

Pl.4, figs 17–18

Remarks: Young & Bown (2014) recombined this taxon with *Umbilicosphaera*, proposing that Paleogene species with clearly open central areas be placed in this genus, whereas those with closed central areas be assigned to *Calcidiscus*. They added that those with narrow central openings may be ambiguous and proposed a criterion of a central area opening >25% of the distal shield diameter to distinguish *Umbilicosphaera* from *Calcidiscus*. Given that they indicated that this division is artificial and additional work needs to be done, we retain *Calcidiscus* as the genus for this study.

Coronocyclus bramlettei (Hay & Towe, 1962) Bown, 2005

Pl.4, figs 19–21

Coronocyclus nitescens (Kamptner, 1963) Bramlette & Wilcoxin, 1967

Pl.12, figs 16–19

Umbilicosphaera jordanii Bown, 2005

Placolith coccoliths incertae sedis

Ellipsolithus bollii Perch-Nielsen, 1977

Pl.4, fig 22–23

Ellipsolithus distichus (Bramlette & Sullivan, 1961) Sullivan, 1964

Pl.4, figs 24–25

Markalius apertus Perch-Nielsen, 1979

Pl.4, figs 26–27

Markalius inversus (Deflandre in Deflandre & Fert, 1954) Bramlette & Martini, 1964

Pl.4, figs 28–30

Tetralithoides symeonidesii Theodoridis, 1984

Pl.5, figs 1–2

Murolith coccoliths

Mesozoic survivor muroliths

Order **EIFFELLITHALES** Rood *et al.*, 1971

Family **CHIASTOZYGACEAE** Rood *et al.*, 1973

Jakubowskia leoniae Varol, 1989

Pl.5, figs 3–5

Cenozoic muroliths

Order **ZYGODISCALES** Young & Bown, 1997

Family **HELICOSPHAERACEAE** Black, 1971

Helicosphaera bramlettei (Muller, 1970) Jafar & Martini, 1975

Pl.5, figs 6–7

Helicosphaera lophota (Bramlette & Sullivan, 1961) Locker, 1973

Pl.12, figs 20–21

Helicosphaera seminulum Bramlette & Sullivan, 1961

Pl.5, figs 8–10

Remarks: This taxon is continuously present from NP12 to upper NP13/14 at mid-Waipara. This is consistent with observations from the South Dover Bridge Core, Maryland, USA (Self-Trail, 2011) where it also makes its first appearance in NP12. It is less consistent at the other three sites but does occur for the first time in NP12 at Site 207. Further work needs to be done to determine if this taxon may be biostratigraphically useful.

Family **PONTOSPHAERACEAE** Lemmermann, 1908

Genus *Pontosphaera* Lohmann, 1902

Used to classify all pontosphaerid coccoliths, including species that are classified as *Transversopontis* by some authors.

Pontosphaera distincta (Bramlette & Sullivan, 1961) Roth & Thierstein, 1972

Pl.5, figs 11–12

Pontosphaera duocava (Bramlette & Sullivan, 1961) Romein, 1979

Pl.5, figs 13–14

Pontosphaera exilis (Bramlette & Sullivan, 1961)

Pl.5, figs 15–17

Pontosphaera pax Stradner & Seifert, 1980

Pontosphaera pectinata (Bramlette & Sullivan, 1961) Sherwood 1974

Pl.5, figs 18–19

Pontosphaera plana (Bramlette & Sullivan, 1961) Haq, 1971

Pl.5, figs 20–21

Pontosphaera pulcheroides (Sullivan, 1964) Romein, 1979

Pl.5, figs 22–23

Pontosphaera pulchra (Deflandre *in* Deflandre & Fert, 1954) Romein, 1979

Pl.5, figs 24–25

Pontosphaera punctosa (Bramlette & Sullivan, 1961) Perch-Nielsen, 1984

Pl.5, fig. 26

Pontosphaera versa (Bramlette & Sullivan, 1961) Sherwood, 1974

Pl.5, figs 27–29

Pontosphaera sp.

Pl.5, fig. 30

Family **ZYGODISCACEAE** Hay & Mohler, 1967

Lophodolithus nascens Bramlette & Sullivan, 1961

Pl.6, figs 1–3

Neochiastozygus distentus (Bramlette & Sullivan, 1961) Perch-Nielsen, 1971

Pl.6, fig. 4

Neochiastozygus imbrii Haq & Lohmann, 1975

Pl.6, figs 5–7

Neochiastozygus junctus (Bramlette & Sullivan, 1961) Perch-Nielsen, 1971

Neococcolithes dubius (Deflandre in Deflandre & Fert, 1954) Black, 1967

Pl.6, figs 8–10

Neococcolithes minutus (Perch-Nielsen, 1967) Perch-Nielsen, 1971

Pl.6, figs 11–13

Neococcolithes protenus (Bramlette & Sullivan, 1961) Black, 1967

Pl.6, figs 14–16

Holococcoliths

Family **CALYPTROSPHAERACEAE** Boudreaux & Hay, 1967

Orthozygus occultus Dunkley Jones *et al.*, 2009

Pl.6, figs 17–22

Remarks: Dunkley Jones *et al.* (2009) described this taxon from the upper Eocene (NP18–20) of Tanzania. This taxon is found in much older sediment at mid-Waipara River (NP12) and Site 207 (NP9–10) than previously reported.

S. cf. Semihololithus biskayae Perch-Nielsen, 1971

Pl.6, fig. 23

Zygrhablithus bijugatus bijugatus (Deflandre in Deflandre & Fert, 1954) Deflandre, 1959

Pl.6, figs 24–27

Zygrhablithus bijugatus cornutus Bown, 2005

Nannoliths

Family **BRAARUDOSPHAERACEAE** Deflandre, 1947

Braarudosphaera bigelowii (Gran & Braarud, 1935) Deflandre, 1947

Pl.13, figs 1–2

Micrantholithus lateralis Sullivan, 1965

Pl.6, figs 28–30

Family **DISCOASTERACEAE** Tan, 1927

Discoaster barbadiensis Tan, 1927

Pl.7, figs 1–6

Discoaster binodosus Martini, 1958

Pl.7, figs 7–10

Discoaster cruciformis Martini, 1958

Pl.7, figs 11–12

Discoaster diastypus Bramlette & Sullivan, 1961

Pl.7, figs 13–16

Remarks: Used here for medium to large rosette-shaped discoasters with prominent bosses on both sides and short rays that typically curve.

Discoaster distinctus Martini, 1958

Pl.7, figs 17–20

Discoaster elegans Bramlette & Sullivan, 1961

Pl. 8, figs 1–4

Remarks: Present in low numbers at mid-Waipara River in the upper part of the combined NP13–14 interval and in the lowermost NP16 sample. Also consistently present at Hampden Beach in the combined lower NP13–14 Zone upper NP14–15 Zone.

D. elegans is easily distinguished from *D. barbadiensis* by the presence of concentric lines.

Discoaster kuepperi Stradner, 1959

Pl.8, figs 5–8

Discoaster lenticularis Bramlette & Sullivan, 1961

Pl.8, figs 9–12

Discoaster lodoensis Bramlette & Riedel, 1954

Pl.8, figs 13–20

Discoaster martini Stradner, 1959

Pl.12, figs 22–23

Discoaster mediosus Bramlette & Sullivan, 1961

Pl.9, figs 1–8

Remarks: *Discoaster* species with 8–10 arms with rounded to pointed tips. Bown (2005) differentiates *D. mediosus* from *D. binodosus* based on the number of arms; however, we do not make that distinction. Instead, we differentiate between the two species based on the presence or absence of prominent lateral nodes.

Discoaster multiradiatus Bramlette & Riedel, 1954

Pl.9, figs 9–12

Discoaster nodifer (Bramlette & Riedel, 1954) Bukry, 1973

Pl.9, figs 13–16

Discoaster saipanensis Bramlette & Riedel, 1954

Pl.9, figs 17–20

Remarks: Perch-Nielsen (1985) indicated sporadic occurrences of this species in NP15, with it more consistently present in NP16. More recently this taxon has been reported from upper NP14 (Self-Trail, 2011). This corresponds with DSDP Site 207, where *D.*

saipanensis ranges from upper NP14 to NP15b. At mid-Waipara this taxon first occurs in the combined NP13–14 zone and at Site 277 a single specimen occurs in NP13.

Discoaster salisburgensis Stradner, 1961

Pl.10, figs 1–4

Discoaster septemradiatus (Klumpp, 1953) Martini 1958

Pl.10, figs 5–8

Discoaster splendidus Martini, 1960

Pl.10, figs 9–10

Discoaster sublodoensis? Bramlette & Sullivan, 1961

Discoaster tanii Bramlette & Riedel, 1954

Pl.10, figs 11–14

Discoaster wemmelensis Achuthan & Stradner, 1969

Pl.10, figs 15–20

Family **FASCICULITHACEAE** Hay & Mohler, 1967

Fasciculithus bobii Perch-Nielsen, 1971

Pl.11, fig. 1

Fasciculithus involutus Bramlette & Sullivan, 1961

Pl.11, figs 2–5

Fasciculithus thomasii Perch-Nielsen, 1971

Pl.11, fig. 6

Fasciculithus tympaniformis Hay & Mohler in Hay *et al.*, 1967

Pl.11, figs 7–8

Family **RHOMBOASTERACEAE** Bown, 2005

Nannotetrina alata (Martini in Martini & Stradner, 1960) Haq & Lohmann, 1976

Pl.13. figs 3–4

Nannotetrina cristata (Martini, 1958) Perch-Nielsen, 1971

Pl.13. figs 5–7

Nannotetrina fulgens (Stradner in Martini & Stradner, 1960) Achuthan & Stradner, 1969

Pl.13. figs 8–10

Nannotetrina spinosa (Stradner in Martini and Stradner, 1960) Bukry, 1963

Pl.13. figs 11–12

Rhomboaster bramlettei (Brönnimann & Stradner, 1960) Bybell & Self-Trail, 1995

Pl.11, figs 9–13

Rhomboaster cuspis Bramlette & Sullivan, 1961

Pl.11, figs 14–17

Tribrachiatus orthostylus Shamrai, 1963

Pl.11, figs 18–19

Tribrachiatus morphotype A

Pl.11, fig. 20

Remarks: Nannolith with two strongly curved arms of equal length and a third, shorter arm that extends perpendicular to the other arms. Generally, shows higher order birefringence than *T. orthostylus*.

Tribrachiatus morphotype B

Pl.11, figs 21–22

Remarks: Nannolith with two arms of equal length that are flattened on upper and lower sides and a third short arm. Well preserved specimens exhibit claw-like structures at the tips of the longer arms. A “vault” is noticeable on the underside of the nannolith.

Family **SPHENOLITHACEAE** Deflandre, 1952

Sphenolithus anarrhopus Bukry & Bramlette, 1969

Sphenolithus editus Perch-Nielsen in Perch-Nielsen *et al.*, 1978

Pl.11, figs 23–24

Sphenolithus moriformis (Brönnimann & Stradner, 1960) Bramlette & Wilcoxon, 1967

Pl.11, figs 25–26

Sphenolithus radians Deflandre in Grassé, 1952

Pl.11, figs 27–28

Sphenolithus spiniger Bukry, 1971

Pl.11, figs 29–30

Nannoliths incertae sedis

Biantholithus sparsus Bramlette & Martini, 1964

Pl.13, figs 13–15

APPENDIX B: PLATES

Plates 1–11 contain images of nannofossil taxa from the mid-Waipara River section, Canterbury Basin and sample numbers are indicated below each individual image. Plates 12–13 contain images of additional taxa from DSDP Sites 207 and 277 and sample numbers are indicated in a separate caption below the plates.

PLATE 1

Prinsiaceae: *Toweius*, *Girgisia*

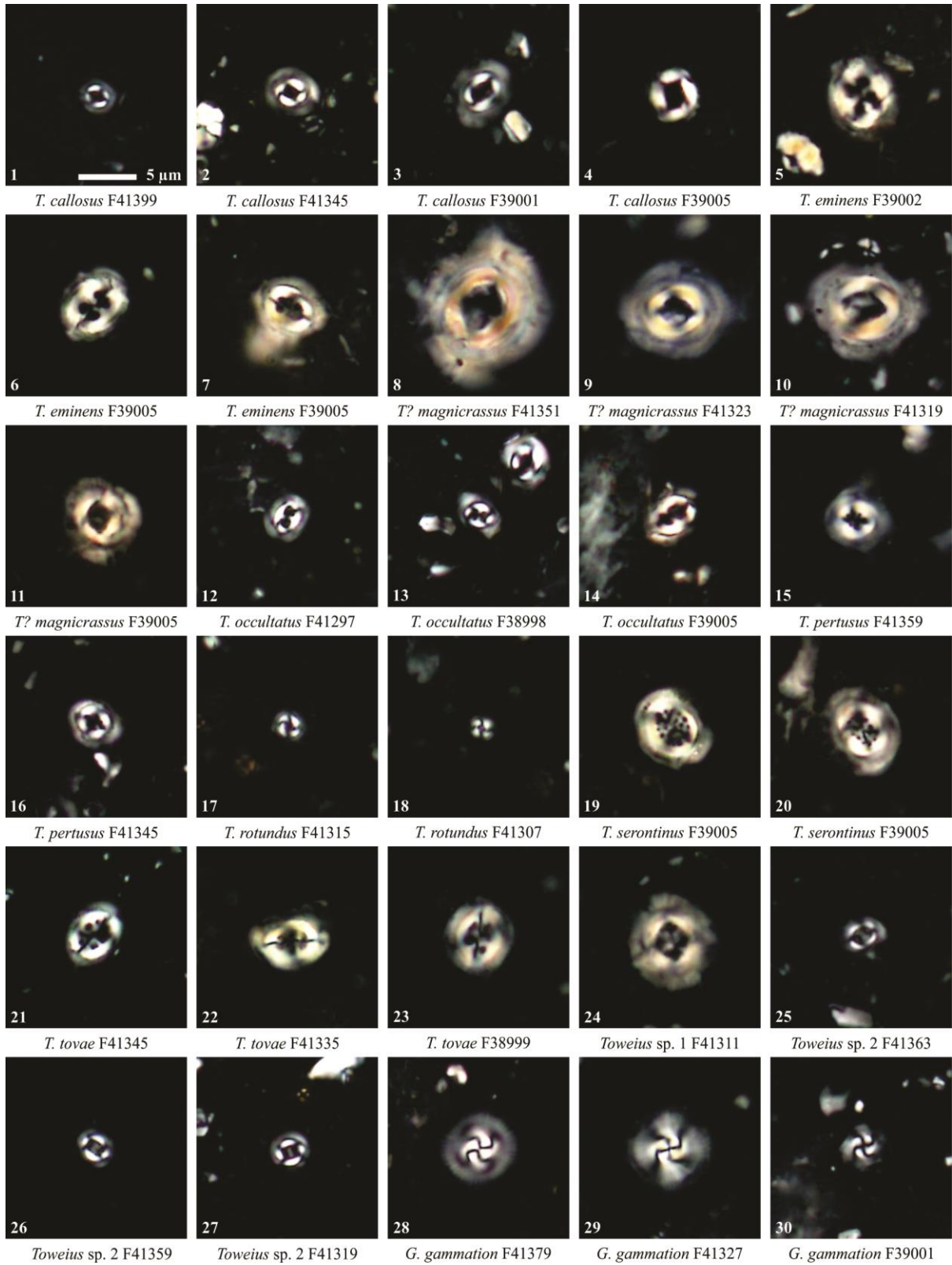


PLATE 2

Noelaerhabdaceae: *Reticulofenestra*

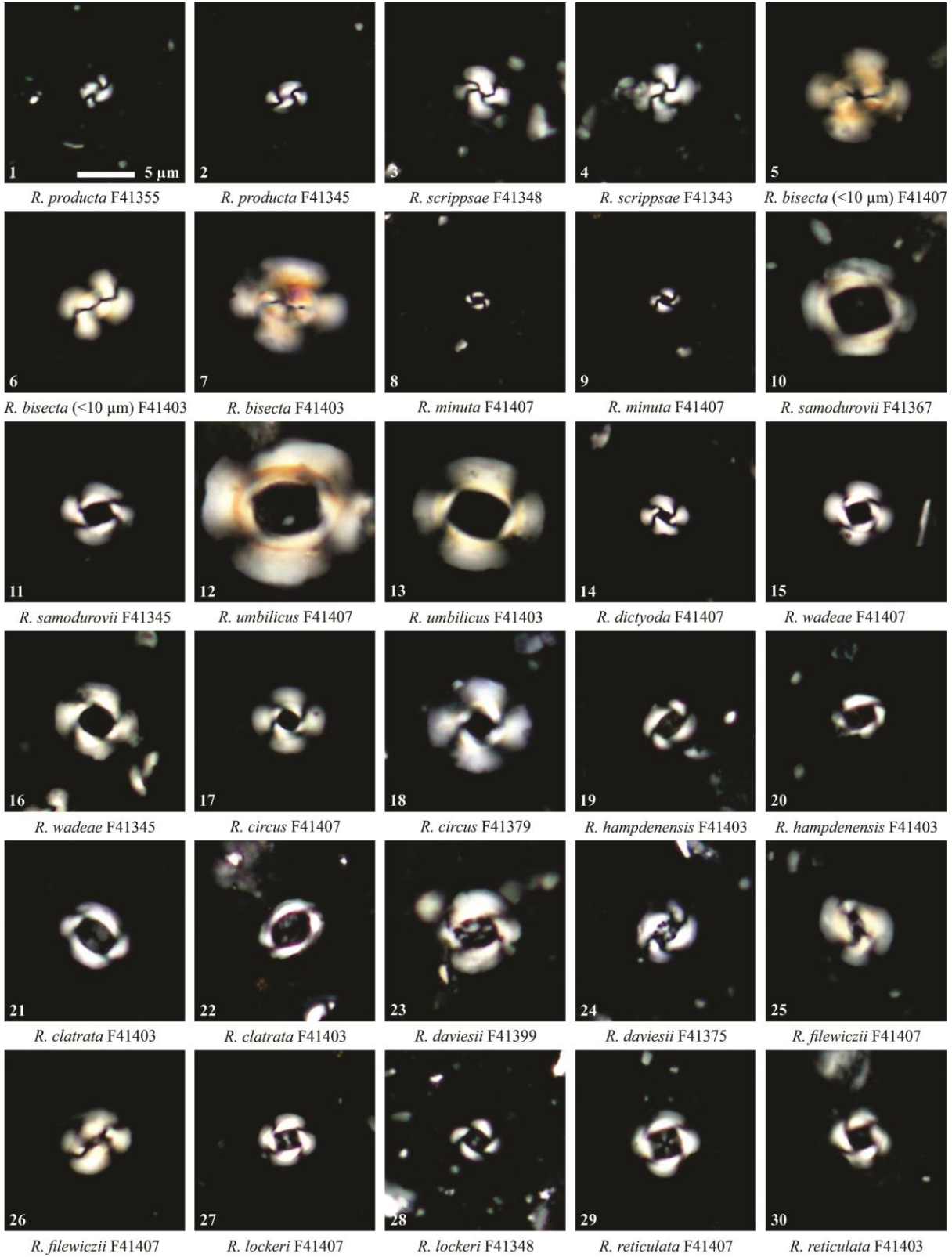


PLATE 3

Noelaerhabdaceae: Cyclicargolithus; Coccolithaceae: Campylosphaera,
Chiasmolithus, Clausicoccus

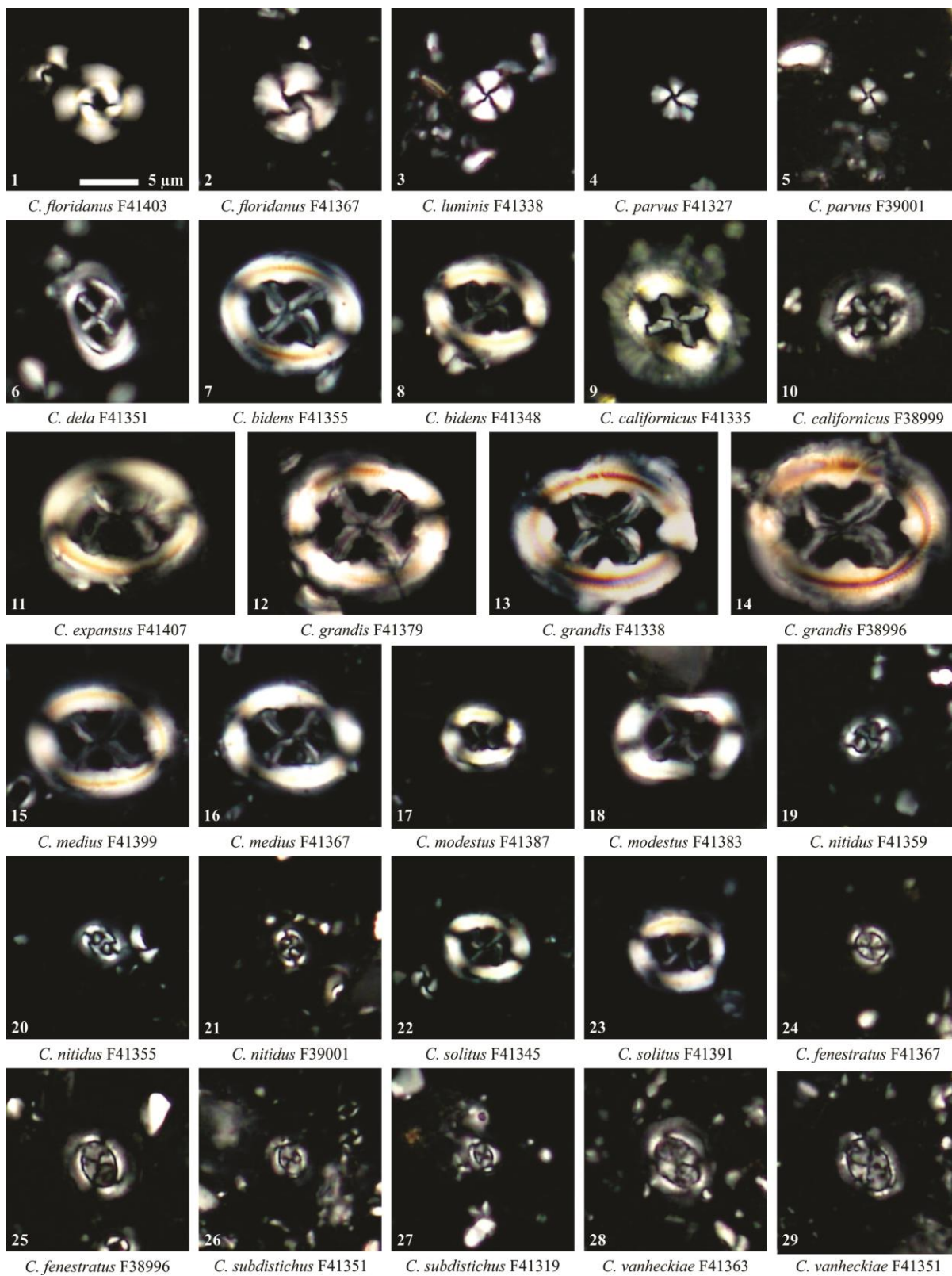


PLATE 4

Coccolithaceae: Coccolithus; Calcidiscaceae: Calcidiscus, Coronocyclus; Incertae sedis
placoliths: Ellipsolithus, Markalius

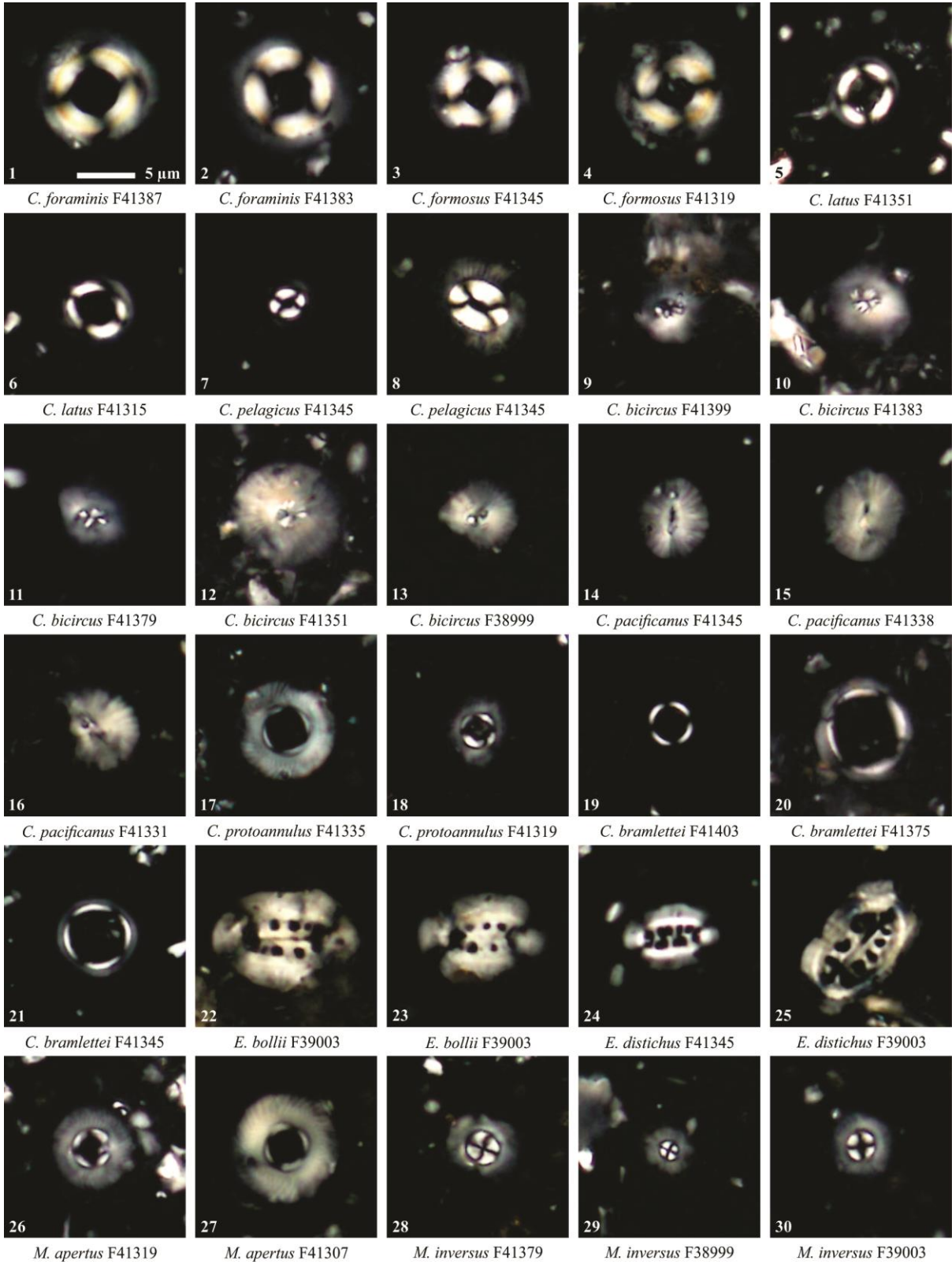


PLATE 5

Incertae sedis placoliths: *Tetralithoides*; Chiastozygaceae: *Jakubowskia*;

Helicosphaeraceae: *Helicosphaera*, Pontosphaeraceae: *Pontosphaera*

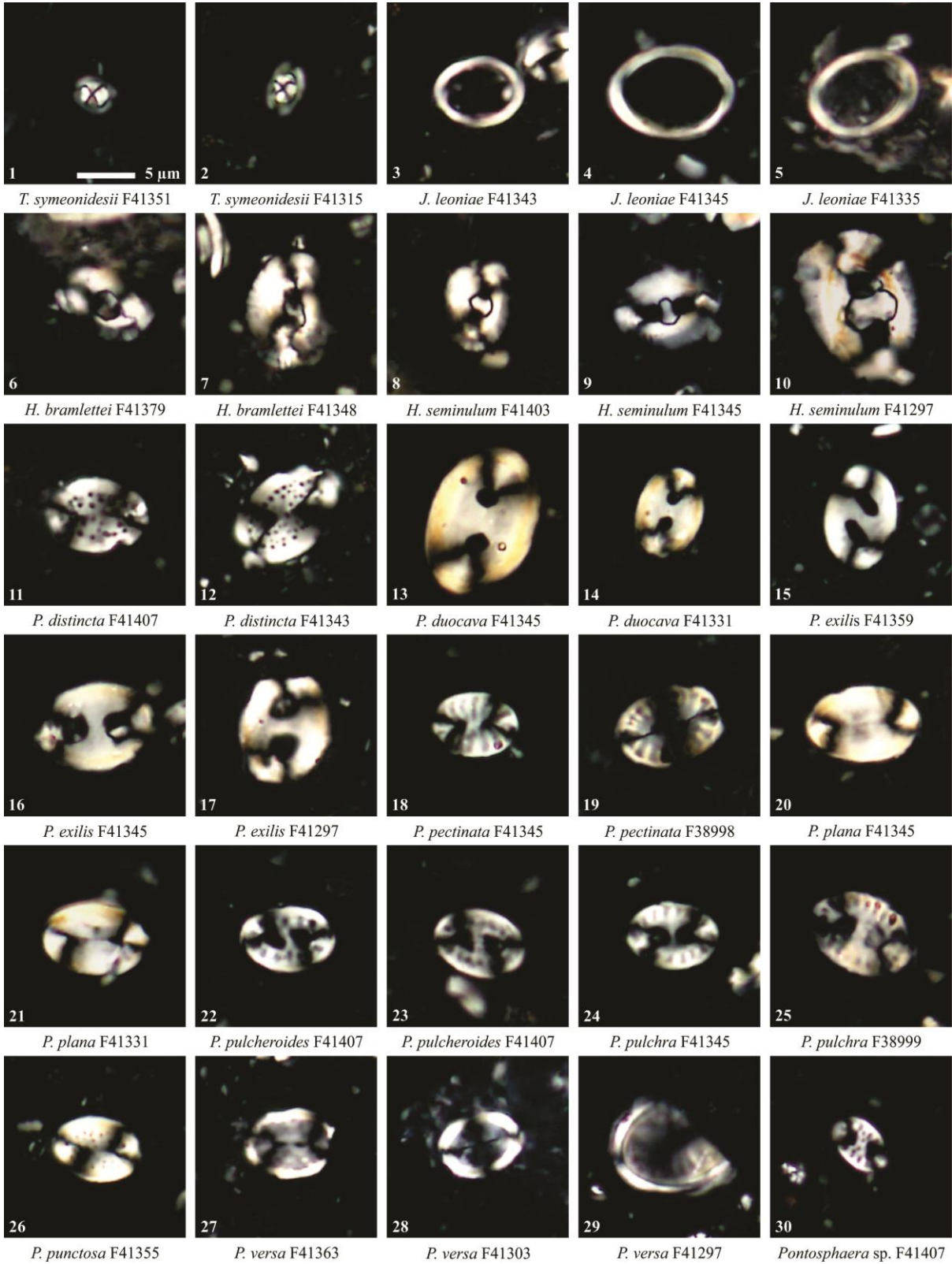


PLATE 6

Zygodiscaceae: Lophodolithus, Neochiastozygus, Neococcolithes; Holococcoliths:
Orthozygus, Semihololithus, Zygrhablithus; Nannoliths: Braarudosphaeraceae

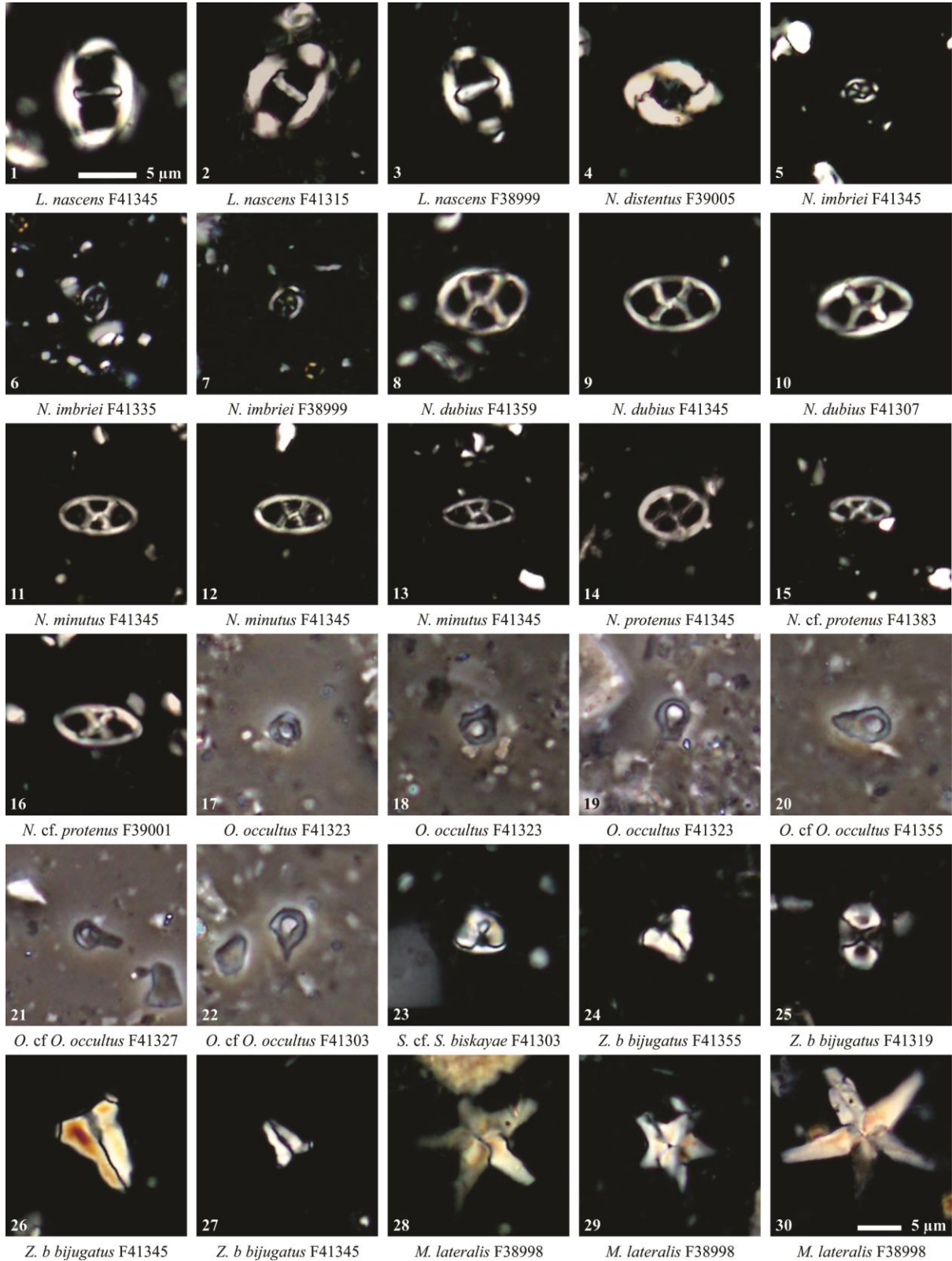
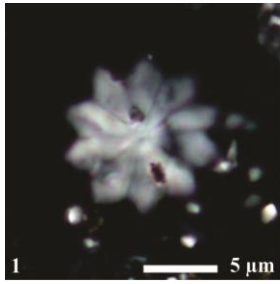
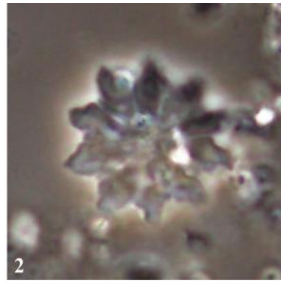


PLATE 7

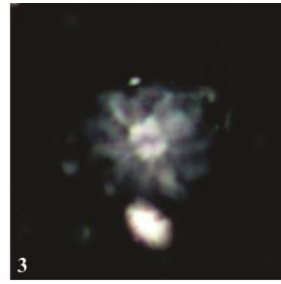
Nannoliths: Discoasteraceae



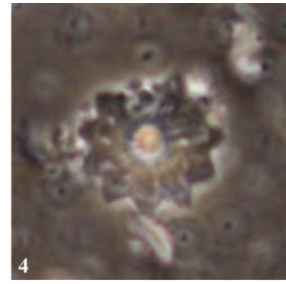
1 *D. barbadensis* F41338



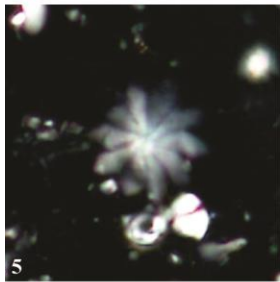
2 *D. barbadensis* F41338



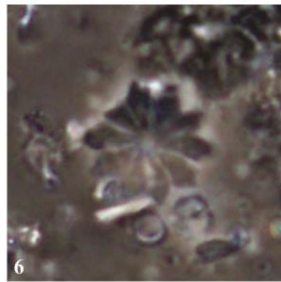
3 *D. barbadensis* F41335



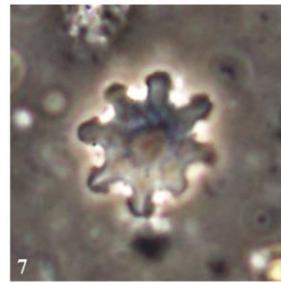
4 *D. barbadensis* F41335



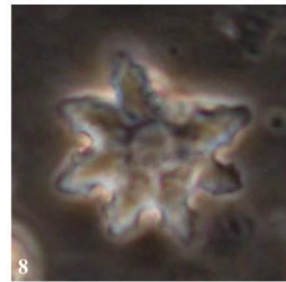
5 *D. barbadensis* F41331



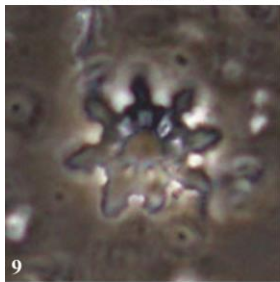
6 *D. barbadensis* F41331



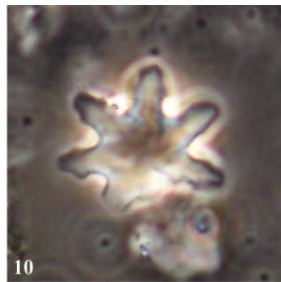
7 *D. binodosus* F41335



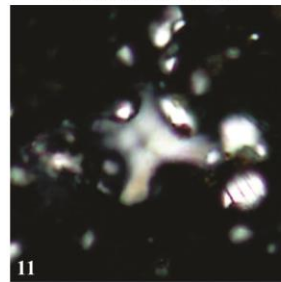
8 *D. binodosus* F41331



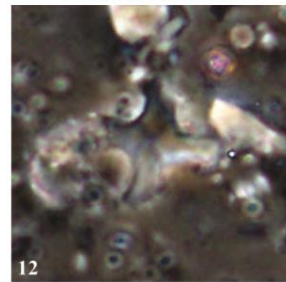
9 *D. binodosus* F41331



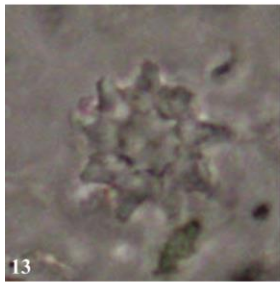
10 *D. binodosus* F41331



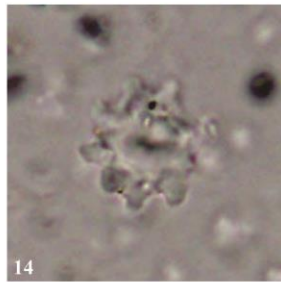
11 *D. cruciformis* F41323



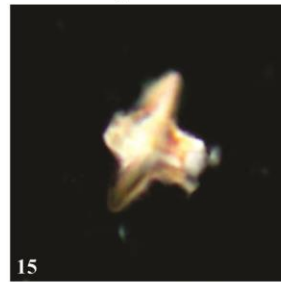
12 *D. cruciformis* F41323



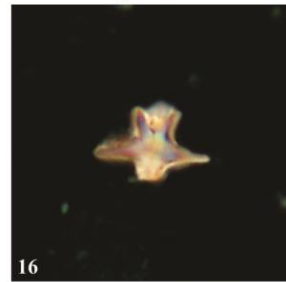
13 *D. diastypus* F39003



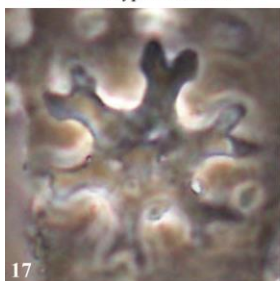
14 *D. diastypus* F39003



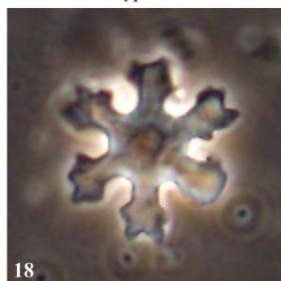
15 *D. diastypus* F39003



16 *D. diastypus* F39003



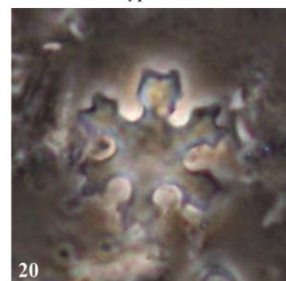
17 *D. distinctus* F41363



18 *D. distinctus* F41345



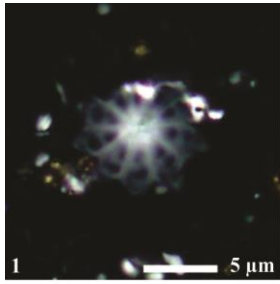
19 *D. distinctus* F41335



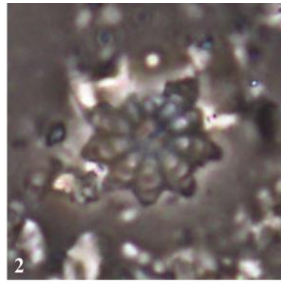
20 *D. distinctus* F41323

PLATE 8

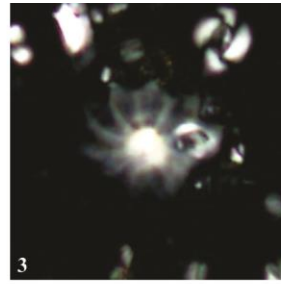
Nannoliths: Discoasteraceae



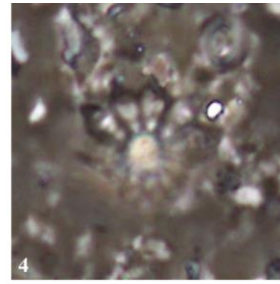
D. elegans F41399



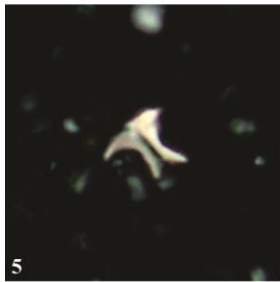
D. elegans F41399



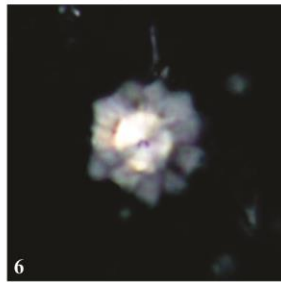
D. elegans F41375



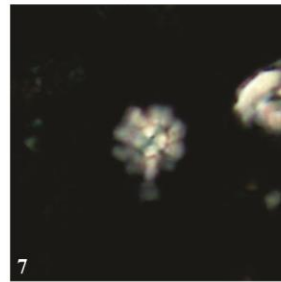
D. elegans F41375



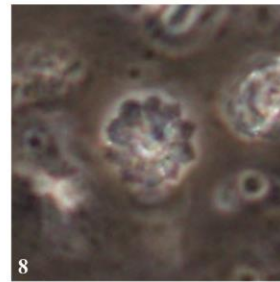
D. kuepperi F41359



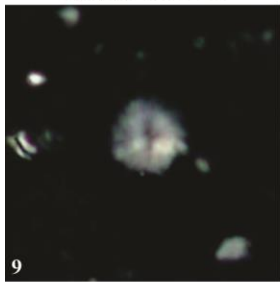
D. kuepperi F41323



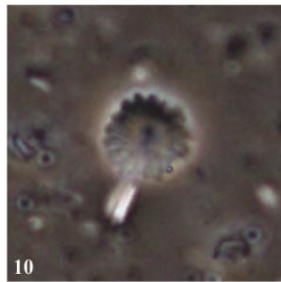
D. kuepperi F38999



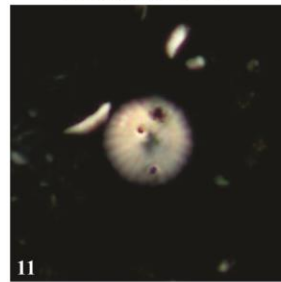
D. kuepperi F38999



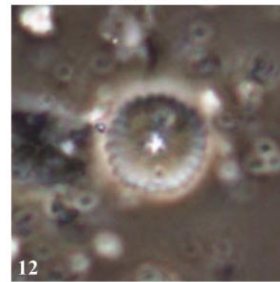
D. lenticularis F41351



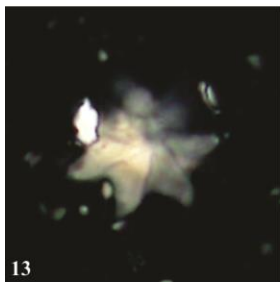
D. lenticularis F41351



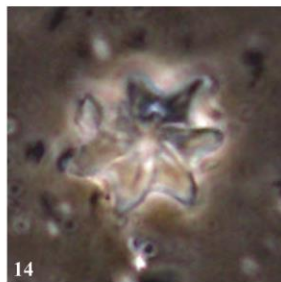
D. lenticularis F39005



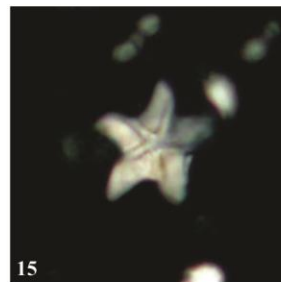
D. lenticularis F39005



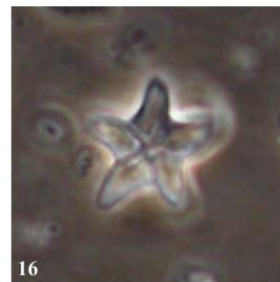
D. lodoensis F41351



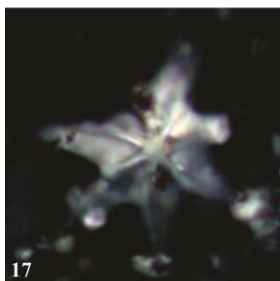
D. lodoensis F41351



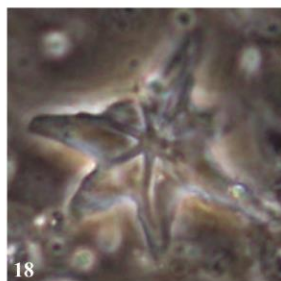
D. lodoensis F41345



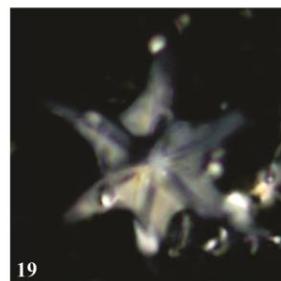
D. lodoensis F41345



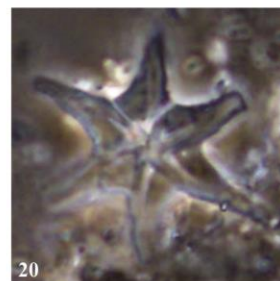
D. lodoensis F41323



D. lodoensis F41323



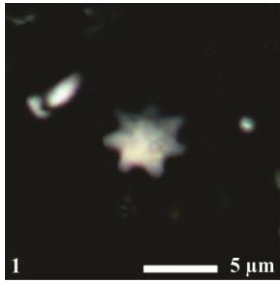
D. lodoensis F41311



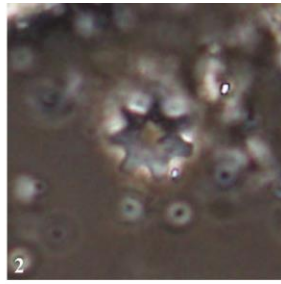
D. lodoensis F41311

PLATE 9

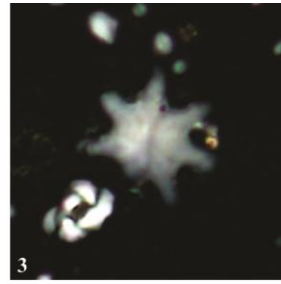
Nannoliths: Discoasteraceae



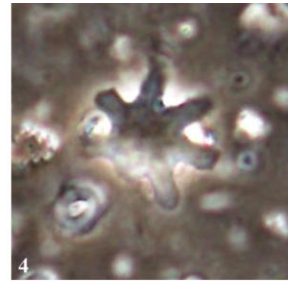
1 *D. mediosus* F41383



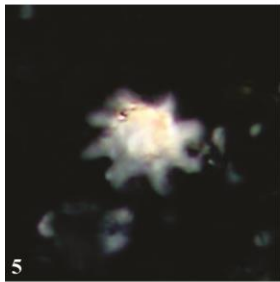
2 *D. mediosus* F41383



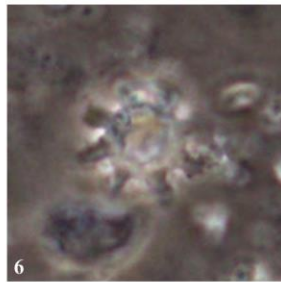
3 *D. mediosus* F41375



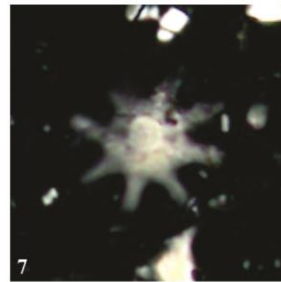
4 *D. mediosus* F41375



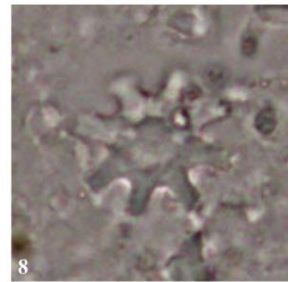
5 *D. mediosus* F41335



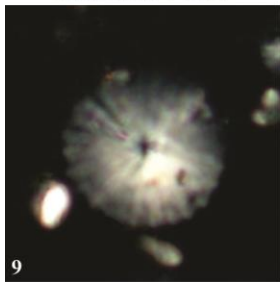
6 *D. mediosus* F41335



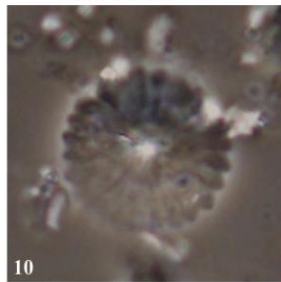
7 *D. mediosus* F41297



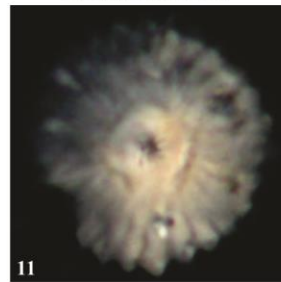
8 *D. mediosus* F41297



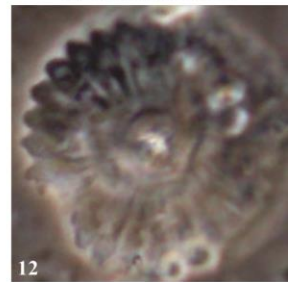
9 *D. multiradiatus* F39005



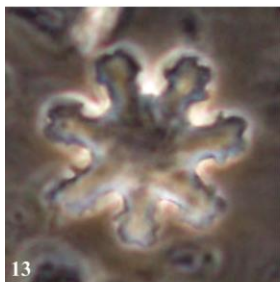
10 *D. multiradiatus* F39005



11 *D. multiradiatus* F39005



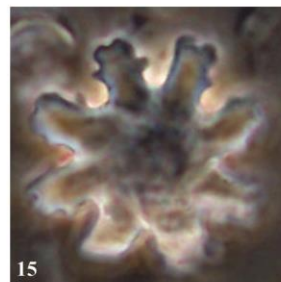
12 *D. multiradiatus* F39005



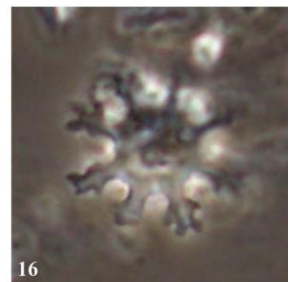
13 *D. nodifer* F41348



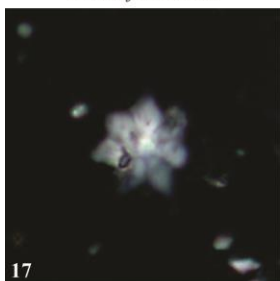
14 *D. nodifer* F41348



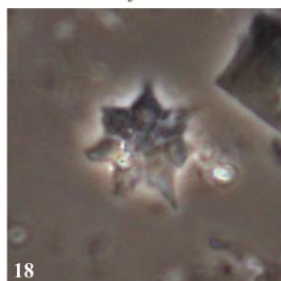
15 *D. nodifer* F41345



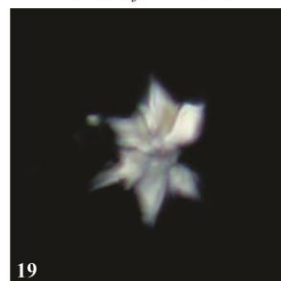
16 *D. nodifer* F41311



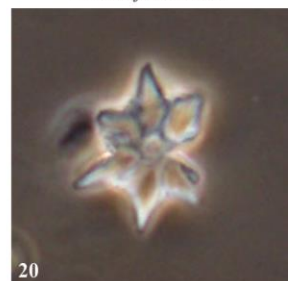
17 *D. saipanensis* F41407



18 *D. saipanensis* F41407



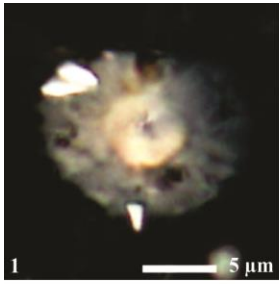
19 *D. saipanensis* F41403



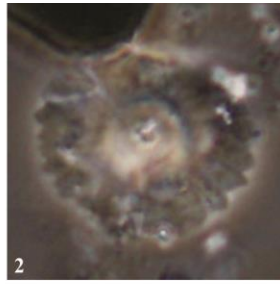
20 *D. saipanensis* F41403

PLATE 10

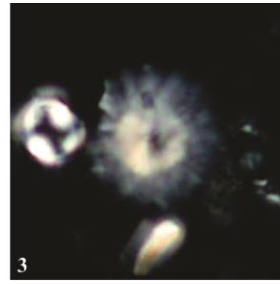
Nannoliths: Discoasteraceae



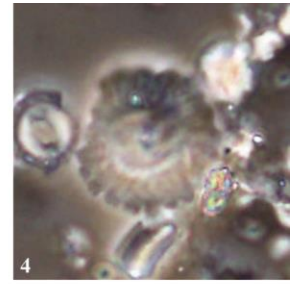
D. salisburgensis F39005



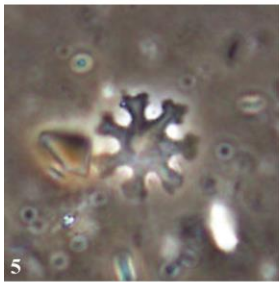
D. salisburgensis F39005



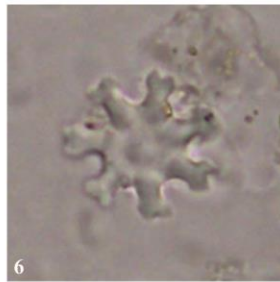
D. salisburgensis F39005



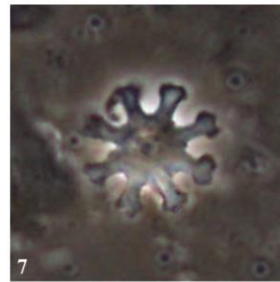
D. salisburgensis F39005



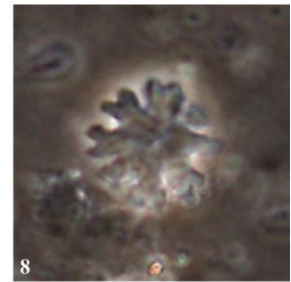
D. septemradiatus F41348



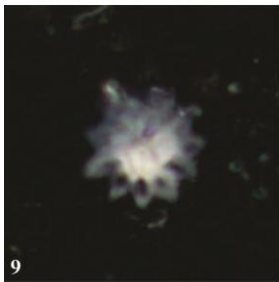
D. septemradiatus F41345



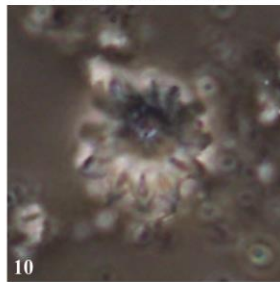
D. septemradiatus F41345



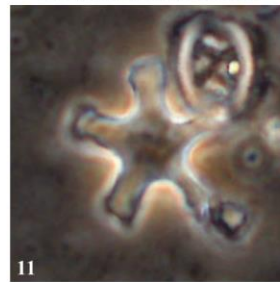
D. septemradiatus F41331



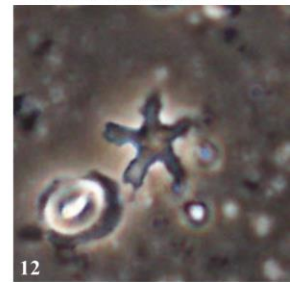
D. splendidus F39005



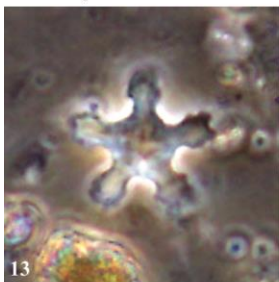
D. splendidus F39005



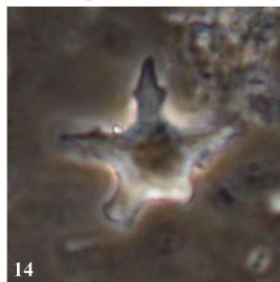
D. tanii F41345



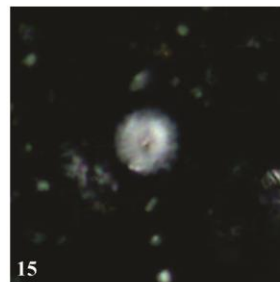
D. tanii F41345



D. tanii F41343



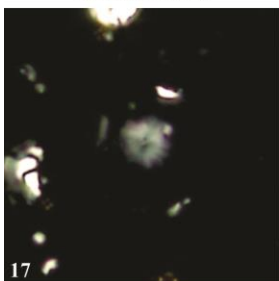
D. tanii F39005



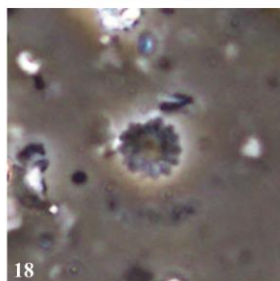
D. wemmelensis F41331



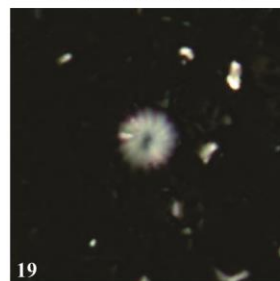
D. wemmelensis F41331



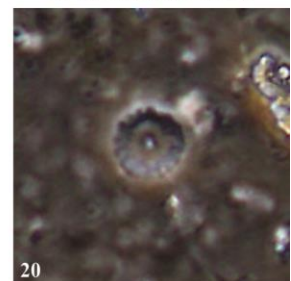
D. wemmelensis F41303



D. wemmelensis F41303



D. wemmelensis F38999



D. wemmelensis F38999

PLATE 11

Nannoliths: Fasciculithaceae, Rhomboasteraceae, Sphenolithaceae

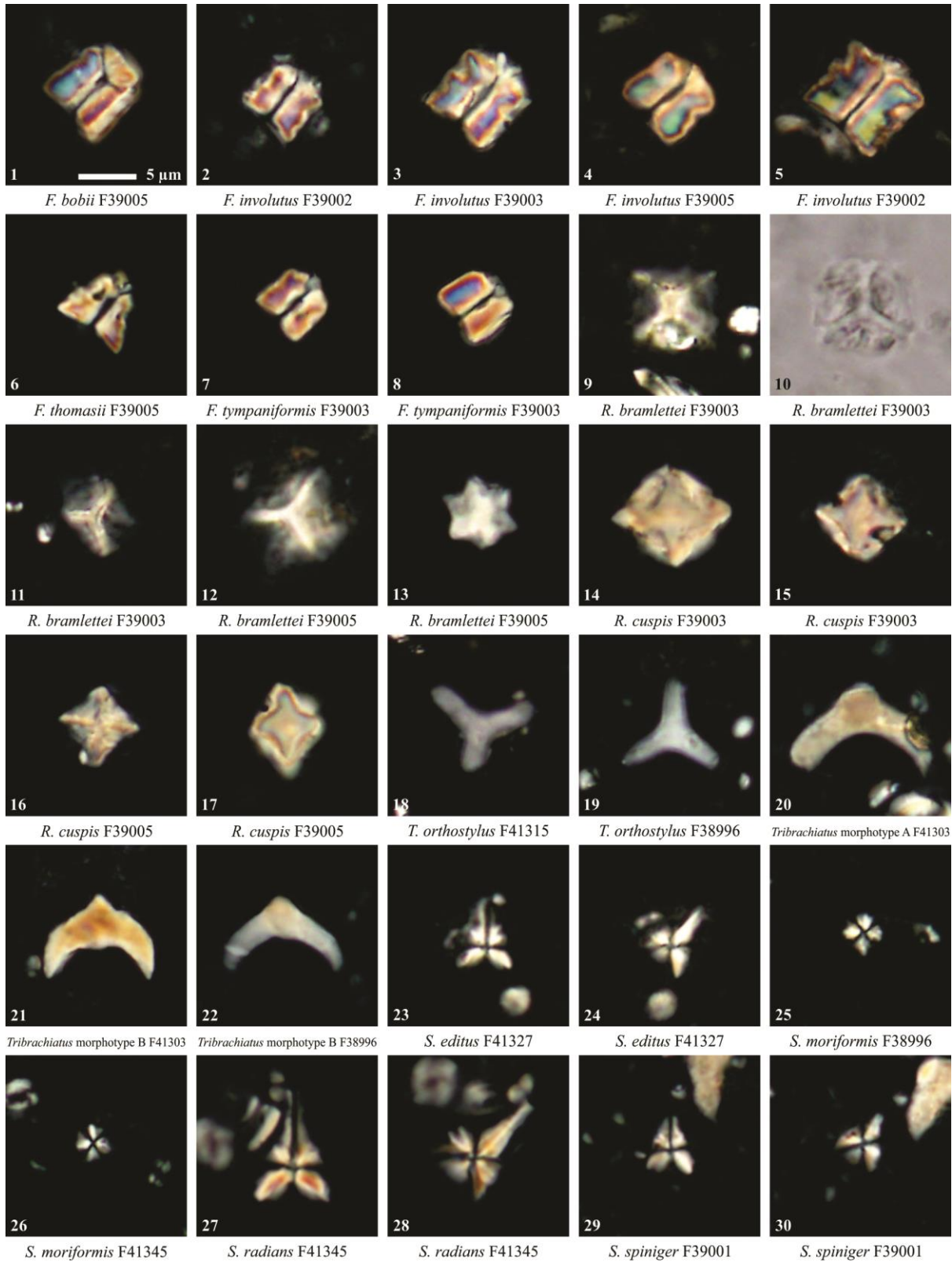


PLATE 12

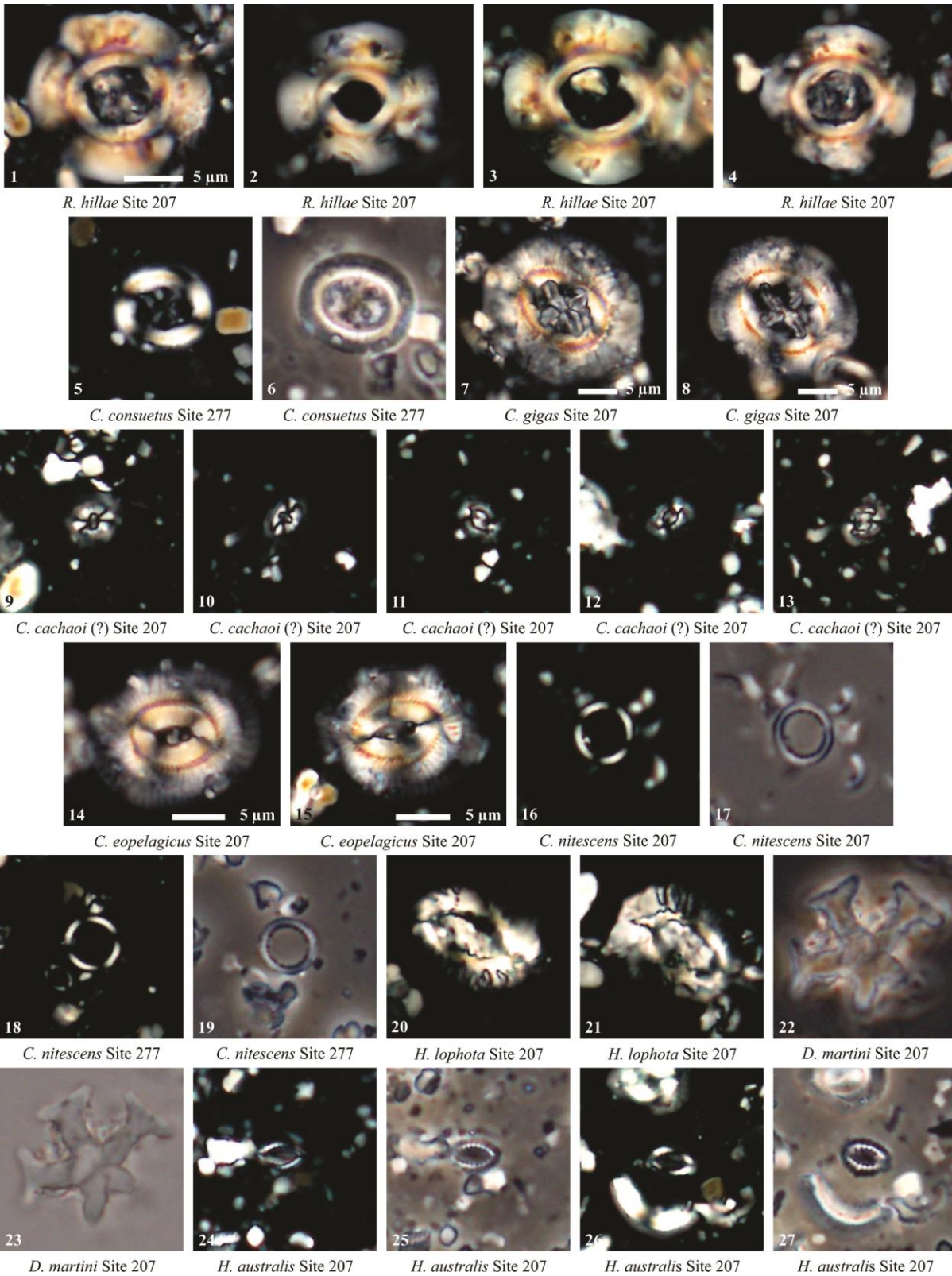


Plate 12: 1, 3, 16-17, 20-21: 207A-14R-1, 119-123. 2, 7-8: 207A-16R-2, 90-94. 4, 22-23: 207A-15R-3, 100-104. 5-6: 277-41-3, 110. 9-10, 24-27: 207A-26R-3, 100-104. 11-13: 207A-26R-2, 70-74. 14: 207A-18R-5, 100-104. 15: 207A-18R-2, 102-106. 18-19: 277-38R-3, 100.

PLATE 13

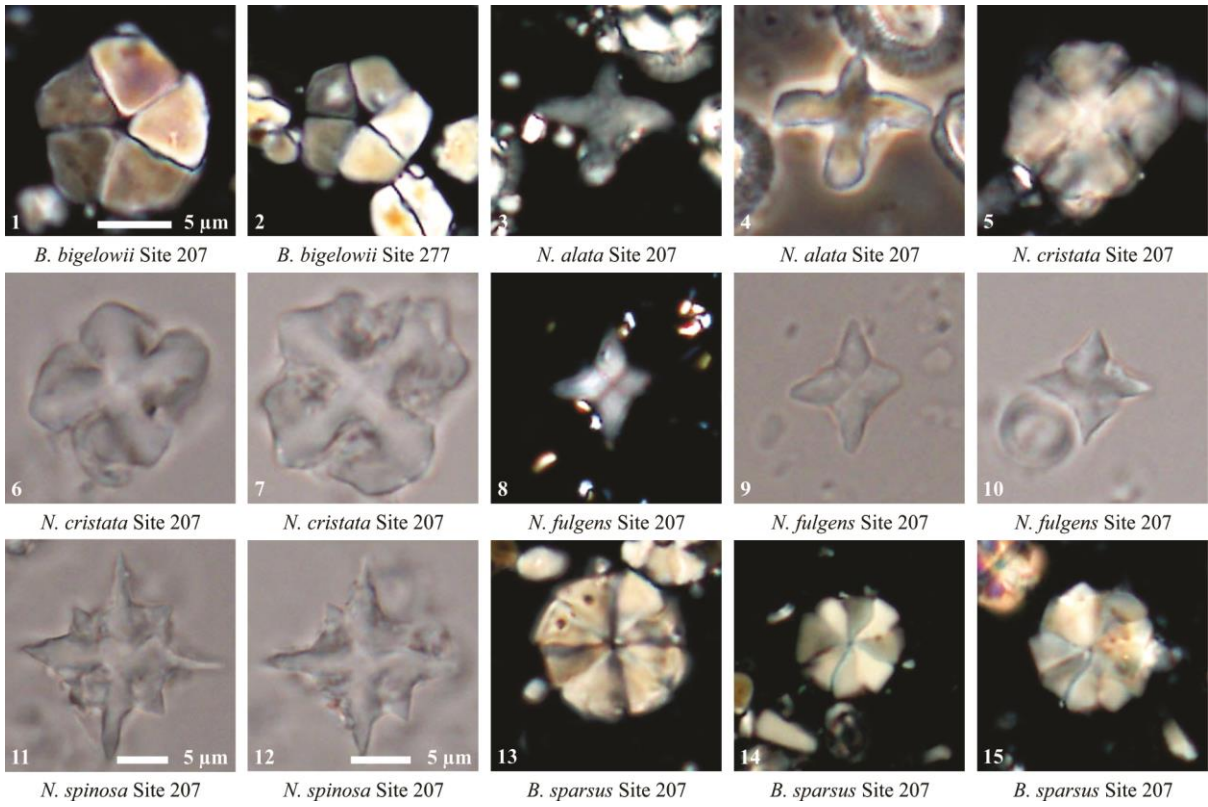


Plate 13: 1: 207A-24R-4, 110-114 2: 277-41R-3, 28. 3-4: 207A-15R-3, 100-104. 5-7: 207A-18R-2, 102-106. 8-12: 207A-14R-1, 119-123. 13-15: 207A-26R-3, 100-104.

Calcareous nannofossil distribution chart for Hampden Beach

Moeraki	Kurinui										Hampden		Formation					
	NP13/14					NP14-15					NP16	NP Zone (Martini, 1971)	Stratigraphic position (m)	Sample Number	Preservation			
11.60	14.2/24.3	B											136.80	14.2/30.3	G	11		<i>Blackites</i> spp.
													131.80	14.2/29.6	P			<i>Calcidiscus bicircus</i>
													127.40	14.2/29.4	P-M			<i>Chiasmolithus bidens</i>
													123.00	14.2/29.2	P-M			<i>Chiasmolithus expansus</i>
													118.60	14.2/29.0	P			<i>Chiasmolithus grandis</i>
													114.20	14.2/28.8	G	1	1	<i>Chiasmolithus solitus</i>
													111.00	14.2/28.7	B			<i>Chiasmolithus spp.</i>
													97.30	14.2/28.4	B			<i>Clathrolithus</i> spp.
													96.80	14.2/28.1	B			<i>Clausiococcus fenestratus</i>
													94.60	14.2/28.0	B			<i>Clausiococcus subdistichus</i>
													92.40	14.2/27.9	B			<i>Clausiococcus vanheckiae</i>
													90.20	14.2/27.8	B			<i>Coccolithus foraminis</i>
													88.00	14.2/27.7	B			<i>Coccolithus formosus</i>
													85.80	14.2/27.6	B			<i>Coccolithus pelagicus</i>
													79.20	14.2/27.3	P-M			<i>Coccolithus staurion</i>
													74.80	14.2/27.1	M			<i>Coronocyclus bramlettei</i>
													70.40	14.2/26.9	M			<i>Coronocyclus</i> spp.
													66.00	14.2/26.7	M			<i>Cruciplacolithus</i> spp.
													61.60	14.2/26.5	M+G			<i>Cyclagospaera</i> spp.
													51.40	14.2/26.3	G	9	3	<i>Cyclicargolithus</i> spp.
													49.70	14.2/26.1	G	6		<i>Discoaster bifax</i>
													46.70	14.2/25.8	B			<i>Discoaster distinctus</i>
													44.60	14.2/25.7	B			<i>Discoaster elegans</i>
													44.10	14.2/25.6	B			<i>Discoaster kuepperi</i>
													43.50	14.2/25.5	B			<i>Discoaster lenticularis</i>
													41.70	14.2/25.4	B			<i>Discoaster lodoensis</i>
													40.60	14.2/25.3	B			<i>Discoaster medius</i>
													36.00	14.2/25.2	B			<i>Discoaster nodifer</i>
													32.90	14.2/25.1	B			<i>Discoaster septemradiatus</i>
													30.00	14.2/25.0	B			<i>Discoaster wemmelensis</i>
													25.40	14.2/24.9	B			<i>Discoaster</i> spp. (5 ray)
													24.00	14.2/24.8	B			<i>Discoaster</i> spp. (6 ray)
													22.30	14.2/24.7	B			<i>Discoaster</i> 7+ ray
													15.20	14.2/24.6	B			<i>Discoaster</i> (rosette)
													13.40	14.2/24.5	B			<i>Discoaster</i> spp.
													11.60	14.2/24.3	B			<i>Ellipsolithus distichus</i>
																		<i>Girgisia gammatum</i>
																		<i>Helicosphaera seminulum</i>
																		<i>Markalius inversus</i>
																		<i>Nannatetrina</i> spp.
																		<i>Neococcolithes dubius</i>
																		<i>Neococcolithes minutus</i>
																		<i>Orthozygus occultus</i>
																		<i>Pontosphaera exilis</i>
																		<i>Pontosphaera pax</i>
																		<i>Pontosphaera plana</i>
																		<i>Pontosphaera pulchroides</i>
																		<i>Pontosphaera pulchra</i>

Moeraki	Kurinu	Hampden		Formation
		NP16	NP14-15	Nannofossil Zone
	NP13/14			Stratigraphic position (m)
				Sample Number
				Preservation
				<i>Pontosphaera punctosa</i>
				<i>Pontosphaera</i> spp.
				<i>Pyrocyclus</i> spp.
				<i>Reticulofenestra bisecta</i> (<10 µm)
				<i>Reticulofenestra circus</i>
				<i>Reticulofenestra daviesii</i>
				<i>Reticulofenestra dictyoda</i>
				<i>Reticulofenestra hamdenensis</i>
				<i>Reticulofenestra minuta</i>
				<i>Reticulofenestra producta</i>
				<i>Reticulofenestra samodurovii</i>
				<i>Reticulofenestra scrippsae</i>
				<i>Reticulofenestra wadeae</i>
				<i>Reticulofenestra</i> spp.
				<i>Sphenolithus moriformis</i>
				<i>Sphenolithus radians</i>
				<i>Sphenolithus spiniger</i>
				<i>Sphenolithus</i> spp.
				<i>Toweius callosus</i>
				<i>Toweius magnicrossus</i>
				<i>Toweius occultatus</i>
				<i>Toweius rotundus</i>
				<i>Toweius</i> sp 1 (Bown)
				<i>Umbilicosphaera jordanii</i>
				<i>Zygrhablithus bijugatus bijugatus</i>
				Placolith, small
				Unidentified rim

Calcareous nannofossil distribution chart for DSDP Site 207

NP9/10	NP11	NP12	NP13		NP14			NP15a-b	NP16	NP Zone (Martini, 1971)											
CNE1	CNE3	CNE4	CNE5		CNE6	CNE7-8		CNE9-11	CNE12-13	CNE Zone (Agnini et al., 2014)											
286.00	284.20	276.51	269.60	269.00	264.00	259.04	247.26	242.46	230.01	219.47	216.40	213.40	212.00	207.52	198.51	189.40	182.00	171.51	170.19	Depth (mbsf)	
26R-3, 100-104	26R-2, 70-74	25R-3, 51-55	24R-4, 110-114	24R-4, 50-54	23R-CC, 0	23R-3, 104-108	22R-1, 126-130	21R-4, 96-100	20R-5, 101-105	19R-4, 97-101	19R-2, 90-94	18R-6, 90-94	18R-5, 100-104	18R-2, 102-106	17R-2, 101-105	16R-2, 90-94	15R-3, 100-104	14R-2, 101-105	14R-1, 119-123	Sample no.	
P-M	M	M	M	M	M	M	M	M-G	M-G	M-G	G	G	G	G	M	M-P	M-P	M	G	Preservation	
x																				<i>Biantholithus sparsus</i>	
																					<i>Blackites</i> spp.
																					<i>Braarudosphaera bigelowii</i>
																					<i>Calcidiscus bicircus</i>
																					<i>Calcidiscus pacificanus</i>
																					<i>Calcidiscus protoannulus</i>
																					<i>Calcidiscus</i> spp.
																					<i>Campylosphaera eo/dela</i>
																					<i>Chiasmolithus bidens</i>
																					<i>Chiasmolithus californicus</i>
																					<i>Chiasmolithus expansus</i>
																					<i>Chiasmolithus gigas</i>
																					<i>Chiasmolithus grandis</i>
																					<i>Chiasmolithus modestus</i>
																					<i>Chiasmolithus nitidus</i>
																					<i>Chiasmolithus solitus</i>
																					<i>Chiasmolithus</i> spp.
																					<i>Clausicoccus fenestratus</i>
																					<i>Clausicoccus subdistichus</i>
																					<i>Clausicoccus vanheckiae</i>
																					<i>Clausicoccus</i> spp.
																					<i>Coccolithus cachaoui</i> (q)
																					<i>Coccolithus eopelagicus</i>
																					<i>Coccolithus foraminis</i>
																					<i>Coccolithus formosus</i>
																					<i>Coccolithus latus</i>
																					<i>Coccolithus pelagicus</i>
																					<i>Coccolithus staurion</i>
																					<i>Coccolithus</i> spp.
																					<i>Coronocyclus bramlettei</i>
																					<i>Coronocyclus nitescens</i>
																					<i>Cruciplacolithus primus</i>
																					<i>Cyclargolithus floridanus</i>
																					<i>Cyclargolithus luminis</i>
																					<i>Cyclargolithus parvus</i>
																					<i>Discoaster barbadiensis</i>
																					<i>Discoaster cruciformis</i>
																					<i>Discoaster kuepperi</i>
																					<i>Discoaster lenticularis</i>
																					<i>Discoaster lodoensis</i>

NP9/10	NP11	NP12	NP13	NP14	NP15a-b	NP16	NP Zone (Martini, 1971)
CNE1	CNE3	CNE4	CNE5	CNE6	CNE9-11	CNE12-13	CNE Zone (Agnini et al., 2014)
286.00	279.00	276.51	269.60	242.46	198.51	170.19	Depth (mbsf)
26R-3, 100-104	26R-2, 70-74	25R-3, 51-55	24R-4, 110-114	21R-4, 96-100	17R-2, 101-105	14R-1, 119-123	Sample no.
P-M	M	M	M	M-G	M	G	Preservation
							<i>Discoaster martinii</i>
							<i>Discoaster multiradiatus</i>
							<i>Discoaster saipanensis</i>
							<i>Discoaster salisburgensis</i>
							<i>Discoaster septemradiatus</i>
							<i>Discoaster sublodoensis</i>
							<i>Discoaster wemmelensis</i>
							<i>Discoaster</i> spp. (5 ray)
							<i>Discoaster</i> spp. (6 ray)
							<i>Discoaster</i> spp. (7+ ray)
							<i>Discoaster</i> spp. (rosette)
							<i>Discoaster</i> spp.
							<i>Ellipsolithus bollii</i>
							<i>Ellipsolithus distichus</i>
							<i>Ellipsolithus macellus</i>
							<i>Fasciculithus involutus</i>
							<i>Fasciculithus tympaniformis</i>
							<i>Fasciculithus</i> spp. (end view)
							<i>Girgsia gammation</i>
							<i>Helicosphaera lophota</i>
							<i>Helicosphaera seminulum</i>
							<i>Hornibrookina australis</i>
							<i>Hornibrookina teurenis</i>
							<i>Jakubowskia leoniae</i>
							<i>Lophodolichus</i> spp.
							<i>Markalius apertus</i>
							<i>Markalius inversus</i>
							<i>Micrantholithus</i> spp.
							<i>Nannotetrina alata</i>
							<i>Nannotetrina cristata</i>
							<i>Nannotetrina fulgens</i>
							<i>Nannotetrina spinosa</i>
							<i>Neochiastozygus distentus</i>
							<i>Neochiastozygus junctus</i>
							<i>Neococcolithes dubius</i>
							<i>Neococcolithes minutus</i>
							<i>Neococcolithes protenus</i>
							<i>Neococcolithes</i> spp.
							<i>Orthozygus occultus</i>
							<i>Pontosphaera exilis</i>

NP9/10	NP11	NP12	NP13		NP14			NP15a-b	NP16	NP Zone (Martini, 1971)
CNE1	CNE3	CNE4	CNE5		CNE6	CNE7-8		CNE9-11	CNE12-13	CNE Zone (Agnini et al., 2014)
286.00	284.20	276.51	269.60	264.00	242.46	213.40	216.40	198.51	171.51	Depth (mbsf)
26R-3, 100-104	26R-2, 70-74	25R-3, 51-55	24R-4, 110-114	24R-4, 50-54	21R-4, 96-100	18R-5, 100-104	19R-2, 90-94	17R-2, 101-105	14R-2, 101-105	Sample no.
P-M	M	M	M	M	M-G	G	G	M	M	Preservation
										<i>Pontosphaera plana</i>
										<i>Pontosphaera pulchra</i>
										<i>Pontosphaera</i> spp.
										<i>Pyrocyclus</i> spp.
										<i>Reticulofenestra circus</i>
										<i>Reticulofenestra daviesii</i>
										<i>Reticulofenestra dictyoda</i>
										<i>Reticulofenestra hillae</i>
										<i>Reticulofenestra minuta</i>
										<i>Reticulofenestra producta</i>
										<i>Reticulofenestra samodurovii</i>
										<i>Reticulofenestra scrippsae</i>
										<i>Reticulofenestra umbilicus</i>
										<i>Reticulofenestra wadeae</i>
										<i>Reticulofenestra</i> spp.
										<i>Sphenolithus editus</i>
										<i>Sphenolithus moriformis</i>
										<i>Sphenolithus radians</i>
										<i>Sphenolithus spiniger</i>
										<i>Sphenolithus</i> spp.
										<i>Tetralithoides symeonidesii</i>
										<i>Toweius callosus</i>
										<i>Toweius eminens</i>
										<i>Toweius magnicrassus</i>
										<i>Toweius occultatus</i>
										<i>Toweius pertusus</i>
										<i>Toweius tovae</i>
										<i>Toweius</i> spp.
										<i>Toweius</i> sp 2 (Bown)
										<i>Tribracliatius orthostylus</i>
										<i>Umbilicosphaera jordani</i>
										<i>Zygrhablithus bijugatus bijugatus</i>
										Placolith, small
										Unidentified
										Unidentified rim

Calcareous nannofossil distribution chart for DSDP Site 277

NP13		NP14			NP16	NP Zone (Martini, 1971)
CNE5		CNE6	CNE7	CNE8	CNE12-13	CNE Zone (Agnini et al., 2014)
Depth (mbsf)	Sample ID	Preservation				
369.00	36-1, 100	M-P				<i>Blackites</i> spp.
		x				<i>Braarudosphaera bigelowii</i>
370.58	36-2, 108	P				<i>Calcidiscus bicircus</i>
		x				<i>Calcidiscus pacificanus</i>
372.08	36-3, 108	P				<i>Calcidiscus protoannulus</i>
						<i>Calcidiscus</i> spp.
381.50	37-3, 100	M-P				<i>Campylosphaera eo/dela</i>
						<i>Chiasmolithus bidens</i>
387.95	38-1, 95	M-P				<i>Chiasmolithus consuetus</i>
						<i>Chiasmolithus expansus</i>
388.75	38-2, 25	P				<i>Chiasmolithus grandis</i>
						<i>Chiasmolithus modestus</i>
389.50	38-2, 100	P				<i>Chiasmolithus nitidus</i>
						<i>Chiasmolithus solitus</i>
391.00	38-3, 100	M-P				<i>Chiasmolithus</i> spp.
						<i>Clasicococcus fenestratus</i>
400.50	39-3, 100	M-P				<i>Clasicococcus subdistichus</i>
						<i>Clasicococcus vanheckiae</i>
407.83	40-2, 33	M				<i>Clasicococcus</i> spp.
						<i>Coccolithus foraminis</i>
408.50	40-2, 100	M-P				<i>Coccolithus formosus</i>
						<i>Coccolithus latus</i>
409.33	40-3, 33	M-P				<i>Coccolithus eopelagicus</i>
						<i>Coccolithus pelagicus</i>
410.00	40-3, 100	M-P				<i>Coccolithus</i> spp.
						<i>Coronocyclus bramlettei</i>
416.20	41-1, 70	M				<i>Coronocyclus nitescens</i>
						<i>Cyclicargolithus luminis</i>
416.62	41-1, 112	M-P				<i>Discoaster barbadiensis</i>
						<i>Discoaster kuepperi</i>
417.28	41-2, 28	M-P				<i>Discoaster lenticularis</i>
						<i>Discoaster lodoensis</i>
418.07	41-2, 107	M-P				<i>Discoaster saipanensis</i>
						<i>Discoaster sublodoensis</i>
418.78	41-3, 28	M				<i>Discoaster wemmelensis</i>
						<i>Discoaster</i> spp. (5 ray)
419.60	41-3, 110	M				<i>Discoaster</i> spp. (6 ray)
						<i>Discoaster</i> spp. (7+ ray)
						<i>Discoaster</i> spp. (rosette)

APPENDIX D: AGE-DEPTH MODELS

The following foraminiferal and radiolarian datums are used in the age-depth models for DSDP Sites 207 and 277.

Taxon	Group	Age	Reference	Depth (m)
DSDP Site 207				
<i>FO Eusyringium fistuligerum</i>	R	43.10	Gradstein et al. (2012), Dallanave et al. (2015)	165.50
<i>FO Zealithapium mitra</i>	R	42.30	Gradstein et al. (2012), Norris et al. (2014)	170.19
<i>LO Zealithapium anoectum</i>	R	42.50	Gradstein et al. (2012), Norris et al. (2014)	168.50
<i>FO Globigerinatheka index</i>	F	42.64	Gradstein et al. (2012)	182.00
<i>FO Eusyringium lagena</i>	R	45.50	Gradstein et al. (2012), Dallanave et al. (2015)	182.00
<i>LO Morozovella crater</i>	F	45.70	Raine et al. (2015)	213.40
<i>FO Theocampe mongolfieri</i>	R	47.98	Gradstein et al. (2012)	216.01
<i>LO Podocyrthis acalles</i>	R	48.13	Gradstein et al. (2012), Norris et al. (2014)	228.20
<i>FO Elphidium hampdenense</i>	F	48.90	Dallanave et al. (2016), Raine et al. (2015)	219.47
<i>FO Morozovella crater</i>	F	52.00	Dallanave et al. (2016), Raine et al. (2015)	269.00
<i>FO Theocampe urceolus</i>	R	52.00	Gradstein et al. (2012)	279.00
<i>FO Calocyclus ampulla</i>	R	46.21	Gradstein et al. (2012), Norris et al. (2014)	276.51
<i>FO Lychnocanium bellum</i>	R	53.00	Gradstein et al. (2012), Norris et al. (2014)	284.20
DSDP Site 277				
<i>LO Morozovella crater</i>	F	45.70	Raine et al. (2015)	380.75
<i>FO Morozovella crater</i>	F	52.00	Dallanave et al. (2016), Raine et al. (2015)	426.90